



# **On the Use of Coupled Wind, Wave, and Current Fields in the Simulation of Loads on Bottom-Supported Offshore Wind Turbines during Hurricanes**

**March 2012 — September 2015**

Eungsoo Kim and Lance Manuel  
*University of Texas at Austin  
Austin, Texas*

Milan Curcic and Shuyi S. Chen  
*University of Miami  
Coral Gables, Florida*

Caleb Phillips and Paul Veers  
*National Renewable Energy Laboratory  
Golden, Colorado*

NREL Technical Monitor: Paul Veers

**NREL is a national laboratory of the U.S. Department of Energy  
Office of Energy Efficiency & Renewable Energy  
Operated by the Alliance for Sustainable Energy, LLC**

This report is available at no cost from the National Renewable Energy Laboratory (NREL) at [www.nrel.gov/publications](http://www.nrel.gov/publications).

**Technical Report**  
NREL/TP-5000-65283  
June 2016

Contract No. DE-AC36-08GO28308

# **On the Use of Coupled Wind, Wave, and Current Fields in the Simulation of Loads on Bottom-Supported Offshore Wind Turbines during Hurricanes**

**March 2012 — September 2015**

Eungsoo Kim and Lance Manuel  
*University of Texas at Austin*  
*Austin, Texas*

Milan Curcic and Shuyi S. Chen  
*University of Miami*  
*Coral Gables, Florida*

Caleb Phillips and Paul Veers  
*National Renewable Energy Laboratory*  
*Golden, Colorado*

NREL Technical Monitor: Paul Veers

**NREL is a national laboratory of the U.S. Department of Energy  
Office of Energy Efficiency & Renewable Energy  
Operated by the Alliance for Sustainable Energy, LLC**

This report is available at no cost from the National Renewable Energy Laboratory (NREL) at [www.nrel.gov/publications](http://www.nrel.gov/publications).

**This publication was reproduced from the best available copy submitted by the subcontractor and received little editorial review at NREL.**

### **NOTICE**

This report was prepared as an account of work sponsored by an agency of the United States government. Neither the United States government nor any agency thereof, nor any of their employees, makes any warranty, express or implied, or assumes any legal liability or responsibility for the accuracy, completeness, or usefulness of any information, apparatus, product, or process disclosed, or represents that its use would not infringe privately owned rights. Reference herein to any specific commercial product, process, or service by trade name, trademark, manufacturer, or otherwise does not necessarily constitute or imply its endorsement, recommendation, or favoring by the United States government or any agency thereof. The views and opinions of authors expressed herein do not necessarily state or reflect those of the United States government or any agency thereof.

This report is available at no cost from the National Renewable Energy Laboratory (NREL) at [www.nrel.gov/publications](http://www.nrel.gov/publications).

Available electronically at SciTech Connect <http://www.osti.gov/scitech>

Available for a processing fee to U.S. Department of Energy and its contractors, in paper, from:

U.S. Department of Energy  
Office of Scientific and Technical Information  
P.O. Box 62  
Oak Ridge, TN 37831-0062  
OSTI <http://www.osti.gov>  
Phone: 865.576.8401  
Fax: 865.576.5728  
Email: [reports@osti.gov](mailto:reports@osti.gov)

Available for sale to the public, in paper, from:

U.S. Department of Commerce  
National Technical Information Service  
5301 Shawnee Road  
Alexandria, VA 22312  
NTIS <http://www.ntis.gov>  
Phone: 800.553.6847 or 703.605.6000  
Fax: 703.605.6900  
Email: [orders@ntis.gov](mailto:orders@ntis.gov)

*Cover Photos by Dennis Schroeder: (left to right) NREL 26173, NREL 18302, NREL 19758, NREL 29642, NREL 19795.*

NREL prints on paper that contains recycled content.

## Acknowledgments

The authors wish to acknowledge the assistance received from project collaborators including Mr. John Michalakes, previously a staff member at the National Renewable Energy Laboratory where he initiated the project summarized in this report, and now at the National Oceanic and Atmospheric Administration. John's leadership was essential in formulating the team and setting the direction for this work. We also acknowledge substantial assistance from Dr. Mark Donelan, of the University of Miami's Rosenstiel School of Marine and Atmospheric Science. Mark was a tireless and insightful collaborator on the wave dynamics simulation and helped interpret the results for use in the loads simulation.

This work was supported by the U.S. Department of Energy under Contract No. DE-AC36-08GO28308 with the National Renewable Energy Laboratory. Funding for the work was provided by the DOE Office of Energy Efficiency and Renewable Energy, Wind and Water Power Technologies Office.



# 1 Overview

In the United States, potential offshore wind plant sites have been identified along the Atlantic seaboard and in the Gulf of Mexico. It is imperative that we define external conditions associated with hurricanes and severe winter storms and consider load cases for which wind turbines may need to be designed. We selected two hurricanes, Ike (2008) and Sandy (2012), and investigated the effect these tropical storms would have on bottom-supported offshore wind turbines that were hypothetically in or close to their path as they made landfall. For realistic turbine loads assessment, it is important that the coupled influences of the changing wind, wave, and current fields are simulated throughout the evolution of the hurricanes. We employed a coupled model—specifically, the University of Miami Coupled Model (UMCM)—that integrates atmospheric, wave, and ocean components to produce needed wind, wave, and current data. The wind data are used to generate appropriate vertical wind profiles and full wind velocity fields including turbulence; the current field over the water column is obtained by interpolated discrete output current data; and short-crested irregular second-order waves are simulated using output directional wave spectra from the coupled model.

We studied two monopile-supported offshore wind turbines sited in 20 meters of water in the Gulf of Mexico to estimate loads during Hurricane Ike, and a jacket space-frame platform-supported offshore wind turbine sited in 50 meters of water in the mid-Atlantic region to estimate loads during Hurricane Sandy. In this report we discuss in detail how the simulated hurricane wind, wave, and current output data are used in turbine loads studies. In addition, important characteristics of the external conditions are studied, including the relative importance of swell versus wind seas, aerodynamic versus hydrodynamic forces, current velocity effects, yaw control options for the turbine, hydrodynamic drag versus inertia forces, and soil-structure interaction effects. A detailed framework is presented that explains how coupled inputs can be included in turbine loads studies during a hurricane. This framework can aid in future efforts aimed at developing offshore wind turbine design criteria and load cases related to hurricanes.

The UMCM was created by the University of Miami for this project and was essential in producing simultaneous wind and wave conditions during all aspects of the hurricane, especially as it approached and passed through areas of potential offshore wind plant development. Appendix A includes a description of the scope and nature of the UMCM and details the modeling capabilities that it possesses. Some example outputs provide a visualization of the kinds of data that are generated. The results for each of the two selected hurricanes (Ike and Sandy) are also detailed. The University of Miami team used extensive buoy data from both storms to validate the UMCM capabilities, some extracts of which are shown here. More documentation of model validation can be found in the References section.

Appendix B describes how users can access this extensive data set of wind and wave conditions for both Hurricane Ike and Hurricane Sandy at user-specified potential development sites. The data have been housed at the National Renewable Energy Laboratory for future use, and software hooks have been created to enable users to extract time series of interest from the more than two Tera-byte data set. Examples time series from the Hurricane Ike and Hurricane Sandy data are plotted to illustrate the types of the data that can be extracted.

## 2 Modeling Hurricane Ike's Influence on a Monopile-Supported Offshore Wind Turbine

### 2.1 Problem description

Over a 5-day period in the evolution of Hurricane Ike (2008) prior to landfall, the response of a monopile-supported 5-MW offshore wind turbine is evaluated in a step-wise procedure. As sites for the turbines to be analyzed, we select locations 60 km to the right and left of the track of Ike, points A and B, respectively, as shown in Fig. 2.1, where the water depth is 20 meters.

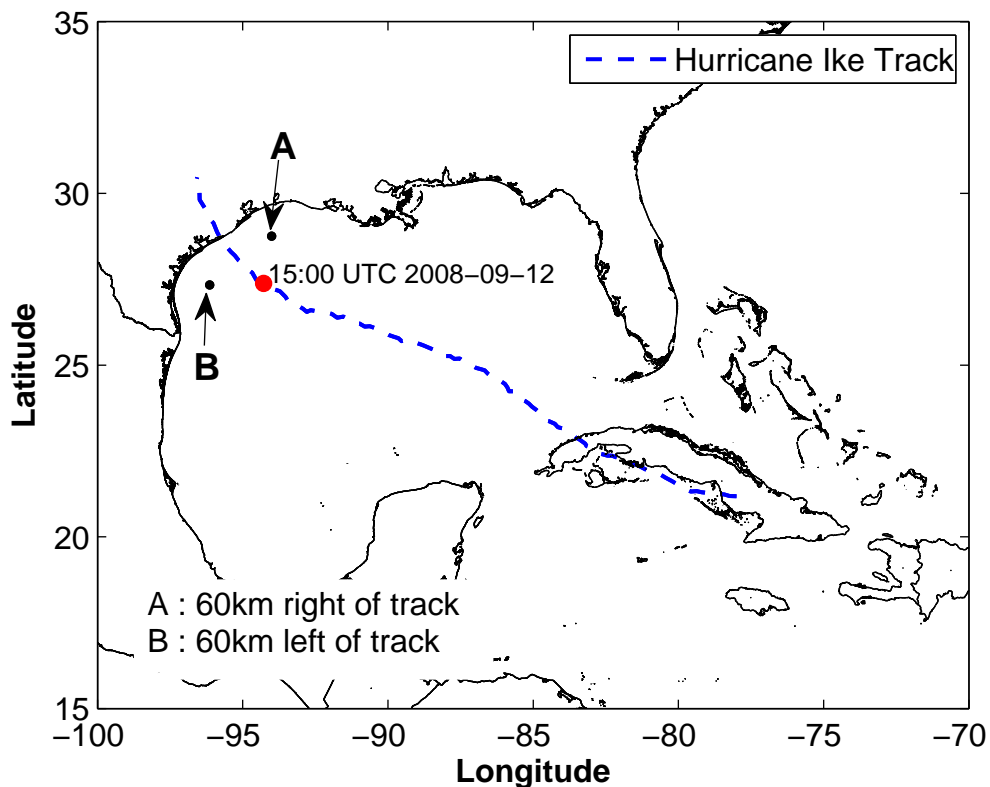


**Figure 2.1. Track of Hurricane Ike and selected locations of two sites, one to the left and the other to the right of the track where the water depth is 20 m.**

Based on output from UCM, coupled wind and wave fields at the two selected locations are simulated and we evaluate the turbine response on a 5-MW offshore wind turbine over a period of the storm's evolution when it is close to landfall. We present the theoretical background and formulation for directional second-order nonlinear irregular wave modeling and outline a procedure for numerical simulation of the sea surface elevation and associated wave kinematics. We also present characteristics of the hurricane wind fields and show how a spectral method is adopted to simulate these hurricane turbulent wind fields. Finally, we investigate how yaw and pitch controls influence the response of the selected offshore wind turbine during a hurricane.

## 2.2 Hurricane Waves

In this study, hurricane-generated wave kinematics are simulated based on directional wave spectra resulting from the UCMC output; the model was initialized at 12:00 UTC on September 9, 2008. A wave spectrum from the UCMC output consists of 36 directional bins and 37 frequency bins covering a range from 0.03 Hz to 2 Hz, over which the discrete frequencies are logarithmically spaced. As an illustration of the development of wave inputs for turbine loads analysis, we present in Fig. 2.2 normalized directional wave spectra with significant wave height ( $H_s$ ) obtained from UCMC that apply to the two selected site A and B; these spectra are for 80 to 120 hours after the start of the simulation (with updates shown every 10 hours). Red and blue arrows in these spectra represent the mean wind and wave direction, respectively. Also, in these wave spectra,  $N$  describe waves propagating toward north, etc., and the dashed circles and the solid circle (inner to outer) correspond to wave frequencies of 0.1, 0.2, 0.3, and 0.4 Hz. In these wave spectra plots, we see that directional spreading of wave energy is significant and that the wave spectrum, before passing the sites, has two well-separated peaks. Although the wave energy at high frequencies is closely linked to the wind field and the mean wave direction is dominated by the low-frequency wave component; this low-frequency wave component is classified as swell which contributes significantly to the total wave energy at the two sites.

### 2.2.1 Wave simulation theory

It is common practice to model the irregular sea surface elevation process as a Gaussian random process using linear Airy wave theory. However, to generate realistic hurricane wave fields, it is essential to account for both wave directionality and nonlinearity. In this study, directionality and nonlinearity of the waves are accounted for by employing directional irregular second-order wave formulations proposed by Sharma and Dean [1] for finite water depths. This second-order wave modeling formulation is an extension of the theory developed by Longuet-Higgins et al. [2] for waters of infinite depth to apply to waters of arbitrary finite depth. A nonlinear boundary value problem is solved up to second order by a perturbation approach accounting for contributions from linear components from arbitrary frequencies and directions. The second-order wave system is one that is forced by the linear system and all information on second-order amplitudes and phases is related to the characteristics of the first-order spectrum.

#### 2.2.1.1 Boundary value problem formulation

If the effects of viscosity and turbulence can be regarded as small, incompressible flows can be described well by a velocity potential. In other words, the velocity components  $u$ ,  $v$ , and  $w$ , can be defined in terms of the gradients of the velocity potential,  $\phi$ , given in terms of the three Cartesian directions,  $x$ ,  $y$ , and  $z$ .

$$(u, v, w) = \left( \frac{\partial \phi}{\partial x}, \frac{\partial \phi}{\partial y}, \frac{\partial \phi}{\partial z} \right) \quad (2.1)$$

The mass conservation equation for an incompressible fluid is

$$\frac{\partial u}{\partial x} + \frac{\partial v}{\partial y} + \frac{\partial w}{\partial z} = 0 \quad (2.2)$$

which can be combined with Eq. 2.1 to yield

$$\nabla^2 \phi = \frac{\partial^2 \phi}{\partial x^2} + \frac{\partial^2 \phi}{\partial y^2} + \frac{\partial^2 \phi}{\partial z^2} = 0 \quad (2.3)$$

where  $-h \leq z \leq \eta$  and  $-\infty \leq x, y \leq \infty$

Sharma and Dean proposed a second-order velocity potential function that satisfies the appropriate boundary conditions for the problem.

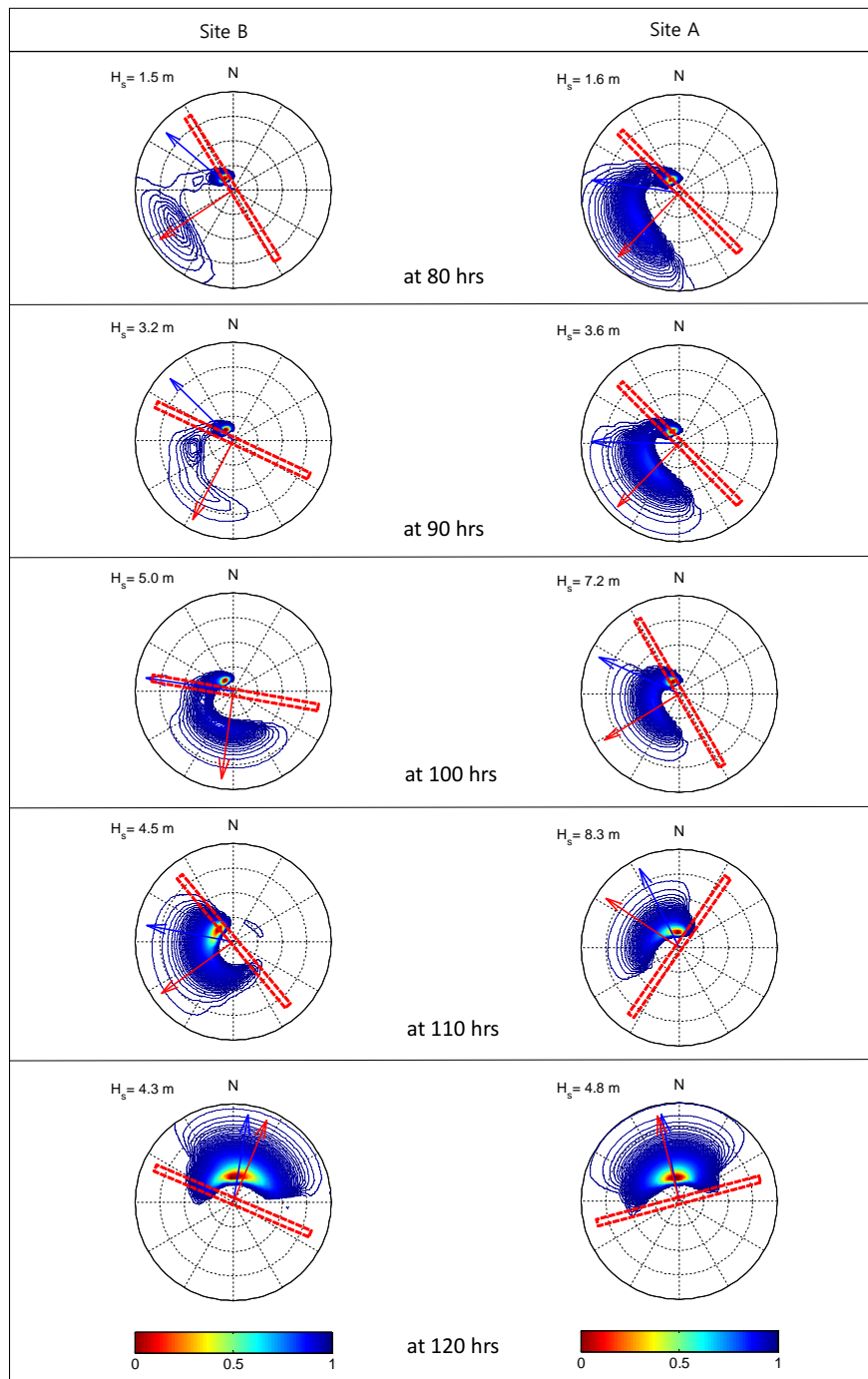


**Figure 2.2. Wave spectra for Sites A and B from over a 40-hour period during Hurricane Ike; N describe waves propagating toward north, etc., and the dashed circles and the solid circle (inner to outer) correspond to wave frequencies of 0.1, 0.2, 0.3, and 0.4 Hz. (blue arrow: wave direction; red arrow: wind direction).**

- **Bottom Boundary Condition (BBC)**

At the bottom boundary, the velocity normal to the boundary is equal to zero. For this case of a horizontal boundary at depth,  $h$ , we have:

$$\left. \frac{\partial \phi}{\partial z} \right|_{z=-h} = 0 \quad (2.4)$$

- **Kinematic Free Surface Boundary Condition (KFSBC)**

A water particle on the free surface remains on the free surface and the vertical velocity at the free surface is equal to the total rate of change of the sea surface elevation:

$$\frac{\partial \eta}{\partial t} + \frac{\partial \phi}{\partial x} \frac{\partial \eta}{\partial x} + \frac{\partial \phi}{\partial y} \frac{\partial \eta}{\partial y} = \frac{\partial \phi}{\partial z} \quad (2.5)$$

where  $z = \eta$ .

- **Dynamic Free Surface Boundary Conditions (DFSBC)**

The pressure,  $p$ , follows from Bernoulli's equation:

$$\frac{p}{\rho} + gz + \frac{\partial \phi}{\partial t} + \frac{1}{2} \nabla \phi \cdot \nabla \phi = -Q(t) \quad (2.6)$$

where  $Q(t)$  is an arbitrary function of time. Instead of including the variation with time of  $Q$  in the velocity potential,  $\phi$ , let  $Q$  be a constant. At the free surface,  $z = \eta$ , the pressure is equal to the atmospheric pressure,  $p_{atm}$  and if we choose  $Q = -p_{atm}/\rho$  in Eq.2.6, we can rewrite the equation as follows [3]:

$$\Rightarrow g\eta + \frac{\partial \phi}{\partial t} + \frac{1}{2} \nabla \phi \cdot \nabla \phi = 0 \quad (2.7)$$

- **Combined Free Surface Boundary Condition (CFSBC)**

We can write an alternative form of Eqs. 2.5 and 2.7 above, by eliminating the unknown free surface elevation  $\eta$ . This then involves only  $\phi$  and its derivatives:

$$-\frac{\partial^2 \phi}{\partial t^2} - g \frac{\partial \phi}{\partial z} - \left( \frac{\partial}{\partial t} + \frac{1}{2} \nabla \phi \cdot \nabla \right) |\nabla \phi|^2 = 0 \quad (2.8)$$

where  $z = \eta$

### 2.2.1.2 Solution of the boundary value problem

A perturbation approach is adopted for solution of the boundary value problem formulated in the previous section. This approach assumes that all variables can be expanded as a convergent power series of a small parameter, such as the wave steepness. Also, it is assumed that the combined free surface boundary condition (CFSBC) can be expanded in a convergent Maclaurin series about the mean water level,  $z = 0$ , in terms of the small parameter.

The velocity potential,  $\phi$ , and sea surface elevation,  $\eta$ , may be represented in the following manner using wave steepness,  $\varepsilon$ , as the perturbation parameter:

$$\phi(x, y, z, t) = \phi^{(1)}(x, y, z, t) + \phi^{(2)}(x, y, z, t) + \dots \quad (2.9)$$

$$\eta(x, y, t) = \eta^{(1)}(x, y, t) + \eta^{(2)}(x, y, t) + \dots \quad (2.10)$$

where  $\eta^{(i)}$  and  $\phi^{(i)}$  (where  $i=1,2$ ) is proportional to  $\varepsilon^i$  or  $O(\varepsilon^i)$ . By substituting the perturbation expansions for  $\phi$  and  $\eta$  into the Laplace equation (Eq. 2.3) and the bottom boundary condition (Eq. 2.4), we obtain two separate boundary conditions as follows:

$$\nabla^2 \phi^{(1)} = 0; \quad \nabla^2 \phi^{(2)} = 0 \quad (2.11)$$

$$\left. \frac{\partial \phi^{(1)}}{\partial z} \right|_{z=-h} = 0; \quad \left. \frac{\partial \phi^{(2)}}{\partial z} \right|_{z=-h} = 0 \quad (2.12)$$

We also have:

$$\frac{\partial^2 \phi^{(1)}}{\partial t^2} + g \frac{\partial \phi^{(1)}}{\partial z} = 0 \quad (2.13)$$

$$\frac{\partial^2 \phi^{(2)}}{\partial t^2} + g \frac{\partial \phi^{(2)}}{\partial z} = -\frac{\partial}{\partial t} |\nabla \phi^{(2)}|^2 - \eta^{(1)} \frac{\partial}{\partial t} \left[ \frac{\partial^2 \phi^{(1)}}{\partial t^2} + g \frac{\partial \phi^{(1)}}{\partial z} \right] \quad (2.14)$$

$$\eta^{(1)} = -\frac{1}{g} \frac{\partial \phi^{(1)}}{\partial t} \quad (2.15)$$

$$\eta^{(2)} = -\frac{1}{g} \left( \frac{\partial \phi^{(2)}}{\partial t} + \frac{1}{2} |\nabla \phi^{(1)}|^2 \right) - \frac{1}{g} \eta^{(1)} \frac{\partial^2 \phi^{(1)}}{\partial z \partial t} \quad (2.16)$$

where  $z = 0$ .

#### • First-Order Solution

We select a first-order velocity potential,  $\phi^{(1)}$  of the following form which satisfies 2.11, 2.12, and 2.13:

$$\phi^{(1)}(\vec{x}, z, t) = (-1) \sum_{i=1}^N \sum_{m=1}^M \frac{g}{\omega_i} a_{im} \frac{\cosh[|\vec{k}_i|(h+z)]}{\cosh(|\vec{k}_i|h)} \cdot \sin(\omega_i t - \vec{k}_{im} \cdot \vec{x} + \epsilon_{im}) \quad (2.17)$$

$$\Rightarrow \phi^{(1)}(\vec{x}, z, t) = \text{Re} \left[ \sum_{i=1}^N \sum_{m=1}^M \iota \frac{g}{\omega_i} A_{im} \frac{\cosh[|\vec{k}_i|(h+z)]}{\cosh(|\vec{k}_{im}h)} \cdot \exp(\iota \omega_i t) \cdot \exp(-\iota (\vec{k}_{im} \cdot \vec{x})) \right] \quad (2.18)$$

where  $A_{im} = a_{im} \exp(-\iota \epsilon_{im})$ ;  $\vec{x} = (x, y)$  is a point on the horizontal  $x$ - $y$  plane;  $\omega_i$  is the angular frequency;  $\vec{k}_i$  is the wave number which is related to the frequency,  $\omega_i$ , through the linear dispersion relation,  $\omega_i^2 = g |\vec{k}_i| \tanh(|\vec{k}_i|h)$  (where  $h$  is the water depth);  $\iota = \sqrt{-1}$  and  $\vec{k}_{im} = (|\vec{k}_i| \cos \theta_m, |\vec{k}_i| \sin \theta_m)$ ;  $N$  and  $M$  are the total number of frequencies and the total number of wave directions considered, respectively. Also,  $a_{im}$  refers to the component spectral amplitudes, which are calculated as follows:

$$E \left[ \frac{a_{im}^2}{2} \right] = S(\omega_i, \theta_m) \Delta \omega \Delta \theta \quad (2.19)$$

where,  $E[\bullet]$  is the expected value of  $\bullet$ .

By substituting Eq. 2.17 into Eq. 2.15, we obtain the first-order component of the surface wave elevation,  $\eta^{(1)}$ , as follows:

$$\eta^{(1)}(\vec{x}, t) = \sum_{i=1}^N \sum_{m=1}^M a_{im} \cos(\omega_i t - \vec{k}_{im} \cdot \vec{x} + \epsilon_{im}) \quad (2.20)$$

$$\Rightarrow \eta^{(1)}(\vec{x}, t) = \text{Re} \left[ \sum_{i=1}^N \sum_{m=1}^M A_{im} \cdot \exp(i\omega_i t) \cdot \exp(-i(\vec{k}_{im} \cdot \vec{x})) \right] \quad (2.21)$$

• **Second-Order Solution**

Second-order waves are obtained as a result of sum and difference interactions between pairs of frequencies and the phases of the second-order contributions are determined by the sum and difference interactions of the phases of the first-order component phases, which are random. The second-order velocity potential which satisfies Eqs. 2.11, 2.12, and 2.14 is given as follows:

$$\phi^{(2)}(\vec{x}, z, t) = (-1) \cdot \sum_{i,j=1}^N \sum_{m,n=1}^M a_{im} a_{jn} \cdot B_{ijmn}^{\pm} \cdot \sin((\omega_i \pm \omega_j)t - (\vec{k}_{im} \cdot \vec{x} \pm \vec{k}_{jn} \cdot \vec{x}) + (\epsilon_{im} \pm \epsilon_{jn})) \quad (2.22)$$

$$\Rightarrow \phi^{(2)}(\vec{x}, z, t) = \text{Re} \left[ \sum_{i,j=1}^N \sum_{m,n=1}^M i A_{im} A_{jn} \cdot B_{ijmn}^{\pm} \cdot \exp(i(\omega_i \pm \omega_j)t) \cdot \exp(-i(\vec{k}_{im} \cdot \vec{x} \pm \vec{k}_{jn} \cdot \vec{x})) \right] \quad (2.23)$$

By employing the first-order potential,  $\phi^{(1)}$ , the first-order surface elevation,  $\eta^{(1)}$ , and the second-order potential,  $\phi^{(2)}$ , in Eq. 2.16, we obtain a second-order correction to the linear sea surface elevation as follows:

$$\eta^{(2)}(\vec{x}, t) = \sum_{i,j=1}^N \sum_{m,n=1}^M a_{im} a_{jn} \cdot K_{ijmn}^{\pm} \cdot \cos((\omega_i \pm \omega_j)t - (\vec{k}_{im} \cdot \vec{x} \pm \vec{k}_{jn} \cdot \vec{x}) + (\epsilon_{im} \pm \epsilon_{jn})) \quad (2.24)$$

$$\Rightarrow \eta^{(2)}(\vec{x}, t) = \text{Re} \left[ \sum_{i,j=1}^N \sum_{m,n=1}^M A_{im} A_{jn} \cdot K_{ijmn}^{\pm} \cdot \exp(i(\omega_i \pm \omega_j)t) \cdot \exp(-i(\vec{k}_{im} \cdot \vec{x} \pm \vec{k}_{jn} \cdot \vec{x})) \right] \quad (2.25)$$

Quadratic transfer functions (QTF),  $K_{ijmn}^{\pm}$  and  $B_{ijmn}^{\pm}$ , derived by Sharma and Dean [1] are given as follows:

$$K_{ijmn}^{\pm} = \frac{1}{4} \left[ \frac{D_{ijmn}^{\pm} - (k_i k_j \cos(\theta_m - \theta_n) \mp R_i R_j)}{\sqrt{R_i R_j}} + (R_i + R_j) \right] \quad (2.26)$$

$$B_{ijmn}^{\pm} = \frac{1}{4} \frac{\cos[k_{ijmn}^{\pm}(h+z)]}{\cos[k_{ijmn}^{\pm}(h)]} \frac{D_{ijmn}^{\pm}}{\omega_i \pm \omega_j} \quad (2.27)$$

where

$$R_i = |\vec{k}_i| \tanh(|\vec{k}_i| h) \quad (2.28)$$

$$D_{ijmn}^{\pm} = \frac{(\sqrt{R_i} \pm \sqrt{R_j})[\sqrt{R_j}(k_i^2 - R_i^2) \pm \sqrt{R_i}(k_j^2 - R_j^2)]}{[(\sqrt{R_i} \pm \sqrt{R_j})^2 - k_{ijmn}^{\pm} \tanh(k_{ijmn}^{\pm} h)]} + \frac{[2(\sqrt{R_i} \pm \sqrt{R_j})^2][k_i k_j \cos(\theta_m - \theta_n) \mp R_i R_j]}{[(\sqrt{R_i} \pm \sqrt{R_j})^2 - k_{ijmn}^{\pm} \tanh(k_{ijmn}^{\pm} h)]} \quad (2.29)$$

In the above,  $k_{ijmn}^+$  and  $k_{ijmn}^-$  are given as follows :

$$k_{ijmn}^+ = \sqrt{k_i^2 + k_j^2 + 2k_i k_j \cos(\theta_m - \theta_n)} \quad (2.30)$$

$$k_{ijmn}^- = \sqrt{k_i^2 + k_j^2 - 2k_i k_j \cos(\theta_m - \theta_n)}$$

For infinite water depth, the equations proposed by Sharma and Dean [1] reduce to those derived by Longuet-Higgins et al. [2] for deep water. Also, for  $\vec{k}_i = \vec{k}_j$  and  $N = 1$ , the formulas for the velocity potential and surface elevation reduce to the familiar Stokes second-order equations [4].

#### • *Validity of Second-Order Wave Theory*

While the second-order irregular wave modeling outlined above is a more accurate representation of irregular seas in shallow waters compared to the linear irregular wave model, it obviously does not model the complete nonlinear characteristics of ocean waves and is not valid for all cases. The physical parameter that determines the range of validity is the wave steepness. When the wave steepness exceeds a certain value, the second-order model is no longer valid and a higher-order model is then required. In fact, when waves become too steep, they can break and no model based on solution of Laplace's equation (given in terms of velocity potential) is valid.

### 2.2.2 *Second-order wave kinematics*

Second-order wave kinematics are evaluated using the wave velocity potentials presented in Sec. 2.2.1.2. It is assumed that the considered fluid is incompressible, inviscid, and irrotational.

#### 2.2.2.1 *Water particle velocity*

The velocity field of the irrotational fluid can be expressed as follows:

$$\vec{u} = \nabla \phi \quad (2.31)$$

$$\vec{u}^{(1)} = (u_x^{(1)}, u_y^{(1)}, u_z^{(1)}) = \nabla \phi^{(1)} = \left( \frac{\partial \phi^{(1)}}{\partial x}, \frac{\partial \phi^{(1)}}{\partial y}, \frac{\partial \phi^{(1)}}{\partial z} \right) \quad (2.32)$$

$$\vec{u}^{(2)} = (u_x^{(2)}, u_y^{(2)}, u_z^{(2)}) = \nabla \phi^{(2)} = \left( \frac{\partial \phi^{(2)}}{\partial x}, \frac{\partial \phi^{(2)}}{\partial y}, \frac{\partial \phi^{(2)}}{\partial z} \right) \quad (2.33)$$



### 2.2.2.2 Water particle acceleration

The acceleration of a water particle can be evaluated by the material or substantial derivative of the velocity vector,  $\vec{u}$ :

$$\frac{D}{Dt} \vec{u} = \underbrace{\frac{\partial \vec{u}}{\partial t}}_{Term 1} + \underbrace{\vec{u} \cdot \nabla \vec{u}}_{Term 2} \quad (2.34)$$

where *Term 1* and *Term 2* are the local acceleration at a fixed point and the convective acceleration, respectively. We are only interested in the acceleration at a fixed point, which is evaluated as follows:

$$\vec{a}^{(1)} = (a_x^{(1)}, a_y^{(1)}, a_z^{(1)}) = \frac{\partial \vec{u}^{(1)}}{\partial t} = \left( \frac{\partial u_x^{(1)}}{\partial t}, \frac{\partial u_y^{(1)}}{\partial t}, \frac{\partial u_z^{(1)}}{\partial t} \right) \quad (2.35)$$

$$\vec{a}^{(2)} = (a_x^{(2)}, a_y^{(2)}, a_z^{(2)}) = \frac{\partial \vec{u}^{(2)}}{\partial t} = \left( \frac{\partial u_x^{(2)}}{\partial t}, \frac{\partial u_y^{(2)}}{\partial t}, \frac{\partial u_z^{(2)}}{\partial t} \right) \quad (2.36)$$

### 2.2.2.3 Dynamic pressure

To obtain the first- and second-order pressure, we substitute the perturbation expansions of the velocity potential into Bernoulli's equation (Eq. 2.6) and separate terms of the same order:

$$\frac{p}{\rho} + gz + \frac{\partial}{\partial t} (\phi^{(1)} + \phi^{(2)} + \dots) + \frac{1}{2} \nabla (\phi^{(1)} + \phi^{(2)} + \dots) \cdot \nabla (\phi^{(1)} + \phi^{(2)} + \dots) = -Q \quad (2.37)$$

$$\frac{p}{\rho} = -gz - Q + \underbrace{\left[ \frac{\partial \phi^{(1)}}{\partial t} \right]}_{O(\varepsilon)} + \underbrace{\left[ \frac{\partial \phi^{(2)}}{\partial t} + \frac{1}{2} \nabla \phi^{(1)} \cdot \nabla \phi^{(1)} \right]}_{O(\varepsilon^2)} + O(\varepsilon^3) + \dots \quad (2.38)$$

Thus, the first- and second-order dynamic pressures,  $p_d^{(1)}$  and  $p_d^{(2)}$ , are obtained as follows [5] [6]:

$$p_d^{(1)} = -\rho \frac{\partial \phi^{(1)}}{\partial t} \quad (2.39)$$

$$p_d^{(2)} = -\rho \left[ \frac{\partial \phi^{(2)}}{\partial t} + \frac{1}{2} \nabla \phi^{(1)} \cdot \nabla \phi^{(1)} \right] = \underbrace{-\rho \left[ \frac{\partial \phi^{(2)}}{\partial t} \right]}_{Term 1} - \underbrace{\rho \left[ \frac{1}{2} \vec{u}^{(1)} \cdot \vec{u}^{(1)} \right]}_{Term 2} \quad (2.40)$$

where *Term 1* and *Term 2* are the second-order potential term and the quadratic interaction term, respectively. The second-order dynamic pressure in this study is evaluated by only including the contribution of the second-order potential term, *Term 1*.

### 2.2.3 Numerical simulation of second-order waves

In this section, the criteria and algorithms used to numerically simulate irregular second-order wave are presented. First, we discuss the issue of validity of the second-order wave theory that was briefly raised in Sec. 2.2.1.2.

### 2.2.3.1 Limitation of Second-Order Wave Theory and Cut-Off Frequency

The solution of the second-order boundary value problem is derived based on a perturbation approach, which uses wave steepness,  $\varepsilon \ll 1$  as an expansion parameter. For a regular wave, Dean and Dalrymple [7] defined  $\varepsilon = ka/2$ , where  $k$  and  $a$  are the wavenumber and wave amplitude, respectively. According to them, the second-order wave theory is valid if two criteria are fulfilled:

- **Convergence:** First, the ratio of the second-order term to the first order term in Eq. 2.9 must be much smaller than unity:

$$\frac{\varepsilon^2 \phi^{(2)}}{\varepsilon \phi^{(1)}} = \frac{ka\phi^{(2)}}{2\phi^{(1)}} \ll 1 \quad (2.41)$$

$$\Rightarrow \frac{3}{8} \frac{ka \cosh(2kh)}{\cosh(kh) \sinh^3(kh)} \ll 1 \quad (2.42)$$

- **No bump in the trough:** Second, the physical properties of the wave profile require that there is no bump in the trough. This is indicated by a negative second derivative of the wave trough, which leads to the criterion:

$$ka < \frac{\sinh^3(kh)}{\cosh(kh)[2 + \cosh(2kh)]} \quad (2.43)$$

In addition to the above two criteria, the breaking criterion for the wave steepness must be fulfilled. For arbitrary water depth, the Miche breaking criterion is as follows [8]:

$$\frac{H}{L} = \frac{2a}{2\pi/k} < 0.142 \tanh(kh) \quad (2.44)$$

$$\Rightarrow ka < 0.142\pi \tanh(kh) \quad (2.45)$$

Figure 2.3 illustrates the different limiting criteria expressed for  $ka$  as a function of  $kh$ . The shaded region in Fig. 2.3 represents wave steepness conditions for which second-order wave theory is valid. According to the figure, we note (except when  $kh \rightarrow 0$ ) that:

- when  $kh < 0.62\pi$ , the maximum wave steepness is restricted by the “no bump in the trough” criterion in Eq. 2.43.
- when  $kh > 0.62\pi$ , the maximum wave steepness is restricted by the breaking wave criterion in Eq. 2.45.

In the regular wave case, the validity of the second-order wave theory can be controlled by simply limiting the considered maximum wavenumber in order to satisfy the three criteria (see Eqs. 2.42, 2.43, and 2.45). However, because these criteria were derived for regular waves, they may not be directly extended for use with irregular wave. The following three criteria can be used to arrive at the maximum wave frequency for valid application of the second-order wave theory:

- **Hu and Zhao [9]:** Based on results from numerical simulations, Hu and Zhao [9] suggested that the second-order wave model presented here is valid as long as  $H_s/L_z$  is less than approximately 0.08, where  $H_s$  is the significant wave height and  $L_z$  is the wavelength corresponding to the zero-crossing frequency,  $\omega_z = \sqrt{\gamma_2/\gamma_0}$ , where  $\gamma_n$  is given by

$$\gamma_n = \int \omega^n S(\omega) d\omega \quad (2.46)$$

- **Stansberg [10]:** Stansberg [10] proposed a useful criterion to establish the highest frequency for which second-order wave theory may be considered valid. It is given in terms of a cut-off wavenumber as follows:

$$k_{cut} = \frac{2}{E(a_{max})[1 + 1/2(k_p E(a_{max}))]} \quad (2.47)$$

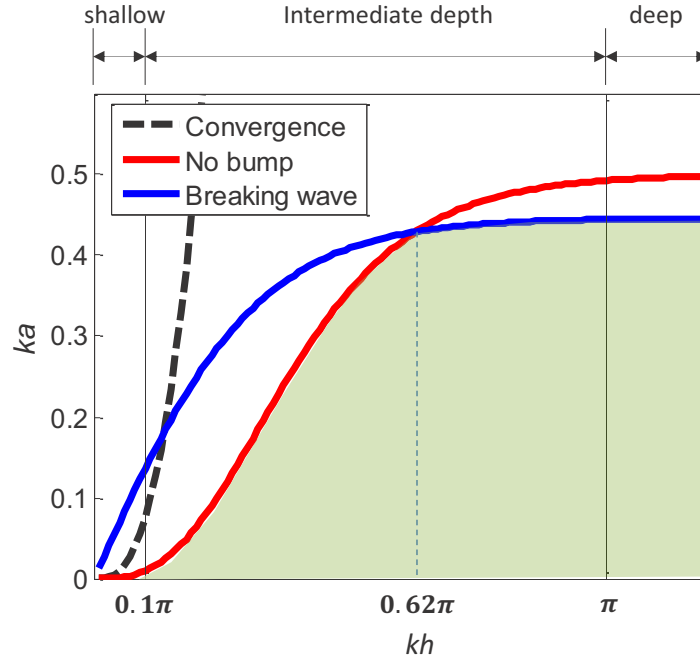


**Figure 2.3. Different limiting criteria for wave steepness,  $ka$ , as a function of normalized water depth,  $kh$ , for second-order waves**

where  $k_{cut}$  is related to the limiting (cut-off) frequency,  $\omega_{cut}$ , through the linear dispersion relation and  $k_p$  is the wavenumber corresponding to the spectral peak period,  $T_p$ ;  $E(a_{max})$  is the expected value of the extreme wave amplitude of a Gaussian wave record, which follows a Rayleigh distribution. The denominator in Eq. 2.47 is a simplified second-order correction for a non-Gaussian wave field. According to extreme value theory,  $E(a_{max})$  is given as follows:

$$E(a_{max}) = \frac{H_s}{4} \left[ \sqrt{2 \ln(N_z)} + \frac{\gamma_{em}}{\sqrt{2 \ln(N_z)}} \right] \quad (2.48)$$

$$N_z = \frac{t_{max}}{T_z} \quad (2.49)$$

where  $\gamma_{em} = 0.577\dots$  is the Euler-Mascheroni constant;  $N_z$  is the number of zero-upcrossing wave cycles and  $t_{max}$  is the duration of the simulation.

- **DNV-RP-C205 [11]:** DNV-RP-C205 [11] guidelines provide a simpler criterion for the application of second-order wave theory by defining a limiting cut-off frequency as follows:

$$\omega_{cut} = \sqrt{\frac{2g}{H_s}} \quad (2.50)$$

For irregular waves, the validity of the use of second-order wave theory is significantly affected by the spectral or statistical properties of the considered irregular waves such as the peak wave period ( $T_p$ ), the significant wave height ( $H_s$ ), and the duration of the simulations ( $t_{max}$ ), which influence the limiting criteria. During a numerical simulation of the second-order wave kinematics, therefore, the maximum wave frequency arbitrarily assigned without considering the spectral properties of the irregular waves may result in the generation of physically incorrect

second-order wave kinematics. In this study, the criterion proposed by Stansberg [10] is employed to simulate the second-order sea surface elevation and associated wave kinematics.

### 2.2.3.2 Sampling Theorem and Additional Requirement of Cut-Off Frequency, $\omega_{cut}$

In digital simulation of the sea surface elevation and associated kinematics, we replace continuous time,  $t$ , by a discrete time array,  $t_p = p\Delta t$ , where  $\Delta t = t_{max}/N_t$ , such that  $p = 1, 2, \dots, N_t$ . By virtue of the periodicity of Fourier series, we have

$$\Delta\omega = \frac{2\pi}{t_{max}} \quad (2.51)$$

Consideration of the Nyquist frequency provides a prescription for the nominal sampling interval required to avoid aliasing. This may be stated simply as follows:

- The sampling frequency,  $\omega_s = 2\pi/\Delta t$ , should be at least twice the highest frequency contained in the signal.

In mathematical terms, we have:

$$\omega_s \geq 2\omega_{cut} \quad (2.52)$$

If  $\omega_{cut} = N_\omega\Delta\omega$ , we must then satisfy the following inequality:

$$\left[ \omega_s = \frac{2\pi}{\Delta t} = \frac{2\pi}{t_{max}/N_t} \right] \geq \left[ 2\omega_{cut} = 2N_\omega\Delta\omega = 2N_\omega \frac{2\pi}{t_{max}} \right] \quad (2.53)$$

$$\Rightarrow N_t \geq 2N_\omega \quad (2.54)$$

In the numerical simulation of second-order wave kinematics, the largest frequency of wave components generated by the second-order wave-wave interaction is  $2N_\omega\Delta\omega$ , which is associated with the sum-frequency interaction. Therefore, to satisfy the sampling theorem for second-order wave simulation, we must ensure that:

$$N_t \geq 4N_\omega \quad (2.55)$$

This simply means that the cut-off frequency,  $\omega_{cut}$ , evaluated by the criterion presented in Sec. 2.2.3.1 must satisfy:

$$\left[ N_t = \frac{t_{max}}{\Delta t} \right] \geq \left[ 4N_\omega = 4 \frac{\omega_{cut}}{\Delta\omega} = 4 \frac{\omega_{cut}}{2\pi/t_{max}} \right] \quad (2.56)$$

$$\Rightarrow \omega_{cut} \leq \frac{\pi}{2\Delta t} \quad (2.57)$$

### 2.2.3.3 Singularity of Quadratic Transfer Function (QTF)

Formulations for the first- and second-order wave kinematics shown in previous sections are determined from the solution of the boundary value problem (see Eqs. 2.3 - 2.8). When we implement these formulations to numerically simulate wave kinematics, some problems arise that stem from the physically correct or weakly-correct assumptions considered in solution of the boundary value problem. One of the issues has to do with the singularity of the first- and second-order wave kinematics transfer functions. This singularity problem is also seen in QTFs proposed by other researchers (Longuet-Higgins [2]; Marthinsen and Winterstein [12]; Nwogu [13]) presented below.

#### QTF proposed by Longuet-Higgins [2]

$$B_{ij}^\pm = \frac{g^2}{\omega_i\omega_j} \frac{(\omega_i \pm \omega_j)(\vec{k}_i \cdot \vec{k}_j \mp |\vec{k}_i||\vec{k}_j|)}{(\omega_i \pm \omega_j)^2 - g|\vec{k}_i \pm \vec{k}_j|} \quad (2.58)$$

**QTF used by Marthinsen and Winterstein [12]**

$$B_{ij}^{\pm} = (1 - \delta_{i,j}) \frac{g^2}{\omega_i \omega_j} \frac{\frac{g^2 |\vec{k}_i| |\vec{k}_j|}{2\omega_i \omega_j} - \frac{1}{4}(\omega_i^2 + \omega_j^2 \pm \omega_i \omega_j) + \frac{g^2}{4} \frac{\omega_i |\vec{k}_j|^2 \pm \omega_j |\vec{k}_i|^2}{\omega_i \omega_j (\omega_i \pm \omega_j)}}{(\omega_i \pm \omega_j) - g \frac{|\vec{k}_i| \pm |\vec{k}_j|}{\omega_i \pm \omega_j} \tanh[(|\vec{k}_i| \pm |\vec{k}_j|)h]} \quad (2.59)$$

where  $\delta_{i,j} = 1$  if  $i = j$  and zero otherwise. This is introduced to avoid the singularity of  $B_{ij}^{\pm}$ .

**QTF proposed by Nwogu [13]**

$$K_{ij}^{\pm} = \frac{\omega_i \omega_j (k_{ij}^{\pm} h)^2 \cos(\theta_i - \theta_j) [1 - (\alpha + 1/3)(k_{ij}^{\pm} h)^2]}{2\lambda k_i' k_j' h^3} + \frac{\omega_{ij}^{\pm} [1 - \alpha(k_{ij}^{\pm} h)^2] [\omega_i k_j' h (|\vec{k}_i| h \pm |\vec{k}_j| h \cos(\theta_i - \theta_j))]}{2\lambda k_i' k_j' h^3} + \frac{\omega_j k_i' h (|\vec{k}_i| h \cos(\theta_i - \theta_j) \pm |\vec{k}_j| h)}{2\lambda k_i' k_j' h^3} \quad (2.60)$$

$$\lambda = (\omega_{ij}^{\pm})^2 [1 - \alpha(k_{ij}^{\pm} h)^2] - g(k_{ij}^{\pm})^2 h [1 - (\alpha + 1/3)(k_{ij}^{\pm} h)^2] \quad (2.61)$$

$$k_i' = |\vec{k}_i| [1 - (\alpha + 1/3)(|\vec{k}_i| h)^2] \quad (2.62)$$

where  $\alpha = (z_{\alpha}/h)^2/2 + (z_{\alpha}/h)$  and  $z_{\alpha} \approx -0.53h$  from shallow water depths up to the deep water depth limit.

• **Singularity at  $\omega = 0$**

When  $\omega_i$  in Eq. 2.17 approaches zero, the denominator of the equation approaches zero. Although the numerator also approaches zero, we may have computational difficulties and special treatment may be required during numerical simulation of the kinematics depending on the software tool used. To avoid discontinuity or singularity problems at zero frequency, one can simply set the kinematics equal to zero there and not attempt evaluation.

QTFs of the second-order wave elevation and the velocity potential, i.e.,  $K_{ijmn}^{\pm}$  and  $B_{ijmn}^{\pm}$ , also have similar singularity issues at zero frequency. As shown in Eq. 2.26, the denominator of the first term in the expression for  $K_{ijmn}^{\pm}$  is  $\sqrt{R_i R_j}$ , which approaches zero when either  $\omega_i$  or  $\omega_j$  approaches zero.

In the numerator of the expression for  $B_{ijmn}^{\pm}$  in Eq. 2.27, the term,  $D_{ijmn}^{\pm}$ , appears that is defined in Eq. 2.29. The numerator in both the first and second terms in the expression for  $D_{ijmn}^{\pm}$  approaches zero when either  $\omega_i$  or  $\omega_j$  goes to zero. In this case, there is no need for any special treatment during numerical simulation because the denominator of  $B_{ijmn}^{\pm}$  is not zero unless  $\omega_i = \omega_j = 0$ .

Based on the possibility of singularities in the first- and second-order transfer functions, we assume that the formulations presented in Sec. 2.2.1.2 are not used to evaluate first- and second-order wave kinematics when  $\omega_i = 0$  or  $\omega_j = 0$ . This assumption is physically acceptable because we are assuming that a zero-frequency regular wave does not have any wave energy and that the zero-energy wave component does not interact with any other wave components.

• **Singularity at diagonal components of  $K_{ijmn}^-$  and  $B_{ijmn}^-$**

Another singularity to be considered during numerical simulation results from the discontinuity in the diagonal component of  $K_{ijmn}^-$  and  $B_{ijmn}^-$ . When  $\omega_i = \omega_j$ , the denominator terms for  $D_{ijmn}^-$  are equal to zero, which makes  $K_{ijmn}^-$  and  $B_{ijmn}^-$  singular along the diagonal components. Physically, the interaction between two wave components propagating in opposite directions with same magnitude results in total energy loss. This can be explained by studying Fig. 2.4, which shows how two wave components interact. As shown in the figure, two free wave components,  $\vec{k}_i$

and  $\vec{k}_j$ , generate new bounded wave components,  $\vec{k}_i + \vec{k}_j$  and  $\vec{k}_i - \vec{k}_j$ , by sum and difference interactions, respectively. Therefore, unlike difference-interaction QTFs for second-order wave (hydrodynamic) forces, in the case of kinematics, all diagonal components of  $K_{ijmn}^-$  and  $B_{ijmn}^-$  should be set to zero; this only means that total energy loss results from the interaction of two wave components with the same magnitude and opposite propagation directions, i.e.,  $\vec{k}_i - \vec{k}_i$ .

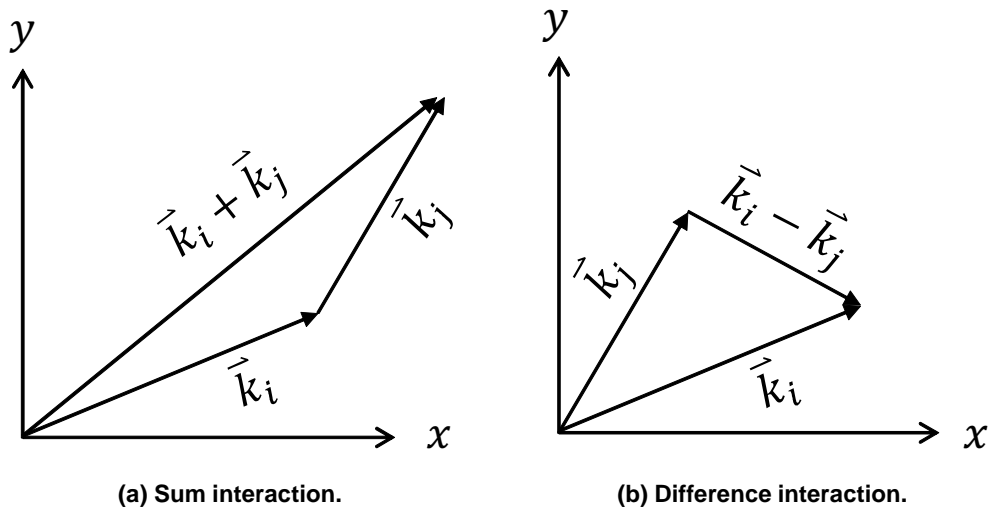


Figure 2.4. Sum and difference interaction of wavenumber vectors

### 2.2.3.4 Inverse Fast Fourier Transform

Agarwal and Manuel [14] discuss the numerical simulation of uni-directional second-order waves in detail. It involves a single sum of component harmonics that can be efficiently computed using the Inverse Fast Fourier Transform (IFFT). On the other hand, simulation of directional irregular second-order waves involves a double sum, which can be computationally expensive. The procedure presented by Agarwal and Manuel [14] made it possible to rewrite the double summation as a single summation by appropriately re-assembling and rewriting indices (or coefficients) of terms involved. Once the indices for an equivalent single summation are assembled, a one-dimensional IFFT procedure, similar to that for linear waves, can be used to carry out the nonlinear (second-order) wave simulations efficiently. We extend this same procedure to the numerical simulation of irregular directional second-order waves. A flowchart for calculation of directional second-order wave kinematics and resulting hydrodynamic loads is presented in Fig. 2.5. This calculation procedure is incorporated into the open-source software, FAST, for coupled aero-servo-hydro-elastic analysis of offshore wind turbines.

## 2.3 Hurricane Winds

UMCM provides mean wind field data corresponding to 10 meters above the mean surface level generated at a 1.3 km grid resolution. This large-scale mean wind field data must be down-scaled using a scale-bridging procedure to provide the needed wind field at about a 10 m resolution around the rotor to allow meaningful aerodynamic load computations. In this study, the turbulent wind fields are simulated using a spectral method based on characteristics of the surface wind field obtained from UMCM; these characteristics consist of the sustained 1-minute surface wind speeds,  $U_{1min}$ , the mean wind direction, the surface drag coefficient,  $C_D$ , and the surface stress,  $\tau$ .

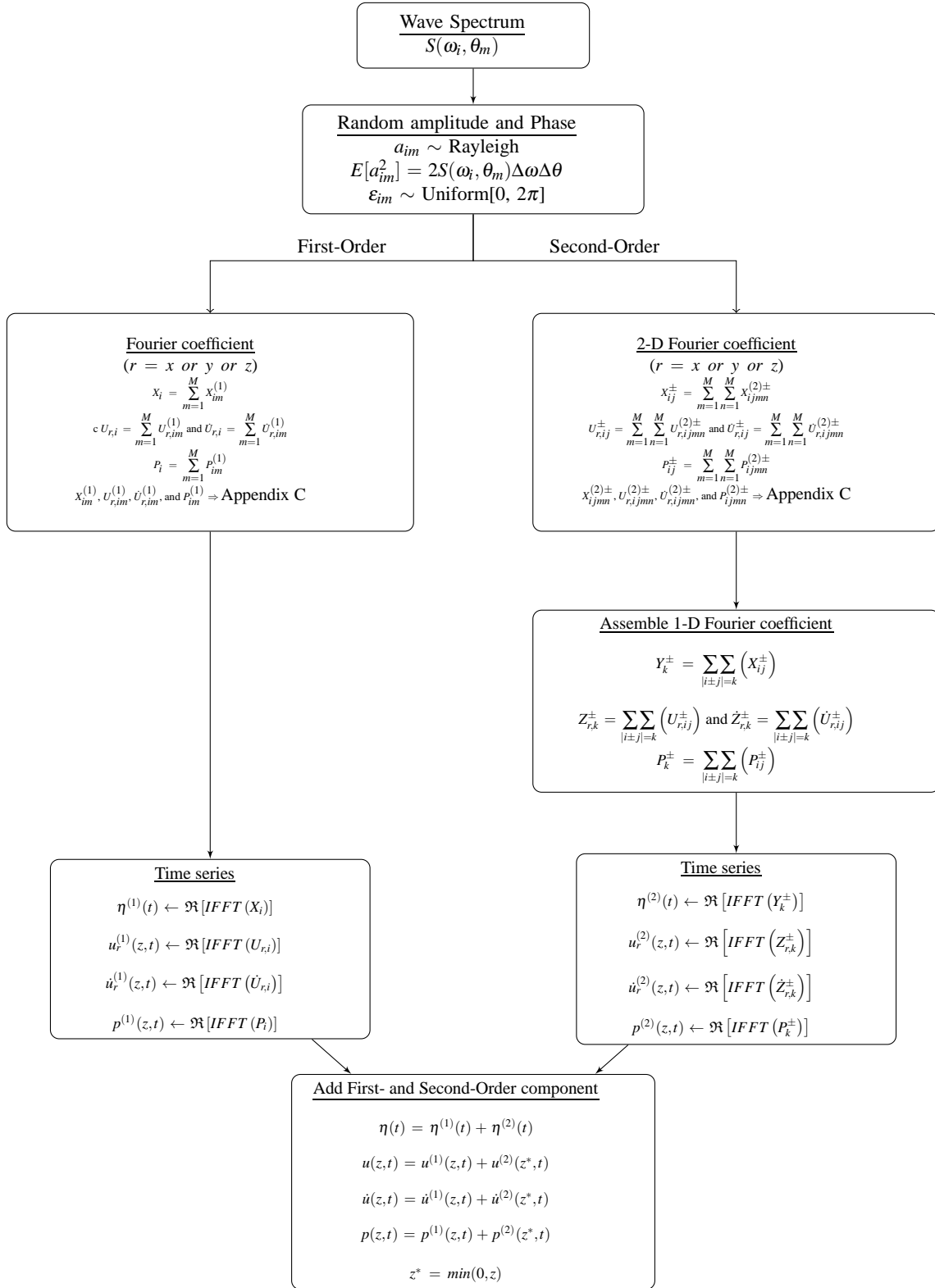


**Figure 2.5. Flowchart for the numerical simulation of second-order directional waves**

### 2.3.1 Mean wind field

We are interested in simulations of 1-hour duration for turbine response statistics; for this, we desire information on the 1-hour mean wind speed at hub height of the turbine. This requires conversion from 1-minute to 1-hour averaging in time as well as adjustment of 10 m winds to elevations corresponding to the rotor swept area of the turbine. In a World Meteorological Organization (WMO) report by Harper et al. [15], conversion factors are recommended for relating the WMO standard 10-minute average wind speed to 1-minute, 2-minute, and 3-minute “sustained” winds in tropical cyclone conditions. The report indicates that an at-sea conversion factor between the 1-minute sustained wind speed and the 10-minute average wind speed should be 0.93, rather than the traditional value of 0.88, which is shown to be associated more with an off-land exposure. Accordingly, this conversion factor of 0.93 is used to estimate the 10-minute mean wind speed from the 1-minute sustained wind speed. Since there is not enough published data to obtain an estimate of the 1-hour mean wind speed from the 1-minute or the 10-minute wind speed, we assume that the 1-hour mean wind speed (needed for this study) is the same as the 10-minute wind speed, without applying any additional conversion factor. Bryan and Rotunno [16] showed that the grid size used in hurricane wind field simulation can significantly affect the wind speed averaged over the grid. Although the mean wind velocity fields from UMCM are generated for a coarse 1.3 km grid resolution, we interpolate these mean wind fields over a finer grid (10 m × 10 m) over the wind turbine rotor swept area, which is used for the dynamic analysis of the selected offshore wind turbine in this study.

Among various approaches adopted to describe the variation of wind speed with elevation in the atmospheric boundary layer, Panofsky and Dutton [17] proposed a form for the vertical wind speed profile that includes a stability term,  $\Psi_m$ , from planetary boundary layer theory, as follows:

$$U_{10min}(z) = \frac{u_*}{\kappa} \left[ \ln\left(\frac{z}{z_0}\right) - \Psi_m \right] \quad (2.63)$$

where  $u_*$  is the friction velocity, equal to  $\sqrt{\tau/\rho_a}$  (where  $\tau$  = wind stress on the ocean surface and  $\rho_a$  = air density),  $\kappa$  is the von Kármán constant, and  $z_0$  is the surface roughness length. Powell et al. [18] showed that logarithmic mean wind profiles apply in tropical cyclones at least in the lowest 200 m and then the profile levels off slightly with a peak near 500 m. Also, Hsu [19] has shown that, during a hurricane, the effect of stability in Eq. 2.63 is negligible. Accordingly, in this study, we use the familiar logarithmic law wind profile to estimate surface mean wind speeds during a hurricane:

$$U_{10min}(z) = \frac{u_*}{\kappa} \ln\left(\frac{z}{z_0}\right) \quad (2.64)$$

The friction velocity,  $u_*$ , and the surface roughness length,  $z_0$ , in Eq. 2.64 were derived based on mean wind field parameters from UMCM as shown in Fig. 2.6. Because the wind stress,  $\tau$ , from UMCM takes into account the influence of wave height, the surface mean wind speeds evaluated by Eq. 2.64 and the wave heights are coupled through  $\tau$ . Vertical wind profiles are evaluated with respect to the mean surface level (MSL); variations in the MSL due to storm surge are not considered.

### 2.3.2 Turbulent wind field

The turbulence intensity is an important controlling parameter for simulating turbulent wind fields; it is dependent on the atmospheric stability and the surface roughness length. Ishizaki [20] evaluated the turbulent intensity of hurricane winds as a function of mean wind speed up to 30 m/s and found that it generally reduces with an increase in mean wind speed. On the other hand, studies by Ochi [21] showed that, for hurricane winds over 40 m/s, turbulence intensity increases slightly with increase in mean wind speed; the increase in sea surface roughness with wind speed may be one of the factors that contributes to this increase in turbulence intensity. Due to the lack of measurement data of hurricane turbulent wind fields over water, in this study, the relationship in IEC 61400-1 [22] between turbulence intensity and wind speed (for a selected wind turbine class) is employed.

The modified Kaimal model, defined in the IEC wind turbine design standard (IEC 61400-1) [22], assumes neutral atmospheric stability. The model is widely used in turbine loads studies and is presented here as the basis for



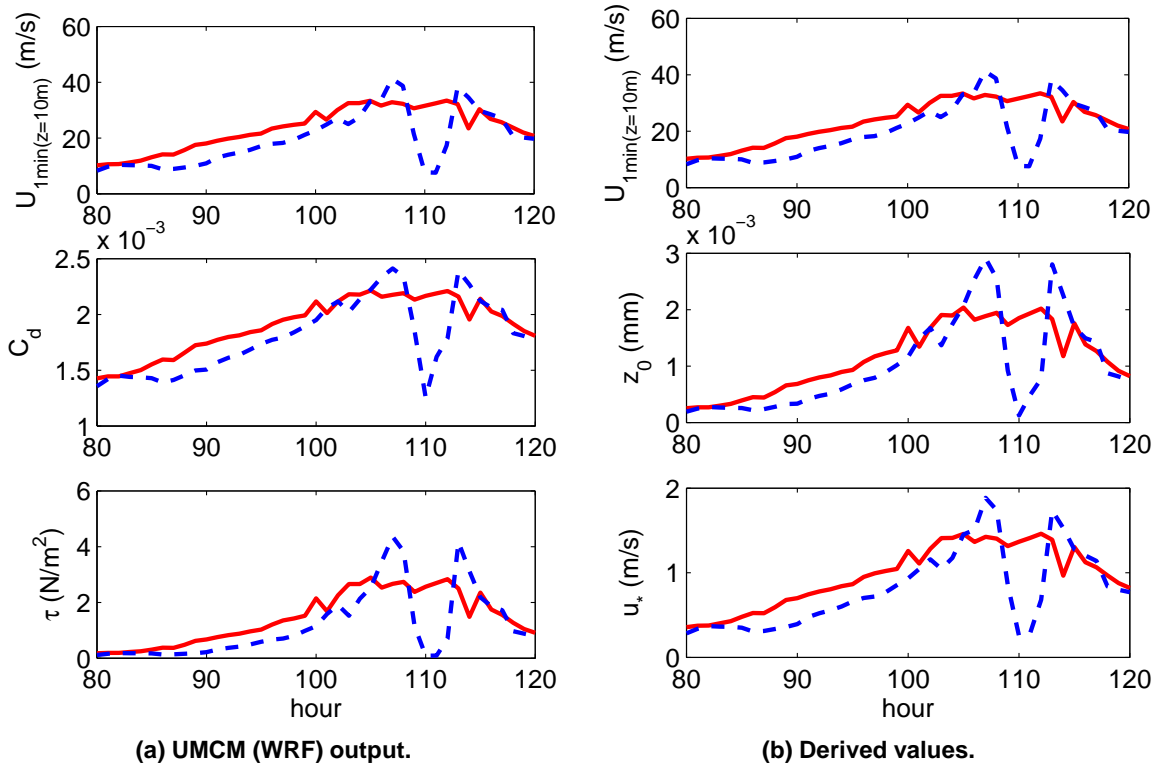


**Figure 2.6. Various mean wind field parameters from UMCM ( $U_{1min}$ ,  $C_d$ , and  $\tau$ ) and derived wind properties ( $z_0$  and  $u_*$ ); where  $U_{1min}$  =1-minute mean wind speed,  $C_d$  =drag coefficient,  $\tau$  =wind stress,  $z_0$  =surface roughness length, and  $u_*$  = friction velocity (note: the blue dashed line corresponds to Site B and the red solid line corresponds to Site A).**

turbulence modeling and, later, it is combined with a steady wind profile to define the neutrally stable boundary layer or neutral boundary layer (NBL). The power spectral density functions for any of the three turbulence components,  $K = u', v',$  or  $w'$ , are given as follows:

$$S_K(f) = \frac{4\sigma_K^2 L_K / U_{hub}}{(1 + 6fL_K / U_{hub})^{5/3}} \quad (2.65)$$

where  $S_K(f)$  (in  $(\text{m/s})^2/\text{Hz}$ ) is the one-sided power spectrum for turbulence component,  $K$ ;  $\sigma_K$  is the standard deviation of turbulence component,  $K$ ;  $f$  refers to the frequency of interest in Hertz (Hz);  $U_{hub}$  is the mean hub-height mean wind speed; and  $L_K$  is an integral length scale parameter that can be computed as follows:

$$\begin{aligned} L_{u'} &= 8.10\Lambda_U \\ L_{v'} &= 2.70\Lambda_U \\ L_{w'} &= 0.66\Lambda_U \end{aligned} \quad (2.66)$$

where  $\Lambda_U$  is a longitudinal turbulence scale parameter taken to be 42 m corresponding to a wind turbine with hub height 90 m above the mean water level [22]. The required turbulence standard deviations may be computed as follows:

$$\begin{aligned} \sigma_{u'} &= I_{ref}(0.75U_{hub} + 5.6 \text{ m/s}) \\ \sigma_{v'} &= 0.8\sigma_{u'} \\ \sigma_{w'} &= 0.5\sigma_{u'} \end{aligned} \quad (2.67)$$

where  $I_{ref}$  is the expected value of the turbulence intensity at a hub-height mean wind speed of 15 m/s. For turbulence category B (medium turbulence characteristics) in wind turbine design,  $I_{ref} = 14\%$ . The cross-power spectral density function corresponding to locations,  $i$  and  $j$ , (for any turbulence component) is defined as follows:

$$S_{ij}(f) = Coh_{ij}(f) \sqrt{S_{ii}(f)S_{jj}(f)} \quad (2.68)$$

where  $Coh_{ij}(f)$  is the coherence function. For turbulence component,  $K$ , we have:

$$K = u', v', w' : \quad Coh_{ij}^{(K)}(r, f) = \exp \left( -12 \sqrt{\left( \frac{fr}{U_{hub}} \right)^2 + \left( 0.12 \frac{r}{L_K} \right)^2} \right) \quad (2.69)$$

in which  $r$  is the separation (distance) between points  $i$  and  $j$ .

## 2.4 Turbine Response

### 2.4.1 Turbine Model

A 5-MW wind turbine model developed at NREL and representative of utility-scale offshore wind turbines being manufactured today is considered. The turbine is a variable-speed, collective pitch-controlled machine with a maximum rotor speed of 12.1 rpm; its rated wind speed is 11.5 m/s. It is assumed to have a hub height of 90 meters (above the mean sea level) and a rotor diameter of 126 meters. The turbine is assumed to be sited in 20 meters of water; it has a monopile support structure of 6-meter diameter, which is assumed to be rigidly connected at the seafloor. Fundamental frequencies for the tower fore-aft and side-to-side bending modes are around 0.32 Hz and 0.31 Hz, respectively. This turbine model with monopile foundation has been the subject of several simulation studies (see, for example, Agarwal and Manuel [23], [24]).

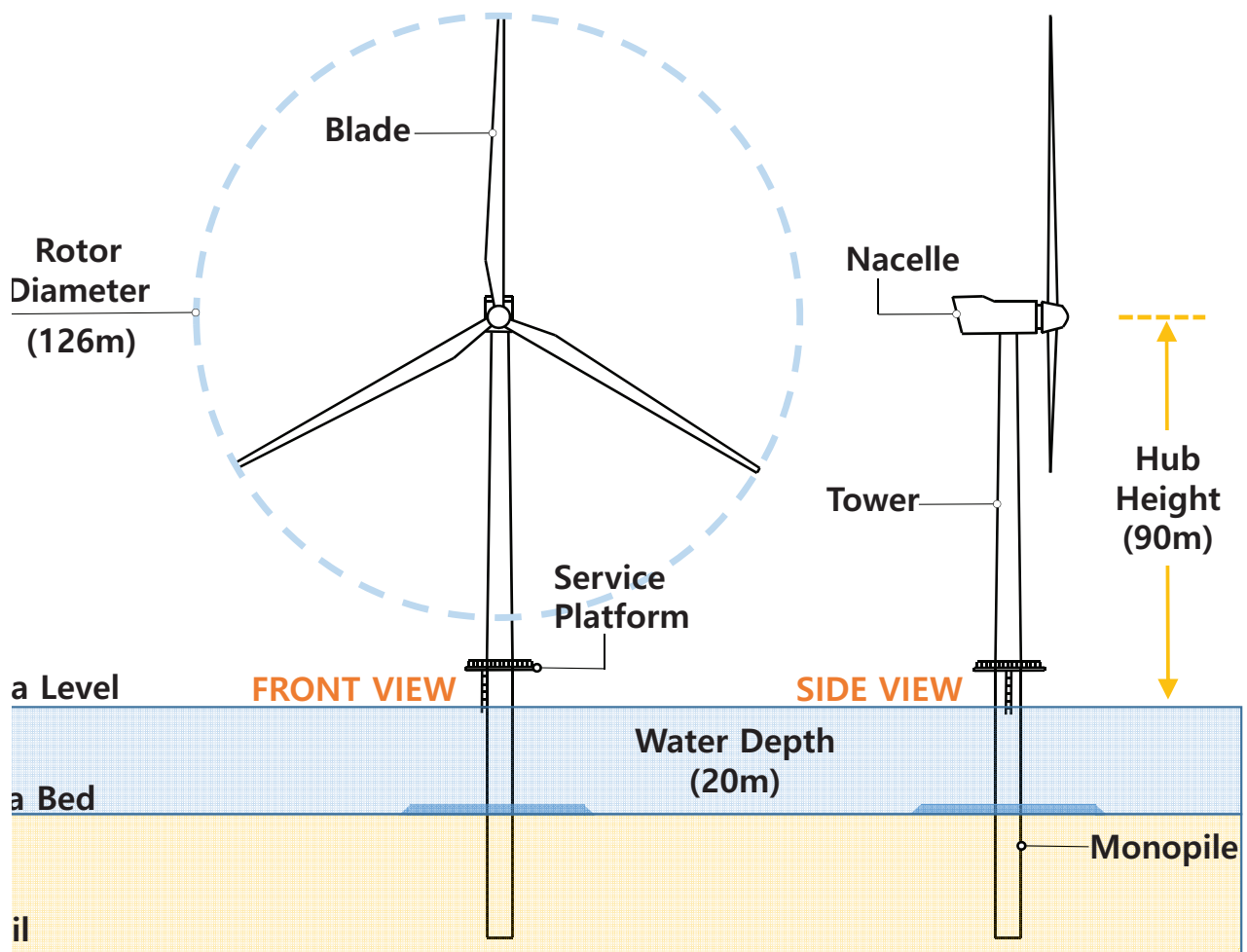
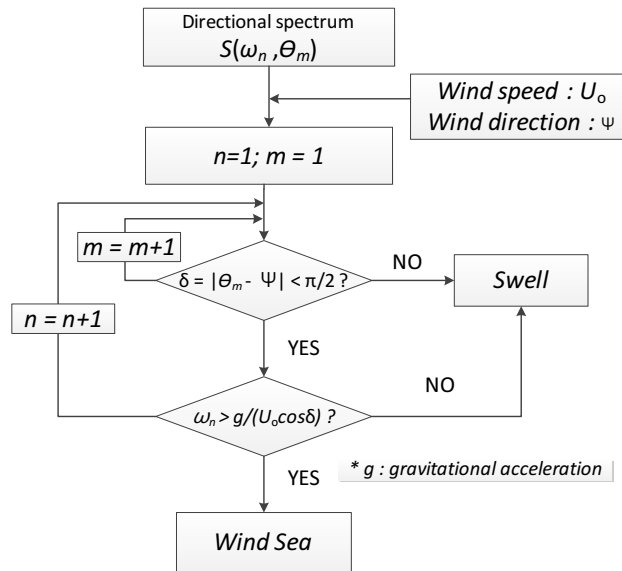


Figure 2.7. Selected 5-MW offshore wind turbine with a monopile support structure

### 2.4.2 Swell versus Wind Seas

As shown in Fig. 2.2, the hurricane directional waves are composed of swell at low frequencies and locally generated waves above approximately three times the spectral peak frequency. There is, however, no tendency for the spectrum to become bimodal in either frequency or direction. Rather, the spectra are directionally skewed, with a smooth directional transition from low frequency to high frequency [25]. Following Holthuijsen [26], wind sea waves are more irregular and short-crested, respond quickly to wind variations, and are characterized by a rather broad spectrum. On the other hand, swell consists of rather regular long-crested waves whose evolution is not as strongly affected by the wind, and its spectrum is narrower. Still, the distinction between wind sea and swell is often not obvious. Under changing winds (in both magnitude and direction) wave systems can overlap in parts of the frequency-direction domain giving rise to a rather continuous spectrum in which the presence of two or more distinct systems is not clearly discernible. Portilla et al. [27] introduced several schemes to separate a swell from a locally generated wave, which include a wind sea and swell identification scheme that uses the directional wave spectrum and available wind data (on the mean wind direction,  $\psi$ , and the mean wind speed,  $U_o$ ). If a directional wave spectrum and this wind information are available, a straightforward step to identify wind sea and swell components is to apply a definition for wind seas based on wave age [28]. The wind sea and swell identification scheme that we use is described in Fig. 2.8. According to this separation scheme, wave components that (1) propagate in wave direction,  $\theta$ , between  $\psi - \pi/2$  and  $\psi + \pi/2$  and (2) travel at a wave phase velocity,  $c_p$ , slower than  $U_o \cos(\theta_m - \psi)$  are classified as being part of a wind sea. In Fig. 2.9, the directional wave spectrum for a location on the left side of the track of Hurricane Ike (i.e., Site B), as obtained from the UMCM at 100 hours after the start of the simulation, is separated into wind sea and swell by the wave age criterion proposed by Komen et al. [28]; in this figure, the wave spectrum is normalized by a maximum wave spectrum value.



**Figure 2.8. Wind sea and swell separation procedure using wave age criterion**

Using the procedure outlined, directional wave spectra from 80 to 120 hours are separated into wind sea and swell. In Fig. 2.10, wave variances ( $\sigma_\eta^2$ ) and mean wave frequencies ( $f_m$ ) of wind sea and swell are evaluated after the separation. Before the hurricane passes the selected sites, the swell components significantly contribute to the overall wave energy. Note that the mean wave frequency of the swell component is significantly below 0.3 Hz (which is the resonant frequency associated with the first tower bending mode for the wind turbine used in this study); this suggests that the contribution of swell to total turbine response may not be significant.

The variation of the mean wave frequency and wave direction for swell and wind seas are presented in Fig. 2.11.

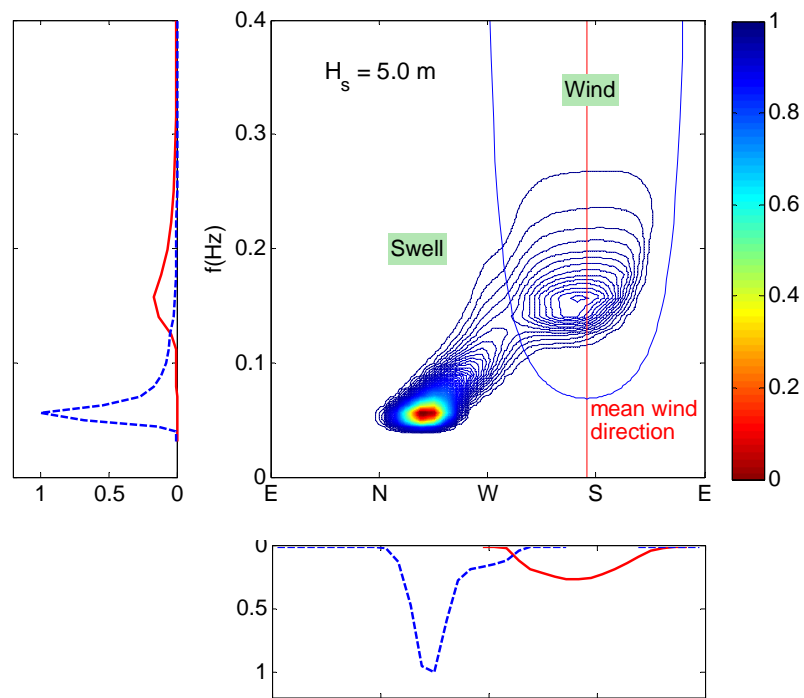
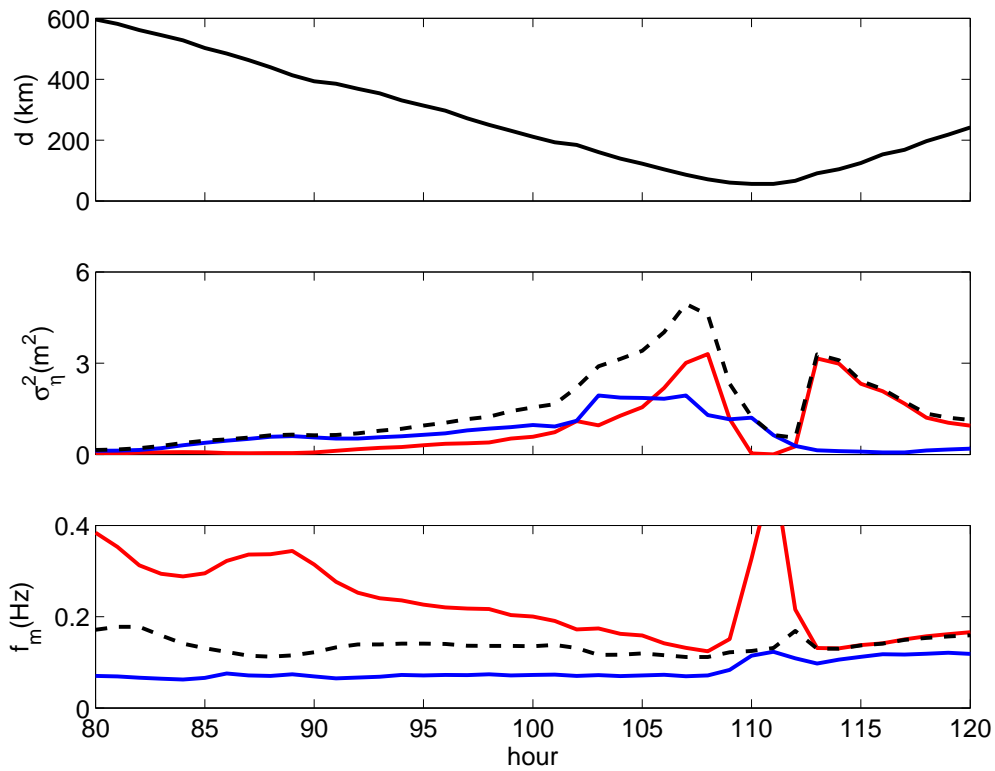
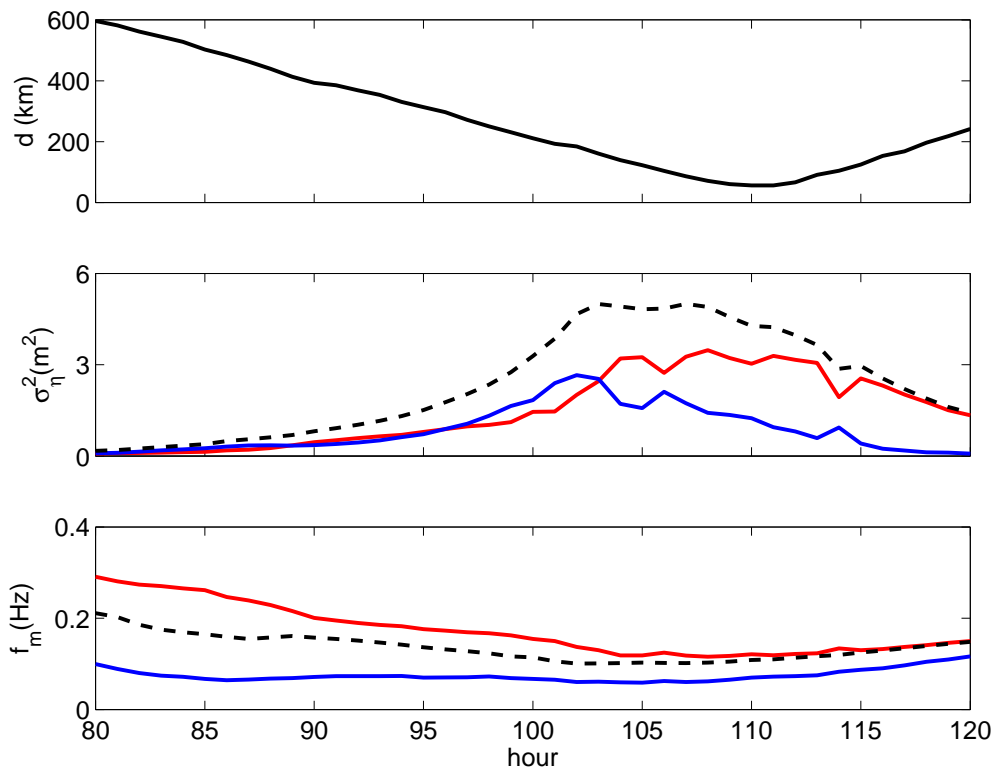


**Figure 2.9. Wind sea and swell separation, normalized by the wave spectrum maximum value (blue line: swell spectrum; red line: wind sea spectrum).**



(a) Site B.



(b) Site A.

Figure 2.10. Variation with time in the distance between the site and hurricane eye ( $d$ ), wave variance ( $\sigma_{\eta}^2$ ), and mean wave frequency ( $f_m$ ) (black dashed line: wind sea + swell; blue solid line: swell; red solid line: wind sea)

While the mean wave frequency and wave direction corresponding to wind seas are significantly changed with the hurricane movement because these wind seas are greatly affected by local wind direction and speed changes, the variation in mean wave frequency and wave direction corresponding to swell is relatively insignificant because the evolution of swell is not as strongly affected by the local wind.

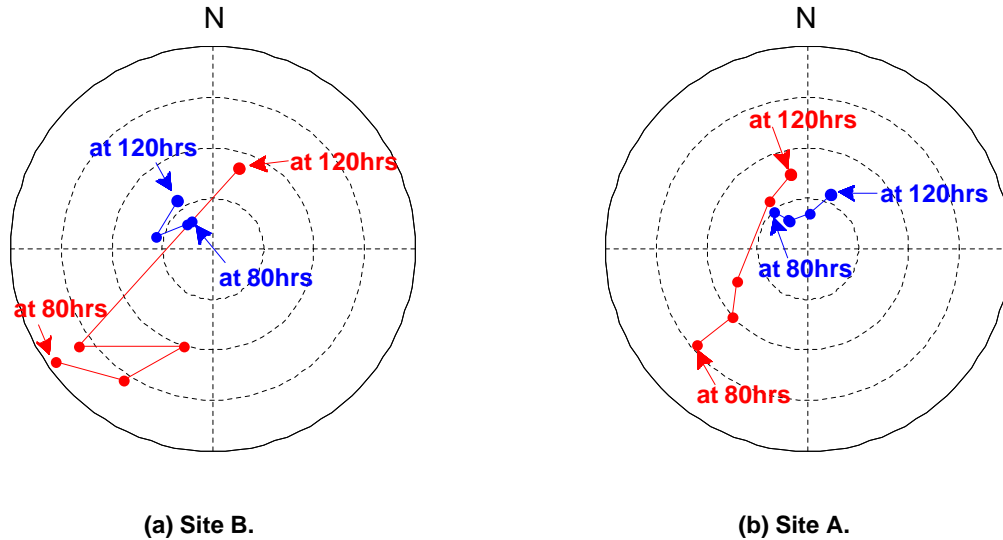


**Figure 2.11. Variation of the mean wave frequency and wave direction every 10 hours; *N* indicates waves propagating toward north, etc., and the dashed and solid circles (inner to outer) correspond to wave frequencies of 0.1, 0.2, 0.3, and 0.4 Hz (blue dots and line: swell sea; red dots and line: wind sea).**

After the hurricane waves are separated into wind sea and swell by the procedure described in Fig. 2.8, the variances of the tower bending moment resulting from the wind sea and swell are compared in Fig. 2.12. Only the effect of wave loads is included in evaluating the turbine response. Although the contribution from swell components to the overall wave energy is comparable with and even sometimes higher than that from wind seas, the contribution of swell to the fore-aft tower bending moment (FATBM) at the base is relatively very small when compared with its contribution to the side-to-side tower bending moment (SSTBM). Two possible factors can explain the small FATBM contribution from swell; these are: (1) the significantly lower mean wave frequency of the swell component is less than 0.3 Hz which is near the resonant frequency associated with first tower bending mode; and (2) the relatively strong misalignment between the mean wind direction (in the direction of bending of FATBM) and the mean direction of the swell sea. This second factor also helps explain the higher contribution of swell to SSTBM than to FATBM. On the other hand, because of the relatively slight misalignment between the wind sea and the mean wind direction, a larger portion of the wind sea energy contributes to FATBM and this leads to higher FATBM response corresponding to wind seas rather than to SSTBM response. Still, for most of the time covered by the simulation, the contribution from the wind sea to the SSTBM response is higher than from swell due to the significantly lower mean wave frequency of the swell component. Overall, it is found that the FATBM response is significantly higher than the SSTBM response.

### 2.4.3 Effect of feathered blades

During the hurricane, the blades of the wind turbine are pitched to feather to minimize turbine loads. The effect of feathering blades on the turbine response is evaluated using turbulent wind velocity fields with a mean longitudinal wind velocity of about 27 m/s at 90 m above MSL. Two difference turbine states are studied: (1) Case 1: the turbine maintains yaw control and can track the changing wind direction perfectly, and (2) Case 2: the turbine experiences

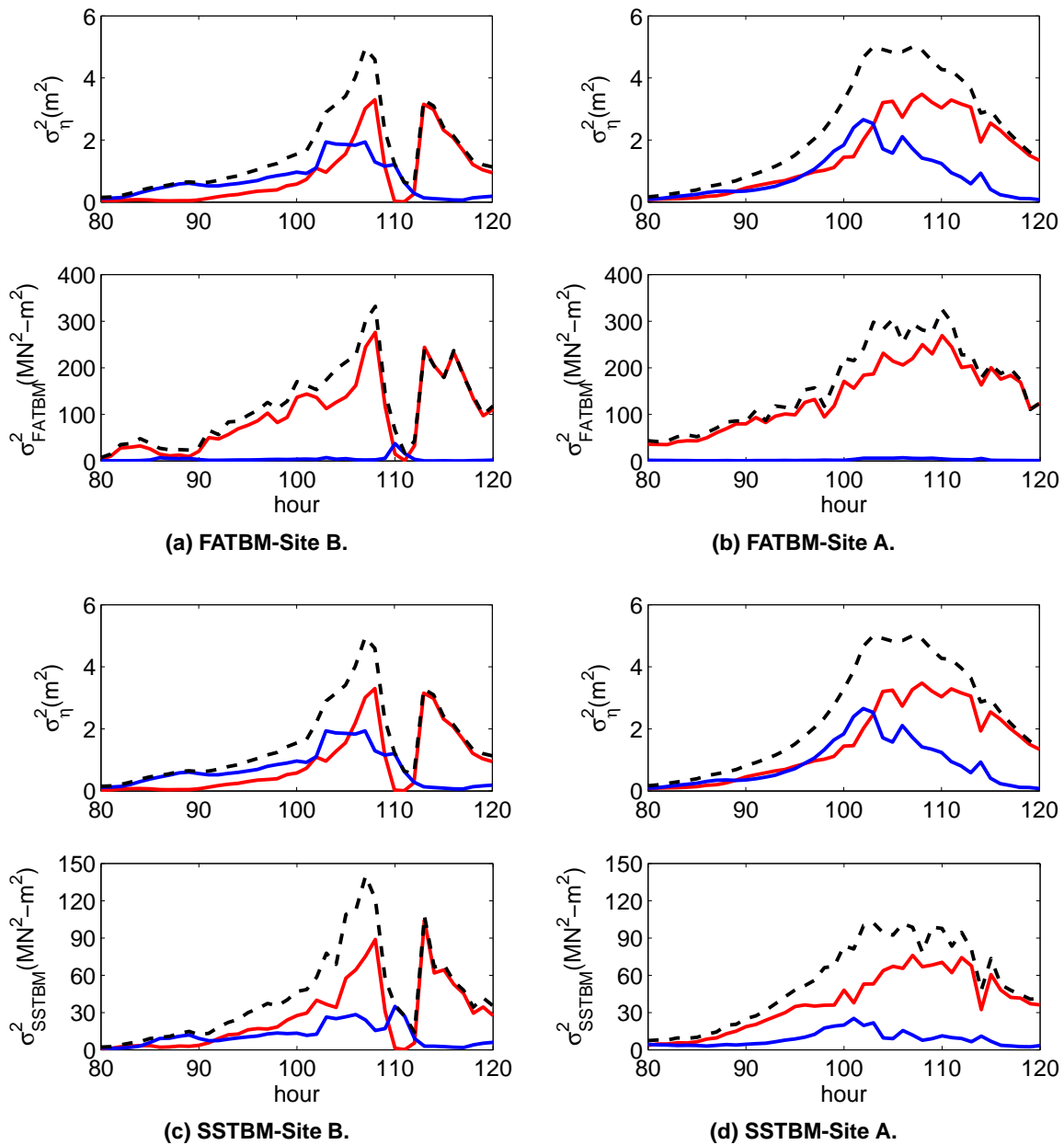
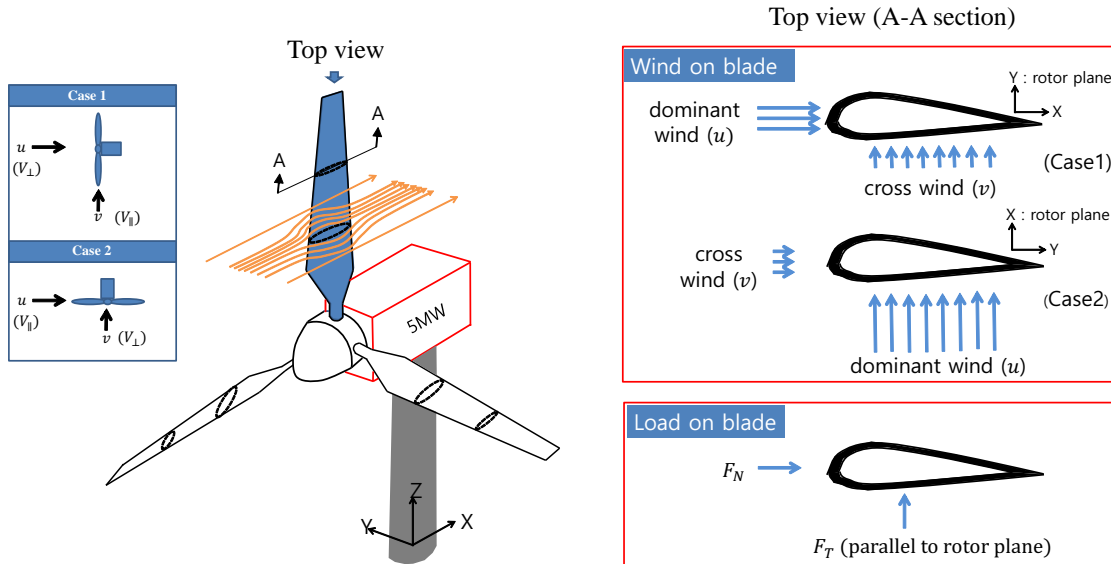


Figure 2.12. Variation in the tower response (bending moment) variance with time indicating contributions from wind sea and swell (black dash line: wind sea + swell; blue solid line: swell; red solid line: wind sea)





**Figure 2.13. Schematic sketch of a parked wind turbine and definition of loads on blades**

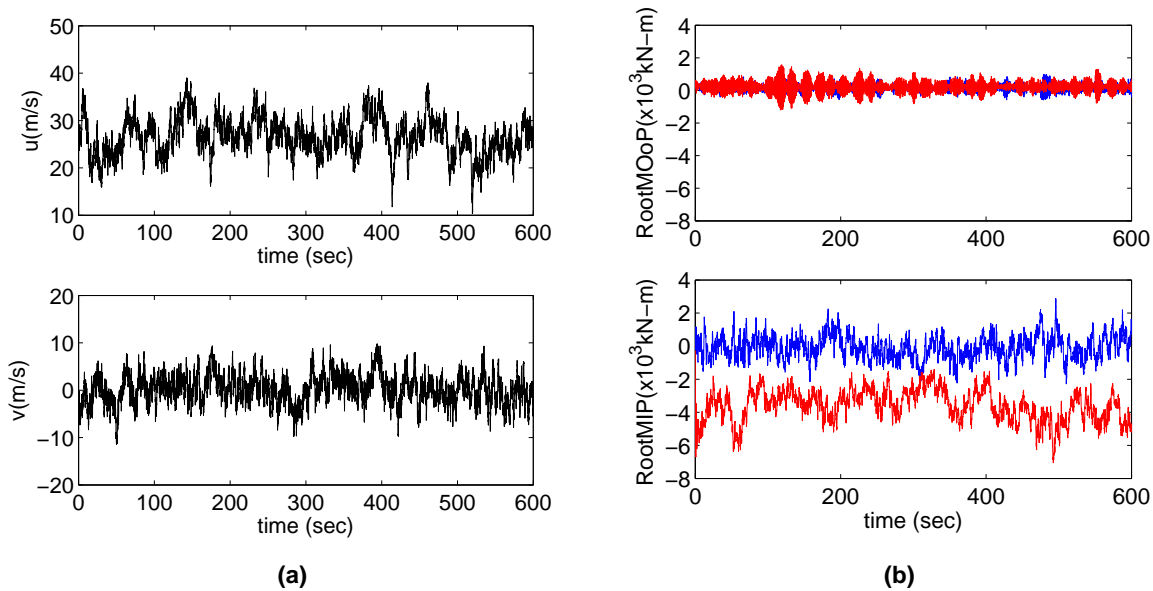
some yaw misalignment or yaw error. In this study, a single yaw misalignment or yaw error case of 90 degrees is evaluated; note that this may not provide the worst-case scenario for turbine loads. Figure 2.13 shows a schematic sketch of a parked wind turbine which is considered in this study; one of blades of the turbine is oriented at a  $0^\circ$  azimuth angle (i.e., in the 12 o'clock position) and is designated as Blade 1. The figure also shows the top view of a cross section of Blade 1 with wind flow directions indicated for both cases. Tangential forces,  $F_T$  and normal forces,  $F_N$ , are defined in the figure for Blade 1. The dominant longitudinal wind and the cross (lateral) wind directions in both cases are aligned with the  $x$  and  $y$  directions, respectively, of the turbine base coordinate system as shown in the figure.

Table 2.1 shows 1-hour maximum bending moments at the root of Blade 1 for two different pitch angle cases. As can be seen, when cross winds are not included, both out-of-plane and in-plane bending moments at the blade root are decreased when the blades are pitched to feather; the in-plane bending moment is decreased from 1,215 kN-m to 563 kN-m and the out-of-plane bending moment is decreased from 8,053 kN-m to 453 kN-m. However, when cross winds are included, while the out-of-plane bending moment is decreased from 8,278 kN-m to 1,065 kN-m by feathering the blades, the in-plane bending moment is increased from 1,688 kN-m to 2,788 kN-m. Also, upon including the cross wind, in-plane and out-of-plane bending moments are both significantly increased, especially when the blades are feathered. Feathering the blades increases the contribution of the cross wind on blade root moments.

**Table 2.1. One-hour maximum bending moment at blade root with and without the cross wind velocity contribution for a blade at a  $0^\circ$  azimuth angle.**

	in-plane bending moment (kN-m)		out-of-plane bending moment (kN-m)	
	pitch angle ( $\beta$ ) = $0^\circ$	pitch angle ( $\beta$ ) = $90^\circ$	pitch angle ( $\beta$ ) = $0^\circ$	pitch angle ( $\beta$ ) = $90^\circ$
without cross wind	1,215	563	8,053	453
with cross wind	1,688	2,788	8,278	1,065

Figure 2.14 shows the effect of yaw misalignment on bending moments at the blade root. The blade root in-plane bending moments are much more significantly influenced by yaw error than the out-of-plane bending moments. As shown in Fig. 2.13, the dominant wind in Case 2 is aligned with the rotor plane, and it increases the



**Figure 2.14. (a) Turbulent wind velocity time series and (b) associated blade root bending moments (blue line: Case 1; red line: Case 2)**

maximum in-plane bending moment as well as the mean in-plane bending moment.

Figure 2.15 shows the variation in aerodynamic forces at several sections along Blade 1 for the two different yaw-control cases. At most blade sections and for both cases, the tangential forces,  $F_T$ , corresponding to bending moments in the rotor plane are significantly larger than the normal forces,  $F_N$ , corresponding to the moments orthogonal to the rotor plane. It is also seen that Case 2 leads to larger tangential forces than Case 1.

#### 2.4.4 Effect of turbine control

We now investigate how yaw and pitch controls influence the response of the selected offshore wind turbine during a hurricane. A wind turbine’s control and safety systems play a vital role in regulating aerodynamic loads by adjusting the blade pitch angle with changing wind speed and the nacelle yaw angle with changing wind direction. In this study, using simulated wind and wave fields, we evaluate: (1) the effect of different nacelle yaw angles relative to the wind direction (i.e., different amounts of yaw error or misalignment); (2) the effect of different blade pitch angles; (3) the effect of different turbine parking strategies—e.g., parked (at standstill) or in an idling state; and (4) load maxima at different blade azimuthal configurations while the turbine is in a standstill state.

##### 2.4.4.1 Effect of yaw misalignment

First, the effect of yaw misalignment on turbine response is studied; seven different yaw misalignments ( $\theta_{yaw} = -90, -60, -30, 0, 30, 60, \text{ and } 90$  degrees) are considered. The 0-degree yaw misalignment corresponds to a case with enough backup power for active yawing so as to have no yaw error; the others could represent cases with insufficient yaw system backup power that, then, lead to varying degrees of yaw misalignment or error. We assume that the wind turbine is in an idling state and that all the blades are feathered, or turned to a 90-degree pitch angle. From Fig. 2.16 for an idling turbine at Site A, it can be seen that while the contribution from hydrodynamic loading to the tower response is only very slightly influenced by the amount of yaw misalignment, the aerodynamic loading contribution is significantly influenced by it. Peak tower bending moment values occur for a yaw misalignment of

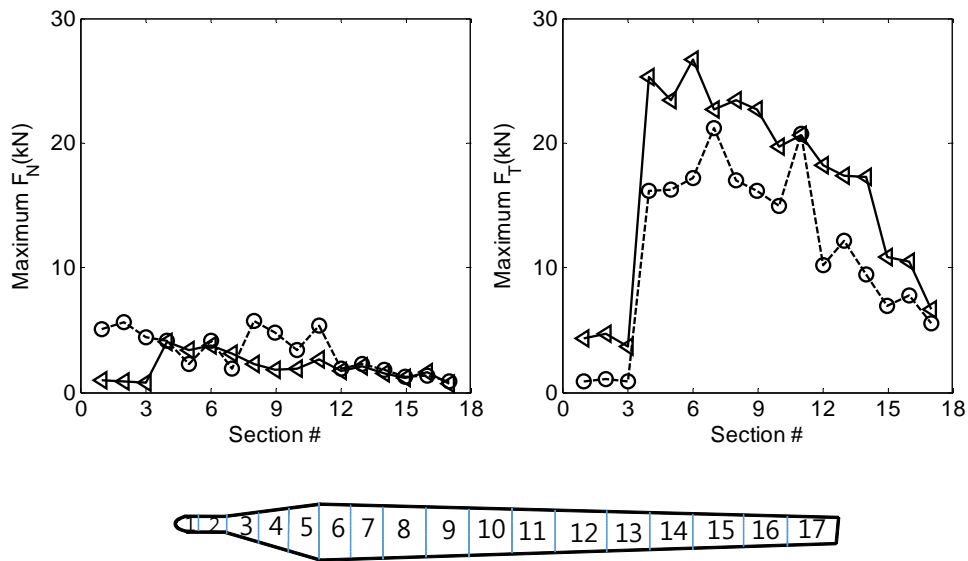


Figure 2.15. Maximum normal force ( $F_N$ ) and tangential force ( $F_T$ ) on blade (circles: Case 1; triangles: Case 2)

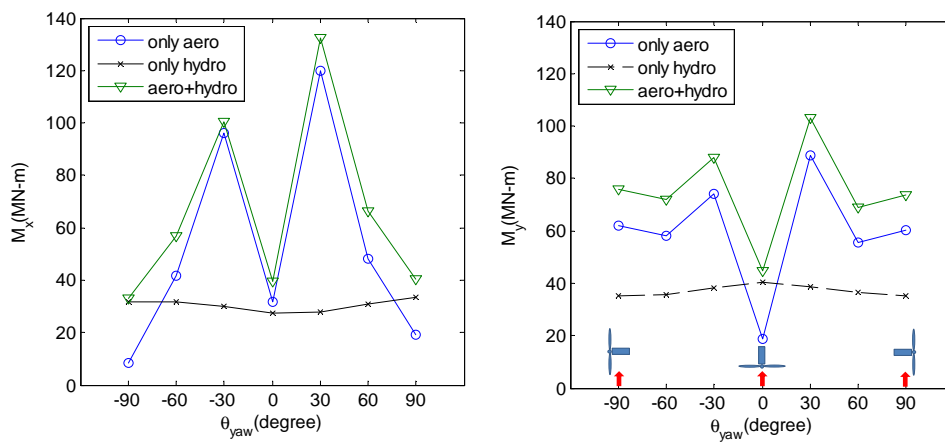


Figure 2.16. Maximum tower bending moment at mudline (at 100 hrs) for an idling turbine at Site A.

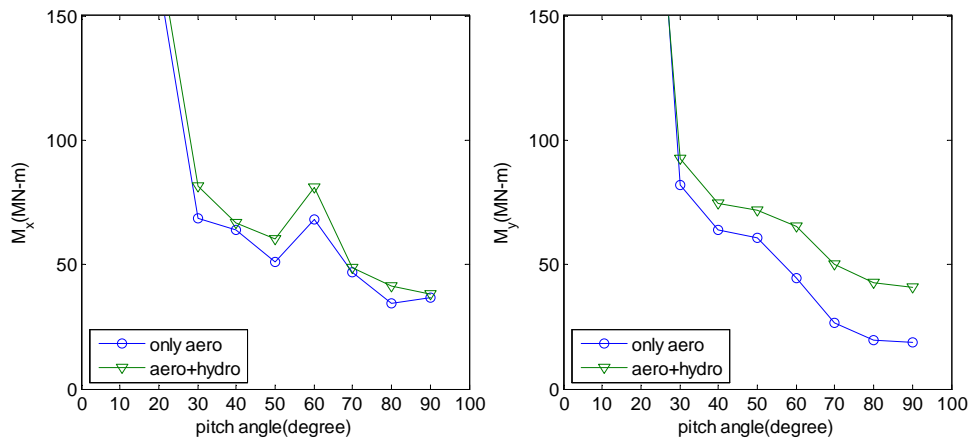
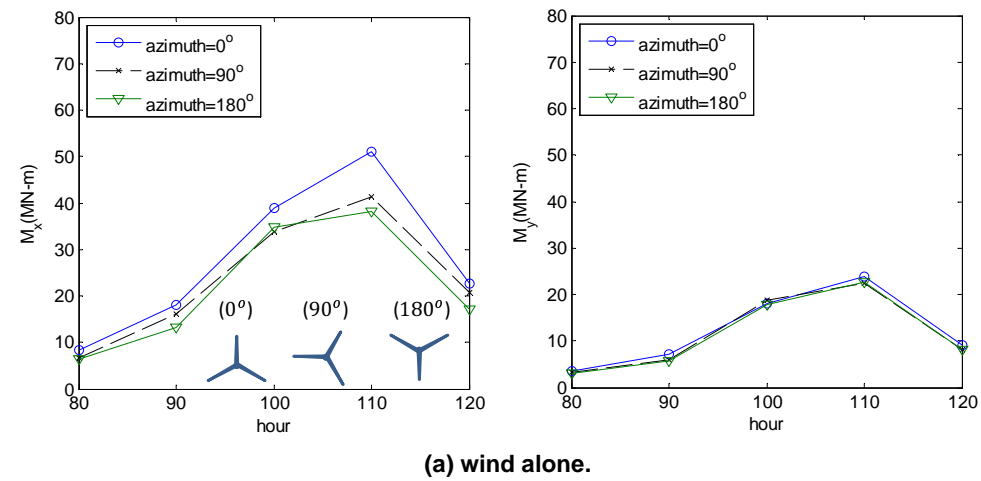
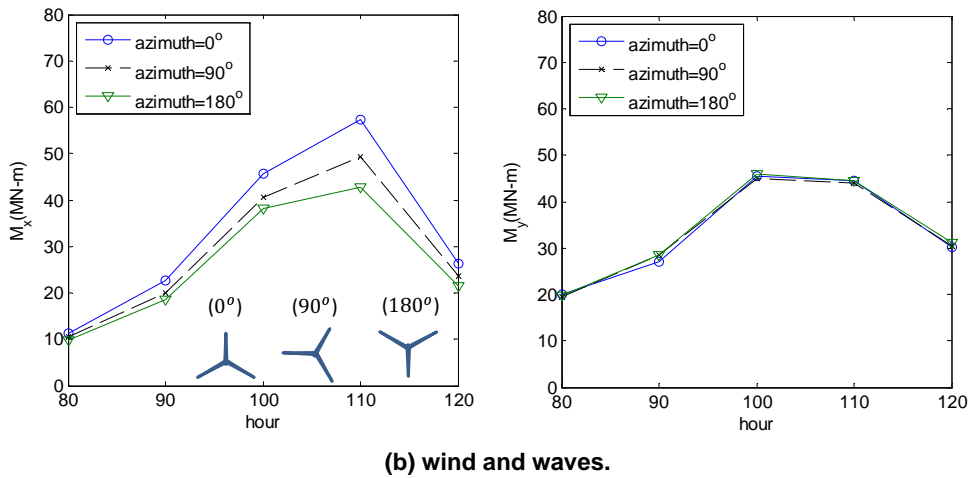


Figure 2.17. Effect of pitch angle on tower bending moment (at 100 hours) for an idling turbine at Site A.



(a) wind alone.



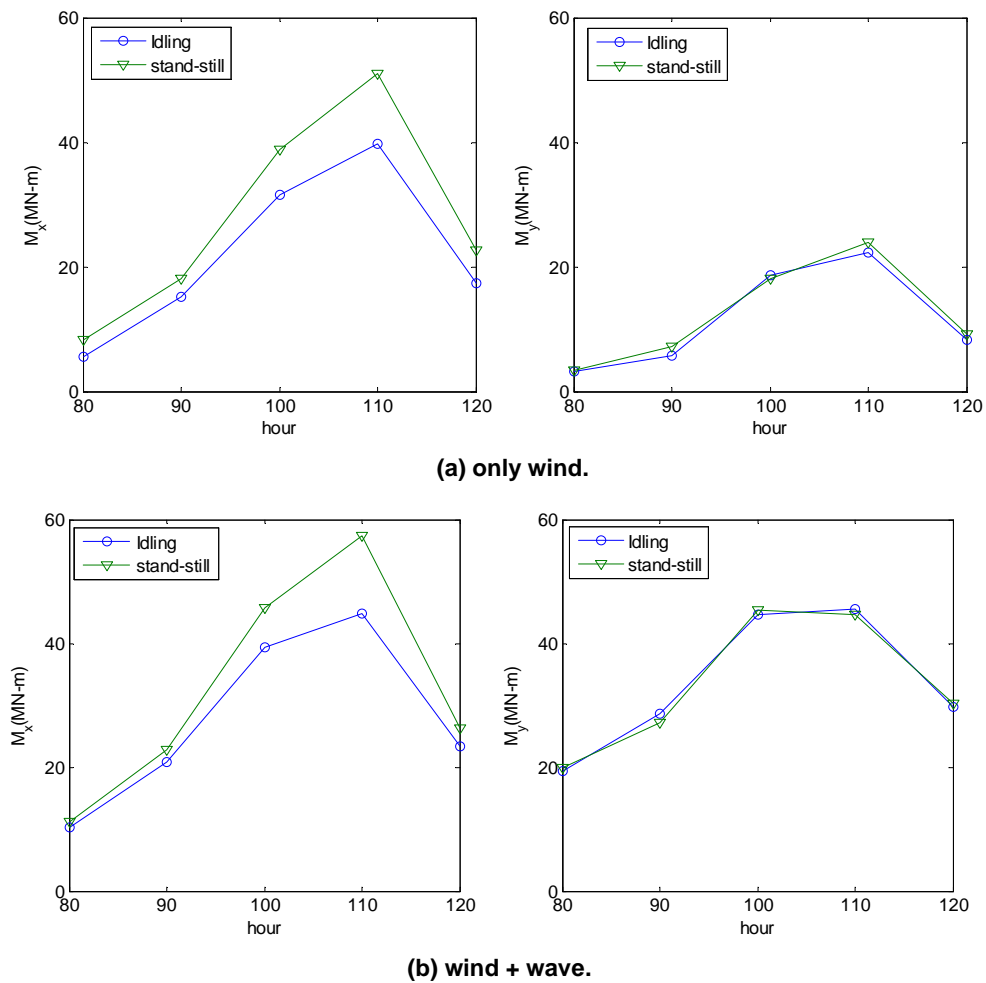
(b) wind and waves.

Figure 2.18. Effect of blade azimuthal position on tower bending moment for a parked-standstill turbine at Site A during Hurricane Ike.

about 30 degrees; when the misalignment changes from 0 to 30 degrees, the tower bending loads are seen to increase by as much as a factor of 4.

### 2.4.4.2 Effect of blade pitch angle

We discuss next the sensitivity of the tower response to the blade pitch angle. In this sensitivity study, all the blades are locked at a set pitch angle selected to be between 20 and 90 degrees. We assume that the wind turbine is in an idling state and that the rotor is yawed to be in alignment with the mean wind direction. From Fig. 2.17, as expected, we see that a 90-degree pitch angle results in the lowest tower response maxima and that, when the pitch angle is reduced from 30 to 20 degrees, an extremely large increase in the maximum tower bending moment results. Clearly, blade pitch control is important during the hurricane.



**Figure 2.19. Effect of turbine parking strategy on tower loads for a turbine at Site A (with no yaw misalignment) during Hurricane Ike.**

#### 2.4.4.3 Effect of blade azimuthal configuration

Next, for the wind turbine assumed to be in a parked-standstill state, we evaluate the tower response at three different blade azimuthal configurations. In the first case, one of blades of the turbine is oriented at a  $0^\circ$  azimuth angle (i.e., in the 12 o'clock position); this blade is designated as Blade 1. In the second and third cases, the azimuth counterclockwise angles of Blade 1 are 90 and 180 degrees, respectively. We assume that the wind turbine is in a parked-standstill state, that the rotor and nacelle are yawed so as to be aligned with the mean wind direction, and that all three blades are feathered. From Fig. 2.18, it can be seen that while  $M_y$  (the tower base fore-aft moment), in this case with zero yaw error, is not significantly different for different blade azimuthal configurations,  $M_x$  (the tower base side-to-side moment) is seen to vary by a considerably larger amount; this range can be as much as 25% of the value, say, at the zero-degree azimuthal configuration. In general, though not at all times during the simulation, the largest and smallest tower loads are observed at the 0 and 180 degree azimuthal configurations, respectively.

#### 2.4.4.4 Effect of alternative turbine parking strategies: standstill versus idling

At very high wind speeds, it is expected that an offshore wind turbine will be parked and held either at a standstill state or allowed to rotate in an idling state. We now discuss the effect that such alternative turbine parking strategies have on turbine loads. We assume that the turbine rotor is yawed so as to be aligned with the mean wind direction and that all three blades are feathered; also, for the parked-standstill case, one of the blades is assumed to be at a zero-degree azimuthal position. From Fig. 2.19, we can see that  $M_y$  (the tower base fore-aft moment), in this case with zero yaw error, is not significantly different for the two different turbine parking strategies. In contrast,  $M_x$  (the tower base side-to-side moment) is seen to be noticeably different and the parked-standstill case leads to larger loads than the idling case.

## 2.5 Result and Discussion

We have carried out in-depth studies of the response of a monopile-supported 5-MW offshore wind turbine during Hurricane Ike. The intensity and track of Hurricane Ike are numerically simulated by a fully coupled atmospheric-wave-ocean model, UMCM. Based on directional wave spectra resulting from the UMCM output, hurricane-generated wave kinematics are simulated using directional irregular second-order waves. We have presented the wave modeling approach adopted as well as a numerical procedure for simulating the directional nonlinear waves. A mean wind field is defined and turbulent wind fields are stochastically simulated using a Fourier-based spectral procedure; both are based on characteristics of the surface wind field obtained from the UMCM output obtained over a duration of 120 hours.

Because hurricane directional waves are composed of two wave components, swell and wind sea which have different characteristics, their characteristics are evaluated after separating swell and wind sea components from directional wave spectra resulting from the UMCM output based on the wave age criterion. Although the swell component significantly contributes to overall wave energy, the mean wave frequency of this swell component is significantly lower than resonant frequencies associated with tower bending. Also, while mean wave frequencies and wave directions corresponding to wind seas are significantly changed with hurricane movement because these wind seas are greatly affected by the local wind direction and speed change; in contrast, the variation of mean wave frequencies and wave directions corresponding to swell is relatively insignificant because the evolution is not as strongly affected by the local wind.

At selected locations, we evaluated the effect on turbine load maxima, during the simulation of Hurricane Ike, of: (i) different nacelle yaw angles relative to the mean wind direction (i.e., different amounts of yaw error or misalignment); (ii) different blade pitch angles; and (iii) different turbine parking strategies (i.e., considering a turbine in either a standstill or idling state). In addition, we studied loads for different blade azimuthal positions. Based on the numerical studies presented, we can make the following general conclusions:

- While the contribution from hydrodynamic loading to the tower response is only very slightly influenced by the amount of yaw misalignment, the aerodynamic loading contribution is significantly influenced by it; peak tower bending moment values occur for a yaw misalignment of about 30 degrees. The significantly lower turbine loads in the case of zero yaw misalignment highlights the importance of a reliable yaw backup power system, which is strongly recommended since a grid failure during a hurricane could result in loss of the needed yaw control.
- Blade pitch control is important during the hurricane; as expected, a 90-degree pitch angle results in the lowest tower response maxima and in a systematic study, it was found that when the pitch angle is reduced from 30 to 20 degrees, a significant increase in the maximum tower bending moment results.
- While the tower base fore-aft moment in a case with zero yaw error does not vary greatly for different blade azimuthal positions, the tower base side-to-side moment is seen to vary by a considerably larger amount; this range can be as much as 25% of the value, say, at the zero-degree azimuthal position. In general, though not at all times during the hurricane, largest and smallest tower load maxima occurred for rotor configurations where one blade is in the 0 and 180 degree azimuthal position, respectively.
- While the tower base fore-aft moment in a case with zero yaw error is not significantly different for the different turbine parking strategies considered, the tower base side-to-side moment is seen to be noticeably different and the parked-standstill case leads to systematically larger loads than the idling case during the hurricane.

## 3 Modeling Hurricane Sandy's Influence on a Jacket-Supported Offshore Wind Turbine

### 3.1 Problem Description

For evaluating the response of an offshore wind turbine (OWT) during the evolution of Hurricane Sandy (2012), we consider ten mid-Atlantic sites identified for potential wind energy development. These selected sites shown in Figure 3.1 were in or close to the path of Hurricane Sandy. Some general information on the selected sites is presented in Table 3.1. The water depth at some of these sites is greater than 30 m. Depending on the water depth range, in our analyses, we considered at many as three fixed water depths (20 m, 45 m, and 50 m) possible at any site. Because a monopile support structure becomes progressively uneconomical as the water depth increases beyond 25-30m [29], other types of support structures such as jackets or tripods might be better candidates at those water depths. To illustrate the detailed procedure related to the response evaluations of an offshore wind turbine with a jacket support structure, we consider only a single site where the water depth is 50 m.

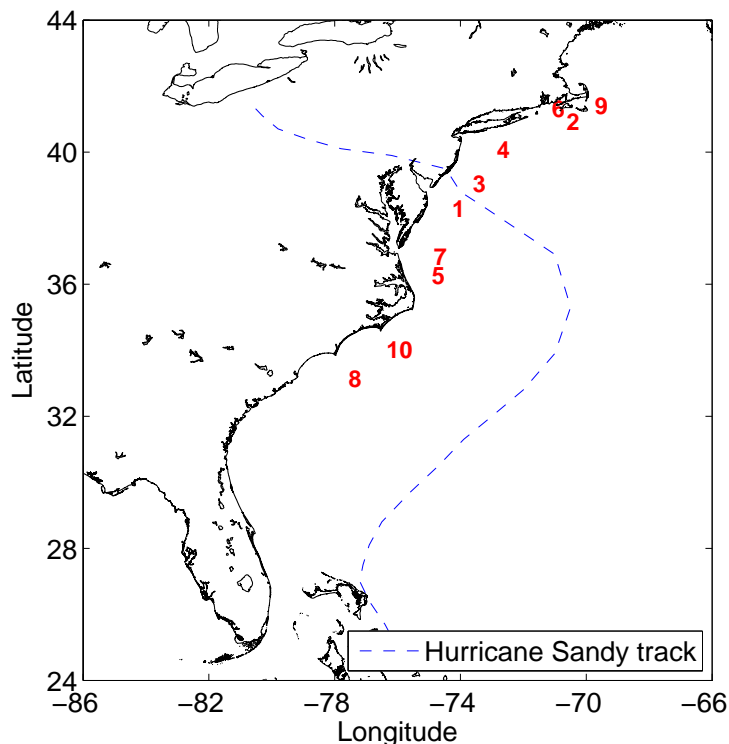
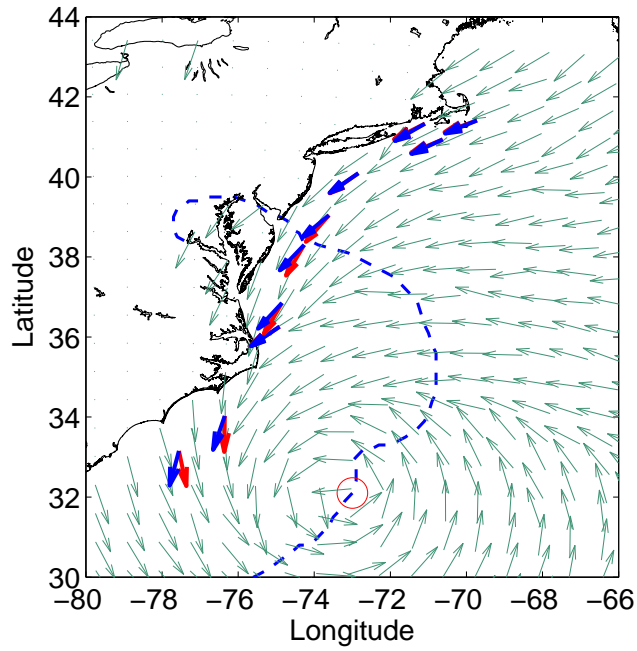


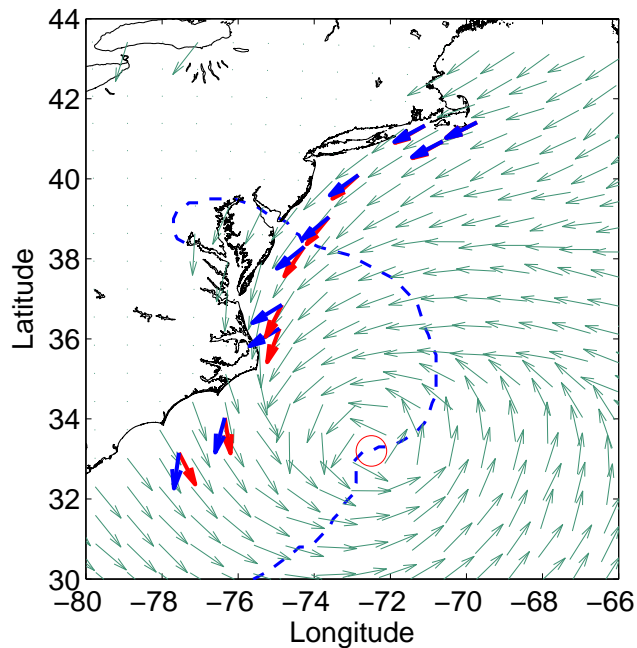
**Figure 3.1. The locations of ten selected offshore wind plant sites and the simulated track of Hurricane Sandy.**

As was the case for Hurricane Ike discussed in Chapter 2, coupled wind and wave fields at the locations of interest are simulated based on the UCMC output. Figure 3.4 shows the variation with time of the wind and wave directions; the red circle indicates the location of the hurricane eye at the specified time. In the figure, the red and blue arrows represent the wind and wave directions, respectively, at the ten selected sites (locally) while the green arrows depict the full-field wind direction over the entire simulation domain. As shown in this figure, the wind and wave directions and the misalignments between the two at each site change noticeably as the hurricane moves along its track.



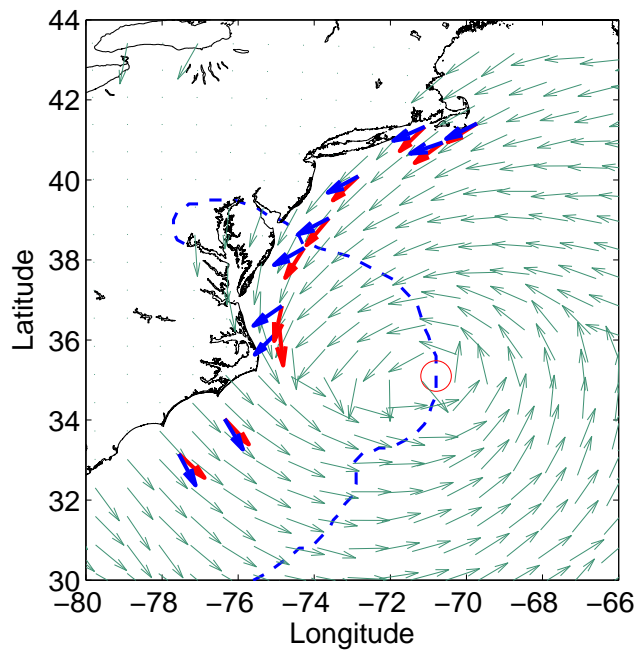


(a) At 10:00 UTC on October 28, 2012 ( $t_0$ ).

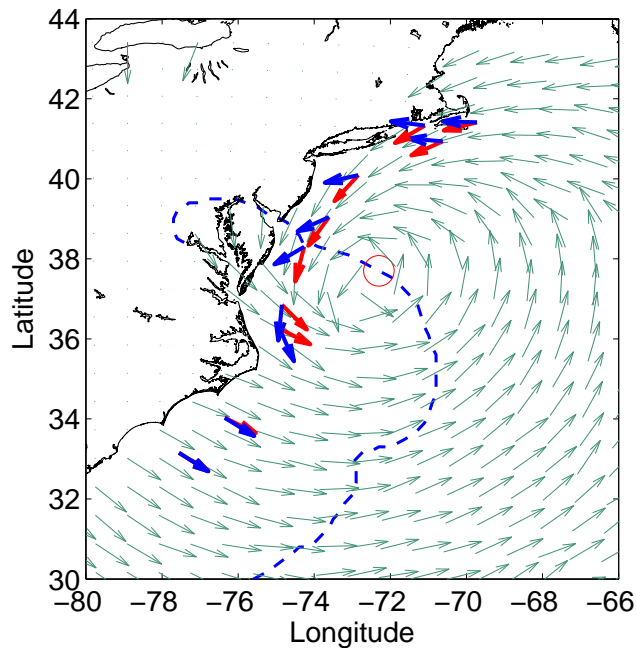


(b) At  $t_0 + 10$  hours.

**Figure 3.2. Variation with time during Hurricane Sandy of the full-field wind direction (green arrows), local wind direction (blue arrows), and local wave direction (red arrows) at the locations of the ten selected sites (at  $t_0$  and  $t_0 + 10$  hours).**

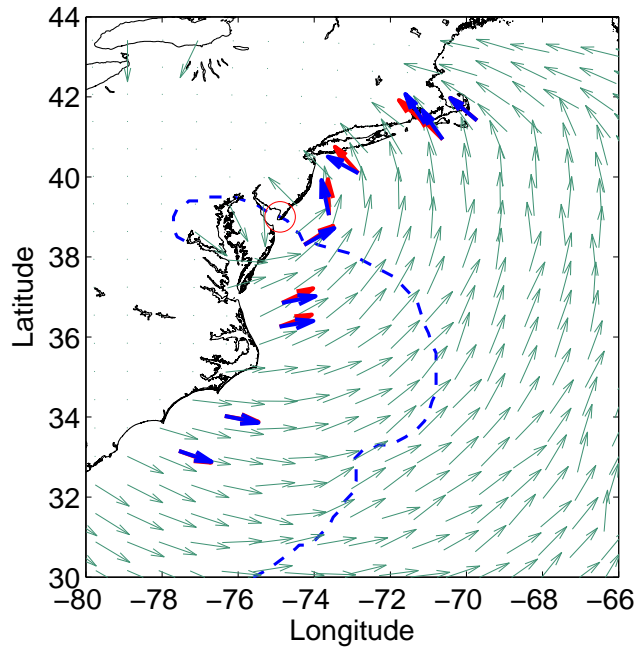


(a) At  $t_0 + 20$  hours.

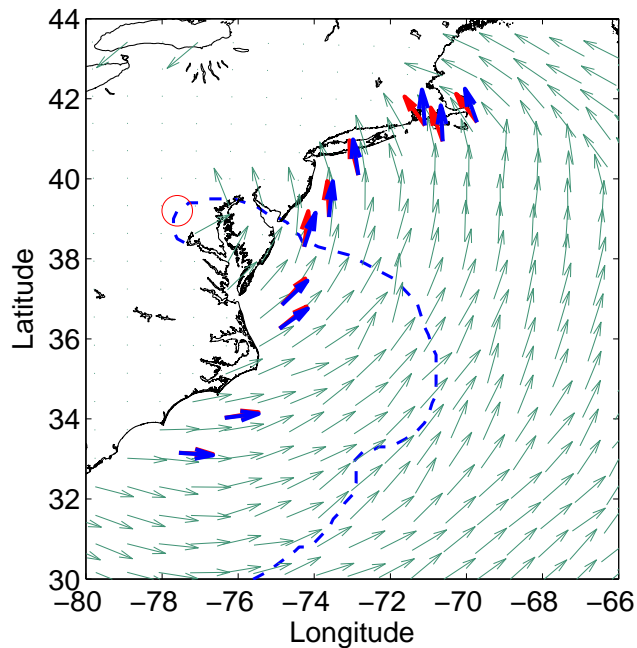


(b) At  $t_0 + 30$  hours.

**Figure 3.3. Variation with time during Hurricane Sandy of the full-field wind direction (green arrows), local wind direction (blue arrows), and local wave direction (red arrows) at the locations of the ten selected sites (at  $t_0 + 20$  and  $t_0 + 30$  hours).**



(a) At  $t_0 + 40$  hours.



(b) At  $t_0 + 50$  hours.

**Figure 3.4. Variation with time during Hurricane Sandy of the full-field wind direction (green arrows), local wind direction (blue arrows), and local wave direction (red arrows) at the locations of the ten selected sites (at  $t_0 + 40$  and  $t_0 + 50$  hour).**

**Table 3.1. General information on ten potential offshore wind plant sites selected for analysis in this study (source: www.4coffshore.com).**

	Wind Energy Area (ID)	Water Depth Range	Distance from shore
1	Maryland WEA South (US4O)	11-36 m	24.4 km
2	Massachusetts WEA (US0V)	31-62 m	38.7 km
3	New Jersey (US4S)	14-32 m	30.1 km
4	New York RFI (US4J)	18-42 m	40.8 km
5	North Carolina(US4E)	15-44 m	41.5 km
6	Rhode Island & MA (US3C)	26-49 m	31.5 km
7	Virginia (US3H)	18-33 m	54.2 km
8	North Carolina(US4E)	15-44 m	41.5 km
9	Cape Wind, MA (US03)	1-18 m	14.2 km
10	Apex Offshore Wind, NC (US99)	26-29 m	32.2 km

In this chapter, we present detailed response results only for an offshore wind turbine at Site No. 1. Figure 3.5 shows the location of Site No. 1 along with the track of Hurricane Sandy as extracted from a best track database and estimated by the UMCM simulation; the larger red star indicates the location of Site No. 1 while the smaller blue stars indicate locations of the other nine sites. The figure serves to display the evolution of track of the hurricane over a 60-hour period beginning at 00:00 UTC on October 28, 2012 (0 hour).

### 3.2 Hurricane-Induced Waves

Irregular hurricane-generated waves are numerically simulated using second-order wave theory and the methodology presented in Chapter 2. Table 3.2 summarizes information on wave spectra from UMWM output and on ocean currents from HYCOM output obtained following the UMCM simulation of Hurricane Sandy. As shown in the table, wave spectra for Hurricane Sandy are continuously generated for separate 1-min periods. However, to simulate 1-hour sea surface elevation process and associated wave kinematics in the time domain for subsequent turbine load calculation, we need to employ a wave spectrum that represents the entire 1-hour period. Figure 3.6a shows the wave spectrum 40 hours after 10:00 UTC on October 28, 2012 at the 50-meter water depth location within Site No. 1. Figures 3.6b, 3.6c, and 3.6d show, respectively, computed wave spectra 1, 10, and 60 minutes later. Differences between the wave spectra over the entire hour are not significant; hence, in this study, we simply assume that the UMWM wave spectrum from the first minute each hour is representative of the spectrum over the entire hour. Of course, as the hurricane progresses, these wave spectra are updated each hour to generate the changing sea surface elevation and wave kinematics.

**Table 3.2. Wave and current information from UMWM and HYCOM.**

Physics model	Output files	Resolution		Data used
		spatial	temporal	
Current (HYCOM)	current_xx.nc	every 2 m depth (at each site)	10 min	$v_{cx}, v_{cy}, v_{cz}$
Wave (UMWM)	umwm_spc_xx.nc	at each site	1 min	$F(\vec{k}), k, \theta$ $U(z = 10 \text{ m})$

Figures 3.7 and 3.8 show the variation with time of the frequency-dependent wave spectrum,  $S(f_n)$ , and the direction-dependent wave spreading function,  $D(\theta_m)$ , defined as follows:

$$S(f_n) = \sum_{m=1}^M S(f_n, \theta_m) \Delta \theta_m; \sigma_{\eta}^2 = \sum_{n=1}^N S(f_n) \Delta f_n \quad (3.1)$$

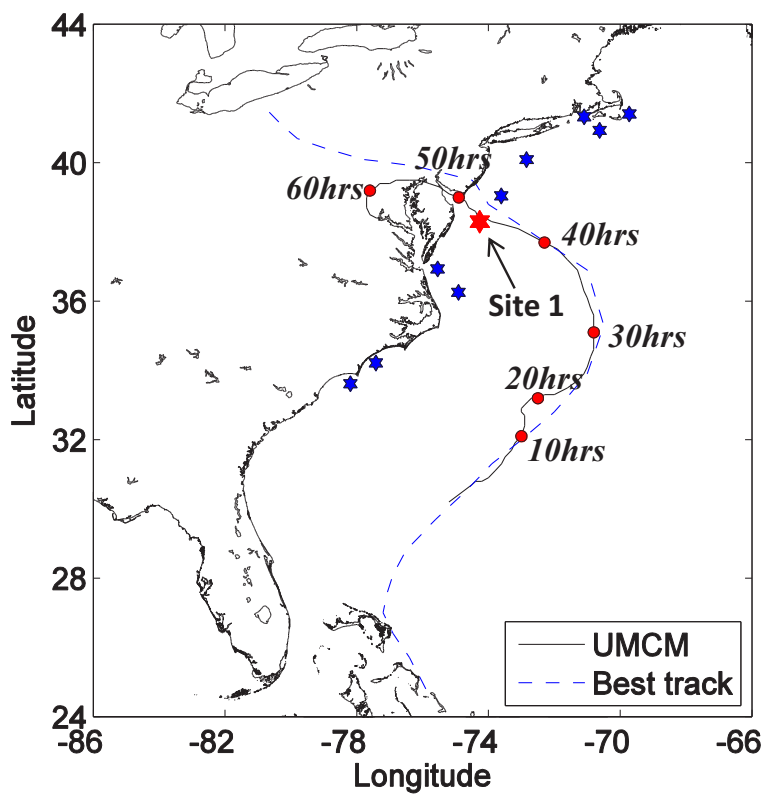


Figure 3.5. Location of Site No. 1 and the simulated track of Hurricane Sandy evaluated based on UMCM output (compared to a best track database).

$$D(\theta_m) = \sum_{n=1}^N S(f_n, \theta_m) \Delta f_n; \sigma_{\eta}^2 = \sum_{m=1}^M D(\theta_m) \Delta \theta_m \quad (3.2)$$

where  $\sigma_{\eta}^2$  is the variance of the sea surface elevation process. From Figs. 3.7 and 3.8, it can be seen that at around 46 hours, both the wave spectrum and the directional spreading change quite abruptly as the hurricane's eye passes the site. During that hour, our assumption that the first minute's wave spectrum is representative of the entire hour would not be an acceptable one.

### 3.3 Hurricane-Induced Wind Field

Table 3.3 summarizes information on the wind field from WRF output obtained following the UMCM simulation of Hurricane Sandy. In the table, a geometric height,  $z$  (elevation above the mean sea level), corresponding to the three output wind velocity components,  $U_x(z)$ ,  $U_y(z)$ , and  $U_z(z)$ , are evaluated as follows, using an initial geopotential,  $PHB$ , and a perturbation geopotential,  $PH$  [30]:

$$\text{geometric height: } z = \frac{PH + PHB}{9.81} \quad (3.3)$$

While turbulent wind fields for Hurricane Ike in Chapter 2 were simulated using mean wind field data sampled every hour and only at a location 10 meters above the mean sea surface level (with an assumed vertical wind shear), we demonstrate how the WRF output can allow us to make use of available wind field data provided every 10 minutes and at several elevations to stochastically simulate turbulent wind fields for Hurricane Sandy.

**Table 3.3. Wind field information from WRF output for Hurricane Sandy.**

Physics model	Output files	Resolution		Data used
		spatial	temporal	
Wind (WRF)	wrf_xx.nc	12 × 12 km	10 min	$u^*(t_p)$
		4 × 4 km		$U_x(z, t_p), U_y(z, t_p), U_z(z, t_p)$
		1.3 × 1.3 km		$PHB(z, t_p), PH(z, t_p)$

Figure 3.9 presents the overall procedure to simulate turbulent wind fields using WRF output for Hurricane Sandy. In order to simulate an hour-long fully turbulent wind field including the vertical wind shear, as a first step, we compute six values of the 10-min sampled total wind speed,  $U(z, t_p)$ , the horizontal wind direction,  $\theta_{hor}(z, t_p)$ , and the vertical wind direction,  $\theta_{ver}(z, t_p)$ , using WRF output  $U_x(z, t_p)$ ,  $U_y(z, t_p)$ , and  $U_z(z, t_p)$  (where  $p = 1, 2, \dots, 6$  during the hour). This is done as follows:

$$U(z, t_p) = \sqrt{[U_x(z, t_p)]^2 + [U_y(z, t_p)]^2 + [U_z(z, t_p)]^2} \quad (3.4)$$

$$\theta_{hor}(z, t_p) = \text{atan2} \left( \frac{U_y(z, t_p)}{U_x(z, t_p)} \right) \quad (3.5)$$

$$\theta_{ver}(z, t_p) = \text{atan2} \left( \frac{U_z(z, t_p)}{\sqrt{(U_x(z, t_p))^2 + (U_y(z, t_p))^2}} \right) \quad (3.6)$$

$$\text{atan2}(y, x) = \begin{cases} \arctan \frac{y}{x} & x > 0 \\ \arctan \frac{y}{x} + \pi & y \geq 0, x < 0 \\ \arctan \frac{y}{x} - \pi & y < 0, x < 0 \\ +\pi/2 & y > 0, x = 0 \\ -\pi/2 & y < 0, x = 0 \\ \text{undefined} & y = 0, x = 0 \end{cases} \quad (3.7)$$

The time-varying non-turbulent wind velocity at time,  $t_n$ , i.e.,  $U(z, t_n)$ , and the wind directions,  $\theta_{hor}(z, t_n)$  and  $\theta_{ver}(z, t_n)$  at intervals equal to  $\Delta t$  may be found by applying the simple interpolation function, `Interp`, using computed values of  $U(z, t_p)$ ,  $\theta_{hor}(z, t_p)$ , and  $\theta_{ver}(z, t_p)$ .

$$U(z, t_n) = \text{Interp}(n\Delta t, t_p, U(z, t_p)) \quad (3.8)$$

$$\theta_{hor}(z, t_n) = \text{Interp}(n\Delta t, t_p, \theta_{hor}(z, t_p)) \quad (3.9)$$

$$\theta_{ver}(z, t_n) = \text{Interp}(n\Delta t, t_p, \theta_{ver}(z, t_p)) \quad (3.10)$$

where  $t_n = n\Delta t$  and  $n = 1, 2, \dots, 3600/\Delta t$ , corresponding to a wind velocity field output every second for one hour.

The zero-mean turbulent wind fields for Hurricane Sandy, i.e.,  $u'(z, t_n)$ ,  $v'(z, t_n)$ , and  $w'(z, t_n)$  are simulated using the original form of the Kaimal turbulence power spectral density functions (Kaimal et al. [31]); needed quantities such as the one-hour mean wind speed,  $U_m(z)$ , and friction velocity,  $u_m^*$ , are evaluated as follows using the six 10-minute interval WRF output variables,  $U(z, t_p)$  and  $u^*(t_p)$ , in each hour:

$$U_m(z) = \frac{1}{6} \sum_{p=1}^6 U(z, t_p) \quad (3.11)$$

$$u_m^* = \frac{1}{6} \sum_{p=1}^6 u^*(t_p) \quad (3.12)$$

Effectively, then,  $u_m^*$ , arising from the WRF output, scales the turbulence intensity during each hour of the simulation of the hurricane.

Finally, the “total” wind velocity field is computed by adding the time-varying non-turbulent wind field to the zero-mean turbulent wind field as follows:

$$u(z, t_n) = U(z, t_n) + u'(z, t_n) \quad (3.13)$$

$$v(z, t_n) = v'(z, t_n) \quad (3.14)$$

$$w(z, t_n) = w'(z, t_n) \quad (3.15)$$

Next, the wind velocities evaluated in Eqs. 3.13-3.15 are rotated relative to a fixed inertial reference frame coordinate system (defined at the wind turbine) by employing two transformation matrices,  $[T_{hor}]$  and  $[T_{ver}]$ . Thus, we have:

$$\begin{pmatrix} u_x \\ u_y \\ u_z \end{pmatrix} = [T_{hor}][T_{ver}] \begin{pmatrix} u \\ v \\ w \end{pmatrix} \quad (3.16)$$

where

$$[T_{hor}] = \begin{bmatrix} \cos \theta_{hor} & -\sin \theta_{hor} & 0 \\ \sin \theta_{hor} & \cos \theta_{hor} & 0 \\ 0 & 0 & 1 \end{bmatrix} \quad (3.17)$$

$$[T_{ver}] = \begin{bmatrix} \cos \theta_{ver} & 0 & -\sin \theta_{ver} \\ 0 & 1 & 0 \\ \sin \theta_{ver} & 0 & \cos \theta_{ver} \end{bmatrix} \quad (3.18)$$

and  $\theta_{hor}$  and  $\theta_{ver}$  are defined in Eqs. 3.9 and 3.10 for every time instant of interest,  $t_n$ .

The overall simulation procedure leading to full 4-D wind fields, presented in Fig. 3.9, is integrated into the open-source aeroelastic simulation program, FAST [32], by making use of the UserWind module there.

### 3.3.1 Mean Wind Field during Hurricane Sandy

The mean vertical wind profile for Hurricane Ike was estimated using the classical log law that was presented in Eq. 2.64. Such a logarithmic profile, which is commonly used to describe vertical wind shear, does not account for atmospheric stability effects. In contrast, because the WRF output provides wind field data at several elevations, we can directly use these data to obtain the mean wind shear for full wind field simulation during Hurricane Sandy. The WRF output for Hurricane Sandy provides mean wind field data at 6 different elevations up to 200 meters above the bottom surface; Fig. 3.10 shows the variation with time of the horizontal mean wind speed and the vertical mean wind speed. The vertical wind direction,  $\theta_{ver}(z, t_p)$ , is less than 2 degrees during the simulation. Even though the WRF output includes a vertical wind velocity component,  $U(z, t_p)$ , the magnitude of this component is very small as can be confirmed from Fig. 3.10.

In Fig. 3.11, the surface wind shear extracted from the WRF output is compared with the wind shear estimated by the classical log law (Eq. 2.64) which does not account for stability effects. The computed wind shear profile presented in Fig. 3.11 corresponds to a time, 40 hours after 00:00 UTC on October 28, 2012 and it applies to a 50-m water depth location at Site No. 1; this profile more closely resembles stable atmospheric boundary layer conditions with greater wind shear than in the log-law profile.

### 3.3.2 Turbulent Wind Field during Hurricane Sandy

In the present study, the Veers method [33], based on Fourier techniques, is utilized to generate a turbulent wind field (over the swept area of the offshore wind turbine rotor) that is comprised of three orthogonal zero-mean velocity components. To this turbulent wind field, the time-varying mean wind field, discussed previously, is added to yield the full wind field over the rotor that is needed for loads analyses. The required inputs for the Veers method are target turbulence power spectral density (PSD) functions and coherence functions; physical parameters in these target functions depend on the WRF output that changes every hour.

#### 3.3.2.1 Turbulence Power Spectral Density Functions

A power spectral density function describes the contribution to the variance of a stochastic process as a function of frequency; it has, for example, dimensions of [variable units]<sup>2</sup> per Hertz (Hz). Intuitively, then, the PSD function describes the frequency content of the stochastic process. In this study, the original Kaimal turbulence power spectra (Kaimal et al. [31]) are used as the basis for simulating the three orthogonal components of turbulence:

$$S_u(f) = \frac{105u_*^2z/U_{ref}}{(1 + 33fz/U_{ref})^{\frac{5}{3}}} \quad (3.19)$$

$$S_v(f) = \frac{17u_*^2z/U_{ref}}{(1 + 9.5fz/U_{ref})^{\frac{5}{3}}} \quad (3.20)$$

$$S_w(f) = \frac{2u_*^2z/U_{ref}}{1 + 5.3(fz/U_{ref})^{\frac{5}{3}}} \quad (3.21)$$

where  $S_u(f)$ ,  $S_v(f)$ , and  $S_w(f)$  (in (m/s)<sup>2</sup>/Hz) are one-sided power spectra for the longitudinal, transverse, and vertical wind velocity components, respectively. Also,  $f$  refers to the frequency of interest in Hertz (Hz),  $u_*$  is the friction velocity (in m/s),  $z$  is the elevation (in meters), and  $U_{ref}$  is a reference wind velocity (in m/s). For Hurricane Sandy,  $U_{ref}$  and  $u_*$ , needed to define the Kaimal power spectra are taken as  $U_m(z)$  and  $u_m^*$  as given by Eqs. 3.11 and 3.12, respectively. It should be noted that the modified Kaimal power spectra as specified in the IEC wind turbine design standard [22] are defined differently from the ones described above in Eqs. 3.19-3.21. One benefit of using the original Kaimal power spectra in Eqs. 3.19-3.21 instead of the IEC Kaimal spectra is that the parameters involved



depend only on physical quantities and they do not require any additional assumptions. With the IEC Kaimal spectra, a pre-determined longitudinal turbulence scale parameter,  $\Lambda_U$ , and reference turbulence intensity,  $I_{ref}$ , have to be assigned.

### 3.3.2.2 Turbulence Coherence Functions

The coherence function for any single turbulence component is a frequency-dependent measure of the correlation of that component at two spatially separated points. In this study, this coherence function is modeled as follows [34] :

$$Coh_{\varepsilon}(j, k, f, U_{jk}) = \exp \left[ -f \frac{[c_y^2(y_j - y_k)^2 + c_z^2(z_j - z_k)^2]^{1/2}}{0.5 [U_{ref}(z_j) + U_{ref}(z_k)]} \right] \quad (3.22)$$

where  $Coh_{\varepsilon}(j, k, f, U_{jk})$  is a dimensionless coherence function for each turbulence component of interest,  $\varepsilon$  (i.e.,  $u$ ,  $v$ , or  $w$ ), at locations,  $(y_j, z_j)$  and  $(y_k, z_k)$ , expressed as a function of frequency,  $f$ ; also,  $c_y$  and  $c_z$  are coherence decay parameters (dimensions:  $L^{-1}$ ) for lateral ( $y$ ) and vertical ( $z$ ) separations, respectively; for  $k = 1$ ,  $c_y = 10$  and  $c_z = 3$ , for  $k = 2$ ,  $c_y = 6.5$  and  $c_z = 3$  and for  $k = 3$ ,  $c_y = 3.0$  and  $c_z = 0.5$  [35]. Again,  $U_{ref}$ , needed to define the coherence functions is taken as  $U_m(z)$  as given by Eq. 3.11. The coherence functions together with the PSD functions are used to assemble the full-field frequency-dependent cross-power spectral density (CPSD) function matrix over the entire simulation domain covering the turbine's rotor; the Veers method provides a means to use this CPSD matrix to generate time series of the wind velocity over the rotor-swept area. Note that even though no coherence is considered between the orthogonal turbulence components, they are intrinsically correlated with each other in time through  $u_m^*$  resulting from the WRF model output.

## 3.4 Offshore Wind Turbine Response during Hurricane Sandy

An uncoupled modeling scheme is used to analyze the response of an offshore wind turbine with a jacket support structure as illustrated in Fig. 3.12. While in a coupled modeling approach, aerodynamic and hydrodynamic load effects are evaluated in a single computation step or software tool, an uncoupled modeling approach uses two separate software tools or computational steps to evaluate the aerodynamic and hydrodynamic load effects. The rotor aerodynamic forces are first evaluated in FAST, using a baseline wind turbine assumed fixed rigidly at the base. Aerodynamic loads evaluated at the nacelle (top of the tower) are applied as point loads in Abaqus [36] to a structural model of the tower and jacket support structure, which is also subjected to hydrodynamic forces resulting from waves and currents.

Unlike monopile-type support structures that have rotational symmetry due to their cylindrical sections, the orientation of its jacket support structure beneath affects the overall response of a wind turbine due to lack of rotational symmetry. Hence, as shown in Fig. 3.13, a combination of three separate considerations should be made in order to evaluate the response of the wind turbine with a jacket support structure during a hurricane. These three considerations are:

- (1) Support structure orientation,  $\theta_1$  (defined with regard to the wind direction),
- (2) Wind and wave misalignment,  $\theta_2$ ,
- (3) Yaw misalignment,  $\theta_3$ .

To simplify the analyses in this study, we assume that the support structure orientation,  $\theta_1$ , and the yaw misalignment,  $\theta_3$ , are each equal to zero. Thus, only wind-wave misalignment varies during the evolution or movement of the hurricane in our analyses. As mentioned earlier, we will present response evaluations of 1-hour duration, beginning at 00:00 UTC on October 28, 2012 (the start of the UCMC simulations). These response computations are repeated every 10 hours, beginning 10 hours after the start of the simulations and ending 60 hours after the start. The response computations are only for a Site No. 1, depicted in Fig. 3.5.

### 3.4.1 Turbine Model

All the investigations in this study are for a 5-MW offshore wind turbine with a jacket support structure as shown in Fig. 3.14. This is the same system used by the Offshore Code Comparison Collaboration Continuation (OC4) project (Phase I). The rotor nacelle assembly (RNA) of the OWT is that of the NREL 5-MW baseline turbine [37]. The jacket support structure has four legs, four levels of X-braces, and mudbraces. This support structure has been described in detail by Vorpahl et al. [38].

#### 3.4.1.1 OC4 Jacket Support Structure

The jacket support structure for the NREL 5-MW turbine is based on a reference design developed as part of the European Union's UpWind project [39]. The UpWind jacket is designed for a site with a water depth of 50 m. The jacket consists of four legs, four levels of X-braces, and mudbraces. The top and bottom widths of the jacket are 8 m and 12 m, respectively. A rigid concrete block with a weight of 660 tons and dimensions of 9.6 m (length)  $\times$  9.6 m (width)  $\times$  4 m (height) is positioned at the top of the jacket and serves as the transition piece (TP) or platform that connects the jacket with the tower of the baseline wind turbine. The geometric configuration and dimensions of the members of the OC4 jacket support structure are presented in Fig. 3.15. The jacket is made up of a medium-grade structural steel with a Young's modulus of 210 GPa. The density is assumed to be 8500 kg/m<sup>3</sup>, which accounts for paint, bolts, welds, and all other additional masses.

As marine growth can influence the overall loading and, thus, the dynamic behavior of the system, it is taken into consideration in the model described herein as per DNV guidelines [40] and as given by Fisher and Kuehn [41]. The depth range with respect to the mean sea level (MSL) over which to consider marine growth is  $-40 \leq z_g(\text{m}) \leq -2$ , its thickness,  $t_g$ , is 100 mm, and its density,  $\rho_g$ , is 1,100 kg/m<sup>3</sup>. The legs of the jacket structure are assumed to be flooded by sea water with density,  $\rho_w$ , equal to 1,025 kg/m<sup>3</sup>; the braces are not assumed flooded.

There is a grouted connection between the piles and the jacket legs as shown in Fig. 3.16. The bottom of the grouted connection is at  $z = -49.5$  m and the upper end of the grout is at  $z = -45.5$  m. The properties of the legs at the lowest level (Level 4) and the piles are included in Fig. 3.15. The density of the grout material between the two steel parts,  $\rho_G$ , is assumed to be 2,000 kg/m<sup>3</sup>. As the stiffness of the two steel members together with the grout material is very high, the grouted part from MSL  $-49.5$  m to MSL  $-45.5$  m (including pile, leg, and grout) is modeled as rigid in Abaqus. The embedded length of the pile is assumed to be 47 m.

As shown in Fig. 3.17, the Abaqus model used in this study consists of a tower top mass, a tower, a transition piece, and the jacket structure. All the separate parts in the model are connected via kinematic coupling constraints in Abaqus. The rotor nacelle assembly (RNA) including the hub is modeled as a nodal mass without rotary inertia and the transition piece between the baseline turbine and the jacket structure is modeled as a rigid body, where the 660 tons dead load of this transition piece is modeled as a rectangular body with the dimensions of 9.6 m (length)  $\times$  9.6 m (width)  $\times$  4 m (height). Because the purpose of this study is not to evaluate localized stress concentration at member joints or local buckling of members, all the jacket members are modeled using Euler-Bernoulli beam elements.

In this study, member forces and reaction forces at a total of 13 locations (referred to as "sensor locations") are evaluated. Figure 3.18 provides detailed information on these sensor location. The structural response of braces and legs are evaluated with respect to the member (local) coordinate system; for axial forces, positive values imply tensile forces while negative values imply compressive forces.

#### 3.4.1.2 Verification of the Abaqus Model

The Abaqus model is verified by comparison with the study presented by Popko et al. [42], which includes results from the IEA Wind Task 30 OC4 Project Phase I, which was focused on the coupled simulation of an offshore wind turbine with a jacket support structure. In the verification studies with our model, it is assumed that the jacket structure is cut and clamped or fixed at the mudline.

### Comparison of Masses

Before comparing the wind turbine or support structure response with any other studies, we first consider the structural mass as well as all additional mass in the model. This is done in Table 3.4. Structural mass includes the jacket, transition piece, tower, and rotor-nacelle assembly (RNA), while additional mass includes marine growth and water in the flooded legs. In general, a very good agreement is observed when our model is compared with that in Popko et al. [42].

**Table 3.4. Comparison of structural and additional mass in our Abaqus model with that in Popko et al. [42].**

	Structural Mass (kg)				Additional mass (kg)		Total
	RNA	Tower	TP	Jacket	Flooded Leg	Marine Growth	
Abaqus Model	350	216	660	674	204	180	2290
Popko et al. [42]	350	220	660	677	200	177	2290
Difference	0	-4	0	-3	+4	+3	0

### Comparison of Natural Frequencies

An eigenvalue analysis is performed to obtain natural frequencies based on our Abaqus model, which are then compared with the natural frequencies evaluated with an Ansys model used by Song et al. [43]. The natural frequencies for the Abaqus and Ansys models are presented in Table 3.5. Generally, values from the two models are in a good agreement with each other. Small discrepancies are expected as the two models include a different number of degrees of freedom (DOF) and somewhat dissimilar structural modeling assumptions. As shown in Fig. 3.19, Popko et al. [42] also provides eigenvalue analysis results based on various OWT modeling codes used as part of the OC4 project. Eigenfrequencies of the first and second global fore-aft and side-to-side modes in the figure are very close to eigenfrequencies for the same modes determined using our Abaqus model.

**Table 3.5. Natural frequencies of the OC4 wind turbine system.**

Mode	Natural frequencies (Hz)		
	Ansys (Song et al.)	Abaqus (this study)	Difference (%)
1	0.3190	0.3333	4.4
2	0.3190	0.3333	4.4
3	1.1936	1.2155	1.8
4	1.1936	1.2155	1.8
5	3.4425	3.3643	2.2
6	4.1253	4.4354	7.5
7	4.1253	4.4354	7.5
8	5.3391	5.3242	0.2
9	6.6953	6.6084	1.2
10	6.6953	6.6084	1.2

### Comparison of Turbine Response

As further verification of the Abaqus model, we consider two response measures under regular wave loading: (1) the fore-aft shear force at the base of the jacket structure; and (2) the out-of-plane displacement (i.e., in the fore-aft direction,  $x$ ) of the central joint of the X-brace at Level 2 on Side 2 (S2) (see Fig. 3.15). Our response calculations are compared with those presented in Popko et al. [42].

First, the fore-aft shear force is evaluated for the offshore wind turbine excited using a regular Airy wave ( $H = 6$  m,  $T = 10$  sec). As shown in Fig. 3.20, good agreement is seen for the evaluated fore-aft force between our model and others reported in Popko et al. [42]. Next, the out-of-plane displacement (effectively, in the fore-aft direction) is

considered for the offshore wind turbine excited by a regular 9<sup>th</sup>-order stream function wave ( $H = 8$  m,  $T = 10$  sec). In Fig. 3.21, the surface wave elevation resulting from using this stream function is compared with the surface wave elevation based on Airy wave theory used with our Abaqus model (the wave profiles for the 9<sup>th</sup>-order stream function and the Airy theory cases are very similar). Figure 3.22 shows that the X-brace out-of-plane displacement evaluated from our Abaqus model (thick black line) matches well with results presented in Popko et al. [42].

### 3.4.1.3 Modeling Soil-Pile Interaction

Because the interaction between the soil and the embedded pile changes the dynamic characteristics of wind turbine, this interaction effect is considered in our Abaqus model of the jacket support structure. In our model, this interaction is represented by a  $p$ - $y$  curve model specified in the American Petroleum Institute (API) RP2A guidelines [44]. The  $p$ - $y$  curve method for designing offshore pile foundations has been utilized by the offshore oil and gas industry for decades and is based largely on work performed in the early 1970s [45, 46]. The method approximates the stiffness of the soil-pile system by a number of discrete nonlinear soil springs arranged along the length of the pile. These springs act independently of one another and therefore do not affect the displacement of neighboring springs. The lateral resistance of the pile is represented by  $p$ - $y$  curves, with “ $p$ ” representing the lateral resistance and “ $y$ ” representing the lateral displacement of the pile. The soil profile assumed for the design of the OC4 Jacket [39] is used to evaluate the lateral soil stiffness characteristics and is presented in Table 3.6.

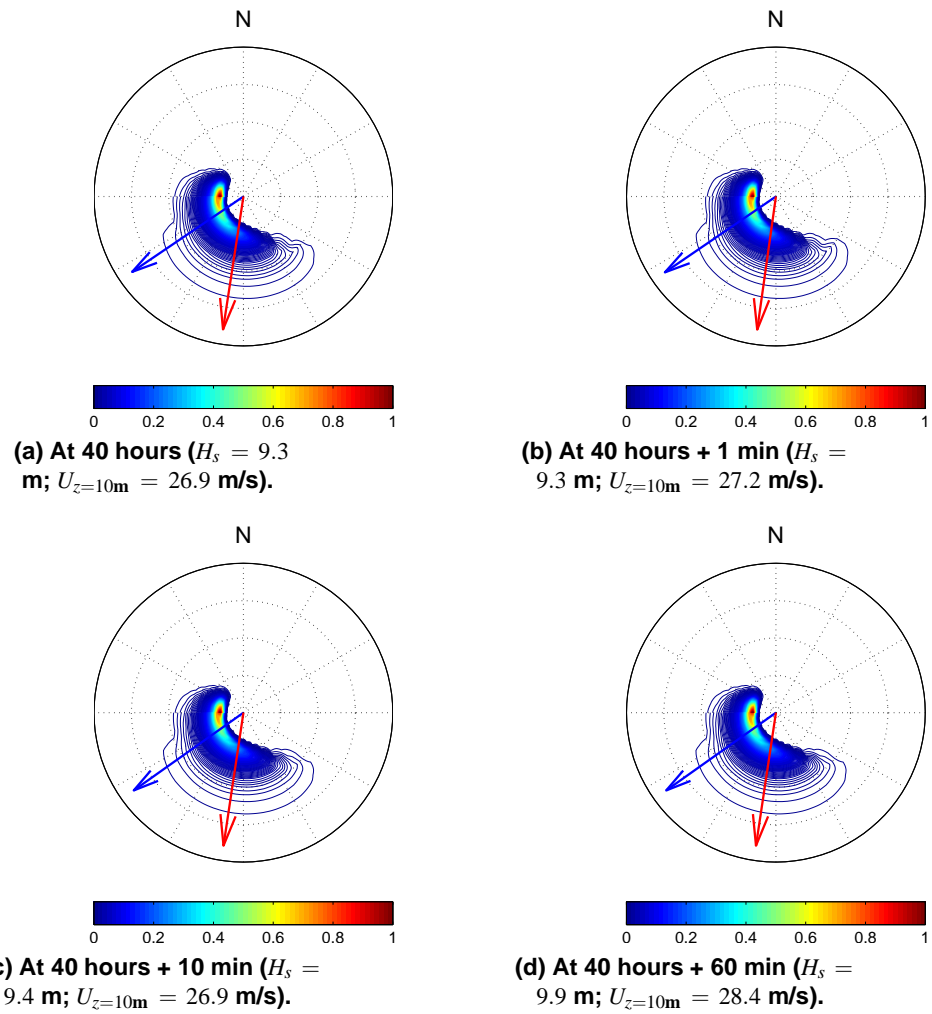


**Figure 3.6. Variation with time of Hurricane Sandy wave spectra (at and after 40 hours) at the location of Site No. 1 with 50-m water depth (blue arrow: wave direction; red arrow: wind direction). Only very small changes are seen over one hour.**

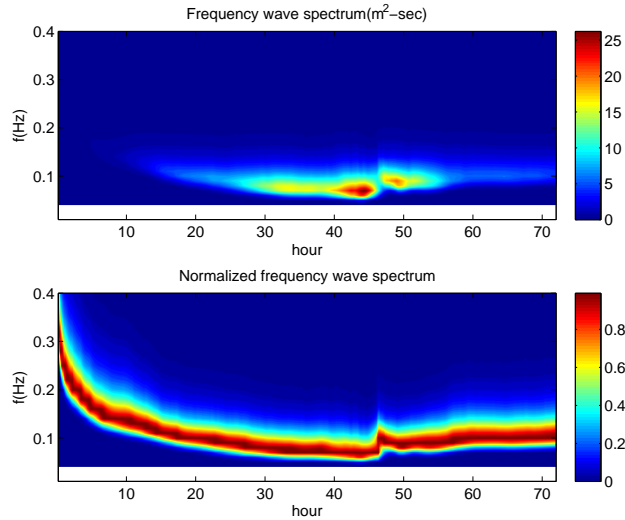


**Figure 3.7. Variation with time of the frequency-dependent wave spectrum during Hurricane Sandy (at the location of Site No. 1 with 50-m water depth. Normalization to unity with variation in time is also shown.)**

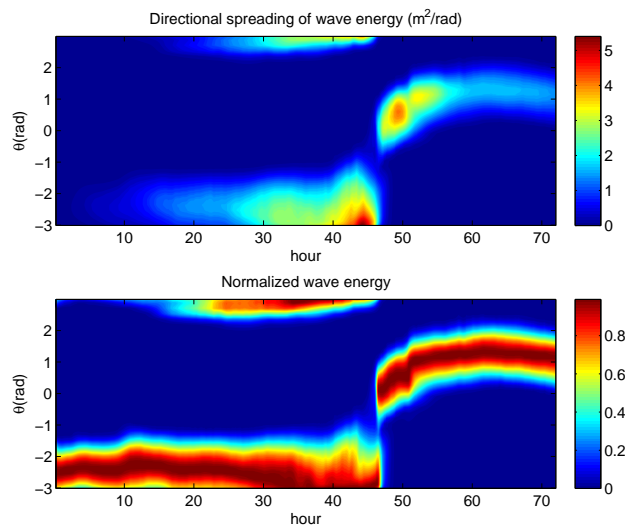


**Figure 3.8. Variation with time of the directional-dependent wave spreading function during Hurricane Sandy (at the location of Site No. 1 with 50-m water depth. Normalization to unity with variation in time is also shown.)**

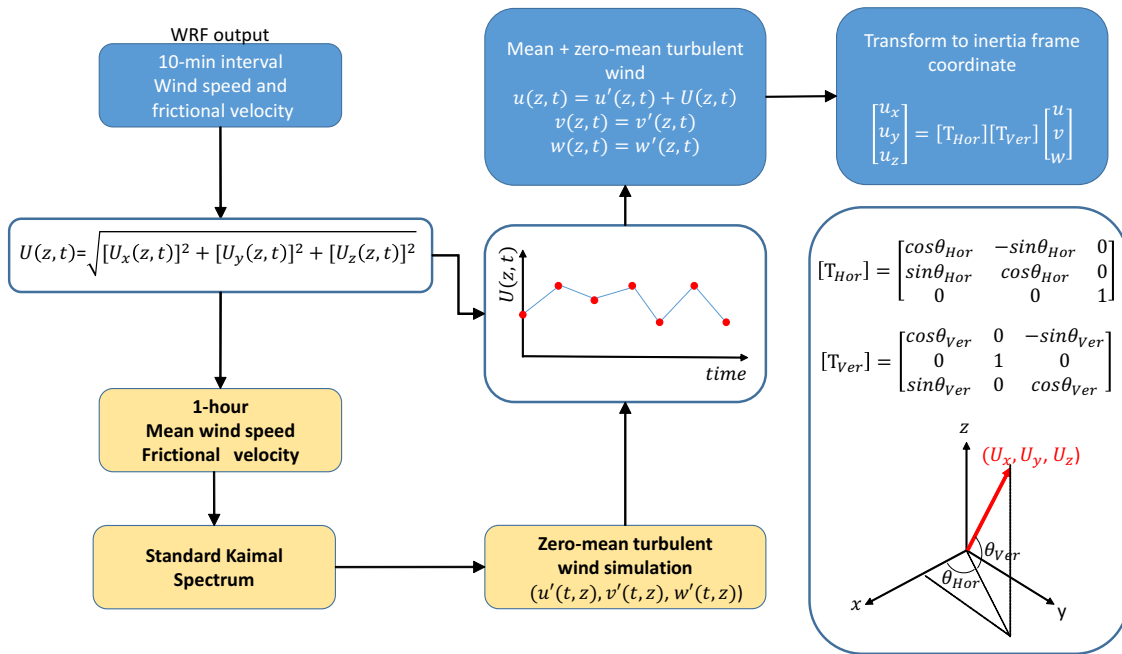


Figure 3.9. Procedure for simulation of the turbulent wind field during Hurricane Sandy.

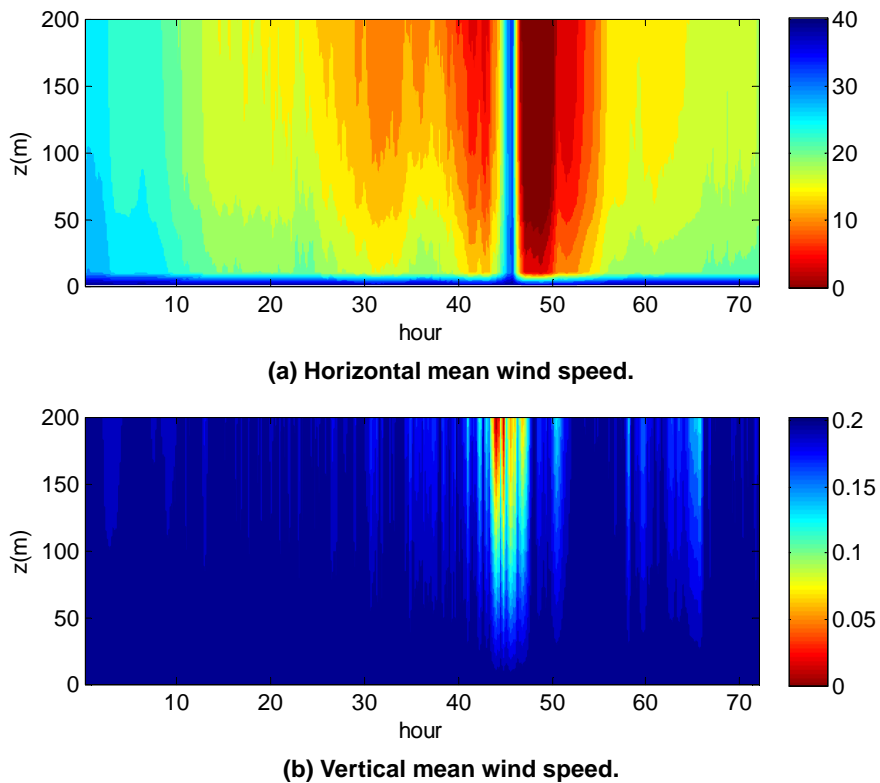


Figure 3.10. Variation with time of the horizontal mean wind speed and the vertical mean wind speed (at the location of Site No. 1 with 50-m water depth).

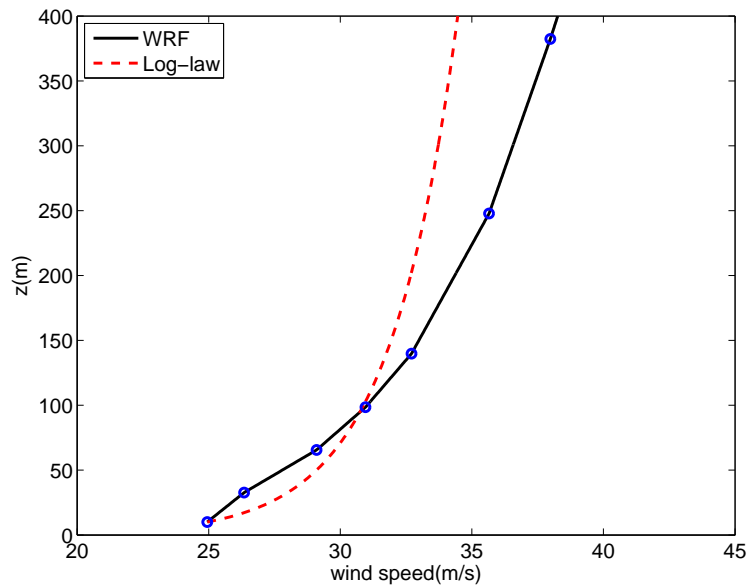


Figure 3.11. Mean wind shear interpolated from the WRF output for Hurricane Sandy versus that estimated by the classical log law (corresponding to the time, 40 hours, and at Site No. 1).

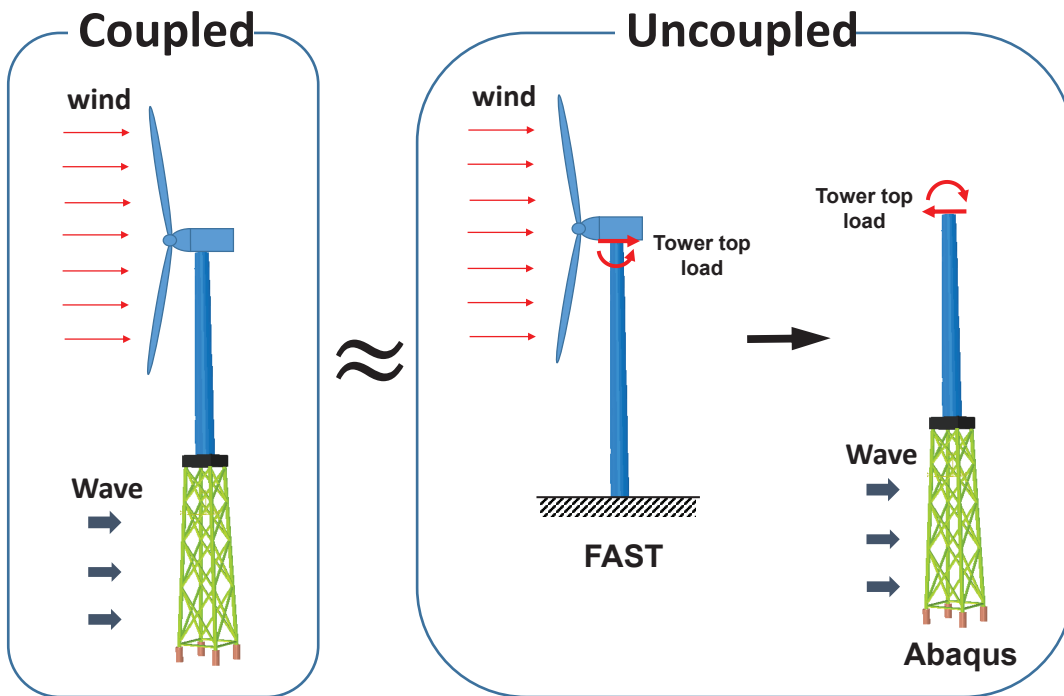
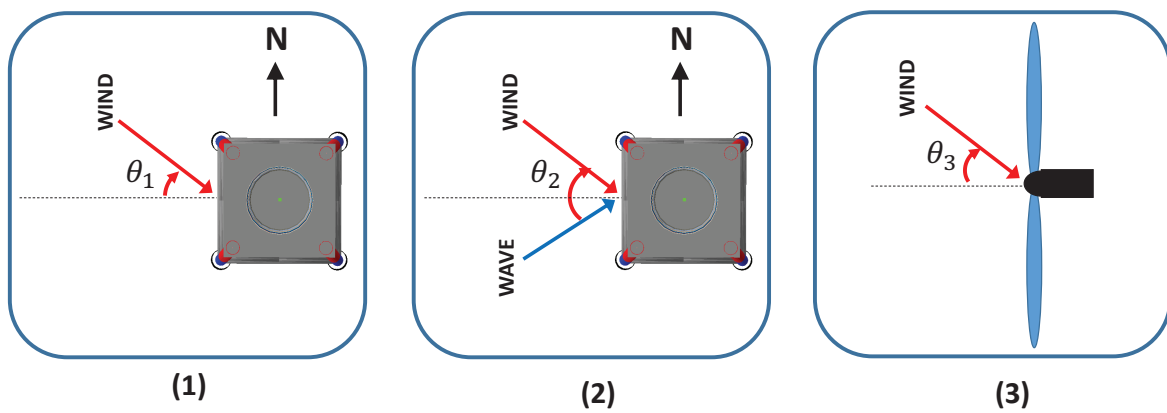


Figure 3.12. Coupled and uncoupled modeling approach for an offshore wind turbine with a jacket support structure.





**Figure 3.13. Three considerations in evaluating the response of a jacket-type structure supporting an offshore wind turbine.**

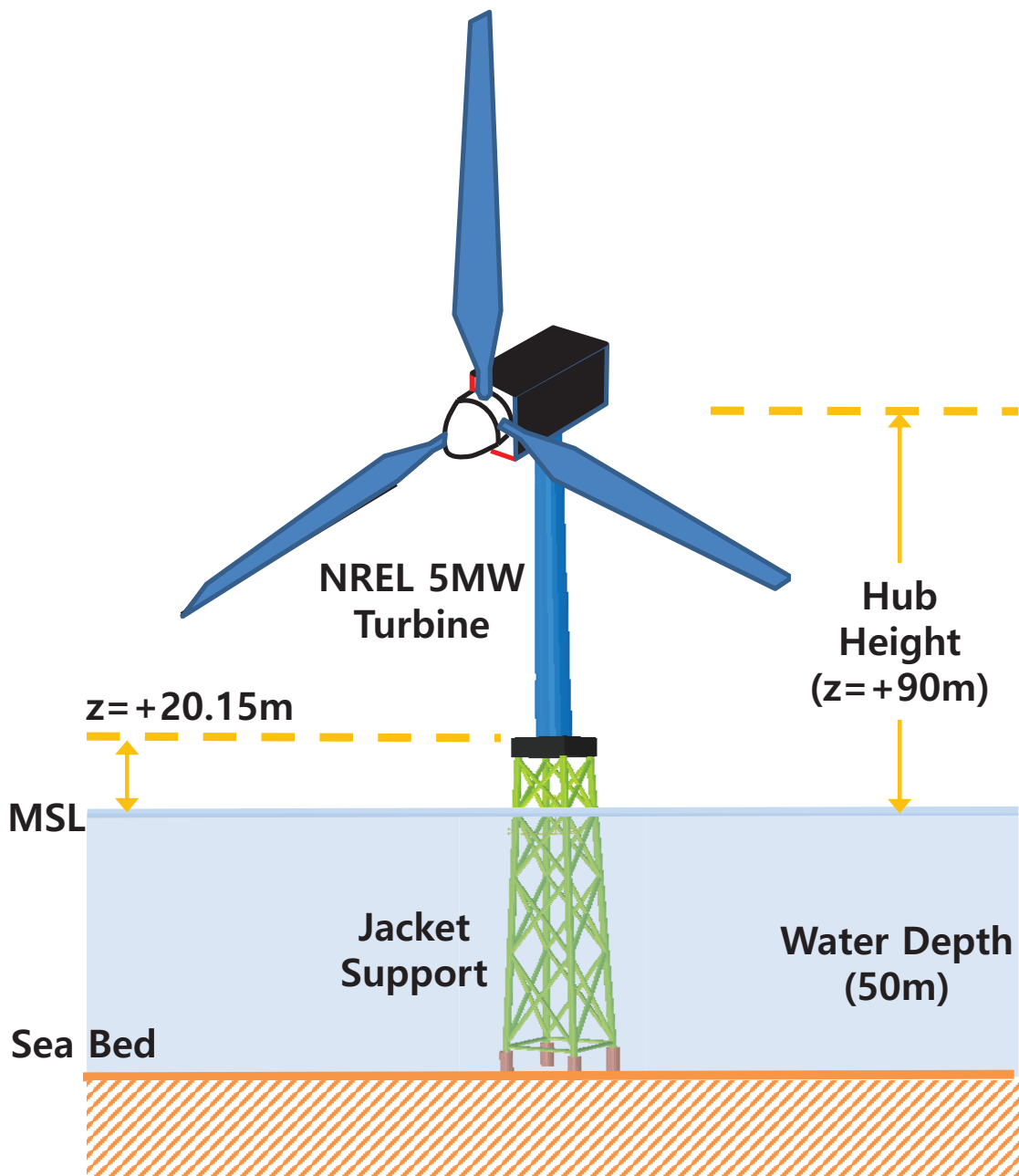


Figure 3.14. Schematic diagram of the jacket-supported NREL 5-MW wind turbine model.

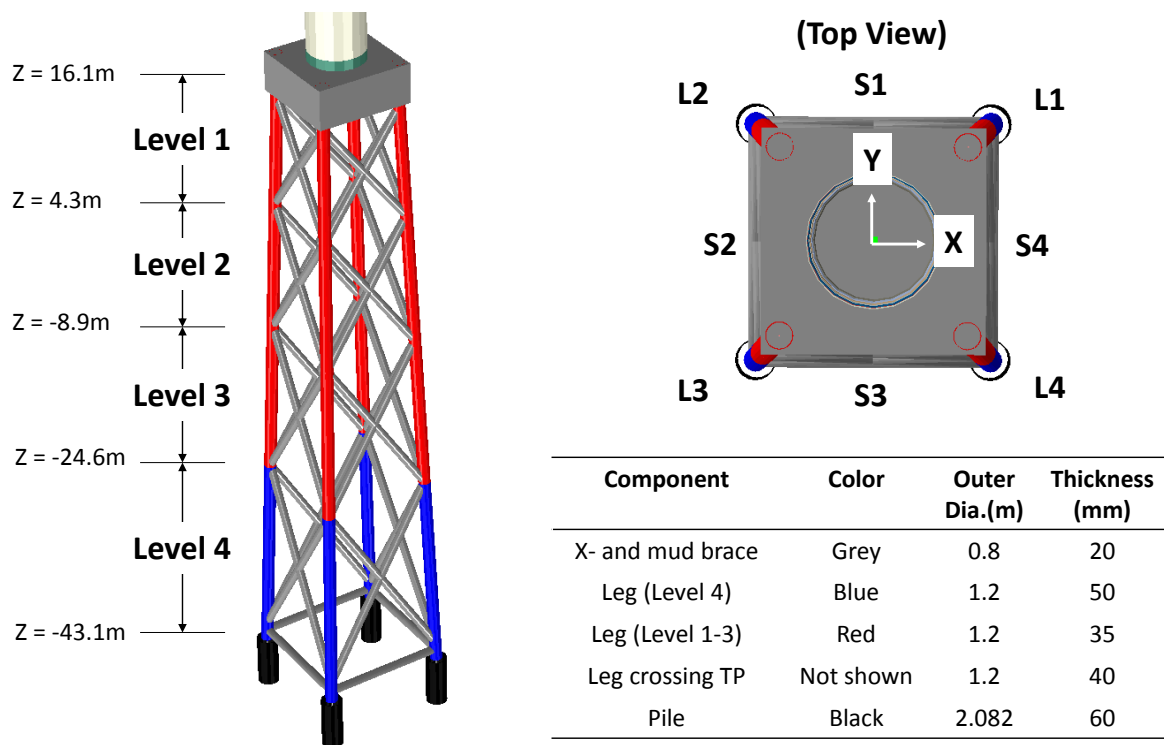


Figure 3.15. Geometric configuration and dimensions of members of the OC4 jacket support structure.

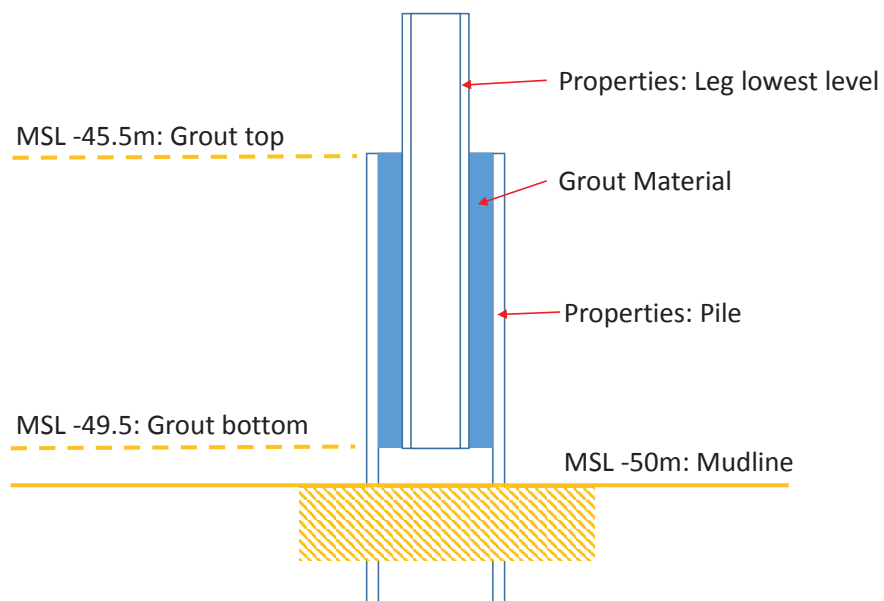


Figure 3.16. Grouted leg and pile connection for the jacket support structure.

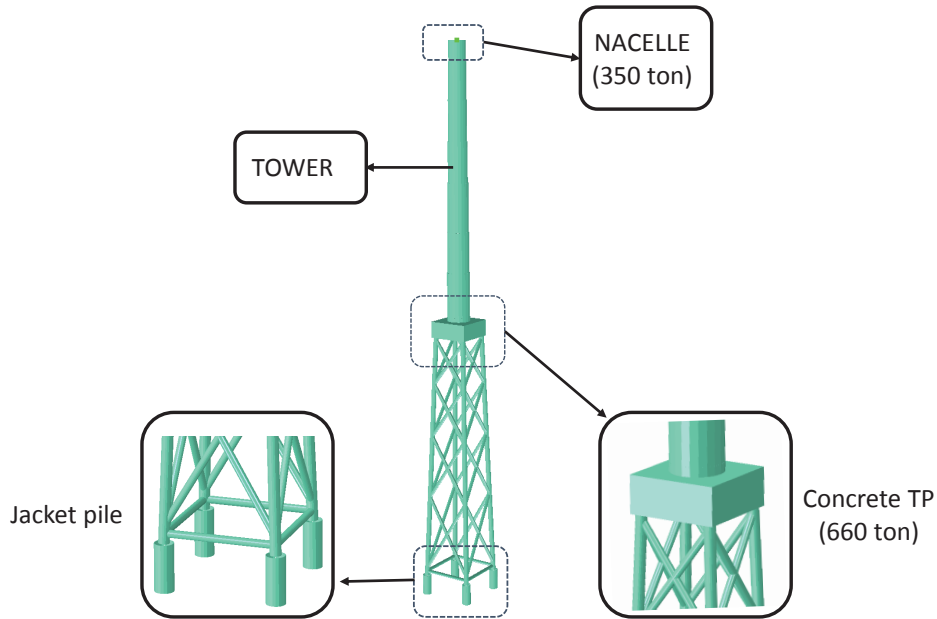


Figure 3.17. Abaqus modeling of the OC4 reference jacket structure used in this study.

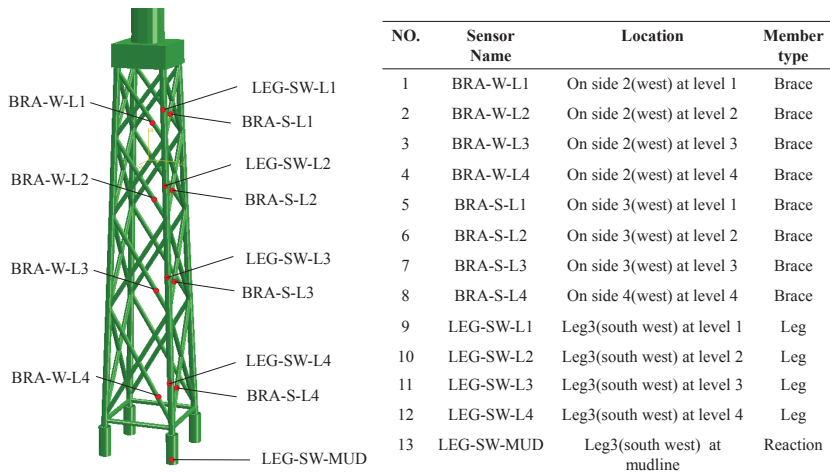


Figure 3.18. Sensor names and locations for the dynamic response analyses of the offshore wind turbine and jacket support structure.

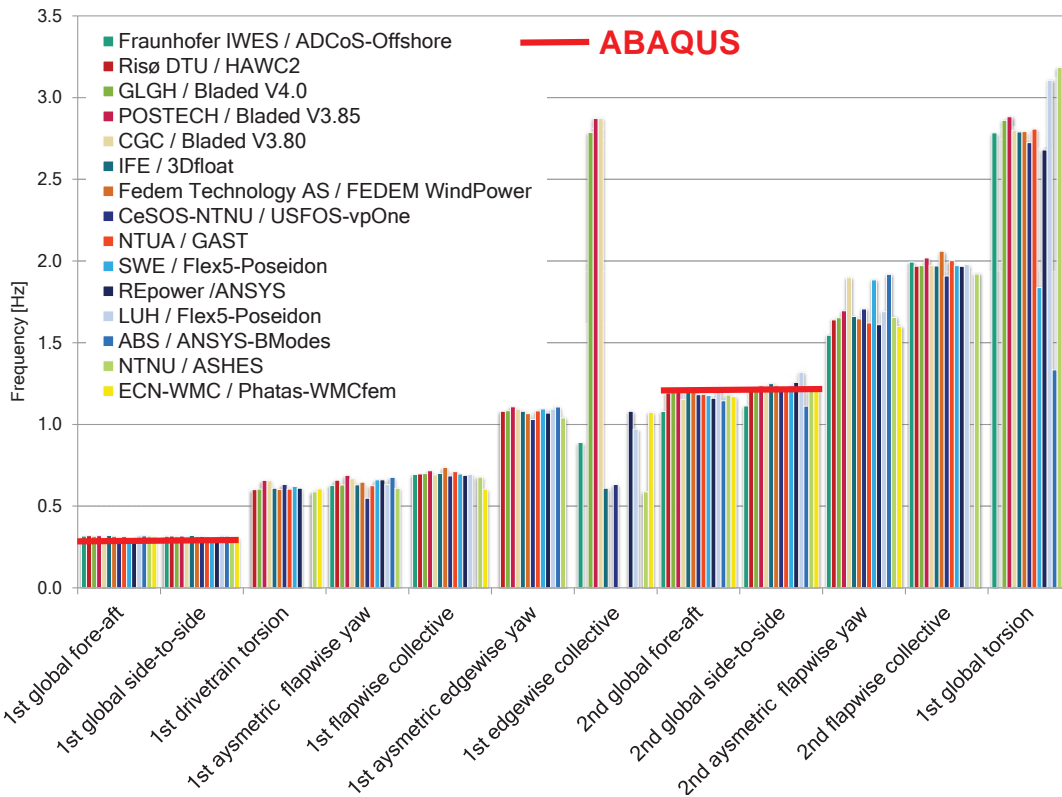


Figure 3.19. Natural frequencies based on various OWT modeling codes [42].

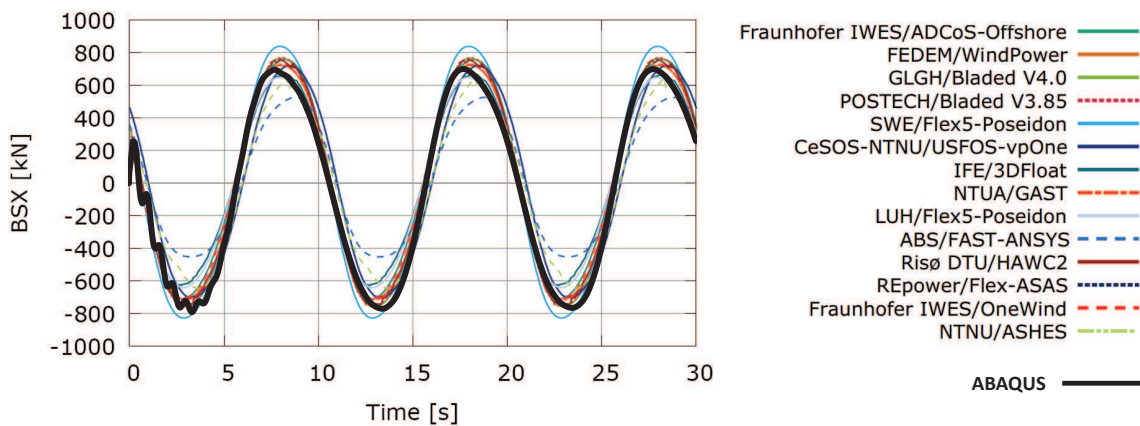


Figure 3.20. Fore-aft shear force at the mudline for our Abaqus model and comparison with results presented in Popko et al. [42].

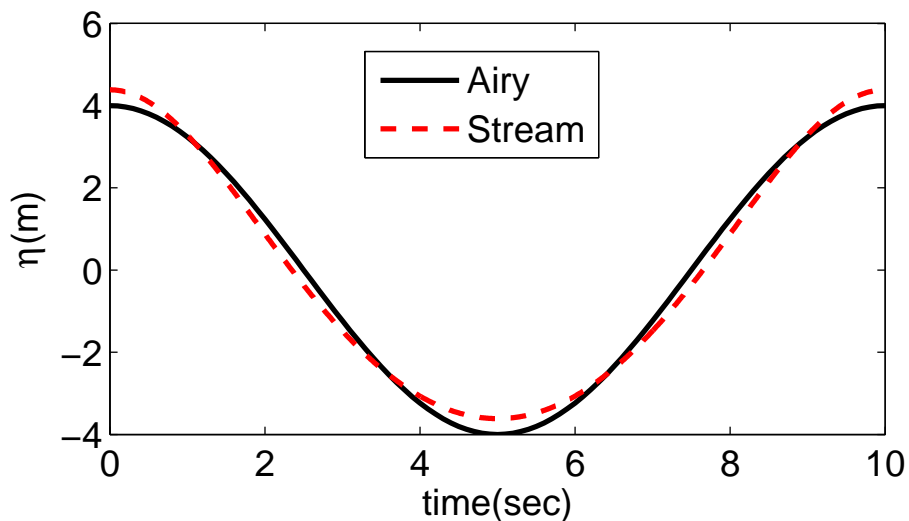


Figure 3.21. Surface wave elevation evaluated using Airy theory and a 9<sup>th</sup>-order stream function approach.

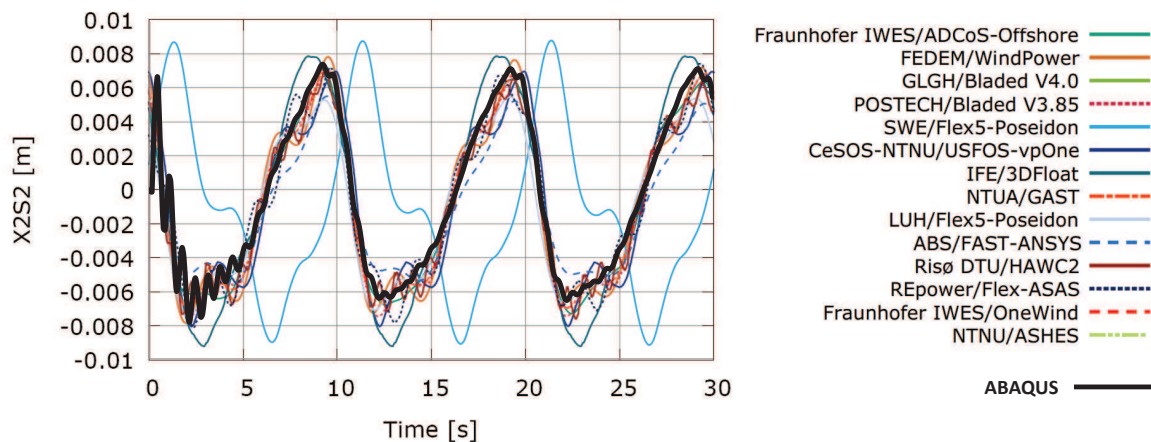


Figure 3.22. Out-of-plane deflection at center of X-brace at Level 2 on Side 2 of our Abqaus model and comparison with results presented in Popko et al. [42].

**Table 3.6. Soil properties assumed for the jacket support structure [39].**

Depth (m)	Soil type	$\gamma'$ (kN/m <sup>3</sup> )	$\phi$ (deg)	$c_u$ (kPa)	$\epsilon_{50}$ (%)
0-3	SAND	10	36.0		
3-5	SAND	10	36.0		
5-7	CLAY	10		60.0	0.7
7-10	SAND	10	37.0		
10-13	SAND	10	35.0		
13-15	SAND	10	35.0		
15-18	SAND	10	37.5		
18-47	SAND	10	37.5		

$\gamma'$ : effective soil weight  
 $\phi$ : angle of internal friction  
 $c_u$ : undrained shear strength  
 $\epsilon_{50}$ : strain that occurs at one-half of the maximum stress in laboratory undrained compression test

**Table 3.7. Development of sand  $p$ - $y$  curves [44].**

1. Theoretical ultimate bearing capacity for wedge failure, $p_{us}$	$p_{us} = (C_1z + C_2D)\gamma'z$
2. Theoretical ultimate bearing capacity for flow failure, $p_{ud}$	$p_{ud} = C_3D\gamma'z$
3. Governing ultimate bearing capacity, $p_u$	$p_u = \min(p_{us}, p_{ud})$
4. Develop $p$ - $y$ curve	$p = Ap_u \tanh\left(\frac{kz}{Ap_u}y\right)$

$D$ : Average pile diameter from surface to depth  
 $A$ : Factor to account for cyclic loading condition (take  $A = 0.9$ )  
 $C_1, C_2,$  and  $C_3$ : Coefficients determined from Figure 6.8.6-1 in API [44]  
 $k$ : Initial modulus of subgrade reaction determined from Figure 6.8.7-1 in API [44]

In the API guidelines,  $p$ - $y$  curves for sand and clay are developed using the procedures presented in Tables 3.7 and 3.8, respectively. Figures 3.23a and 3.23b present characteristic shapes of the  $p$ - $y$  curves for sand and clay, respectively. In our Abaqus model, the lateral stiffness of the soil is modeled using a nonlinear spring element, SPRING1. Table 3.9 shows the effect of soil-structure interaction on the eigenfrequencies of the model; consideration of soil-structure interaction (SSI) effects leads to noticeable reduction in the system natural frequencies.

### 3.4.2 Hydrodynamic Loads and Associated Response on Jacket Members during Hurricane Sandy

The hydrodynamic loading experienced by a jacket member is comprised of drag and inertia force components. Morison's equation is used to compute the hydrodynamic load per unit member length,  $\Delta f$ , as follows:

$$\Delta f = \Delta f_D + \Delta f_M = \frac{1}{2}C_D\rho D u_r |u_r| + \frac{\pi D^2}{4}C_M\rho_w \dot{u}_r \quad (3.23)$$

where  $\Delta f_D$  and  $\Delta f_M$  are the drag and inertia forces per unit length, respectively,  $C_D$  is the drag coefficient taken as 1.0, and  $C_M$  is the inertia coefficient taken as 2.0. Also, in Eq. 3.23,  $u_r$  and  $\dot{u}_r$ , respectively, are the "relative" velocity and acceleration (accounting for the motions of the water particles and the structure),  $\rho_w$  is the density of water, and

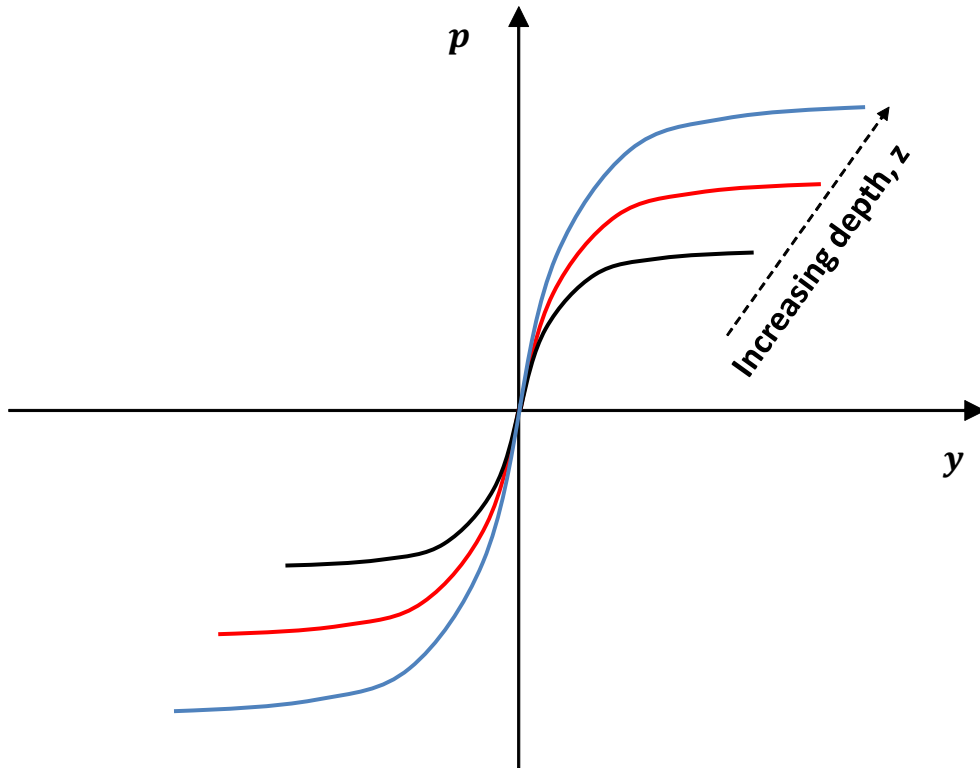
**Table 3.8. Development of clay  $p$ - $y$  curves [44].**

Static Loading	
1. Compute ultimate soil resistance, $p_u$	$p_{u1} = \left[ 3 + \frac{\gamma'}{c_u}z + \frac{J}{D}z \right] c_u D$ $p_{u2} = 0.9c_u D$ $p_u = \min(p_{u1}, p_{u2})$
2. Compute deflection at one-half the ultimate soil resistance, $y_{50}$	$y_{50} = 2.5\varepsilon_{50}D$
3. Develop $p$ - $y$ curves	$\frac{p}{p_u} = 0.5 \left( \frac{y}{y_{50}} \right)^{1/3}$
Dynamic Loading	
1. Develop $p$ - $y$ curves	Construct $p$ - $y$ curve in the same manner as for static loading for values of $p < 0.72p_u$
2. Determine transition depth, $z_r$	$z_r = \frac{6c_u D}{\gamma' D + Jc_u}$
3. If depth $z \geq z_r$	$p = 0.72p_u \text{ for } y > 3y_{50}$
4. If depth $z < z_r$	$p = 0.72p_u \text{ at } y = 3y_{50}$ $p = 0.72p_u \left( \frac{z}{z_r} \right) \text{ at } y = 15y_{50}$

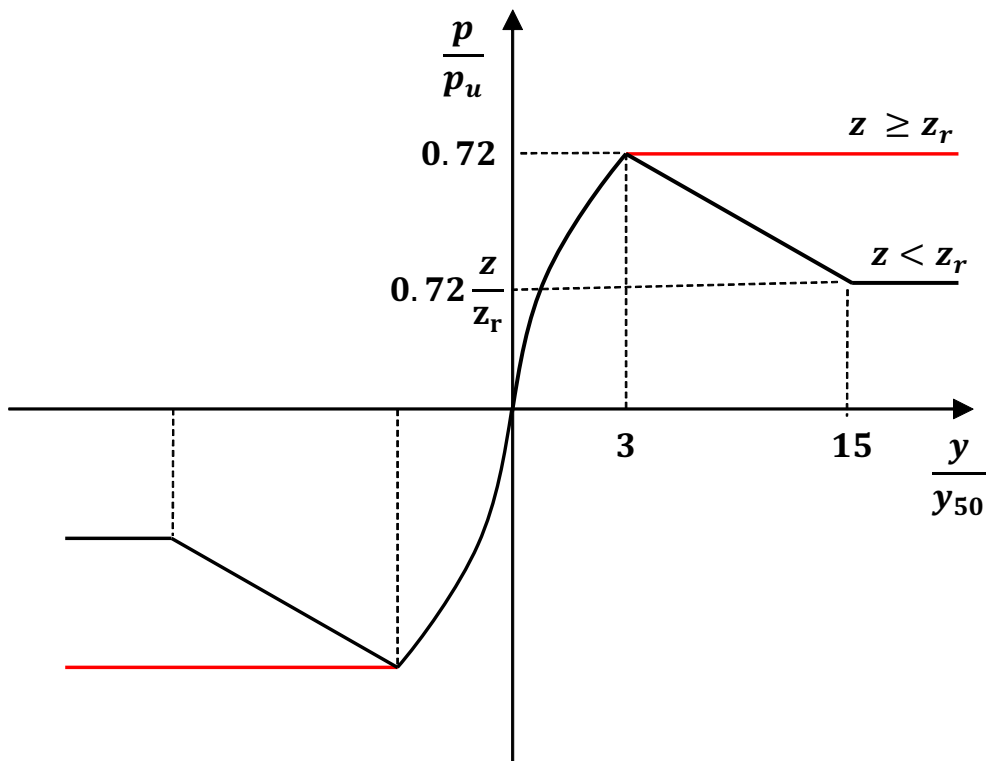
**Table 3.9. Variation of system natural frequencies under different foundation modeling assumptions.**

Mode	Natural frequencies (Hz)		
	Abaqus (clamped at mudline)	Abaqus (including SSI)	Difference [%]
1	0.3333	0.3053	8.4
2	0.3333	0.3053	8.4
3	1.2155	0.9592	21.0
4	1.2155	0.9592	21.0
5	3.3643	2.3932	28.8
6	4.4354	3.4427	22.3
7	4.4354	3.4427	22.3
8	5.3242	4.7326	11.1
9	6.6084	5.1140	22.6
10	6.6084	5.1140	22.6





(a) Representative  $p$ - $y$  curves for sand.



(b) Representative  $p$ - $y$  curve for clay.

Figure 3.23. Characteristic Shapes of the  $p$ - $y$  curves used in this study.

$D$  is the diameter of the jacket member. In the case of linear Gaussian waves, the inertia force in Morison’s equation is a Gaussian process as it is a linear of the water particle acceleration which is a Gaussian process; the drag force, however, is a non-Gaussian process as it is a nonlinear function of the water particle velocity.

We are interested in the response of the jacket support structure as various locations—braces, legs, and at the mudline. The four response measures that we consider here are: axial force in brace, **BRA-W-L4**; axial force in leg, **LEG-SW-L4**; vertical reaction force,  $F_z$ , at mudline, **LEG-SW-MUD**; and bending moment,  $M_y$ , at mudline, **LEG-SW-MUD**. Refer to Fig. 3.18 which helps to identify these response variables and their locations on the jacket structure. Response statistics are for hydrodynamic loading alone and apply to a single hour during Hurricane Sandy for the wind turbine at Site No. 1.

Table 3.10 summarizes response statistics considering hydrodynamic drag and inertia loads separately as well as in combined (total) effect. Based on an estimate of the number of upcrossings of the mean of the response process, one can compute a theoretical peak factor for response extremes, assuming the process were Gaussian [47]. As shown in Table 3.10 for the axial force in brace, **BRA-W-L4**, the response due to inertia forces has skewness close to zero, kurtosis close to 3, and peak factor close to the corresponding Gaussian peak factor—all of these findings are in line with expected Gaussian characteristics of the response due to inertial load effects alone. Similar observations can be made as well for the other response measures’ statistics under inertia loads, as can be seen in Tables 3.11, 3.12, and 3.13. In contrast, the response due to drag forces has a significantly higher kurtosis and a peak factor larger than the corresponding Gaussian peak factor—therefore, the response due to drag forces is clearly strongly non-Gaussian.

**Table 3.10. Statistics of the axial force in a brace, **BRA-W-L4**, due to hydrodynamic loading during Hurricane Sandy (corresponding to 50 hours after 00:00 UTC on October 28, 2012).**

	Axial force in a brace member, <b>BRA-W-L4</b>		
	drag	inertia	total
Mean (kN)	212	162	210
Max (kN)	1053	668	1100
Min (kN)	-1334	-1084	-1499
SD (kN)	271	299	403
Skewness	0.31	-0.10	0.16
Kurtosis	6.62	2.79	3.35
Peak Factor (PF) <sup>1</sup>	4.66	3.08	3.25
PF (Gaussian) <sup>2</sup>	2.97	3.02	3.00

<sup>1</sup> PF = Maximum(|Max – Mean|, |Min – Mean|)/SD

SD = standard deviation

<sup>2</sup> Peak factor evaluated from the mean upcrossing rate of the process, assuming it were Gaussian

Agarwal [48] studied the relative importance of drag and inertia forces to the tower base bending moment of an offshore wind turbine supported by a monopile, which was a cylinder of 6 m diameter installed in 20 meters of water. It was found in that study that the response due to hydrodynamic loading was dominated by inertia forces and the response was close to a Gaussian process. However, the OC4 reference jacket support structure used in the present study is composed of brace members of 1.0 m diameter and leg members of 1.2 m diameter, which are much smaller sized sections than the monopile studied by Agarwal [48]. Thus, the relative contribution of drag to inertia forces toward the total response is greatly increased in our study. From Tables 3.10, 3.11, 3.12, and 3.13, it is clear that inertia and drag force effects are of comparable importance for all the response variables studied. The ratios of the maximum response due to drag loads alone to the maximum response due to inertia loads alone are about 1.23, 1.00, 0.90, and 1.33, respectively, for the brace axial force (**BRA-W-L4**), the leg axial force (**LEG-SW-L4**), the vertical reaction force at mudline ( $F_y$  at **LEG-SW-MUD**), and the bending moment at mudline ( $M_y$  at **LEG-SW-MUD**); the corresponding ratios for the response standard deviation are about 0.91, 0.92, 0.98, and 0.90, respectively.

**Table 3.11. Statistics of the axial force in a leg, **LEG-SW-L4**, due to hydrodynamic loading during Hurricane Sandy (corresponding to 50 hours after 00:00 UTC on October 28, 2012).**

	Axial force in a leg, <b>LEG-SW-L4</b>		
	drag	inertia	total
Mean (kN)	-3237	-3110	-3231
Max (kN)	629	-1394	853
Min (kN)	-5332	-5319	-5760
SD (kN)	533	577	781
Skewness	1.12	-0.17	0.47
Kurtosis	10.05	3.05	4.33
Peak Factor(PF)	7.26	3.83	5.23
PF (Gaussian)	3.02	3.06	3.03

**Table 3.12. Statistics of the vertical reaction force,  $F_z$ , at the mudline, **LEG-SW-MUD**, due to hydrodynamic loading during Hurricane Sandy (corresponding to 50 hours after 00:00 UTC on October 28, 2012).**

	Vertical reaction force at mudline, <b>LEG-SW-MUD</b>		
	drag	inertia	total
Mean (kN)	-3330	-3575	-3326
Max (kN)	3024	-467	3501
Min (kN)	-5877	-6538	-6409
SD (kN)	874	890	1259
Skewness	2.22	-0.08	0.99
Kurtosis	12.88	3.44	5.87
Peak Factor(PF)	7.27	3.49	5.42
PF (Gaussian)	3.01	3.05	3.02

We note from the preceding results that although the drag and inertia contributions to the different response variables are comparable, the response due to the combined or total hydrodynamic load effects, accounting for drag and inertia, depends on the location and type of the evaluated response. For example, for axial force evaluated in a brace (**BRA-W-L4**) and for the mudline reaction moment,  $M_y$  (at **LEG-SW-MUD**), the computed response extreme peak factors are quite close to the peak factors theoretically estimated based on the assumption of a Gaussian response process. This implies that the 1-hour maximum values of these two response variables during Hurricane Sandy can be estimated based on Gaussian response assumptions. In contrast, the computed response extreme peak factors for the axial force in a leg (**LEG-SW-L4**) and for the mudline vertical reaction force,  $F_z$  (at **LEG-SW-MUD**) are significantly higher than the corresponding Gaussian peak factors.

### 3.4.3 Effect of Hurricane-Induced Currents

For the case of a monopile-supported offshore wind turbine, because the contribution of drag loads to the total hydrodynamic loads is insignificant as was shown by Agarwal [48], we might expect that the contribution of wave currents to the total response would also be negligible in that case. In the present study, we know that drag load effects for the OC4 jacket support structure are of comparable importance to the inertia load effects. Since the drag load effects must include the contribution from ocean currents, we are interested in learning to what extent these currents influence the total response.

For Hurricane Sandy, available depth-dependent ocean current velocities from HYCOM are vectorially combined with the wave particle velocities before computing drag forces. Figure 3.24 shows the variation with time of the ocean current velocities, evaluated by post-processing HYCOM output at Site No. 1, during the UMCM simulation of Hurricane Sandy. Figure 3.25 shows how the ocean current velocity components,  $u_{cx}$  and  $u_{cy}$ , influence the

**Table 3.13. Statistics of the bending moment,  $M_y$ , at the mudline, **LEG-SW-MUD**, due to hydrodynamic loading during Hurricane Sandy (corresponding to 50 hours after 00:00 UTC on October 28, 2012).**

	Bending moment at mudline, <b>LEG-SW-MUD</b>		
	drag	inertia	total
Mean (kN)	61	-2	57
Max (kN)	1641	1290	1846
Min (kN)	-1714	-1170	-1779
SD (kN)	393	438	582
Skewness	-0.35	0.09	-0.17
Kurtosis	6.36	2.73	3.17
Peak Factor(PF)	4.52	2.95	3.16
PF (Gaussian)	2.98	3.01	3.01

axial force in a brace (**BRA-W-L4**); including the ocean currents increases the maximum axial force in the brace by about 19% (from 1255 kN to 1499 kN).

### 3.4.4 Hydrodynamic versus Aerodynamic Loads

In this section, we evaluate the relative importance of hydrodynamic loads versus aerodynamic loads toward different jacket response measures. Figures 3.28 and 3.31 show, respectively, simulated time series of axial forces in diagonal braces on Side 2 and in leg L3 at different vertical levels (refer to Fig. 3.15). These time series plots are taken from a 1-hour simulation during Hurricane Sandy. In the brace members, while the wind load effect is dominant at the upper levels of the jacket (e.g., Level 1), the wave load effect becomes dominant at the lower level (e.g. Levels 2-4). In contrast, the axial force in the leg member (L3), even at the lowest levels, is significantly affected by both wind and wave loads.

Figure 3.32 shows maximum mudline reaction forces and moments evaluated from 1-hour simulations (carried out every 10 hours) over a period from 10 to 60 hours into the UCMC simulation of Hurricane Sandy. As can be seen in this figure, the contribution of wind loads to the various mudline reaction forces and moments is not significant. It is only for the vertical reaction force,  $F_z$ , at the mudline that the wind loads are relatively more important, but even there, when wind and wave load effects are combined, the very largest maximum  $F_z$  value (which occurs at 50 hours) shows that the total effect on the 1-hour maximum  $F_z$  of wind and waves together is almost the same as that due to waves alone.

## 3.5 Discussion and Conclusions

In-depth studies of the response, during Hurricane Sandy, of a 5-MW offshore wind turbine with a jacket support structure have been presented. To evaluate the response of offshore wind turbines during the evolution of this hurricane, ten mid-Atlantic potential offshore wind plant sites were selected. The track and intensity of Hurricane Sandy were numerically simulated by a fully coupled atmospheric-wave-ocean model, UCMC.

Based on directional wave spectra resulting from the UCMC output, hurricane-generated wave kinematics were simulated using second-order wave theory that was presented in Chapter 2. It was shown that wave spectra based on the first 1 minute each hour could be used to represent the entire 1-hour period and to simulate waves for that hour as needed for subsequent turbine response computations.

While the vertical wind shear profile for Hurricane Ike in Chapter 2 was estimated using the classical log law, in this chapter, we used wind field data from the WRF output, updated every 10 minutes and provided at several elevations, to stochastically simulate needed wind velocity fields for Hurricane Sandy. The WRF output for Hurricane Sandy provided mean wind velocity data at 6 different levels up to 200 m above the surface. The vertical

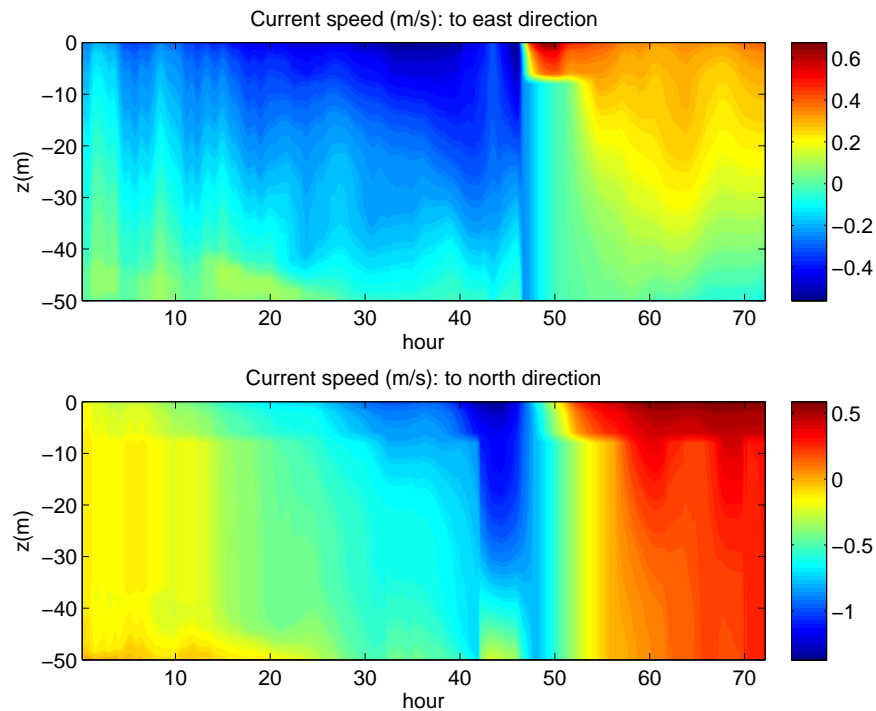


**Figure 3.24. Variation with time of the depth-dependent current velocities during Hurricane Sandy (at the 50-m water depth location within Site No. 1).**

wind profile that resulted, based on the WRF output, showed significant difference from the log law, which ignores atmospheric stability effects. Because the mean wind velocity and wind direction during the hurricane show some variation with time in each hour, the time-varying non-turbulent part of the full wind field was developed by using an interpolation function based on six 10-min sampled wind field data values from the WRF output. The turbulent wind part was stochastically simulated using standard Kaimal power spectra and coherence functions; the reference wind velocity and friction velocity needed to define parameters of the Kaimal power spectra were evaluated using the 10-min wind speed and friction velocity values provided as part of the WRF output.

Due to the limitation of available software tools, an uncoupled modeling scheme was used to analyze the response of an offshore wind turbine with a jacket support structure. While in a coupled modeling approach, aerodynamic and hydrodynamic load effects can be evaluated simultaneously, an uncoupled modeling approach requires separate computational steps to evaluate the aerodynamic loads and the hydrodynamic loads. The aerodynamic load effects on the turbine rotor was first evaluated using a wind turbine model in FAST with a fixed base; the rotor aerodynamic loads were then applied as point loads at the top of a model of a tower that was supported by a jacket structure in Abaqus. Before evaluating the response of the offshore wind turbine with the jacket support during Hurricane Sandy, the uncoupled model was verified by comparing masses, natural frequencies, and the turbine response in regular waves against results presented in the OC4 project report. For verification purposes, it was assumed that the jacket structure was fixed at the mudline. We found that the masses, the natural frequencies, and the turbine response in regular waves, evaluated using our uncoupled model, were all comparable to the results presented in the OC4 project report.

Because interaction between the soil and an embedded pile can change the dynamic characteristics of the wind turbine, this interaction effect was included in our Abaqus model of the jacket support structure. In this model, the interaction between the soil and the embedded pile was modeled using the  $p$ - $y$  curve approach specified in the American Petroleum Institute (API) RP2A guidelines. The soil profile used for the design of the OC4 jacket was used

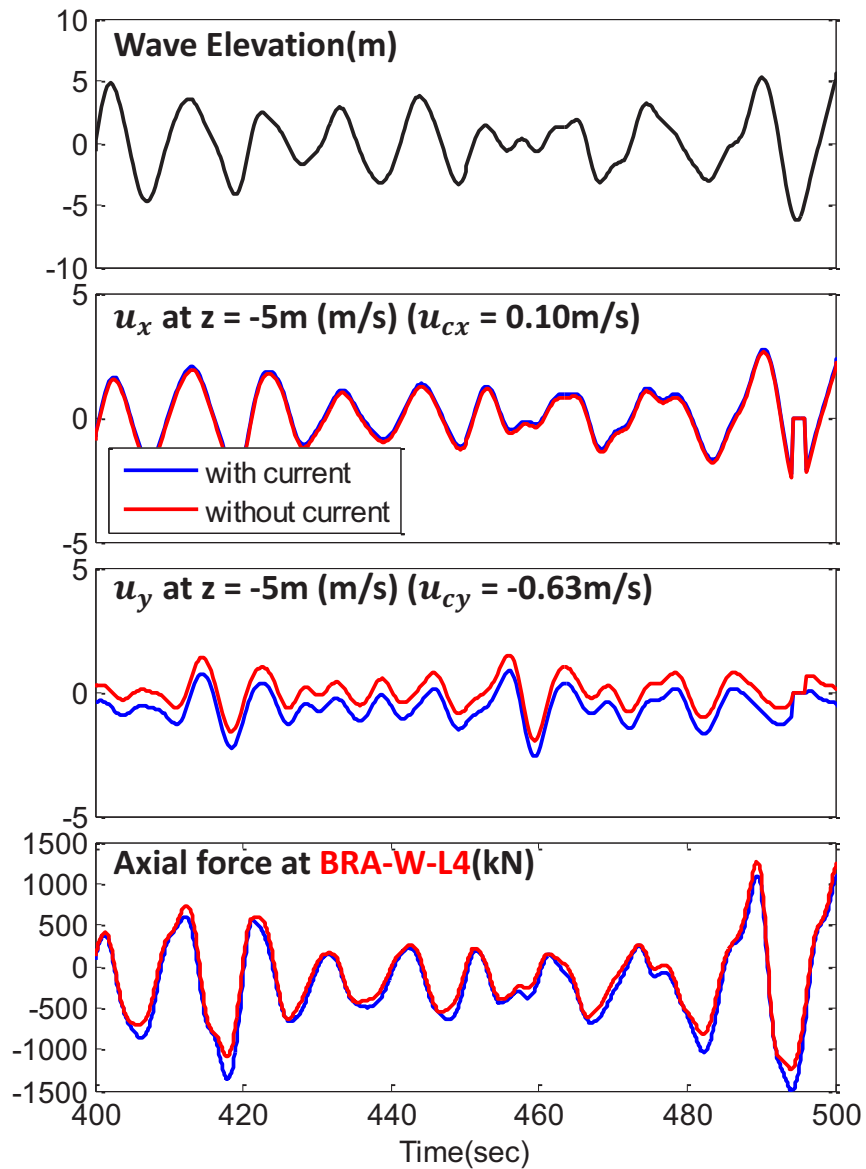
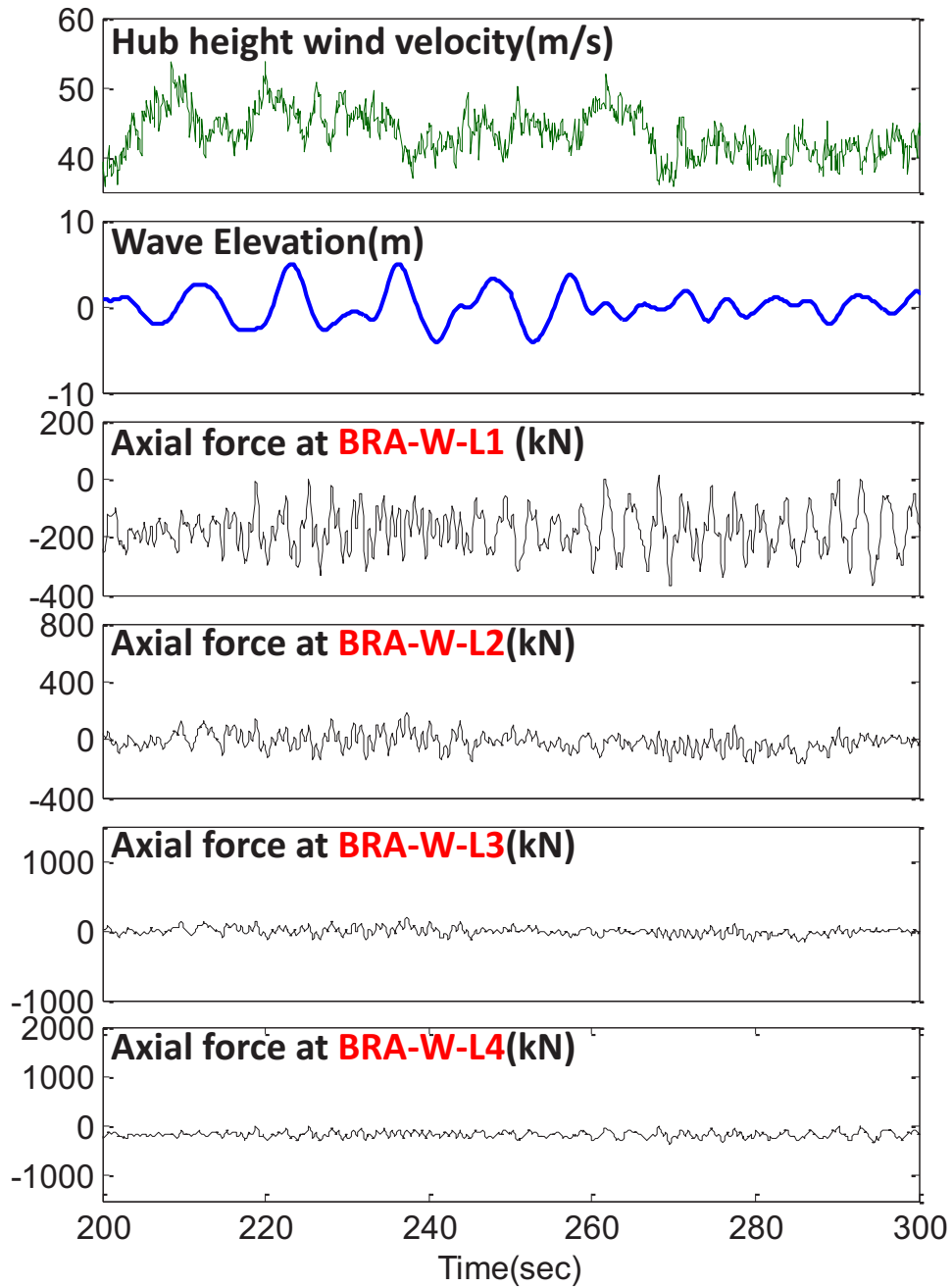
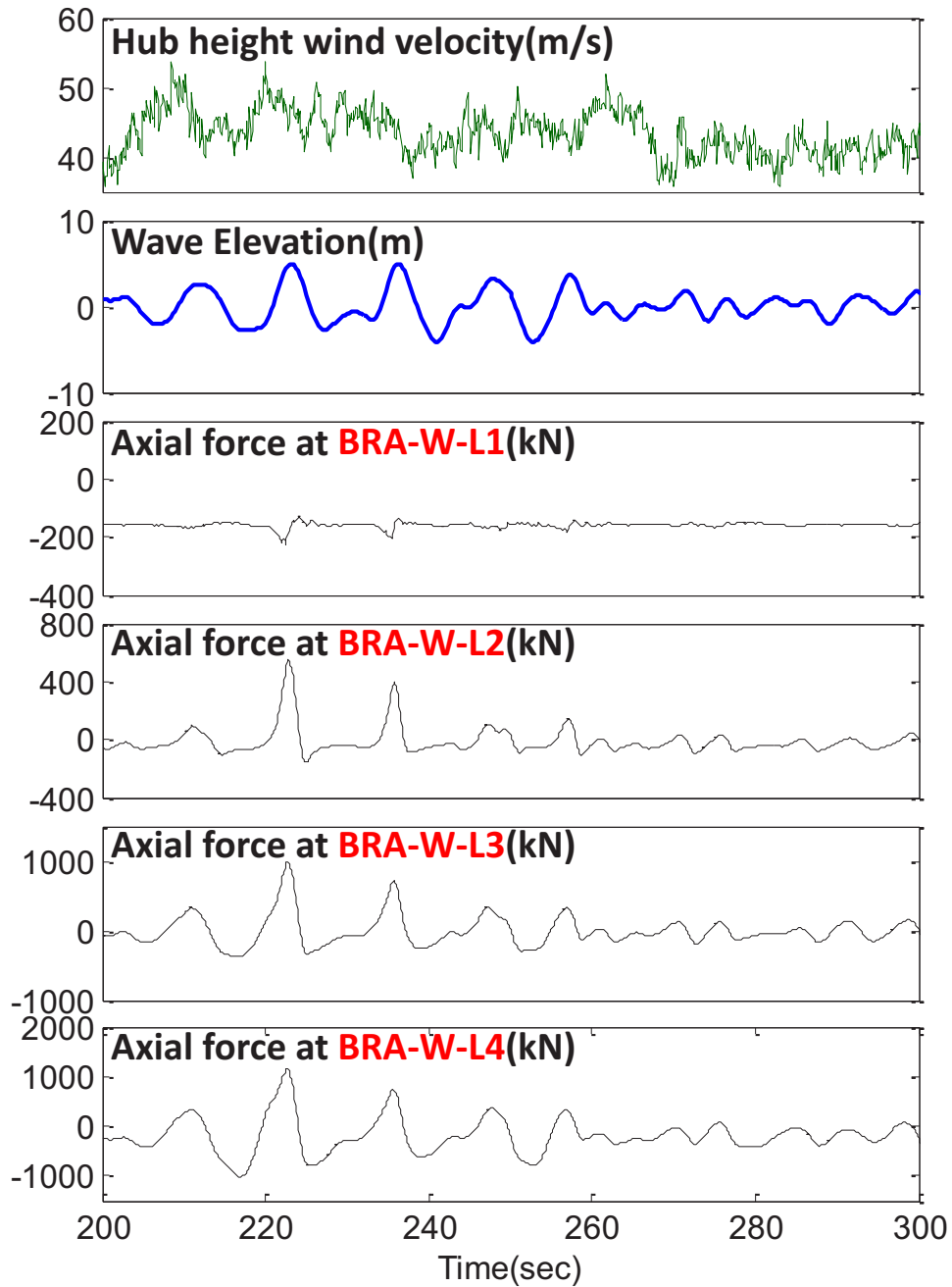


Figure 3.25. Time series at Site No. 1 of the wave elevation, the near-surface  $x$ -direction wave and current velocities, the near-surface  $y$ -direction wave and current velocities, and the axial force in a brace, **BRA-W-L4**, after including and excluding the ocean current contribution (corresponding to 50 hours after 00:00 UTC on October 28, 2012 during Hurricane Sandy).



(a) only wind loads.

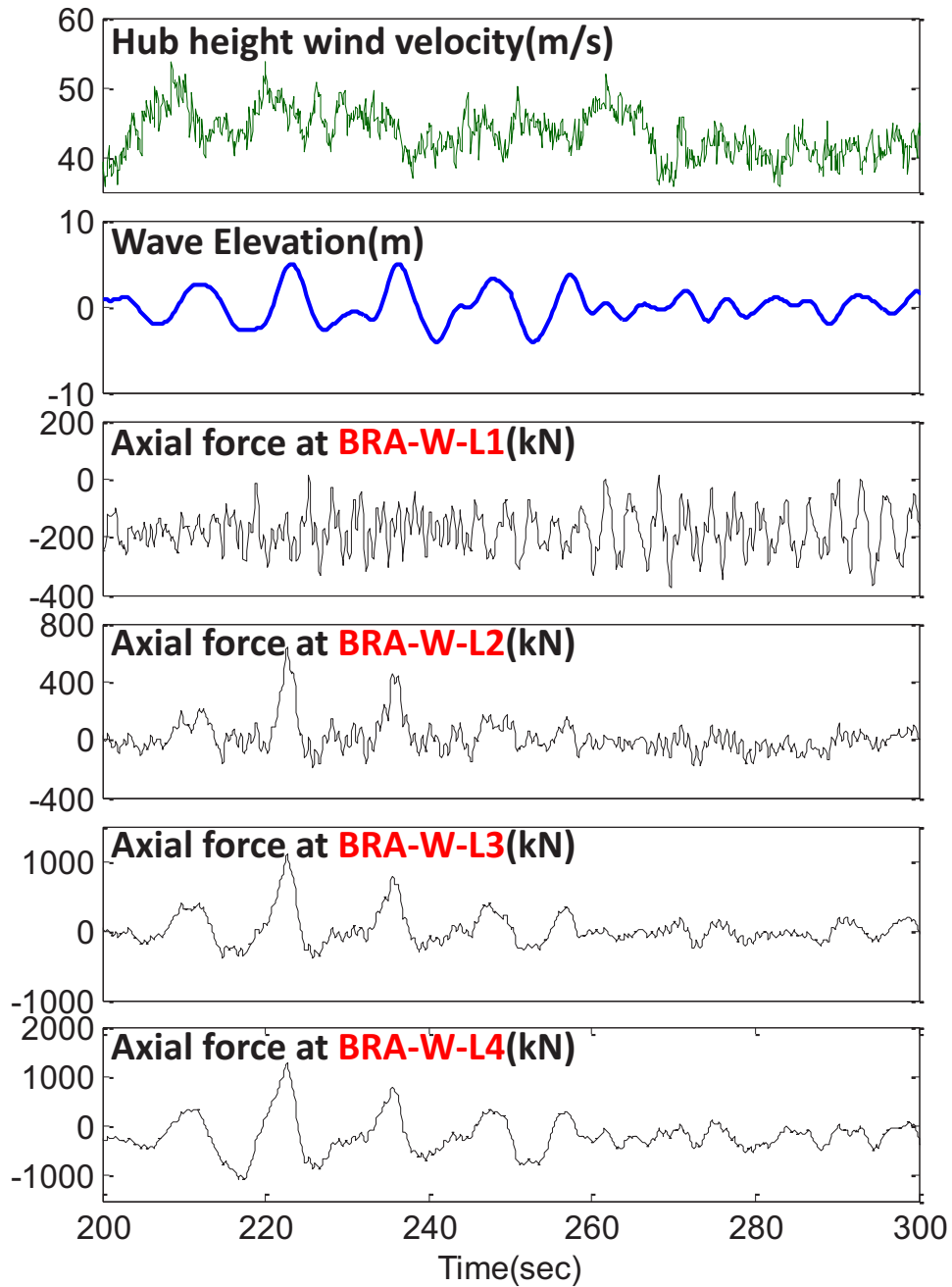
Figure 3.26. Time history of diagonal brace axial forces on Side 2 at various vertical levels of the jacket support structure at Site No. 1 during Hurricane Sandy (only wind loads).



(a) only wave loads.

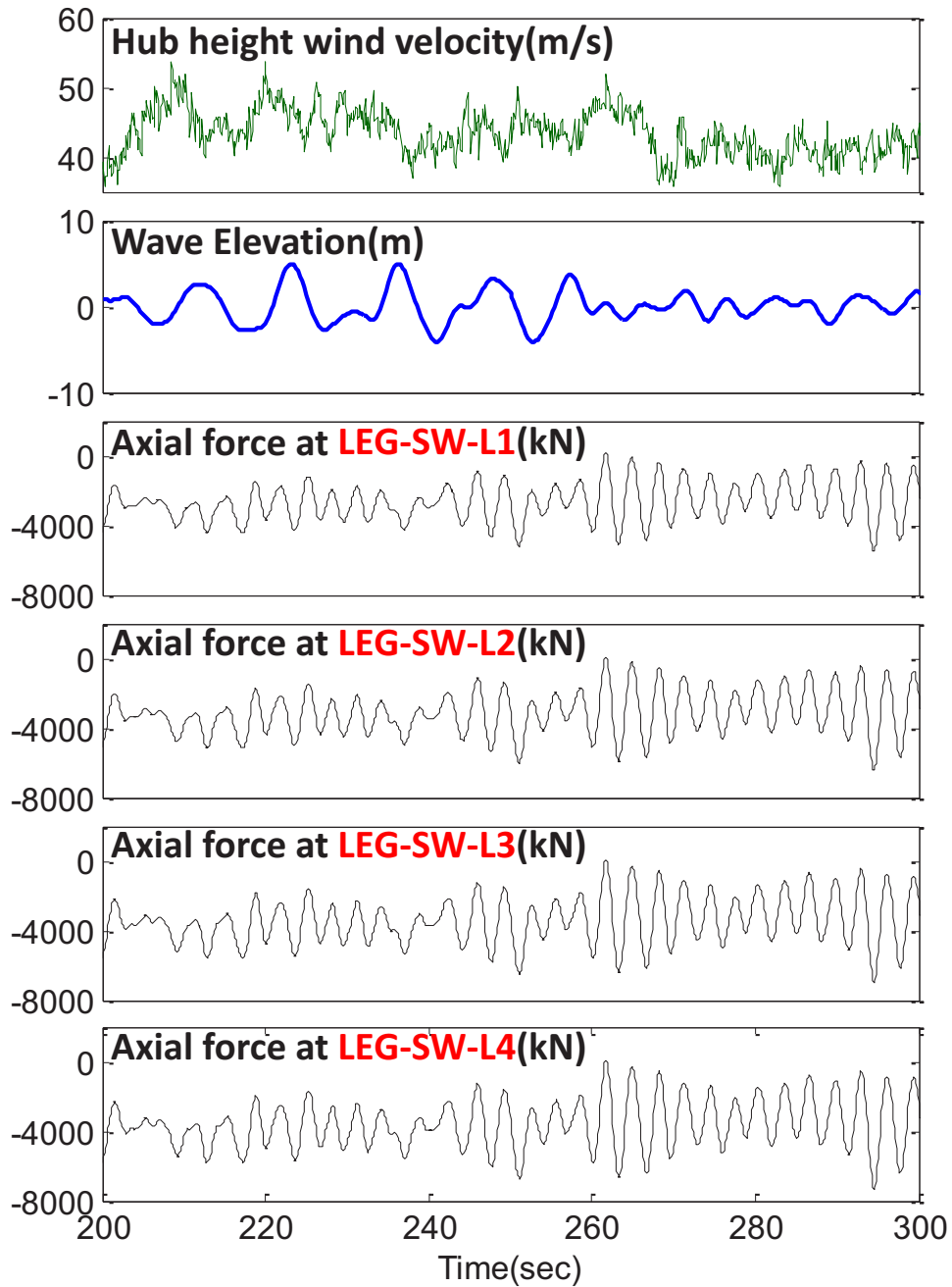
Figure 3.27. Time history of diagonal brace axial forces on Side 2 at various vertical levels of the jacket support structure at Site No. 1 during Hurricane Sandy (only wave loads).





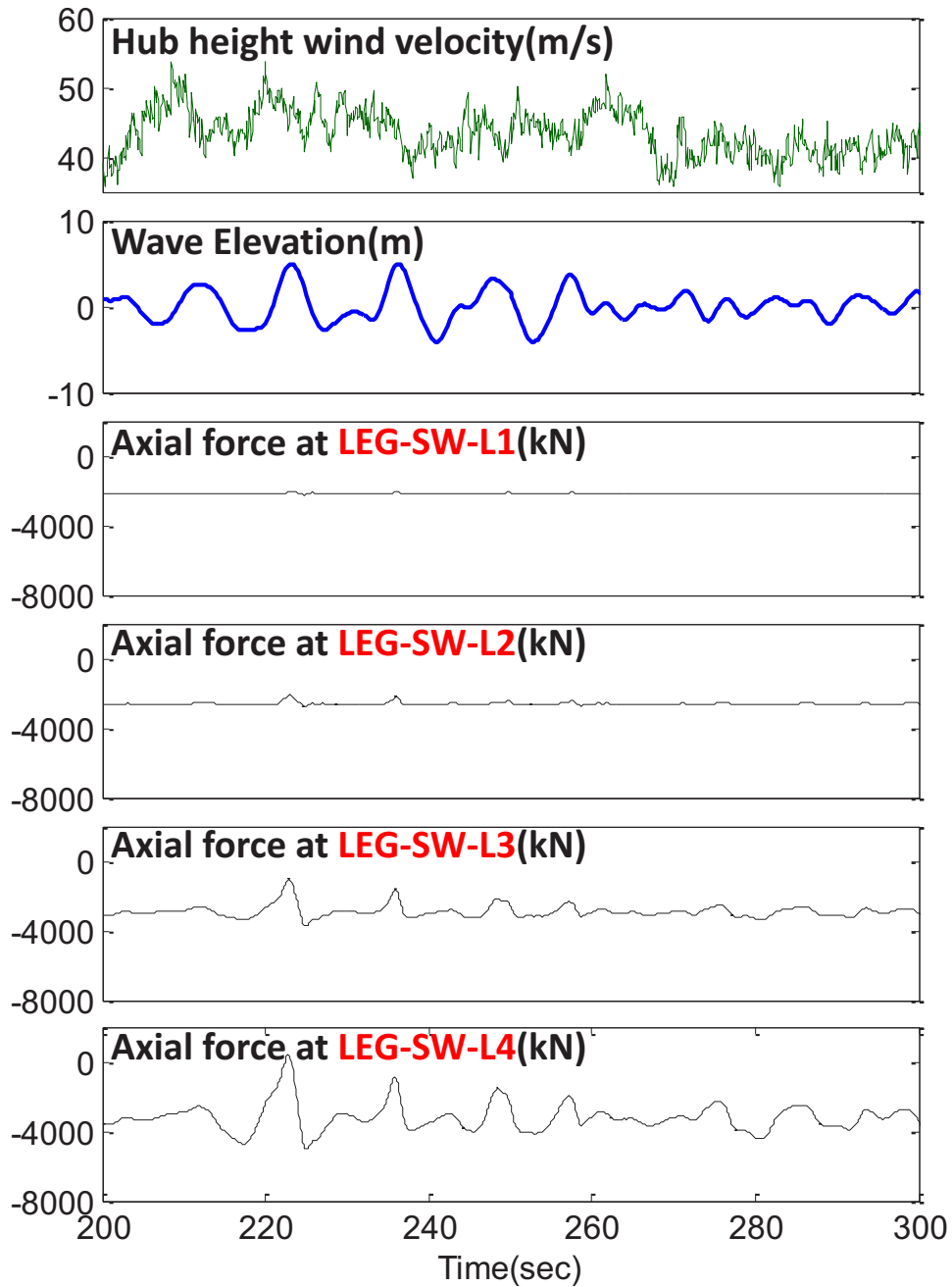
(a) considering wind and wave loads.

Figure 3.28. Time history of diagonal brace axial forces on Side 2 at various vertical levels of the jacket support structure at Site No. 1 during Hurricane Sandy (considering wind and wave loads).



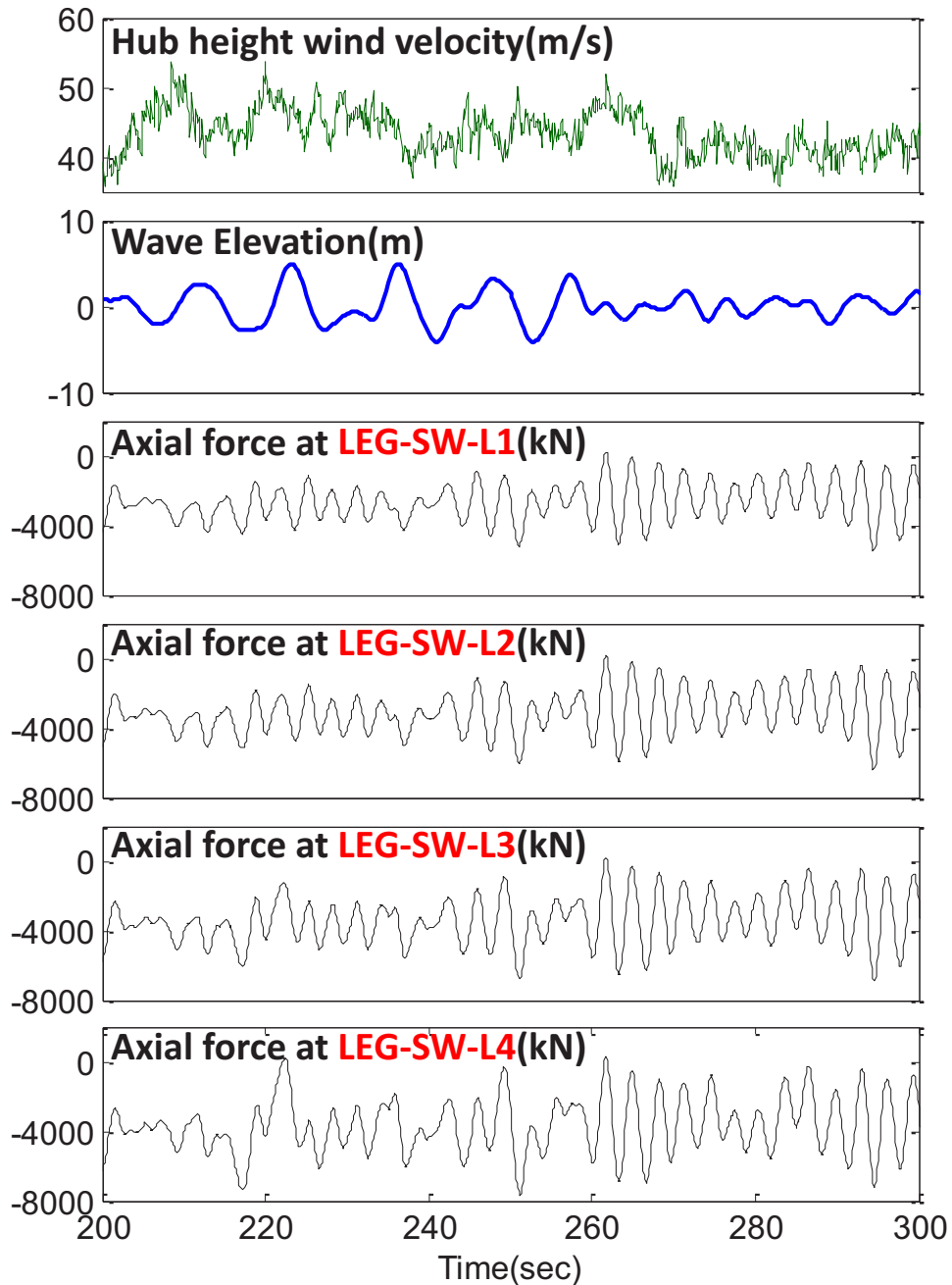
(a) only wind loads.

Figure 3.29. Time history of leg (L3) axial forces at various vertical levels of the jacket support structure at Site No. 1 during Hurricane Sandy (only wind loads).



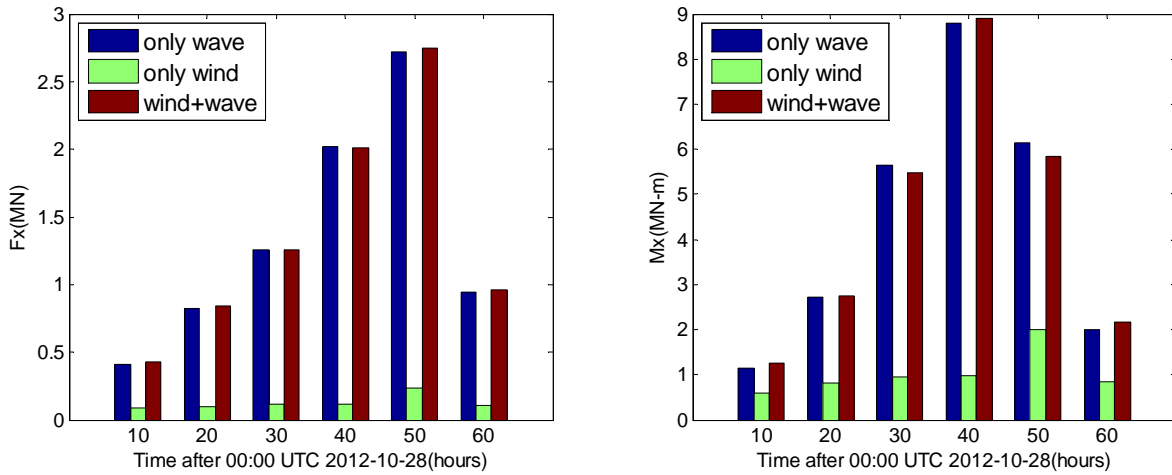
(a) only wave loads.

Figure 3.30. Time history of leg (L3) axial forces at various vertical levels of the jacket support structure at Site No. 1 during Hurricane Sandy (only wave loads).

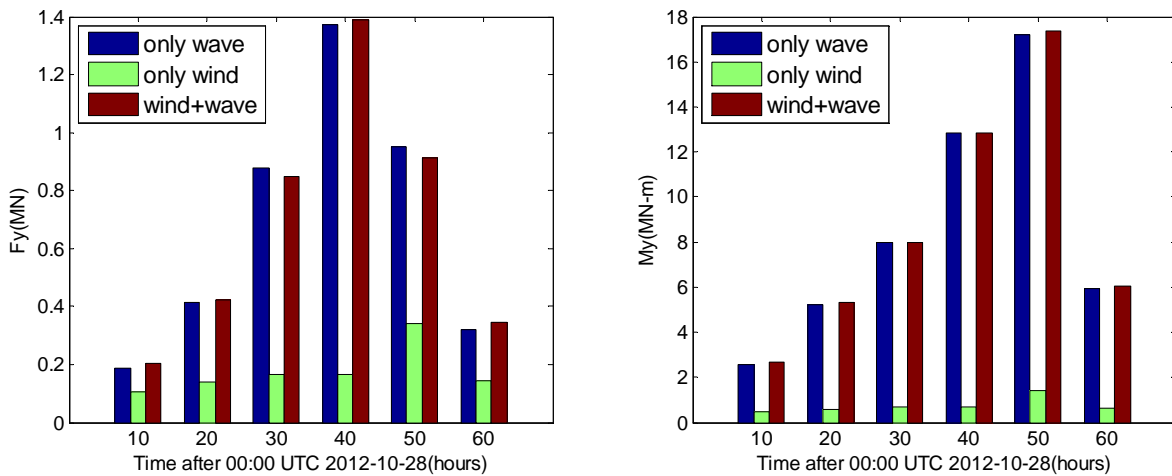


(a) considering wind and wave loads.

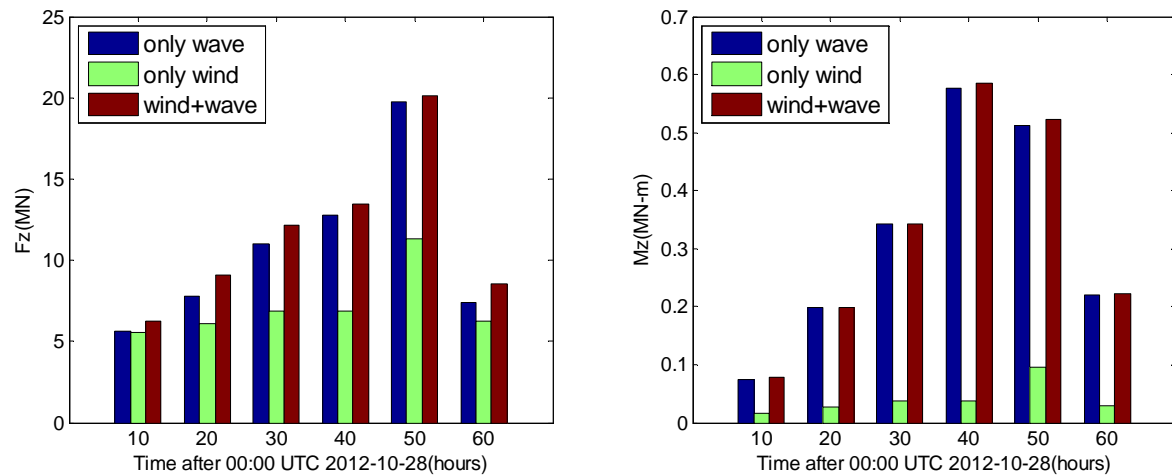
Figure 3.31. Time history of leg (L3) axial forces at various vertical levels of the jacket support structure at Site No. 1 during Hurricane Sandy (considering wind and wave loads).



(a) x-direction.



(b) y-direction.



(c) z-direction.

Figure 3.32. Maximum mudline reaction forces (LEG-SW-MUD) at Site No. 1 during Hurricane Sandy.

to evaluate the soil lateral stiffness characteristics. Because soil-structure interaction effects can significantly influence the overall dynamic characteristics of the structural system, we evaluated the effect of different soil-interaction models on overall system eigenfrequencies.

In turbine response studies related to Hurricane Sandy, we first studied the hydrodynamic loads experienced by a jacket member. As was shown by Agarwal [48], hydrodynamic loading on a monopile-supported wind turbine is dominated by inertia force and the turbine response can then be close to a Gaussian process, especially for linear waves. With the OC4 reference jacket used in this study, composed of brace members of 1.0 m diameter and leg members of 1.2 m diameter, which are more slender than the 6-meter diameter monopile studied by Agarwal [48], we found that drag load effects were comparable to inertia load effects and that the nonlinearity and non-Gaussian character of the total hydrodynamic load effect increased. As a result, maximum response values estimated based on Gaussian assumptions were significantly different from the actual response maxima computed in hour-long simulations during Hurricane Sandy.

We also evaluated the effect of ocean currents on turbine response during Hurricane Sandy. Because drag load effects for the OC4 jacket are comparable in importance to inertia load effects and because drag loads depend on current velocities, the effect of including ocean currents toward the total response was found to be non-negligible as was seen when we studied maximum axial forces in a jacket brace member. This finding suggests that it is important to have fully coupled wave and ocean current inputs for realistic evaluation of the response of an offshore wind turbine during a hurricane.

Finally, we evaluated the relative importance of hydrodynamic versus aerodynamic loads on the overall jacket response during Hurricane Sandy. We found that the relative contribution of wind and wave loads varied depending on the type and location of the jacket member being considered. For a diagonal brace member's axial forces that were studied, while the wind load effect was found to be dominant at upper levels in the jacket, the wave load effect was dominant at the lower levels. In contrast, the axial force in a leg member at lower level was significantly influenced by both wind and wave loads. The contribution of wind load effects to the total mudline vertical reaction force was found to be insignificant.

## 4 Summary and Conclusions

### 4.1 Summary of Research Objectives

The simulation of a coupled wind, wave, and current inputs based on UMCM output and the response evaluation of an offshore wind turbine using these coupled inputs were the primary goals of this study. In particular, we had three main research objectives: (i) to investigate the characteristics of hurricane-generated wind, waves, and currents; (ii) to generate time series input of turbulent wind fields and wave kinematics using the hurricane simulation output; and (iii) to predict and interpret the turbine response during Hurricanes Ike (2008) and Sandy (2012) using the assembled turbulent wind fields, wave kinematics, and current fields.

### 4.2 Summary of the Problem Descriptions

In order to assess the risks to potential U.S. offshore wind farms from the destructive environmental conditions induced by hurricanes, Hurricane Ike(2008) and Sandy(2012) were numerically simulated by a state-of-the-art hurricane numerical simulation model, the University of Miami Coupled Model (UMCM). We used the wind, wave, and current output data provided from these numerical simulations of the two hurricanes. UMCM consists of atmosphere (WRF), ocean surface wave (UMWM), and ocean (HYCOM) component models.

We selected two and ten sites, respectively, for Hurricanes Ike (2008) and Sandy (2008). For Ike, single turbine units at the two sites in the Gulf of Mexico were studied. For Sandy, a detailed turbine response at one of ten potential mid-Atlantic wind energy development sites was undertaken.

The coupled wind and wave fields at selected locations were stochastically simulated and we evaluated the turbine response of a 5-MW offshore wind turbine supported by a monopile or a jacket structure over important periods when the storm is close to making landfall.

For Hurricane Ike, we investigated:

- swell versus wind seas;
- the effect of yaw misalignment;
- the effect of blade pitch angle variation and control;
- the effect of blade azimuthal position on loads; and
- the effect of turbine parking strategies.

Also, under the assumption of zero yaw misalignment and of blades pitched to feather for Hurricane Sandy, we investigated:

- hydrodynamic loads and associated response on jacket members;
- the effect of hurricane-induced currents; and
- a comparison of hurricane-induced hydrodynamic versus aerodynamic loads.

### 4.3 Conclusions

#### 4.3.1 Modeling Hurricane Ike's Influence

Because hurricane directional waves can be thought of as composed of two wave components, swell and wind seas, which have different characteristics, their characteristics are evaluated after separating swell and wind seas from the directional wave spectra resulting from the UMCM output by the wave age criterion. The mean wave frequencies of swell components are significantly lower than resonant frequencies associated with tower bending. Also, the

variation of mean wave frequency and wave direction corresponding to swell is relatively insignificant because the evolution is not as strongly affected by the local wind.

While the contribution from hydrodynamic loading to the tower response is only very slightly influenced by the amount of yaw misalignment, the aerodynamic loading contribution is significantly influenced by it. The significantly lower turbine loads in the case of zero yaw misalignment highlights the importance of a reliable yaw backup power system, which is strongly recommended since a grid failure during a hurricane could result in loss of the needed yaw control.

Blade pitch control is important during the hurricane; as expected, blades pitched to feather result in the lowest tower response maxima.

While the tower base fore-aft moment in a case with zero yaw error does not vary greatly for different blade azimuthal positions, the tower base side-to-side moment is seen to vary by a considerably larger amount. In general, though not at all times during the hurricane, largest and smallest tower load maxima occurred for rotor configurations where one blade is in the 0 and 180 degree azimuthal position, respectively.

While the tower base fore-aft moment in a case with zero yaw error is not significantly different with the different turbine parking strategies, the tower base side-to-side moment is seen to be noticeably different and the parked-standstill case leads to systematically larger loads than the idling case during the hurricane.

#### **4.3.2 Modeling Hurricane Sandy's Influence**

First, we evaluated the nature of the hydrodynamic loads experienced by a jacket member. The small section size of jacket members makes the drag load effect comparable to the inertia load effect; it also makes the nonlinearity of the total hydrodynamic load effect increase. Consequently, this high nonlinearity of the response process makes differences between actual response maxima relative to Gaussian-based maxima significant.

We also evaluated the effect of ocean currents on the overall turbine response. Because the drag load effects for the selected OC4 jacket are of comparable importance to the inertia load effect and because drag loads include contributions from the ocean current, we found that the influence of ocean currents on the total response was non-negligible. This was confirmed by studying maximum axial forces in a diagonal brace member of the jacket structure.

The relative importance of hydrodynamic and aerodynamic loads was also investigated. We found that the relative contribution of wind versus wave loads depends on the type and location of the jacket member of interest. For example, in the brace members studied, while wind load effects were dominant at the higher levels of the jacket structure, wave load effects were dominant at the lower levels. Axial forces in leg members at the lower level, however, were significantly affected by both wind and wave loads. The contribution of wind load effects on total mudline reaction forces was not significant.



# Appendices

# Appendix A

## UMCM input files

### A.1 Hurricane Ike Simulation

#### A.1.1 WRF(namelist.input)

```
&time_control
run_days           = 8,
run_hours          = 0,
run_minutes        = 0,
run_seconds        = 0,
start_year         = 2008, 2008, 2008,
start_month        = 09, 09, 09,
start_day          = 08, 08, 08,
start_hour         = 12, 12, 12,
start_minute       = 00, 00, 00,
start_second       = 00, 00, 00,
end_year           = 2008, 2008, 2008,
end_month          = 09, 09, 09,
end_day            = 13, 13, 13,
end_hour           = 12, 12, 12,
end_minute         = 00, 00, 00,
end_second         = 00, 00, 00,
interval_seconds   = 21600
input_from_file    = .true., .false., .false.,
history_interval   = 60, 60, 60
frames_per_outfile = 1, 1, 1,
restart            = .f.,
restart_interval   = 360,
io_form_history    = 2
io_form_restart    = 2
io_form_input      = 2
io_form_boundary   = 2
debug_level        = 0
input_from_hires   = .f., .t., .t.,
rsmas_data_path    = "/home/disk/manta9/joe/topo/ts",
/

&domains
sr_x               = 0, 0, 0,
sr_y               = 0, 0, 0,
time_step          = 60,
time_step_fract_num = 0,
time_step_fract_den = 1,
max_dom            = 3,
s_we               = 1, 1, 1,
e_we               = 400, 700, 331,
s_sn               = 1, 1, 1,
e_sn               = 360, 502, 331,
s_vert             = 1, 1, 1,
e_vert             = 36, 36, 36,
num_metgrid_levels = 22
eta_levels         = 1.000, 0.996, 0.992, 0.988, 0.983, 0.970, 0.954,
                   0.934, 0.909, 0.880, 0.845, 0.807,
                   0.765, 0.719, 0.672, 0.622, 0.571,
                   0.520, 0.468, 0.420, 0.376, 0.335,
                   0.298, 0.263, 0.231, 0.202, 0.175,
                   0.150, 0.127, 0.106, 0.088, 0.070,
                   0.055, 0.040, 0.026, 0.000

use_surface        = .false.
dx                 = 12000, 4000, 1333.33,
dy                 = 12000, 4000, 1333.33,
grid_id            = 1, 2, 3,
parent_id          = 0, 1, 2,
i_parent_start     = 1, 35, 473,
j_parent_start     = 1, 85, 90,
parent_grid_ratio  = 1, 3, 3,
parent_time_step_ratio = 1, 3, 3,
feedback           = 1,
smooth_option      = 0
```

```

vortex_interval          = 20, 20, 20, 20,
max_vortex_speed        = 40, 40, 40, 40,
time_to_move            = 0, 9999, 0
corral_dist              = 0, 25, 25, 25,
/

&physics
mp_physics               = 4, 4, 4,
ra_lw_physics            = 1, 1, 1,
ra_sw_physics            = 1, 1, 1,
radt                     = 15, 15, 15,
sf_sfclay_physics        = 1, 1, 1,
sf_surface_physics        = 1, 1, 1,
bl_pbl_physics           = 1, 1, 1,
bldt                     = 0, 0, 0,
cu_physics                = 1, 0, 0,
cudt                     = 5, 0, 0,
isfflx                   = 1,
isftcflx                 = 2,
ifsnow                   = 0,
icloud                   = 1,
surface_input_source      = 1,
num_soil_layers          = 5,
sf_urban_physics         = 0,
mp_zero_out              = 0,
maxiens                  = 1,
maxens                   = 3,
maxens2                  = 3,
maxens3                  = 16,
ensdim                   = 144,
slope_rad                = 0,
topo_shading             = 0,
omlcall                  = 0,
oml_hml0                 = 100,
oml_gamma                 = 0.14,
/

&fdda
grid_fdda                = 1, 0, 0,
gfdda_inname             = "wrfdda_d<domain>",
gfdda_end_h              = 24, 24, 24,
gfdda_interval_m         = 360, 360, 360,
fgdt                     = 0, 0, 0,
fgdtzero                 = 0, 0, 0,
if_no_pbl_nudging_uv    = 0, 0, 0,
if_no_pbl_nudging_t     = 0, 0, 0,
if_no_pbl_nudging_ph    = 0, 0, 0,
if_zfac_uv               = 0, 0, 0,
k_zfac_uv                = 10, 10, 10,
if_zfac_t                = 0, 0, 0,
k_zfac_t                 = 10, 10, 10,
if_zfac_ph               = 0, 0, 0,
k_zfac_ph                = 10, 10, 10,
dk_zfac_uv               = 1, 1, 1,
dk_zfac_t                = 1, 1, 1,
dk_zfac_ph               = 1, 1, 1,
guv                      = 0.0003, 0.0000, 0.0000,
gt                      = 0.0000, 0.0000, 0.0000,
gph                      = 0.0000, 0.0000, 0.0000,
if_ramping               = 1,
dtramp_min               = 60.0,
io_form_gfdda            = 2,
/

&dynamics
iso_temp                 = 0.,
w_damping                = 1,
diff_opt                 = 1,
km_opt                   = 4,
diff_6th_opt            = 0,
diff_6th_factor          = 0.12,
base_temp                = 290.,
damp_opt                 = 0,
zdamp                    = 5000., 5000., 5000.,
dampcoef                 = 0.2, 0.2, 0.2,
khdif                   = 0, 0, 0,

```

```

kvdif                = 0,      0,      0,
non_hydrostatic      = .true., .true., .true.,
moist_adv_opt        = 0, 0, 0,
scalar_adv_opt       = 0, 0, 0,
use_baseparam_fr_nml = .true.
/

&bdy_control
spec_bdy_width       = 5,
spec_zone            = 1,
relax_zone           = 4,
specified            = .true., .false.,.false.,
nested               = .false., .true., .true.,
/

&grib2
/

&namelist_quilt
nio_tasks_per_group = 0,
nio_groups = 1,
/

```

## A.1.2 UMWM(main.nml)

```

&DOMAIN
isGlobal             = .F.           ! Global (.T.) or regional (.F.)
mm                  = 1195          ! Domain size in x
nm                  = 1075          ! Domain size in y
om                  = 37            ! Number of frequency bins
pm                  = 36            ! Number of directions
fmin                = 0.0313        ! Lowest frequency bin [Hz]
fmax                = 2.0           ! Highest frequency bin [Hz]
fprog               = 0.5           ! Highest prognostic frequency bin [Hz]
startTimeStr        = '2008-09-08_12:00:00' ! Simulation start time
stopTimeStr         = '2008-09-13_12:00:00' ! Simulation end time
dtg                 = 60            ! Global (I/O) time step [s]
restart              = .f.           ! Restart from file
/

&PHYSICS
g                   = 9.80665       ! Gravitational acceleration [m/s^2]
nu_air              = 1.56E-5       ! Kinematic viscosity of air [m^2/s]
nu_water            = 0.9E-6        ! Kinematic viscosity of water [m^2/s]
sfct                = 0.07          ! Surface tension [N/m]
kappa               = 0.4           ! Von Karman constant
z                   = 10.           ! Height of the input wind speed [m]
gustiness           = 0.0           ! Random wind gustiness factor (should be between 0 and 0.2)
dmin                = 20.           ! Depth limiter [m]
explim              = 1.1           ! Exponent limiter (0.69 ~ 100% growth)
sin_fac             = 0.11          ! Input factor from following winds
sin_diss1           = 0.10          ! Damping factor from opposing winds
sin_diss2           = 0.01          ! Damping factor from swell overrunning wind
sds_fac             = 42.           ! Breaking dissipation factor
sds_power           = 2.5           ! Saturation spectrum power
mss_fac             = 120.          ! Mean-square-slope adjustment to Sds
snl_fac             = 5.            ! Wave energy downshifting factor
sdt_fac             = 0.01          ! Dissipation due to turbulence factor
sbf_fac             = 0.003         ! Bottom friction coefficient [m/s]
sbp_fac             = 0.003         ! Bottom percolation coefficient [m/s]
/

&GRID
gridFromFile        = .T.           ! Set to .T. if lon/lat fields are input from file
delx                 = 12000        ! Grid spacing in x [m] if gridFromFile = .F.
dely                 = 12000        ! Grid spacing in y [m] if gridFromFile = .F.
topoFromFile         = .T.           ! Set to .T. to input bathymetry from file
dpt                  = 1000         ! Constant water depth [m] if topoFromFile = .F.
fillEstuaries        = .F.          ! Set to .T. to fill cells with 3 land neighbours
fillLakes            = .F.          ! Set to .T. to fill user chosen seas/lakes
/

&FORCING
winds                = .F.          ! Wind input from file
currents             = .F.          ! Currents input from file
air_density          = .F.          ! Air density input from file
water_density        = .F.          ! Water density input from file

```

```

/
&FORCING_CONSTANT
  wspd0      = 25  ! Wind speed [m/s]
  wdir0      = 0.  ! Wind direction [rad]
  uc0        = 0.  ! x-component ocean current [m/s]
  vc0        = 0.  ! y-component ocean current [m/s]
  rhoa0      = 1.2 ! Air density [kg/m^3]
  rhow0      = 1025 ! Water density [kg/m^3]
/
&OUTPUT
  outgrid    = 1  ! Gridded output interval [hours]
  outspec    = -1 ! Spectrum output interval [hours]
  outrst     = 6  ! Restart output interval [hours]
  xpl        = 600 ! Grid cell in x for stdout (screen)
  ypl        = 400 ! Grid cell in y for stdout (screen)
  stokes     = .T. ! Output Stokes drift velocity fields
/
&STOKES
  depths     = 0 1 2 3 4 5 6 7 8 9 10 12 14 16 18 20 25 30 35 40 50 60 70 80 90 100

```

### A.1.3 HYCOM(blkdat.input)

```

ERA-15 forcing; flx-s14w; LWcorr; precip+2mm; SSSrlx; FCT2 tsadv; 0-tracer.
Sigma0; GDEM3 init; KPP mixed layer; SeaWiFS mon KPAR; nested in ATLD0.08 2.6;
S-Z(15-11): dp00/f/x/i=3m/1.125/12m/1m; ds=1m/1.125/4m; src_2.2.34;
1234567890123456789012345678901234567890123456789012345678901234567890123456789012345678901234567890
22  'iversn' = hycom version number x10
201  'iexpt' = experiment number x10
1000 'idm'   = longitudinal array size
1000 'jdm'   = latitudinal array size
700  'itest' = grid point where detailed diagnostics are desired
700  'jtest' = grid point where detailed diagnostics are desired
32   'kdm'   = number of layers
32   'nhybrd' = number of hybrid levels (0=all isopycnal)
14   'nsigma' = number of sigma levels (nhybrd-nsigma z-levels)
3.0  'dp00'  = deep z-level spacing minimum thickness (m)
450.0 'dp00x' = deep z-level spacing maximum thickness (m)
1.18 'dp00f' = deep z-level spacing stretching factor (1.0=const.space)
0.5  'ds00'  = shallow z-level spacing minimum thickness (m)
75.0 'ds00x' = shallow z-level spacing maximum thickness (m)
1.18 'ds00f' = shallow z-level spacing stretching factor (1.0=const.space)
1.0  'dp00i' = deep iso-pycnal spacing minimum thickness (m)
6.0  'isotop' = shallowest depth for isopycnal layers (m, <0 from file)
35.0 'saln0' = initial salinity value (psu), only used for iniflg<2
1    'locsig' = locally-referenced pot. density for stability (0=F,1=T)
2    'kapref' = thermobaric ref. state (-1=input,0=none,1,2,3=constant)
2    'thflag' = reference pressure flag (0=Sigma-0, 2=Sigma-2)
34.0 'thbase' = reference density (sigma units)
0    'vsigma' = spacially varying isopycnal target densities (0=F,1=T)
28.10 'sigma' = layer 1 isopycnal target density (sigma units)
28.90 'sigma' = layer 2 isopycnal target density (sigma units)
29.70 'sigma' = layer 3 isopycnal target density (sigma units)
30.50 'sigma' = layer 4 isopycnal target density (sigma units)
30.95 'sigma' = layer 5 isopycnal target density (sigma units)
31.50 'sigma' = layer 6 isopycnal target density (sigma units)
32.05 'sigma' = layer 7 isopycnal target density (sigma units)
32.60 'sigma' = layer 8 isopycnal target density (sigma units)
33.15 'sigma' = layer 9 isopycnal target density (sigma units)
33.70 'sigma' = layer 10 isopycnal target density (sigma units)
34.25 'sigma' = layer 11 isopycnal target density (sigma units)
34.75 'sigma' = layer 12 isopycnal target density (sigma units)
35.15 'sigma' = layer 13 isopycnal target density (sigma units)
35.50 'sigma' = layer 14 isopycnal target density (sigma units)
35.80 'sigma' = layer 15 isopycnal target density (sigma units)
36.04 'sigma' = layer 16 isopycnal target density (sigma units)
36.20 'sigma' = layer 17 isopycnal target density (sigma units)
36.38 'sigma' = layer 18 isopycnal target density (sigma units)
36.52 'sigma' = layer 19 isopycnal target density (sigma units)
36.62 'sigma' = layer 20 isopycnal target density (sigma units)
36.70 'sigma' = layer 21 isopycnal target density (sigma units)
36.77 'sigma' = layer 22 isopycnal target density (sigma units)
36.83 'sigma' = layer 23 isopycnal target density (sigma units)
36.89 'sigma' = layer 24 isopycnal target density (sigma units)
36.97 'sigma' = layer 25 isopycnal target density (sigma units)

```

```

37.02 'sigma' = layer 26 isopycnal target density (sigma units)
37.06 'sigma' = layer 27 isopycnal target density (sigma units)
37.10 'sigma' = layer 28 isopycnal target density (sigma units)
37.17 'sigma' = layer 29 isopycnal target density (sigma units)
37.30 'sigma' = layer 30 isopycnal target density (sigma units)
37.42 'sigma' = layer 31 isopycnal target density (sigma units)
37.48 'sigma' = layer 32 isopycnal target density (sigma units)
3 'iniflg' = initial state flag (0=level, 1=zonl, 2=clim)
0 'jerlv0' = initial jerlov water type (1 to 5; 0 to use KPAR)
3 'yrflag' = days in year flag (0=360, 1=366, 2=366J1, 3=actual)
0 'sshflg' = diagnostic SSH flag (0=SSH,1=SSH&stericSSH)
0.0416667 'dsurfq' = number of days between model diagnostics at the surface
0.0416667 'diagfq' = number of days between model diagnostics
0.0 'proffq' = number of days between model diagnostics at selected locs
0.0 'tilefq' = number of days between model diagnostics on selected tiles
0.0 'meanfq' = number of days between model diagnostics (time averaged)
9999.0 'rstrfq' = number of days between model restart output
1.0 'bnstfq' = number of days between baro nesting archive input
1.0 'nestfq' = number of days between 3-d nesting archive input
0.125 'cplifq' = number of days (or time steps) between sea ice coupling
120.0 'baclin' = baroclinic time step (seconds), int. divisor of 86400
5.0 'batrop' = barotropic time step (seconds), int. div. of baclin/2
0 'incflg' = incremental update flag (0=no, 1=yes, 2=full-velocity)
100 'incstp' = no. timesteps for full update (1=direct insertion)
1 'incupf' = number of days of incremental updating input
0.125 'wbaro' = barotropic time smoothing weight
1 'btrlfr' = leapfrog barotropic time step (0=F,1=T)
0 'btrmas' = barotropic is mass conserving (0=F,1=T)
8.0 'hybrlx' = HYBGEN: inverse relaxation coefficient (time steps)
0.01 'hybiso' = HYBGEN: Use PCM if layer is within hybiso of target density
3 'hybmap' = hybrid remapper flag (0=PCM, 1=PLM, 2=PPM, 3=WENO-like)
0 'hybflg' = hybrid generator flag (0=T&S, 1=th&S, 2=th&T)
0 'advflg' = thermal advection flag (0=T&S, 1=th&S, 2=th&T)
2 'advtyp' = scalar advection type (0=PCM,1=MPDATA,2=FCT2,4=FCT4)
2 'momtyp' = momentum advection type (2=2nd order, 4=4th order)
-1.0 'slip' = +1 for free-slip, -1 for non-slip boundary conditions
0.05 'visco2' = deformation-dependent Laplacian viscosity factor
0.0 'visco4' = deformation-dependent biharmonic viscosity factor
0.0 'facdf4' = speed-dependent biharmonic viscosity factor
0.003 'veldf2' = diffusion velocity (m/s) for Laplacian momentum dissip.
0.02 'veldf4' = diffusion velocity (m/s) for biharmonic momentum dissip.
0.0 'thkdf2' = diffusion velocity (m/s) for Laplacian thickness diffus.
0.01 'thkdf4' = diffusion velocity (m/s) for biharmonic thickness diffus.
0.005 'temdf2' = diffusion velocity (m/s) for Laplacian temp/saln diffus.
1.0 'temdfc' = temp diffusion conservation (0.0,1.0 all dens,temp resp.)
0.0 'vertmx' = diffusion velocity (m/s) for momentum at MICOM M.L.base
0.05 'cbar' = rms flow speed (m/s) for linear bottom friction
2.2e-3 'cb' = coefficient of quadratic bottom friction
0.0 'drglim' = limiter for explicit friction (1.0 none, 0.0 implicit)
0.0 'dragscl' = scale factor for tidal drag (0.0 for no tidal drag)
500.0 'thkdrq' = thickness of bottom boundary layer for tidal drag (m)
10.0 'thkbot' = thickness of bottom boundary layer (m)
0.02 'sigjmp' = minimum density jump across interfaces (kg/m**3)
0.3 'tmljmp' = equivalent temperature jump across mixed-layer (degC)
15.0 'thkmls' = reference mixed-layer thickness for SSS relaxation (m)
0.0 'thkmlt' = reference mixed-layer thickness for SST relaxation (m)
5.0 'thkriv' = nominal thickness of river inflow (m)
20.0 'thkfrz' = maximum thickness of near-surface freezing zone (m)
0 'iceflg' = sea ice model flag (0=none,1=energy loan,2=coupled/esmf)
0.0 'tfrz_0' = ENLN: ice melting point (degC) at S=0psu
-0.054 'tfrz_s' = ENLN: gradient of ice melting point (degC/psu)
0.0 'ticegr' = ENLN: temp. grad. inside ice (deg/m); =0 use surtmp
0.5 'hicemx' = ENLN: minimum ice thickness (m)
10.0 'hicemx' = ENLN: maximum ice thickness (m)
0 'ntracr' = number of tracers (0=none,negative to initialize)
0 'trcflg' = tracer flags (one digit per tr, most sig. replicated)
240 'tsofrq' = number of time steps between anti-drift offset calcs
0.0 'tofset' = temperature anti-drift offset (degC/century)
0.0 'sofset' = salinity anti-drift offset (psu/century)
1 'mlflag' = mixed layer flag (0=none,1=KPP,2-3=KT,4=PWP,5=MY,6=GISS)
1 'pensol' = KT: activate penetrating solar rad. (0=F,1=T)
999.0 'dtrate' = KT: maximum permitted m.l. detrainment rate (m/day)
19.2 'thkmin' = KT/PWP: minimum mixed-layer thickness (m)
1 'dypflg' = KT/PWP: diapycnal mixing flag (0=none, 1=KPP, 2=explicit)
240 'mixfrq' = KT/PWP: number of time steps between diapycnal mix calcs
1.e-7 'diapyc' = KT/PWP: diapycnal diffusivity x buoyancy freq. (m**2/s**2)

```

```

0.25 'rigr' = PWP: critical gradient richardson number
0.65 'ribc' = PWP: critical bulk richardson number
0.7 'rinfty' = KPP: maximum gradient richardson number (shear inst.)
0.25 'ricr' = KPP: critical bulk richardson number
0.0 'bldmin' = KPP: minimum surface boundary layer thickness (m)
1200.0 'bldmax' = K-PROF: maximum surface boundary layer thickness (m)
0.7 'cekman' = KPP/KT: scale factor for Ekman depth
1.0 'cmonob' = KPP: scale factor for Monin-Obukov depth
0 'bblkpp' = KPP: activate bottom boundary layer (0=F,1=T)
1 'shinst' = KPP: activate shear instability mixing (0=F,1=T)
1 'dbdiff' = KPP: activate double diffusion mixing (0=F,1=T)
1 'nonloc' = KPP: activate nonlocal b. layer mixing (0=F,1=T)
0 'botdiw' = K-PROF: activate bot.enhan.int.wav mixing (0=F,1=T)
1 'difout' = K-PROF: output visc/diff coeffs in archive (0=F,1=T)
0 'difsmo' = K-PROF: number of layers with horiz smooth diff coeffs
50.0e-4 'difm0' = KPP: max viscosity due to shear instability (m**2/s)
50.0e-4 'difs0' = KPP: max diffusivity due to shear instability (m**2/s)
0.3e-4 'difmiw' = KPP: background/internal wave viscosity (m**2/s)
0.1e-4 'difsiw' = KPP: background/internal wave diffusivity (m**2/s)
10.0e-4 'dsfmax' = KPP: salt fingering diffusivity factor (m**2/s)
1.9 'rrrho0' = KPP: salt fingering  $rp=(\alpha*\delta t)/(\beta*\delta ls)$ 
98.96 'cs' = KPP: value for nonlocal flux term
10.0 'cstar' = KPP: value for nonlocal flux term
0.0 'cv' = KPP: buoyancy frequency ratio (0.0 to use a fn. of N)
5.0 'c11' = KPP: value for turb velocity scale
2 'hblflg' = KPP: b. layer interp. flag (0=const.,1=linear,2=quad.)
2 'niter' = KPP: iterations for semi-implicit soln. (2 recommended)
0 'fltflg' = FLOATS: synthetic float flag (0=no; 1=yes)
4 'nfladv' = FLOATS: advect every nfladv bac1. time steps (even, >=4)
1 'nflsam' = FLOATS: output (0=every nfladv steps; >0=no. of days)
0 'intpfl' = FLOATS: horiz. interp. (0=2nd order+n.n.; 1=n.n. only)
0 'iturbv' = FLOATS: add horiz. turb. advection velocity (0=no; 1=yes)
1 'ismpfl' = FLOATS: sample water properties at float (0=no; 1=yes)
4.63e-6 'tbvar' = FLOATS: horizontal turb. vel. variance scale (m**2/s**2)
0.4 'tdecri' = FLOATS: inverse decorrelation time scale (1/day)
2 'lbflag' = lateral barotropic bndy flag (0=none, 1=port, 2=input)
2 'tidflg' = TIDES: tidal forcing flag (0=none,1=open-bdy,2=bdy&body)
11111111 'tidcon' = TIDES: 1 digit per (Q1K2P1N201K1S2M2), 0=off,1=on
0.06 'tidsal' = TIDES: scalar self attraction and loading factor (<0: file)
1 'tidgen' = TIDES: generic time (0=F,1=T)
1.0 'tidrmp' = TIDES: ramp time (days)
0.0 'tid_t0' = TIDES: origin for ramp time (model day)
12 'clmflg' = climatology frequency flag (6=bimonthly, 12=monthly)
2 'wndflg' = wind stress input flag (0=none,1=u/v-grid,2,3=p-grid)
1 'ustflg' = ustar forcing flag (3=input,1,2=wndspd,4=stress)
3 'flxflg' = thermal forcing flag (0=none,3=net-flux,1,2,4=sst-based)
0 'empflg' = E-P forcing flag (0=none,3=net_E-P, 1,2,4=sst-bas_E)
0 'dswflg' = diurnal shortwave flag (0=none,1=daily to diurnal corr.)
0 'sssflg' = SSS relaxation flag (0=none,1=clim,-1=clim&rmx)
0 'lwflg' = longwave (SST) flag (0=none,1=clim,2=atmos)
0 'sstflg' = SST relaxation flag (0=none,1=clim,2=atmos,3=observed)
0 'icmflg' = ice mask flag (0=none,1=clim,2=atmos,3=obs/coupled)
0 'flxoff' = net flux offset flag (0=F,1=T)
0 'flxsmo' = smooth surface fluxes (0=F,1=T)
0 'relax' = activate lateral boundary nudging (0=F,1=T)
0 'trcrlx' = activate lat. bound. tracer nudging (0=F,1=T)
0 'priver' = rivers as a precipitation bogas (0=F,1=T)
0 'epmass' = treat evap-precip as a mass exchange (0=F,1=T)

```

## A.2 Hurricane Sandy Simulation

### A.2.1 WRF(namelist.input)

```

&time_control
run_days = 7,
run_hours = 0,
run_minutes = 0,
run_seconds = 0,
start_year = 2012, 2012, 2012,
start_month = 10, 10, 10,
start_day = 27, 27, 27,
start_hour = 00, 00, 00,
start_minute = 00, 00, 00,

```

```

start_second = 00, 00, 00,
end_year      = 2012, 2012, 2012,
end_month     = 10, 10, 10,
end_day       = 31, 31, 31,
end_hour      = 00, 00, 00,
end_minute    = 00, 00, 00,
end_second    = 00, 00, 00,
interval_seconds = 21600
input_from_file = .t., .f., .f.,
input_from_hires = .f., .t., .t.,
history_interval = 60, 60, 60,
frames_per_outfile = 1, 1, 1,
restart         = .f.,
restart_interval = 360,
io_form_history = 2
io_form_restart = 2
io_form_input   = 2
io_form_boundary = 2
debug_level     = 0
rsmas_data_path = "/home/disk/manta9/joe/topo/ts",
/

&domains
hypsothetic_opt = 1,
time_step       = 60,
time_step_fract_num = 0,
time_step_fract_den = 1,
max_dom         = 2,
s_we            = 1, 1, 1,
e_we            = 400, 562, 361,
s_sn            = 1, 1, 1,
e_sn            = 360, 622, 361,
s_vert          = 1, 1, 1,
e_vert          = 36, 36, 36,
num_metgrid_levels = 27
eta_levels      = 1.000, 0.996, 0.992, 0.988, 0.983, 0.970, 0.954,
                 0.934, 0.909, 0.880, 0.845, 0.807,
                 0.765, 0.719, 0.672, 0.622, 0.571,
                 0.520, 0.468, 0.420, 0.376, 0.335,
                 0.298, 0.263, 0.231, 0.202, 0.175,
                 0.150, 0.127, 0.106, 0.088, 0.070,
                 0.055, 0.040, 0.026, 0.000

use_surface     = .false.
dx              = 12000, 4000, 1333.33,
dy              = 12000, 4000, 1333.33,
grid_id         = 1, 2, 3,
parent_id       = 0, 1, 2,
i_parent_start  = 1, 130, 257,
j_parent_start  = 1, 130, 205,
parent_grid_ratio = 1, 3, 3,
parent_time_step_ratio = 1, 3, 3,
feedback        = 1,
smooth_option   = 0
vortex_interval = 20, 20, 20,
max_vortex_speed = 40, 40, 40,
time_to_move    = 0, 9999, 0,
corral_dist     = 0, 15, 15,
track_level     = 85000
/

&physics
mp_physics      = 4, 4, 4,
ra_lw_physics   = 4, 4, 4,
ra_sw_physics   = 4, 4, 4,
radt            = 15, 15, 15,
sf_sfclay_physics = 1, 1, 1,
sf_surface_physics = 1, 1, 1,
bl_pbl_physics  = 1, 1, 1,
bldt            = 0, 0, 0,
cu_physics      = 1, 0, 0,
cudt            = 5, 0, 0,
kfeta_trigger   = 2,
isfflx          = 1,
isftcflx        = 2,
ifsnof          = 0,
icloud          = 1,

```



```

surface_input_source      = 1,
num_soil_layers          = 5,
sf_urban_physics        = 0,
mp_zero_out              = 0,
maxiens                  = 1,
maxens                   = 3,
maxens2                  = 3,
maxens3                  = 16,
ensdim                   = 144,
slope_rad                = 0,
topo_shading             = 0,
omlcall                  = 0,
oml_hml0                 = 100,
oml_gamma                 = 0.14,
stoch_force_opt          = 0, 0, 0, ! turns SKEBS on (0=off)
stoch_vertstruc_opt      = 1, 1, 1, ! makes SKEBS pattern vary with height
tot_backscat_psi         = 1E-05, ! default perturbation amplitude for streamfunction field
tot_backscat_t           = 1E-06, !default perturbation amplitude for temperature field
nens                      = 9,    !random seed
/

&fdda
grid_fdda                = 0,    0,    0,
gfdda_inname             = "wrffdda_d<domain>",
gfdda_end_h              = 120,  120,  24,
gfdda_interval_m         = 360,  360,  360,
fgdt                     = 0,    0,    0,
fgdtzero                 = 0,    0,    0,
if_no_pbl_nudging_uv     = 0,    0,    0,
if_no_pbl_nudging_t      = 0,    0,    0,
if_no_pbl_nudging_ph     = 0,    0,    0,
if_zfac_uv               = 0,    0,    0,
k_zfac_uv                = 10,   10,   10,
if_zfac_t                = 0,    0,    0,
k_zfac_t                 = 10,   10,   10,
if_zfac_ph               = 0,    0,    0,
k_zfac_ph                = 10,   10,   10,
dk_zfac_uv               = 1,    1,    1,
dk_zfac_t                = 1,    1,    1,
dk_zfac_ph               = 1,    1,    1,
guv                      = 0.0003, 0.0000, 0.0000,
gt                      = 0.0000, 0.0000, 0.0000,
gph                      = 0.0000, 0.0000, 0.0000,
if_ramping               = 1,
dtramp_min               = 60.0,
io_form_gfdda            = 2,
/

&dynamics
iso_temp                 = 0.,
w_damping                = 1,
diff_opt                 = 1,
km_opt                   = 4,
diff_6th_opt             = 0,
diff_6th_factor          = 0.12,
base_temp                = 290.
damp_opt                 = 0,
zdamp                    = 5000., 5000., 5000.,
dampcoef                 = 0.2,  0.2,  0.2
khdif                    = 0,    0,    0,
kvdif                    = 0,    0,    0,
non_hydrostatic          = .true., .true., .true.,
moist_adv_opt            = 0, 0, 0,
scalar_adv_opt           = 0, 0, 0,
use_baseparam_fr_nml    = .true.
/

&bdy_control
spec_bdy_width           = 5,
spec_zone                = 1,
relax_zone               = 4,
specified                = .true., .false., .false.,
nested                   = .false., .true., .true.,
perturb_bdy              = 1,    !boundary perturbations on (0=off)
/

```

```

&grib2
/

&namelist_quilt
nio_tasks_per_group = 0,
nio_groups = 1,
/

```

## A.2.2 UMWM(main.nml)

```

&DOMAIN
  isGlobal      = .F.           ! Global (.T.) or regional (.F.)
  nm            = 1195          ! Domain size in x
  nm            = 1075          ! Domain size in y
  om            = 37            ! Number of frequency bins
  pm            = 36            ! Number of directions
  fmin          = 0.0313        ! Lowest frequency bin [Hz]
  fmax          = 2.0           ! Highest frequency bin [Hz]
  fprog         = 0.5           ! Highest prognostic frequency bin [Hz]
  startTimeStr  = '2008-09-08_00:00:00' ! Simulation start time
  stopTimeStr   = '2008-09-08_01:00:00' ! Simulation end time
  dtg           = 60            ! Global (I/O) time step [s]
  restart       = .f.           ! Restart from file
/

&PHYSICS
  g             = 9.80665       ! Gravitational acceleration [m/s^2]
  nu_air        = 1.56E-5       ! Kinematic viscosity of air [m^2/s]
  nu_water      = 0.9E-6       ! Kinematic viscosity of water [m^2/s]
  sfct          = 0.07         ! Surface tension [N/m]
  kappa         = 0.4           ! Von Karman constant
  z             = 10.           ! Height of the input wind speed [m]
  gustiness     = 0.0           ! Random wind gustiness factor (should be between 0 and 0.2)
  dmin          = 20.           ! Depth limiter [m]
  explim        = 1.1           ! Exponent limiter (0.69 ~ 100% growth)
  sin_fac       = 0.11          ! Input factor from following winds
  sin_diss1     = 0.10          ! Damping factor from opposing winds
  sin_diss2     = 0.01          ! Damping factor from swell overrunning wind
  sds_fac       = 42.           ! Breaking dissipation factor
  sds_power     = 2.5           ! Saturation spectrum power
  mss_fac       = 120.          ! Mean-square-slope adjustment to Sds
  snl_fac       = 5.            ! Wave energy downshifting factor
  sdt_fac       = 0.01          ! Dissipation due to turbulence factor
  sbf_fac       = 0.003         ! Bottom friction coefficient [m/s]
  sbp_fac       = 0.003         ! Bottom percolation coefficient [m/s]
/

&GRID
  gridFromFile  = .T.           ! Set to .T. if lon/lat fields are input from file
  delx          = 12000         ! Grid spacing in x [m] if gridFromFile = .F.
  dely          = 12000         ! Grid spacing in y [m] if gridFromFile = .F.
  topoFromFile  = .T.           ! Set to .T. to input bathymetry from file
  dpt           = 1000         ! Constant water depth [m] if topoFromFile = .F.
  fillEstuaries = .F.           ! Set to .T. to fill cells with 3 land neighbours
  fillLakes     = .F.           ! Set to .T. to fill user chosen seas/lakes
/

&FORCING
  winds         = .F.           ! Wind input from file
  currents      = .F.           ! Currents input from file
  air_density   = .F.           ! Air density input from file
  water_density = .F.           ! Water density input from file
/

&FORCING_CONSTANT
  wspd0         = 25            ! Wind speed [m/s]
  wdir0         = 0.            ! Wind direction [rad]
  uc0           = 0.            ! x-component ocean current [m/s]
  vc0           = 0.            ! y-component ocean current [m/s]
  rhoa0         = 1.2           ! Air density [kg/m^3]
  rhow0         = 1030          !
/

  Water density [kg/m^3]
/

&OUTPUT
  outgrid       = 1            ! Gridded output interval [hours]
  outspec       = 1            ! Spectrum output interval [hours]
  outrst        = 6            ! Restart output interval [hours]

```

```

xpl          = 400 ! Grid cell in x for stdout (screen)
ypl          = 500 ! Grid cell in y for stdout (screen)
stokes       = .T. ! Output Stokes drift velocity fields
/
&STOKES
  depths     = 0 0.2 0.4 0.6 0.8 1 2 5 10 30 50 100

```

### A.2.3 HYCOM(blkdat.input)

```

ERA-15 forcing; flx-s14w; LWcorr; precip+2mm; SSSrlx; FCT2 tsadv; 0-tracer.
Sigma0; GDEM3 init; KPP mixed layer; SeaWiFS mon KPAR; nested in ATld0.08 2.6;
S-Z(15-11): dp00/f/x/i=3m/1.125/12m/1m; ds=1m/1.125/4m; src_2.2.34;
1234567890123456789012345678901234567890123456789012345678901234567890123456789012345678901234567890
 22 'iversn' = hycom version number xl0
 201 'iexpt' = experiment number xl0
1000 'idm'   = longitudinal array size
1000 'jdm'   = latitudinal array size
 700 'itest' = grid point where detailed diagnostics are desired
 700 'jtest' = grid point where detailed diagnostics are desired
 32  'kdm'   = number of layers
 32  'nhybrd' = number of hybrid levels (0=all isopycnal)
 14  'nsigma' = number of sigma levels (nhybrd-nsigma z-levels)
 3.0 'dp00'  = deep z-level spacing minimum thickness (m)
450.0 'dp00x' = deep z-level spacing maximum thickness (m)
 1.18 'dp00f' = deep z-level spacing stretching factor (1.0=const.space)
 0.5  'ds00'  = shallow z-level spacing minimum thickness (m)
 75.0 'ds00x' = shallow z-level spacing maximum thickness (m)
 1.18 'ds00f' = shallow z-level spacing stretching factor (1.0=const.space)
 1.0  'dp00i' = deep iso-pycnal spacing minimum thickness (m)
 6.0  'isotop' = shallowest depth for isopycnal layers (m, <0 from file)
35.0  'saln0' = initial salinity value (psu), only used for iniflg<2
 1  'locsig' = locally-referenced pot. density for stability (0=F,1=T)
 2  'kapref' = thermobaric ref. state (-1=input,0=none,1,2,3=constant)
 2  'thflag' = reference pressure flag (0=Sigma-0, 2=Sigma-2)
34.0  'thbase' = reference density (sigma units)
 0  'vsigma' = spacially varying isopycnal target densities (0=F,1=T)
28.10 'sigma' = layer 1 isopycnal target density (sigma units)
28.90 'sigma' = layer 2 isopycnal target density (sigma units)
29.70 'sigma' = layer 3 isopycnal target density (sigma units)
30.50 'sigma' = layer 4 isopycnal target density (sigma units)
30.95 'sigma' = layer 5 isopycnal target density (sigma units)
31.50 'sigma' = layer 6 isopycnal target density (sigma units)
32.05 'sigma' = layer 7 isopycnal target density (sigma units)
32.60 'sigma' = layer 8 isopycnal target density (sigma units)
33.15 'sigma' = layer 9 isopycnal target density (sigma units)
33.70 'sigma' = layer 10 isopycnal target density (sigma units)
34.25 'sigma' = layer 11 isopycnal target density (sigma units)
34.75 'sigma' = layer 12 isopycnal target density (sigma units)
35.15 'sigma' = layer 13 isopycnal target density (sigma units)
35.50 'sigma' = layer 14 isopycnal target density (sigma units)
35.80 'sigma' = layer 15 isopycnal target density (sigma units)
36.04 'sigma' = layer 16 isopycnal target density (sigma units)
36.20 'sigma' = layer 17 isopycnal target density (sigma units)
36.38 'sigma' = layer 18 isopycnal target density (sigma units)
36.52 'sigma' = layer 19 isopycnal target density (sigma units)
36.62 'sigma' = layer 20 isopycnal target density (sigma units)
36.70 'sigma' = layer 21 isopycnal target density (sigma units)
36.77 'sigma' = layer 22 isopycnal target density (sigma units)
36.83 'sigma' = layer 23 isopycnal target density (sigma units)
36.89 'sigma' = layer 24 isopycnal target density (sigma units)
36.97 'sigma' = layer 25 isopycnal target density (sigma units)
37.02 'sigma' = layer 26 isopycnal target density (sigma units)
37.06 'sigma' = layer 27 isopycnal target density (sigma units)
37.10 'sigma' = layer 28 isopycnal target density (sigma units)
37.17 'sigma' = layer 29 isopycnal target density (sigma units)
37.30 'sigma' = layer 30 isopycnal target density (sigma units)
37.42 'sigma' = layer 31 isopycnal target density (sigma units)
37.48 'sigma' = layer 32 isopycnal target density (sigma units)
 3  'iniflg' = initial state flag (0=levl, 1=zonl, 2=clim)
 0  'jerlv0' = initial jerlov water type (1 to 5; 0 to use KPAR)
 3  'yrflag' = days in year flag (0=360, 1=366, 2=366J1, 3=actual)
 0  'sshflg' = diagnostic SSH flag (0=SSH,1=SSH&stericSSH)
0.0416667 'dsurfq' = number of days between model diagnostics at the surface
0.0416667 'diagfq' = number of days between model diagnostics

```

```

0.0 'proffq' = number of days between model diagnostics at selected locs
0.0 'tilefq' = number of days between model diagnostics on selected tiles
0.0 'meanfq' = number of days between model diagnostics (time averaged)
9999.0 'rstrfq' = number of days between model restart output
1.0 'bnstfq' = number of days between baro nesting archive input
1.0 'nestfq' = number of days between 3-d nesting archive input
0.125 'cplifq' = number of days (or time steps) between sea ice coupling
120.0 'baclin' = baroclinic time step (seconds), int. divisor of 86400
5.0 'batrop' = barotropic time step (seconds), int. div. of baclin/2
0 'incflg' = incremental update flag (0=no, 1=yes, 2=full-velocity)
100 'incstp' = no. timesteps for full update (1=direct insertion)
1 'incupf' = number of days of incremental updating input
0.125 'wbaro' = barotropic time smoothing weight
1 'btrlfr' = leapfrog barotropic time step (0=F,1=T)
0 'btrmas' = barotropic is mass conserving (0=F,1=T)
8.0 'hybrlx' = HYBGEN: inverse relaxation coefficient (time steps)
0.01 'hybiso' = HYBGEN: Use PCM if layer is within hybiso of target density
3 'hybmap' = hybrid remapper flag (0=PCM, 1=PLM, 2=PPM, 3=WENO-like)
0 'hybflg' = hybrid generator flag (0=T&S, 1=th&S, 2=th&T)
0 'advflg' = thermal advection flag (0=T&S, 1=th&S, 2=th&T)
2 'advtyp' = scalar advection type (0=PCM,1=MPDATA,2=FCT2,4=FCT4)
2 'momtyp' = momentum advection type (2=2nd order, 4=4th order)
-1.0 'slip' = +1 for free-slip, -1 for non-slip boundary conditions
0.05 'visco2' = deformation-dependent Laplacian viscosity factor
0.0 'visco4' = deformation-dependent biharmonic viscosity factor
0.0 'facdf4' = speed-dependent biharmonic viscosity factor
0.003 'veldf2' = diffusion velocity (m/s) for Laplacian momentum dissip.
0.02 'veldf4' = diffusion velocity (m/s) for biharmonic momentum dissip.
0.0 'thkdf2' = diffusion velocity (m/s) for Laplacian thickness diffus.
0.01 'thkdf4' = diffusion velocity (m/s) for biharmonic thickness diffus.
0.005 'temdf2' = diffusion velocity (m/s) for Laplacian temp/saln diffus.
1.0 'temdfc' = temp diffusion conservation (0.0,1.0 all dens,temp resp.)
0.0 'vertmx' = diffusion velocity (m/s) for momentum at MICOM M.L.base
0.05 'cbar' = rms flow speed (m/s) for linear bottom friction
2.2e-3 'cb' = coefficient of quadratic bottom friction
0.0 'drglim' = limiter for explicit friction (1.0 none, 0.0 implicit)
0.0 'drgscl' = scale factor for tidal drag (0.0 for no tidal drag)
500.0 'thkdrq' = thickness of bottom boundary layer for tidal drag (m)
10.0 'thkbot' = thickness of bottom boundary layer (m)
0.02 'sigjmp' = minimum density jump across interfaces (kg/m**3)
0.3 'tmljmp' = equivalent temperature jump across mixed-layer (degC)
15.0 'thkmls' = reference mixed-layer thickness for SSS relaxation (m)
0.0 'thkmlt' = reference mixed-layer thickness for SST relaxation (m)
5.0 'thkriv' = nominal thickness of river inflow (m)
20.0 'thkfrz' = maximum thickness of near-surface freezing zone (m)
0 'iceflg' = sea ice model flag (0=none,1=energy loan,2=coupled/esmf)
0.0 'tfrz_0' = ENLN: ice melting point (degC) at S=0psu
-0.054 'tfrz_s' = ENLN: gradient of ice melting point (degC/psu)
0.0 'ticegr' = ENLN: temp. grad. inside ice (deg/m); =0 use surtmp
0.5 'hicemn' = ENLN: minimum ice thickness (m)
10.0 'hicemx' = ENLN: maximum ice thickness (m)
0 'ntracr' = number of tracers (0=none,negative to initialize)
0 'trcflg' = tracer flags (one digit per tr, most sig. replicated)
240 'tsofrq' = number of time steps between anti-drift offset calcs
0.0 'tofset' = temperature anti-drift offset (degC/century)
0.0 'sofset' = salnity anti-drift offset (psu/century)
1 'mlflag' = mixed layer flag (0=none,1=KPP,2-3=KT,4=PWP,5=MY,6=GISS)
1 'pensol' = KT: activate penetrating solar rad. (0=F,1=T)
999.0 'dtrate' = KT: maximum permitted m.l. detrainment rate (m/day)
19.2 'thkmin' = KT/PWP: minimum mixed-layer thickness (m)
1 'dypflg' = KT/PWP: diapycnal mixing flag (0=none, 1=KPP, 2=explicit)
240 'mixfrq' = KT/PWP: number of time steps between diapycnal mix calcs
1.e-7 'diapyc' = KT/PWP: diapycnal diffusivity x buoyancy freq. (m**2/s**2)
0.25 'rigr' = PWP: critical gradient richardson number
0.65 'ribc' = PWP: critical bulk richardson number
0.7 'rinfty' = KPP: maximum gradient richardson number (shear inst.)
0.25 'ricr' = KPP: critical bulk richardson number
0.0 'bldmin' = KPP: minimum surface boundary layer thickness (m)
1200.0 'bldmax' = K-PROF: maximum surface boundary layer thickness (m)
0.7 'cekman' = KPP/KT: scale factor for Ekman depth
1.0 'cmonob' = KPP: scale factor for Monin-Obukov depth
0 'bblkpp' = KPP: activate bottom boundary layer (0=F,1=T)
1 'shinst' = KPP: activate shear instability mixing (0=F,1=T)
1 'dbdiff' = KPP: activate double diffusion mixing (0=F,1=T)
1 'nonloc' = KPP: activate nonlocal b. layer mixing (0=F,1=T)
0 'botdiw' = K-PROF: activate bot.enhan.int.wav mixing (0=F,1=T)

```

```

1  'difout' = K-PROF: output visc/diff coeffs in archive (0=F,1=T)
0  'difsmo' = K-PROF: number of layers with horiz smooth diff coeffs
50.0e-4 'difm0' = KPP: max viscosity due to shear instability (m**2/s)
50.0e-4 'difs0' = KPP: max diffusivity due to shear instability (m**2/s)
0.3e-4 'difmiw' = KPP: background/internal wave viscosity (m**2/s)
0.1e-4 'difsiw' = KPP: background/internal wave diffusivity (m**2/s)
10.0e-4 'dsfmax' = KPP: salt fingering diffusivity factor (m**2/s)
1.9 'rrho0' = KPP: salt fingering  $rp=(\alpha*\delta T)/(\beta*\delta S)$ 
98.96 'cs' = KPP: value for nonlocal flux term
10.0 'cstar' = KPP: value for nonlocal flux term
0.0 'cv' = KPP: buoyancy frequency ratio (0.0 to use a fn. of N)
5.0 'c11' = KPP: value for turb velocity scale
2  'hblflg' = KPP: b. layer interp. flag (0=const.,1=linear,2=quad.)
2  'niter' = KPP: iterations for semi-implicit soln. (2 recommended)
0  'fltflg' = FLOATS: synthetic float flag (0=no; 1=yes)
4  'nfladv' = FLOATS: advect every nfladv bacl. time steps (even, >=4)
1  'nflsam' = FLOATS: output (0=every nfladv steps; >0=no. of days)
0  'intpfl' = FLOATS: horiz. interp. (0=2nd order+n.n.; 1=n.n. only)
0  'iturbv' = FLOATS: add horiz. turb. advection velocity (0=no; 1=yes)
1  'ismpfl' = FLOATS: sample water properties at float (0=no; 1=yes)
4.63e-6 'tbvar' = FLOATS: horizontal turb. vel. variance scale (m**2/s**2)
0.4 'tdecri' = FLOATS: inverse decorrelation time scale (1/day)
2  'lbflag' = lateral barotropic bndy flag (0=none, 1=port, 2=input)
2  'tidflg' = TIDES: tidal forcing flag (0=none,1=open-bdy,2=bdy&body)
11111111 'tidcon' = TIDES: 1 digit per (Q1K2P1N201K1S2M2), 0=off,1=on
0.06 'tidsal' = TIDES: scalar self attraction and loading factor (<0: file)
1  'tidgen' = TIDES: generic time (0=F,1=T)
1.0 'tidrmp' = TIDES: ramp time (days)
0.0 'tid_t0' = TIDES: origin for ramp time (model day)
12 'clmflg' = climatology frequency flag (6=bimonthly, 12=monthly)
1  'wndflg' = wind stress input flag (0=none,1=u/v-grid,2,3=p-grid)
2  'ustflg' = ustar forcing flag (3=input,1,2=wndspd,4=stress)
3  'flxflg' = thermal forcing flag (0=none,3=net-flux,1,2,4=sst-based)
0  'empflg' = E-P forcing flag (0=none,3=net_E-P, 1,2,4=sst-bas_E)
0  'dswflg' = diurnal shortwave flag (0=none,1=daily to diurnal corr.)
0  'sssflg' = SSS relaxation flag (0=none,1=clim,-1=clim&rmx)
0  'lwflg' = longwave (SST) flag (0=none,1=clim,2=atmos)
0  'sstflg' = SST relaxation flag (0=none,1=clim,2=atmos,3=observed)
0  'icmflg' = ice mask flag (0=none,1=clim,2=atmos,3=obs/coupled)
0  'flxoff' = net flux offset flag (0=F,1=T)
0  'flxsmo' = smooth surface fluxes (0=F,1=T)
0  'relax' = activate lateral boundary nudging (0=F,1=T)
0  'trcrlx' = activate lat. bound. tracer nudging (0=F,1=T)
0  'priver' = rivers as a precipitation bogas (0=F,1=T)
0  'epmass' = treat evap-precip as a mass exchange (0=F,1=T)

```

# Appendix B

## List of UMCM output

### B.1 List of WRF output

```
dimensions:
  Time = UNLIMITED; // (1 currently)
  DateStrLen = 19;
  west_east = 399;
  south_north = 359;
  bottom_top = 35;
  bottom_top_stag = 36;
  soil_layers_stag = 5;
  west_east_stag = 400;
  south_north_stag = 360;
variables:
  char Times(Time=1, DateStrLen=19);

  float XLAT(Time=1, south_north=359, west_east=399);
    :FieldType = 104; // int
    :MemoryOrder = "XY ";
    :description = "LATITUDE, SOUTH IS NEGATIVE";
    :units = "degree_north";
    :stagger = "";

  float XLONG(Time=1, south_north=359, west_east=399);
    :FieldType = 104; // int
    :MemoryOrder = "XY ";
    :description = "LONGITUDE, WEST IS NEGATIVE";
    :units = "degree_east";
    :stagger = "";

  float LU_INDEX(Time=1, south_north=359, west_east=399);
    :FieldType = 104; // int
    :MemoryOrder = "XY ";
    :description = "LAND USE CATEGORY";
    :units = "";
    :stagger = "";
    :coordinates = "XLONG XLAT";

  float ZNU(Time=1, bottom_top=35);
    :FieldType = 104; // int
    :MemoryOrder = "Z ";
    :description = "eta values on half (mass) levels";
    :units = "";
    :stagger = "";

  float ZNW(Time=1, bottom_top_stag=36);
    :FieldType = 104; // int
    :MemoryOrder = "Z ";
    :description = "eta values on full (w) levels";
    :units = "";
    :stagger = "Z";

  float ZS(Time=1, soil_layers_stag=5);
    :FieldType = 104; // int
    :MemoryOrder = "Z ";
    :description = "DEPTHS OF CENTERS OF SOIL LAYERS";
    :units = "m";
    :stagger = "Z";

  float DZS(Time=1, soil_layers_stag=5);
    :FieldType = 104; // int
    :MemoryOrder = "Z ";
    :description = "THICKNESSES OF SOIL LAYERS";
    :units = "m";
    :stagger = "Z";

  float VAR_SSO(Time=1, south_north=359, west_east=399);
    :FieldType = 104; // int
    :MemoryOrder = "XY ";
    :description = "variance of subgrid-scale orography";
    :units = "m2";
```

```

:stagger = "";
:coordinates = "XLONG XLAT";

float LAP_HGT(Time=1, south_north=359, west_east=399);
:FieldType = 104; // int
:MemoryOrder = "XY ";
:description = "Laplacian of orography";
:units = "m";
:stagger = "";
:coordinates = "XLONG XLAT";

float U(Time=1, bottom_top=35, south_north=359, west_east_stag=400);
:FieldType = 104; // int
:MemoryOrder = "XYZ";
:description = "x-wind component";
:units = "m s-1";
:stagger = "X";
:coordinates = "XLONG_U XLAT_U";

float V(Time=1, bottom_top=35, south_north_stag=360, west_east=399);
:FieldType = 104; // int
:MemoryOrder = "XYZ";
:description = "y-wind component";
:units = "m s-1";
:stagger = "Y";
:coordinates = "XLONG_V XLAT_V";

float W(Time=1, bottom_top_stag=36, south_north=359, west_east=399);
:FieldType = 104; // int
:MemoryOrder = "XYZ";
:description = "z-wind component";
:units = "m s-1";
:stagger = "Z";
:coordinates = "XLONG XLAT";

float PH(Time=1, bottom_top_stag=36, south_north=359, west_east=399);
:FieldType = 104; // int
:MemoryOrder = "XYZ";
:description = "perturbation geopotential";
:units = "m2 s-2";
:stagger = "Z";
:coordinates = "XLONG XLAT";

float PHB(Time=1, bottom_top_stag=36, south_north=359, west_east=399);
:FieldType = 104; // int
:MemoryOrder = "XYZ";
:description = "base-state geopotential";
:units = "m2 s-2";
:stagger = "Z";
:coordinates = "XLONG XLAT";

float T(Time=1, bottom_top=35, south_north=359, west_east=399);
:FieldType = 104; // int
:MemoryOrder = "XYZ";
:description = "perturbation potential temperature (theta-t0)";
:units = "K";
:stagger = "";
:coordinates = "XLONG XLAT";

float HFX_FORCE(Time=1);
:FieldType = 104; // int
:MemoryOrder = "0 ";
:description = "SCM ideal surface sensible heat flux";
:units = "W m-2";
:stagger = "";

float LH_FORCE(Time=1);
:FieldType = 104; // int
:MemoryOrder = "0 ";
:description = "SCM ideal surface latent heat flux";
:units = "W m-2";
:stagger = "";

float TSK_FORCE(Time=1);
:FieldType = 104; // int
:MemoryOrder = "0 ";

```

```

:description = "SCM ideal surface skin temperature";
:units = "W m-2";
:stagger = "";

float HFX_FORCE_TEND(Time=1);
:FieldType = 104; // int
:MemoryOrder = "0 ";
:description = "SCM ideal surface sensible heat flux tendency";
:units = "W m-2 s-1";
:stagger = "";

float LH_FORCE_TEND(Time=1);
:FieldType = 104; // int
:MemoryOrder = "0 ";
:description = "SCM ideal surface latent heat flux tendency";
:units = "W m-2 s-1";
:stagger = "";

float TSK_FORCE_TEND(Time=1);
:FieldType = 104; // int
:MemoryOrder = "0 ";
:description = "SCM ideal surface skin temperature tendency";
:units = "W m-2 s-1";
:stagger = "";

float MU(Time=1, south_north=359, west_east=399);
:FieldType = 104; // int
:MemoryOrder = "XY ";
:description = "perturbation dry air mass in column";
:units = "Pa";
:stagger = "";
:coordinates = "XLONG XLAT";

float MUB(Time=1, south_north=359, west_east=399);
:FieldType = 104; // int
:MemoryOrder = "XY ";
:description = "base state dry air mass in column";
:units = "Pa";
:stagger = "";
:coordinates = "XLONG XLAT";

float NEST_POS(Time=1, south_north=359, west_east=399);
:FieldType = 104; // int
:MemoryOrder = "XY ";
:description = "-";
:units = "-";
:stagger = "";
:coordinates = "XLONG XLAT";

float P(Time=1, bottom_top=35, south_north=359, west_east=399);
:FieldType = 104; // int
:MemoryOrder = "XYZ";
:description = "perturbation pressure";
:units = "Pa";
:stagger = "";
:coordinates = "XLONG XLAT";

float PB(Time=1, bottom_top=35, south_north=359, west_east=399);
:FieldType = 104; // int
:MemoryOrder = "XYZ";
:description = "BASE STATE PRESSURE";
:units = "Pa";
:stagger = "";
:coordinates = "XLONG XLAT";

float FNM(Time=1, bottom_top=35);
:FieldType = 104; // int
:MemoryOrder = "Z ";
:description = "upper weight for vertical stretching";
:units = "";
:stagger = "";

float FNP(Time=1, bottom_top=35);
:FieldType = 104; // int
:MemoryOrder = "Z ";
:description = "lower weight for vertical stretching";

```



```

:units = "";
:stagger = "";

float RDNW(Time=1, bottom_top=35);
:FieldType = 104; // int
:MemoryOrder = "Z ";
:description = "inverse d(eta) values between full (w) levels";
:units = "";
:stagger = "";

float RDN(Time=1, bottom_top=35);
:FieldType = 104; // int
:MemoryOrder = "Z ";
:description = "inverse d(eta) values between half (mass) levels";
:units = "";
:stagger = "";

float DNW(Time=1, bottom_top=35);
:FieldType = 104; // int
:MemoryOrder = "Z ";
:description = "d(eta) values between full (w) levels";
:units = "";
:stagger = "";

float DN(Time=1, bottom_top=35);
:FieldType = 104; // int
:MemoryOrder = "Z ";
:description = "d(eta) values between half (mass) levels";
:units = "";
:stagger = "";

float CFN(Time=1);
:FieldType = 104; // int
:MemoryOrder = "0 ";
:description = "extrapolation constant";
:units = "";
:stagger = "";

float CFN1(Time=1);
:FieldType = 104; // int
:MemoryOrder = "0 ";
:description = "extrapolation constant";
:units = "";
:stagger = "";

float P_HYD(Time=1, bottom_top=35, south_north=359, west_east=399);
:FieldType = 104; // int
:MemoryOrder = "XYZ";
:description = "hydrostatic pressure";
:units = "Pa";
:stagger = "";
:coordinates = "XLONG XLAT";

float Q2(Time=1, south_north=359, west_east=399);
:FieldType = 104; // int
:MemoryOrder = "XY ";
:description = "QV at 2 M";
:units = "kg kg-1";
:stagger = "";
:coordinates = "XLONG XLAT";

float T2(Time=1, south_north=359, west_east=399);
:FieldType = 104; // int
:MemoryOrder = "XY ";
:description = "TEMP at 2 M";
:units = "K";
:stagger = "";
:coordinates = "XLONG XLAT";

float TH2(Time=1, south_north=359, west_east=399);
:FieldType = 104; // int
:MemoryOrder = "XY ";
:description = "POT TEMP at 2 M";
:units = "K";
:stagger = "";
:coordinates = "XLONG XLAT";

```

```

float PSFC(Time=1, south_north=359, west_east=399);
:FieldType = 104; // int
:MemoryOrder = "XY ";
:description = "SFC PRESSURE";
:units = "Pa";
:stagger = "";
:coordinates = "XLONG XLAT";

float U10(Time=1, south_north=359, west_east=399);
:FieldType = 104; // int
:MemoryOrder = "XY ";
:description = "U at 10 M";
:units = "m s-1";
:stagger = "";
:coordinates = "XLONG XLAT";

float V10(Time=1, south_north=359, west_east=399);
:FieldType = 104; // int
:MemoryOrder = "XY ";
:description = "V at 10 M";
:units = "m s-1";
:stagger = "";
:coordinates = "XLONG XLAT";

float RDX(Time=1);
:FieldType = 104; // int
:MemoryOrder = "0 ";
:description = "INVERSE X GRID LENGTH";
:units = "";
:stagger = "";

float RDY(Time=1);
:FieldType = 104; // int
:MemoryOrder = "0 ";
:description = "INVERSE Y GRID LENGTH";
:units = "";
:stagger = "";

float RESM(Time=1);
:FieldType = 104; // int
:MemoryOrder = "0 ";
:description = "TIME WEIGHT CONSTANT FOR SMALL STEPS";
:units = "";
:stagger = "";

float ZETATOP(Time=1);
:FieldType = 104; // int
:MemoryOrder = "0 ";
:description = "ZETA AT MODEL TOP";
:units = "";
:stagger = "";

float CF1(Time=1);
:FieldType = 104; // int
:MemoryOrder = "0 ";
:description = "2nd order extrapolation constant";
:units = "";
:stagger = "";

float CF2(Time=1);
:FieldType = 104; // int
:MemoryOrder = "0 ";
:description = "2nd order extrapolation constant";
:units = "";
:stagger = "";

float CF3(Time=1);
:FieldType = 104; // int
:MemoryOrder = "0 ";
:description = "2nd order extrapolation constant";
:units = "";
:stagger = "";

int ITIMESTEP(Time=1);
:FieldType = 106; // int

```

```

:MemoryOrder = "0 ";
:description = "";
:units = "";
:stagger = "";

float XTIME(Time=1);
:FieldType = 104; // int
:MemoryOrder = "0 ";
:description = "minutes since simulation start";
:units = "";
:stagger = "";

float QVAPOR(Time=1, bottom_top=35, south_north=359, west_east=399);
:FieldType = 104; // int
:MemoryOrder = "XYZ";
:description = "Water vapor mixing ratio";
:units = "kg kg-1";
:stagger = "";
:coordinates = "XLONG XLAT";

float QCLOUD(Time=1, bottom_top=35, south_north=359, west_east=399);
:FieldType = 104; // int
:MemoryOrder = "XYZ";
:description = "Cloud water mixing ratio";
:units = "kg kg-1";
:stagger = "";
:coordinates = "XLONG XLAT";

float QRAIN(Time=1, bottom_top=35, south_north=359, west_east=399);
:FieldType = 104; // int
:MemoryOrder = "XYZ";
:description = "Rain water mixing ratio";
:units = "kg kg-1";
:stagger = "";
:coordinates = "XLONG XLAT";

float QICE(Time=1, bottom_top=35, south_north=359, west_east=399);
:FieldType = 104; // int
:MemoryOrder = "XYZ";
:description = "Ice mixing ratio";
:units = "kg kg-1";
:stagger = "";
:coordinates = "XLONG XLAT";

float QSNOW(Time=1, bottom_top=35, south_north=359, west_east=399);
:FieldType = 104; // int
:MemoryOrder = "XYZ";
:description = "Snow mixing ratio";
:units = "kg kg-1";
:stagger = "";
:coordinates = "XLONG XLAT";

float SHDMAX(Time=1, south_north=359, west_east=399);
:FieldType = 104; // int
:MemoryOrder = "XY ";
:description = "ANNUAL MAX VEG FRACTION";
:units = "";
:stagger = "";
:coordinates = "XLONG XLAT";

float SHDMIN(Time=1, south_north=359, west_east=399);
:FieldType = 104; // int
:MemoryOrder = "XY ";
:description = "ANNUAL MIN VEG FRACTION";
:units = "";
:stagger = "";
:coordinates = "XLONG XLAT";

float SNOALB(Time=1, south_north=359, west_east=399);
:FieldType = 104; // int
:MemoryOrder = "XY ";
:description = "ANNUAL MAX SNOW ALBEDO IN FRACTION";
:units = "";
:stagger = "";
:coordinates = "XLONG XLAT";

```

```

float TSLB(Time=1, soil_layers_stag=5, south_north=359, west_east=399);
:FieldType = 104; // int
:MemoryOrder = "XYZ";
:description = "SOIL TEMPERATURE";
:units = "K";
:stagger = "Z";
:coordinates = "XLONG XLAT";

float SMOIS(Time=1, soil_layers_stag=5, south_north=359, west_east=399);
:FieldType = 104; // int
:MemoryOrder = "XYZ";
:description = "SOIL MOISTURE";
:units = "m3 m-3";
:stagger = "Z";
:coordinates = "XLONG XLAT";

float SH2O(Time=1, soil_layers_stag=5, south_north=359, west_east=399);
:FieldType = 104; // int
:MemoryOrder = "XYZ";
:description = "SOIL LIQUID WATER";
:units = "m3 m-3";
:stagger = "Z";
:coordinates = "XLONG XLAT";

float SMCREL(Time=1, soil_layers_stag=5, south_north=359, west_east=399);
:FieldType = 104; // int
:MemoryOrder = "XYZ";
:description = "RELATIVE SOIL MOISTURE";
:units = "";
:stagger = "Z";
:coordinates = "XLONG XLAT";

float SEAICE(Time=1, south_north=359, west_east=399);
:FieldType = 104; // int
:MemoryOrder = "XY ";
:description = "SEA ICE FLAG";
:units = "";
:stagger = "";
:coordinates = "XLONG XLAT";

float XICEM(Time=1, south_north=359, west_east=399);
:FieldType = 104; // int
:MemoryOrder = "XY ";
:description = "SEA ICE FLAG (PREVIOUS STEP)";
:units = "";
:stagger = "";
:coordinates = "XLONG XLAT";

float SPROFF(Time=1, south_north=359, west_east=399);
:FieldType = 104; // int
:MemoryOrder = "XY ";
:description = "SURFACE RUNOFF";
:units = "mm";
:stagger = "";
:coordinates = "XLONG XLAT";

float UDROFF(Time=1, south_north=359, west_east=399);
:FieldType = 104; // int
:MemoryOrder = "XY ";
:description = "UNDERGROUND RUNOFF";
:units = "mm";
:stagger = "";
:coordinates = "XLONG XLAT";

int IVGTYP(Time=1, south_north=359, west_east=399);
:FieldType = 106; // int
:MemoryOrder = "XY ";
:description = "DOMINANT VEGETATION CATEGORY";
:units = "";
:stagger = "";
:coordinates = "XLONG XLAT";

int ISLTYP(Time=1, south_north=359, west_east=399);
:FieldType = 106; // int
:MemoryOrder = "XY ";
:description = "DOMINANT SOIL CATEGORY";

```

```

:units = "";
:stagger = "";
:coordinates = "XLONG XLAT";

float VEGFRA(Time=1, south_north=359, west_east=399);
:FieldType = 104; // int
:MemoryOrder = "XY ";
:description = "VEGETATION FRACTION";
:units = "";
:stagger = "";
:coordinates = "XLONG XLAT";

float GRDFLX(Time=1, south_north=359, west_east=399);
:FieldType = 104; // int
:MemoryOrder = "XY ";
:description = "GROUND HEAT FLUX";
:units = "W m-2";
:stagger = "";
:coordinates = "XLONG XLAT";

float ACGRDFLX(Time=1, south_north=359, west_east=399);
:FieldType = 104; // int
:MemoryOrder = "XY ";
:description = "ACCUMULATED GROUND HEAT FLUX";
:units = "J m-2";
:stagger = "";
:coordinates = "XLONG XLAT";

float ACSNOM(Time=1, south_north=359, west_east=399);
:FieldType = 104; // int
:MemoryOrder = "XY ";
:description = "ACCUMULATED MELTED SNOW";
:units = "kg m-2";
:stagger = "";
:coordinates = "XLONG XLAT";

float SNOW(Time=1, south_north=359, west_east=399);
:FieldType = 104; // int
:MemoryOrder = "XY ";
:description = "SNOW WATER EQUIVALENT";
:units = "kg m-2";
:stagger = "";
:coordinates = "XLONG XLAT";

float SNOWH(Time=1, south_north=359, west_east=399);
:FieldType = 104; // int
:MemoryOrder = "XY ";
:description = "PHYSICAL SNOW DEPTH";
:units = "m";
:stagger = "";
:coordinates = "XLONG XLAT";

float CANWAT(Time=1, south_north=359, west_east=399);
:FieldType = 104; // int
:MemoryOrder = "XY ";
:description = "CANOPY WATER";
:units = "kg m-2";
:stagger = "";
:coordinates = "XLONG XLAT";

float SSTSK(Time=1, south_north=359, west_east=399);
:FieldType = 104; // int
:MemoryOrder = "XY ";
:description = "SKIN SEA SURFACE TEMPERATURE";
:units = "K";
:stagger = "";
:coordinates = "XLONG XLAT";

float LAI(Time=1, south_north=359, west_east=399);
:FieldType = 104; // int
:MemoryOrder = "XY ";
:description = "Leaf area index";
:units = "area/area";
:stagger = "";
:coordinates = "XLONG XLAT";

```

```

float VAR(Time=1, south_north=359, west_east=399);
:FieldType = 104; // int
:MemoryOrder = "XY ";
:description = "OROGRAPHIC VARIANCE";
:units = "";
:stagger = "";
:coordinates = "XLONG XLAT";

float MAPFAC_M(Time=1, south_north=359, west_east=399);
:FieldType = 104; // int
:MemoryOrder = "XY ";
:description = "Map scale factor on mass grid";
:units = "";
:stagger = "";
:coordinates = "XLONG XLAT";

float MAPFAC_U(Time=1, south_north=359, west_east_stag=400);
:FieldType = 104; // int
:MemoryOrder = "XY ";
:description = "Map scale factor on u-grid";
:units = "";
:stagger = "X";
:coordinates = "XLONG_U XLAT_U";

float MAPFAC_V(Time=1, south_north_stag=360, west_east=399);
:FieldType = 104; // int
:MemoryOrder = "XY ";
:description = "Map scale factor on v-grid";
:units = "";
:stagger = "Y";
:coordinates = "XLONG_V XLAT_V";

float MAPFAC_MX(Time=1, south_north=359, west_east=399);
:FieldType = 104; // int
:MemoryOrder = "XY ";
:description = "Map scale factor on mass grid, x direction";
:units = "";
:stagger = "";
:coordinates = "XLONG XLAT";

float MAPFAC_MY(Time=1, south_north=359, west_east=399);
:FieldType = 104; // int
:MemoryOrder = "XY ";
:description = "Map scale factor on mass grid, y direction";
:units = "";
:stagger = "";
:coordinates = "XLONG XLAT";

float MAPFAC_UX(Time=1, south_north=359, west_east_stag=400);
:FieldType = 104; // int
:MemoryOrder = "XY ";
:description = "Map scale factor on u-grid, x direction";
:units = "";
:stagger = "X";
:coordinates = "XLONG_U XLAT_U";

float MAPFAC_UY(Time=1, south_north=359, west_east_stag=400);
:FieldType = 104; // int
:MemoryOrder = "XY ";
:description = "Map scale factor on u-grid, y direction";
:units = "";
:stagger = "X";
:coordinates = "XLONG_U XLAT_U";

float MAPFAC_VX(Time=1, south_north_stag=360, west_east=399);
:FieldType = 104; // int
:MemoryOrder = "XY ";
:description = "Map scale factor on v-grid, x direction";
:units = "";
:stagger = "Y";
:coordinates = "XLONG_V XLAT_V";

float MF_VX_INV(Time=1, south_north_stag=360, west_east=399);
:FieldType = 104; // int
:MemoryOrder = "XY ";
:description = "Inverse map scale factor on v-grid, x direction";

```

```

:units = "";
:stagger = "Y";
:coordinates = "XLONG_V XLAT_V";

float MAPFAC_VY(Time=1, south_north=360, west_east=399);
:FieldType = 104; // int
:MemoryOrder = "XY ";
:description = "Map scale factor on v-grid, y direction";
:units = "";
:stagger = "Y";
:coordinates = "XLONG_V XLAT_V";

float F(Time=1, south_north=359, west_east=399);
:FieldType = 104; // int
:MemoryOrder = "XY ";
:description = "Coriolis sine latitude term";
:units = "s-1";
:stagger = "";
:coordinates = "XLONG XLAT";

float E(Time=1, south_north=359, west_east=399);
:FieldType = 104; // int
:MemoryOrder = "XY ";
:description = "Coriolis cosine latitude term";
:units = "s-1";
:stagger = "";
:coordinates = "XLONG XLAT";

float SINALPHA(Time=1, south_north=359, west_east=399);
:FieldType = 104; // int
:MemoryOrder = "XY ";
:description = "Local sine of map rotation";
:units = "";
:stagger = "";
:coordinates = "XLONG XLAT";

float COSALPHA(Time=1, south_north=359, west_east=399);
:FieldType = 104; // int
:MemoryOrder = "XY ";
:description = "Local cosine of map rotation";
:units = "";
:stagger = "";
:coordinates = "XLONG XLAT";

float HGT(Time=1, south_north=359, west_east=399);
:FieldType = 104; // int
:MemoryOrder = "XY ";
:description = "Terrain Height";
:units = "m";
:stagger = "";
:coordinates = "XLONG XLAT";

float TAUX_ESMF(Time=1, south_north=359, west_east=399);
:FieldType = 104; // int
:MemoryOrder = "XY ";
:description = "WIND STRESS X-COMPONENT FROM UCMC";
:units = "N/m^2";
:stagger = "";
:coordinates = "XLONG XLAT";

float TAUY_ESMF(Time=1, south_north=359, west_east=399);
:FieldType = 104; // int
:MemoryOrder = "XY ";
:description = "WIND STRESS Y-COMPONENT FROM UCMC";
:units = "N/m^2";
:stagger = "";
:coordinates = "XLONG XLAT";

float TSK(Time=1, south_north=359, west_east=399);
:FieldType = 104; // int
:MemoryOrder = "XY ";
:description = "SURFACE SKIN TEMPERATURE";
:units = "K";
:stagger = "";
:coordinates = "XLONG XLAT";

```

```

float P_TOP(Time=1);
:FieldType = 104; // int
:MemoryOrder = "0 ";
:description = "PRESSURE TOP OF THE MODEL";
:units = "Pa";
:stagger = "";

float T00(Time=1);
:FieldType = 104; // int
:MemoryOrder = "0 ";
:description = "BASE STATE TEMPERATURE";
:units = "K";
:stagger = "";

float P00(Time=1);
:FieldType = 104; // int
:MemoryOrder = "0 ";
:description = "BASE STATE PRESURE";
:units = "Pa";
:stagger = "";

float TLP(Time=1);
:FieldType = 104; // int
:MemoryOrder = "0 ";
:description = "BASE STATE LAPSE RATE";
:units = "";
:stagger = "";

float TISO(Time=1);
:FieldType = 104; // int
:MemoryOrder = "0 ";
:description = "TEMP AT WHICH THE BASE T TURNS CONST";
:units = "K";
:stagger = "";

float MAX_MSTFX(Time=1);
:FieldType = 104; // int
:MemoryOrder = "0 ";
:description = "Max map factor in domain";
:units = "";
:stagger = "";

float MAX_MSTFY(Time=1);
:FieldType = 104; // int
:MemoryOrder = "0 ";
:description = "Max map factor in domain";
:units = "";
:stagger = "";

float RAINC(Time=1, south_north=359, west_east=399);
:FieldType = 104; // int
:MemoryOrder = "XY ";
:description = "ACCUMULATED TOTAL CUMULUS PRECIPITATION";
:units = "mm";
:stagger = "";
:coordinates = "XLONG XLAT";

float RAINSH(Time=1, south_north=359, west_east=399);
:FieldType = 104; // int
:MemoryOrder = "XY ";
:description = "ACCUMULATED SHALLOW CUMULUS PRECIPITATION";
:units = "mm";
:stagger = "";
:coordinates = "XLONG XLAT";

float RAINNC(Time=1, south_north=359, west_east=399);
:FieldType = 104; // int
:MemoryOrder = "XY ";
:description = "ACCUMULATED TOTAL GRID SCALE PRECIPITATION";
:units = "mm";
:stagger = "";
:coordinates = "XLONG XLAT";

float PRATEC(Time=1, south_north=359, west_east=399);
:FieldType = 104; // int
:MemoryOrder = "XY ";

```



```

:description = "PRECIP RATE FROM CUMULUS SCHEME";
:units = "mm s-1";
:stagger = "";
:coordinates = "XLONG XLAT";

float PRATESH(Time=1, south_north=359, west_east=399);
:FieldType = 104; // int
:MemoryOrder = "XY ";
:description = "PRECIP RATE FROM SHALLOW CUMULUS SCHEME";
:units = "mm s-1";
:stagger = "";
:coordinates = "XLONG XLAT";

float RAINCV(Time=1, south_north=359, west_east=399);
:FieldType = 104; // int
:MemoryOrder = "XY ";
:description = "TIME-STEP CUMULUS PRECIPITATION";
:units = "mm";
:stagger = "";
:coordinates = "XLONG XLAT";

float RAINSHV(Time=1, south_north=359, west_east=399);
:FieldType = 104; // int
:MemoryOrder = "XY ";
:description = "TIME-STEP SHALLOW CUMULUS PRECIPITATION";
:units = "mm";
:stagger = "";
:coordinates = "XLONG XLAT";

float RAINNCV(Time=1, south_north=359, west_east=399);
:FieldType = 104; // int
:MemoryOrder = "XY ";
:description = "TIME-STEP NONCONVECTIVE PRECIPITATION";
:units = "mm";
:stagger = "";
:coordinates = "XLONG XLAT";

float RAINBL(Time=1, south_north=359, west_east=399);
:FieldType = 104; // int
:MemoryOrder = "XY ";
:description = "PBL TIME-STEP TOTAL PRECIPITATION";
:units = "mm";
:stagger = "";
:coordinates = "XLONG XLAT";

float SNOWNC(Time=1, south_north=359, west_east=399);
:FieldType = 104; // int
:MemoryOrder = "XY ";
:description = "ACCUMULATED TOTAL GRID SCALE SNOW AND ICE";
:units = "mm";
:stagger = "";
:coordinates = "XLONG XLAT";

float GRAUPELNC(Time=1, south_north=359, west_east=399);
:FieldType = 104; // int
:MemoryOrder = "XY ";
:description = "ACCUMULATED TOTAL GRID SCALE GRAUPEL";
:units = "mm";
:stagger = "";
:coordinates = "XLONG XLAT";

float HAILNC(Time=1, south_north=359, west_east=399);
:FieldType = 104; // int
:MemoryOrder = "XY ";
:description = "ACCUMULATED TOTAL GRID SCALE HAIL";
:units = "mm";
:stagger = "";
:coordinates = "XLONG XLAT";

float SNOWNCV(Time=1, south_north=359, west_east=399);
:FieldType = 104; // int
:MemoryOrder = "XY ";
:description = "TIME-STEP NONCONVECTIVE SNOW AND ICE";
:units = "mm";
:stagger = "";
:coordinates = "XLONG XLAT";

```

```

float GRAUPELNCV(Time=1, south_north=359, west_east=399);
:FieldType = 104; // int
:MemoryOrder = "XY ";
:description = "TIME-STEP NONCONVECTIVE GRAUPEL";
:units = "mm";
:stagger = "";
:coordinates = "XLONG XLAT";

float HAILNCV(Time=1, south_north=359, west_east=399);
:FieldType = 104; // int
:MemoryOrder = "XY ";
:description = "TIME-STEP NONCONVECTIVE HAIL";
:units = "mm";
:stagger = "";
:coordinates = "XLONG XLAT";

float REFL_10CM(Time=1, bottom_top=35, south_north=359, west_east=399);
:FieldType = 104; // int
:MemoryOrder = "XYZ";
:description = "Radar reflectivity (lamda = 10 cm)";
:units = "dBZ";
:stagger = "";
:coordinates = "XLONG XLAT";

float CLDFRA(Time=1, bottom_top=35, south_north=359, west_east=399);
:FieldType = 104; // int
:MemoryOrder = "XYZ";
:description = "CLOUD FRACTION";
:units = "";
:stagger = "";
:coordinates = "XLONG XLAT";

float SWDOWN(Time=1, south_north=359, west_east=399);
:FieldType = 104; // int
:MemoryOrder = "XY ";
:description = "DOWNWARD SHORT WAVE FLUX AT GROUND SURFACE";
:units = "W m-2";
:stagger = "";
:coordinates = "XLONG XLAT";

float GLW(Time=1, south_north=359, west_east=399);
:FieldType = 104; // int
:MemoryOrder = "XY ";
:description = "DOWNWARD LONG WAVE FLUX AT GROUND SURFACE";
:units = "W m-2";
:stagger = "";
:coordinates = "XLONG XLAT";

float SWNORM(Time=1, south_north=359, west_east=399);
:FieldType = 104; // int
:MemoryOrder = "XY ";
:description = "NORMAL SHORT WAVE FLUX AT GROUND SURFACE (SLOPE-DEPENDENT)";
:units = "W m-2";
:stagger = "";
:coordinates = "XLONG XLAT";

float OLR(Time=1, south_north=359, west_east=399);
:FieldType = 104; // int
:MemoryOrder = "XY ";
:description = "TOA OUTGOING LONG WAVE";
:units = "W m-2";
:stagger = "";
:coordinates = "XLONG XLAT";

float XLAT_U(Time=1, south_north=359, west_east_stag=400);
:FieldType = 104; // int
:MemoryOrder = "XY ";
:description = "LATITUDE, SOUTH IS NEGATIVE";
:units = "degree_north";
:stagger = "X";
:coordinates = "XLONG_U XLAT_U";

float XLONG_U(Time=1, south_north=359, west_east_stag=400);
:FieldType = 104; // int
:MemoryOrder = "XY ";

```

```

:description = "LONGITUDE, WEST IS NEGATIVE";
:units = "degree_east";
:stagger = "X";
:coordinates = "XLONG_U XLAT_U";

float XLAT_V(Time=1, south_north_stag=360, west_east=399);
:FieldType = 104; // int
:MemoryOrder = "XY ";
:description = "LATITUDE, SOUTH IS NEGATIVE";
:units = "degree_north";
:stagger = "Y";
:coordinates = "XLONG_V XLAT_V";

float XLONG_V(Time=1, south_north_stag=360, west_east=399);
:FieldType = 104; // int
:MemoryOrder = "XY ";
:description = "LONGITUDE, WEST IS NEGATIVE";
:units = "degree_east";
:stagger = "Y";
:coordinates = "XLONG_V XLAT_V";

float ALBEDO(Time=1, south_north=359, west_east=399);
:FieldType = 104; // int
:MemoryOrder = "XY ";
:description = "ALBEDO";
:units = "-";
:stagger = "";
:coordinates = "XLONG XLAT";

float CLAT(Time=1, south_north=359, west_east=399);
:FieldType = 104; // int
:MemoryOrder = "XY ";
:description = "COMPUTATIONAL GRID LATITUDE, SOUTH IS NEGATIVE";
:units = "degree_north";
:stagger = "";
:coordinates = "XLONG XLAT";

float ALBBCK(Time=1, south_north=359, west_east=399);
:FieldType = 104; // int
:MemoryOrder = "XY ";
:description = "BACKGROUND ALBEDO";
:units = "";
:stagger = "";
:coordinates = "XLONG XLAT";

float EMISS(Time=1, south_north=359, west_east=399);
:FieldType = 104; // int
:MemoryOrder = "XY ";
:description = "SURFACE EMISSIVITY";
:units = "";
:stagger = "";
:coordinates = "XLONG XLAT";

float NOAHRES(Time=1, south_north=359, west_east=399);
:FieldType = 104; // int
:MemoryOrder = "XY ";
:description = "RESIDUAL OF THE NOAH SURFACE ENERGY BUDGET";
:units = "W m{-2}";
:stagger = "";
:coordinates = "XLONG XLAT";

float TMN(Time=1, south_north=359, west_east=399);
:FieldType = 104; // int
:MemoryOrder = "XY ";
:description = "SOIL TEMPERATURE AT LOWER BOUNDARY";
:units = "K";
:stagger = "";
:coordinates = "XLONG XLAT";

float XLAND(Time=1, south_north=359, west_east=399);
:FieldType = 104; // int
:MemoryOrder = "XY ";
:description = "LAND MASK (1 FOR LAND, 2 FOR WATER)";
:units = "";
:stagger = "";
:coordinates = "XLONG XLAT";

```

```

float UST(Time=1, south_north=359, west_east=399);
:FieldType = 104; // int
:MemoryOrder = "XY ";
:description = "U* IN SIMILARITY THEORY";
:units = "m s-1";
:stagger = "";
:coordinates = "XLONG XLAT";

float PBLH(Time=1, south_north=359, west_east=399);
:FieldType = 104; // int
:MemoryOrder = "XY ";
:description = "PBL HEIGHT";
:units = "m";
:stagger = "";
:coordinates = "XLONG XLAT";

float HFX(Time=1, south_north=359, west_east=399);
:FieldType = 104; // int
:MemoryOrder = "XY ";
:description = "UPWARD HEAT FLUX AT THE SURFACE";
:units = "W m-2";
:stagger = "";
:coordinates = "XLONG XLAT";

float QFX(Time=1, south_north=359, west_east=399);
:FieldType = 104; // int
:MemoryOrder = "XY ";
:description = "UPWARD MOISTURE FLUX AT THE SURFACE";
:units = "kg m-2 s-1";
:stagger = "";
:coordinates = "XLONG XLAT";

float LH(Time=1, south_north=359, west_east=399);
:FieldType = 104; // int
:MemoryOrder = "XY ";
:description = "LATENT HEAT FLUX AT THE SURFACE";
:units = "W m-2";
:stagger = "";
:coordinates = "XLONG XLAT";

float ACHFX(Time=1, south_north=359, west_east=399);
:FieldType = 104; // int
:MemoryOrder = "XY ";
:description = "ACCUMULATED UPWARD HEAT FLUX AT THE SURFACE";
:units = "J m-2";
:stagger = "";
:coordinates = "XLONG XLAT";

float ACLHF(Time=1, south_north=359, west_east=399);
:FieldType = 104; // int
:MemoryOrder = "XY ";
:description = "ACCUMULATED UPWARD LATENT HEAT FLUX AT THE SURFACE";
:units = "J m-2";
:stagger = "";
:coordinates = "XLONG XLAT";

float SNOWC(Time=1, south_north=359, west_east=399);
:FieldType = 104; // int
:MemoryOrder = "XY ";
:description = "FLAG INDICATING SNOW COVERAGE (1 FOR SNOW COVER)";
:units = "";
:stagger = "";
:coordinates = "XLONG XLAT";

float SR(Time=1, south_north=359, west_east=399);
:FieldType = 104; // int
:MemoryOrder = "XY ";
:description = "fraction of frozen precipitation";
:units = "-";
:stagger = "";
:coordinates = "XLONG XLAT";

int SAVE_TOPO_FROM_REAL(Time=1);
:FieldType = 106; // int
:MemoryOrder = "0 ";

```

```

:description = "1=original topo from real/0=topo modified by WRF";
:units = "flag";
:stagger = "";

float VERTSTRUCC(Time=1, bottom_top=35, south_north=359, west_east=399);
:FieldType = 104; // int
:MemoryOrder = "XYZ";
:description = "vertical structure for stoch. forcing";
:units = "";
:stagger = "";
:coordinates = "XLONG XLAT";

float VERTSTRUCS(Time=1, bottom_top=35, south_north=359, west_east=399);
:FieldType = 104; // int
:MemoryOrder = "XYZ";
:description = "vertical structure for stoch. forcing";
:units = "";
:stagger = "";
:coordinates = "XLONG XLAT";

float RU_TENDF_STOCH(Time=1, bottom_top=35, south_north=359, west_east_stag=400);
:FieldType = 104; // int
:MemoryOrder = "XYZ";
:description = "stochastic forcing, U";
:units = "m/s";
:stagger = "X";
:coordinates = "XLONG_U XLAT_U";

float RV_TENDF_STOCH(Time=1, bottom_top=35, south_north_stag=360, west_east=399);
:FieldType = 104; // int
:MemoryOrder = "XYZ";
:description = "stochastic forcing, V";
:units = "m/s";
:stagger = "Y";
:coordinates = "XLONG_V XLAT_V";

float RT_TENDF_STOCH(Time=1, bottom_top=35, south_north=359, west_east=399);
:FieldType = 104; // int
:MemoryOrder = "XYZ";
:description = "stochastic forcing, T";
:units = "K/s";
:stagger = "";
:coordinates = "XLONG XLAT";

int SEED1(Time=1);
:FieldType = 106; // int
:MemoryOrder = "0 ";
:description = "RANDOM SEED NUMBER 1";
:units = "";
:stagger = "";

int SEED2(Time=1);
:FieldType = 106; // int
:MemoryOrder = "0 ";
:description = "RANDOM SEED NUMBER 2";
:units = "";
:stagger = "";

float LANDMASK(Time=1, south_north=359, west_east=399);
:FieldType = 104; // int
:MemoryOrder = "XY ";
:description = "LAND MASK (1 FOR LAND, 0 FOR WATER)";
:units = "";
:stagger = "";
:coordinates = "XLONG XLAT";

float SST(Time=1, south_north=359, west_east=399);
:FieldType = 104; // int
:MemoryOrder = "XY ";
:description = "SEA SURFACE TEMPERATURE";
:units = "K";
:stagger = "";
:coordinates = "XLONG XLAT";

```

## B.2 List of UMWM output

```
dimensions:
  x = 1195;
  y = 1075;
  f = 37;
  th = 36;
  z = 19;
variables:
  float z(z=19);
    :description = "Depth";
    :units = "m";

  float u_stokes(z=19, y=1075, x=1195);
    :description = "Stokes drift x-component";
    :units = "m/s";

  float v_stokes(z=19, y=1075, x=1195);
    :description = "Stokes drift y-component";
    :units = "m/s";

  float frequency(f=37);
    :description = "Frequency";
    :units = "Hz";

  float theta(th=36);
    :description = "Directions";
    :units = "rad";

  float lon(y=1075, x=1195);
    :description = "Longitude";
    :units = "degrees East";

  float lat(y=1075, x=1195);
    :description = "Latitude";
    :units = "degrees North";

  int seamask(y=1075, x=1195);
    :description = "Seamask";
    :units = "non-dimensional";

  float depth(y=1075, x=1195);
    :description = "Ocean depth";
    :units = "m";

  float wspd(y=1075, x=1195);
    :description = "Wind speed";
    :units = "m/s";

  float wdir(y=1075, x=1195);
    :description = "Water density";
    :units = "kg/m^3";

  float uc(y=1075, x=1195);
    :description = "Ocean current y-component";
    :units = "m/s";

  float vc(y=1075, x=1195);

  float rhoa(y=1075, x=1195);

  float rhow(y=1075, x=1195);

  float momx(y=1075, x=1195);
    :description = "Momentum, x-component";
    :units = "kgm/s";

  float momy(y=1075, x=1195);
    :description = "Momentum, y-component";
    :units = "kgm/s";

  float cgmxx(y=1075, x=1195);
    :description = "Cg*Momentum, xx-component";
    :units = "kgm^2/s^2";
```

```

float cgmxy(y=1075, x=1195);
:description = "Cg*Momentum, xy-component";
:units = "kgm^2/s^2";

float cgmyy(y=1075, x=1195);
:description = "Cg*Momentum, yy-component";
:units = "kgm^2/s^2";

float taux_form(y=1075, x=1195);
:description = "Form drag, x-component";
:units = "N/m^2";

float tauy_form(y=1075, x=1195);
:description = "Form drag, y-component";
:units = "N/m^2";

float taux_form_1(y=1075, x=1195);
:description = "Form drag, part 1, x-component";
:units = "N/m^2";

float tauy_form_1(y=1075, x=1195);
:description = "Form drag, part 1, y-component";
:units = "N/m^2";

float taux_form_2(y=1075, x=1195);
:description = "Form drag, part 2, x-component";
:units = "N/m^2";

float tauy_form_2(y=1075, x=1195);
:description = "Form drag, part 2, y-component";
:units = "N/m^2";

float taux_form_3(y=1075, x=1195);
:description = "Form drag, part 3, x-component";
:units = "N/m^2";

float tauy_form_3(y=1075, x=1195);
:description = "Form drag, part 3, y-component";
:units = "N/m^2";

float taux_skin(y=1075, x=1195);
:description = "Skin drag, x-component";
:units = "N/m^2";

float tauy_skin(y=1075, x=1195);
:description = "Skin drag, y-component";
:units = "N/m^2";

float taux_ocn(y=1075, x=1195);
:description = "Momentum flux from breaking waves to ocean top, x-component";
:units = "N/m^2";

float tauy_ocn(y=1075, x=1195);
:description = "Momentum flux from breaking waves to ocean top, y-component";
:units = "N/m^2";

float taux_bot(y=1075, x=1195);
:description = "Momentum flux from waves to ocean bottom, x-component";
:units = "N/m^2";

float tauy_bot(y=1075, x=1195);
:description = "Momentum flux from waves to ocean bottom, y-component";
:units = "N/m^2";

float taux_snl(y=1075, x=1195);
:description = "Momentum flux due to Snl, x-component";
:units = "N/m^2";

float tauy_snl(y=1075, x=1195);
:description = "Momentum flux due to Snl, y-component";
:units = "N/m^2";

float tailatmx(y=1075, x=1195);
:description = "Atmosphere tail stress part, x-component";
:units = "N/m^2";

```

```

float tailatmy(y=1075, x=1195);
  :description = "Atmosphere tail stress part, y-component";
  :units = "N/m^2";

float tailocnx(y=1075, x=1195);
  :description = "Ocean tail stress part, x-component";
  :units = "N/m^2";

float tailocny(y=1075, x=1195);
  :description = "Ocean tail stress part, y-component";
  :units = "N/m^2";

float cd(y=1075, x=1195);
  :description = "Drag coefficient of air";
  :units = "non-dimensional";

float ust(y=1075, x=1195);
  :description = "Friction velocity of air";
  :units = "m/s";

float swl(y=1075, x=1195);
  :description = "Significant wave height";
  :units = "m";

float mss(y=1075, x=1195);
  :description = "Mean-squared slope";
  :units = "non-dimensional";

float mwp(y=1075, x=1195);
  :description = "Mean wave period";
  :units = "s";

float mwl(y=1075, x=1195);
  :description = "Mean wavelength";
  :units = "m";

float mwd(y=1075, x=1195);
  :description = "Mean wave direction";
  :units = "rad";

float dwp(y=1075, x=1195);
  :description = "Dominant wave period";
  :units = "s";

float dwl(y=1075, x=1195);
  :description = "Dominant wavelength";
  :units = "m";

float dwd(y=1075, x=1195);
  :description = "Dominant wave direction";
  :units = "rad";

float dcp0(y=1075, x=1195);
  :description = "Dominant phase speed, intrinsic";
  :units = "m/s";

float dcg0(y=1075, x=1195);
  :description = "Dominant group speed, intrinsic";
  :units = "m/s";

float dcp(y=1075, x=1195);
  :description = "Dominant phase speed";
  :units = "m/s";

float dcg(y=1075, x=1195);
  :description = "Dominant group speed";
  :units = "m/s";
}

```

### B.3 List of HYCOM output

```

dimensions:
  MT = UNLIMITED; // (1 currently

```



```

Latitude = 1000;
Longitude = 1000;
Depth = 40;
variables:
double MT(MT=1);
  :long_name = "time";
  :units = "days since 1900-12-31 00:00:00";
  :calendar = "gregorian";
  :axis = "T";

double Date(MT=1);
  :long_name = "date";
  :units = "day as %Y%m%d.%f";
  :C_format = "%13.4f";
  :FORTRAN_format = "(f13.4)";

float Depth(Depth=40);
  :standard_name = "depth";
  :units = "m";
  :positive = "down";
  :axis = "Z";

float Latitude(Latitude=1000);
  :standard_name = "latitude";
  :units = "degrees_north";
  :axis = "Y";

float Longitude(Longitude=1000);
  :standard_name = "longitude";
  :units = "degrees_east";
  :point_spacing = "even";
  :axis = "X";

float u(MT=1, Depth=40, Latitude=1000, Longitude=1000);
  :coordinates = "Date";
  :standard_name = "eastward_sea_water_velocity";
  :units = "m/s";
  :_FillValue = 1.2676506E30f; // float
  :valid_range = -1.975024f, 1.876598f; // float
  :long_name = " u-veloc. [20.1H]";

float v(MT=1, Depth=40, Latitude=1000, Longitude=1000);
  :coordinates = "Date";
  :standard_name = "northward_sea_water_velocity";
  :units = "m/s";
  :_FillValue = 1.2676506E30f; // float
  :valid_range = -1.3474879f, 2.665912f; // float
  :long_name = " v-veloc. [20.1H]";

float w_velocity(MT=1, Depth=40, Latitude=1000, Longitude=1000);
  :coordinates = "Date";
  :standard_name = "upward_sea_water_velocity";
  :units = "m/s";
  :_FillValue = 1.2676506E30f; // float
  :valid_range = -0.037467636f, 0.017186552f; // float
  :long_name = " w-veloc. [20.1H]";

float water_temp(MT=1, Depth=40, Latitude=1000, Longitude=1000);
  :coordinates = "Date";
  :standard_name = "sea_water_temperature";
  :units = "degC";
  :_FillValue = 1.2676506E30f; // float
  :valid_range = 2.6080048f, 30.902374f; // float
  :long_name = " temp [20.1H]";

float salinity(MT=1, Depth=40, Latitude=1000, Longitude=1000);
  :coordinates = "Date";
  :standard_name = "sea_water_salinity";
  :units = "psu";
  :_FillValue = 1.2676506E30f; // float
  :valid_range = 12.106584f, 38.24341f; // float
  :long_name = " salinity [20.1H]";

float pot_density(MT=1, Depth=40, Latitude=1000, Longitude=1000);
  :coordinates = "Date";
  :standard_name = "sea_water_potential_density";

```

```

:units = "sigma";
:_FillValue = 1.2676506E30f; // float
:valid_range = 13.050988f, 36.986603f; // float
:long_name = " p.dens [20.1H]";

float bathymetry(MT=1, Latitude=1000, Longitude=1000);
:coordinates = "Date";
:units = "m";
:_FillValue = 1.2676506E30f; // float
:valid_range = 9.999999f, 8477.0f; // float
:long_name = " bathymetry [20.1H]";

float ilt(MT=1, Latitude=1000, Longitude=1000);
:coordinates = "Date";
:standard_name = "ocean_mixed_layer_thickness";
:units = "m";
:_FillValue = 1.2676506E30f; // float
:valid_range = 1.0797554f, 1146.0001f; // float
:long_name = " ILT (0.50 degC) [20.1H]";

float mlt(MT=1, Latitude=1000, Longitude=1000);
:coordinates = "Date";
:standard_name = "ocean_mixed_layer_thickness";
:units = "m";
:_FillValue = 1.2676506E30f; // float
:valid_range = 0.715755f, 1146.0001f; // float
:long_name = " MLT (0.50 kg/m3) [20.1H]";

float ssh(MT=1, Latitude=1000, Longitude=1000);
:coordinates = "Date";
:standard_name = "sea_surface_elevation";
:units = "m";
:_FillValue = 1.2676506E30f; // float
:valid_range = -0.95362926f, 0.84672445f; // float
:long_name = " sea surf. height [20.1H]";

```

## Appendix C

### Fourier coefficients for wave kinematics

#### C.1 Wave Surface Elevation

##### C.1.1 First-Order

$$X_{im}^{(1)} = a_{im} \cdot \exp(-t\varepsilon_{im}) \cdot \exp(-t(\vec{k}_{im} \cdot \vec{x})) \quad (1)$$

where  $\vec{x} = (x, y)$  is a point on the horizontal  $x$ - $y$  plane;  $t = \sqrt{-1}$  and  $\vec{k}_{im} = (|\vec{k}_i| \cos \theta_m, |\vec{k}_i| \sin \theta_m)$ ;  $\omega_i$  is the angular frequency;  $\vec{k}_i$  is the wave number which is related to the frequency,  $\omega$ , through the linear dispersion relation,  $\omega^2 = g|\vec{k}_i| \tanh(|\vec{k}_i|h)$  (where  $h$  is the water depth).

##### C.1.2 Second-Order

$$X_{ijmn}^{(2)\pm} = a_{im} a_{jn} \cdot \exp(-\text{sgn}(\omega_{ij}^\pm) t \varepsilon_{ijmn}^\pm) \cdot K_{ijmn}^\pm \cdot \exp(-\text{sgn}(\omega_{ij}^\pm) t (\vec{k}_{im} \cdot \vec{x} \pm \vec{k}_{jn} \cdot \vec{x})) \quad (2)$$

where,

$$\varepsilon_{ijmn}^\pm = \varepsilon_{im} \pm \varepsilon_{jn} \quad \text{and} \quad \omega_{ij}^\pm = \omega_i \pm \omega_j \quad (3)$$

$$\text{sgn}(x) = \begin{cases} 1 & x > 0 \\ 0 & x = 0 \\ -1 & x < 0 \end{cases} \quad (4)$$

#### C.2 Wave Particle Velocity

##### C.2.1 First-Order

$$U_{x,im}^{(1)} = a_{im} \cdot \exp(-t\varepsilon_{im}) \omega_i \frac{\cosh[|\vec{k}_i|(h+z)]}{\sinh(|\vec{k}_i|h)} \cos \theta_m \cdot \exp(-t(\vec{k}_{im} \cdot \vec{x})) \quad (5)$$

$$U_{y,im}^{(1)} = a_{im} \cdot \exp(-t\varepsilon_{im}) \omega_i \frac{\cosh[|\vec{k}_i|(h+z)]}{\sinh(|\vec{k}_i|h)} \sin \theta_m \cdot \exp(-t(\vec{k}_{im} \cdot \vec{x})) \quad (6)$$

$$U_{z,im}^{(1)} = (t) a_{im} \cdot \exp(-t\varepsilon_{im}) \omega_i \frac{\sinh[|\vec{k}_i|(h+z)]}{\sinh(|\vec{k}_i|h)} \cdot \exp(-t(\vec{k}_{im} \cdot \vec{x})) \quad (7)$$

##### C.2.2 Second-Order

$$U_{x,ijmn}^{(2\pm)} = a_{im} a_{jn} \cdot \exp(-\text{sgn}(\omega_{ij}^\pm) t \varepsilon_{ijmn}^\pm) \cdot B_{ijmn}^\pm \cdot (|\vec{k}_i| \cos \theta_m \pm |\vec{k}_j| \cos \theta_n) \cdot \exp(-\text{sgn}(\omega_{ij}^\pm) t (\vec{k}_{im} \cdot \vec{x} \pm \vec{k}_{jn} \cdot \vec{x})) \quad (8)$$

$$U_{x,ijmn}^{(2\pm)} = a_{im} a_{jn} \cdot \exp(-\text{sgn}(\omega_{ij}^\pm) t \varepsilon_{ijmn}^\pm) \cdot B_{ijmn}^\pm \cdot (|\vec{k}_i| \sin \theta_m \pm |\vec{k}_j| \sin \theta_n) \cdot \exp(-\text{sgn}(\omega_{ij}^\pm) t (\vec{k}_{im} \cdot \vec{x} \pm \vec{k}_{jn} \cdot \vec{x})) \quad (9)$$

$$U_{x,ijmn}^{(2\pm)} = (t) \cdot a_{im} a_{jn} \cdot \exp(-\text{sgn}(\omega_{ij}^\pm) t \varepsilon_{ijmn}^\pm) \cdot B_{ijmn}^\pm \cdot k_{ijmn}^\pm \cdot \tanh[k_{ijmn}^\pm (h+z)] \cdot \exp(-\text{sgn}(\omega_{ij}^\pm) t (\vec{k}_{im} \cdot \vec{x} \pm \vec{k}_{jn} \cdot \vec{x})) \quad (10)$$

## C.3 Wave Particle Acceleration

### C.3.1 First-Order

$$\dot{U}_{x,im}^{(1)} = (\mathbf{t}) \cdot \boldsymbol{\omega}_i \cdot U_{x,im}^{(1)} \quad (11)$$

$$\dot{U}_{y,im}^{(1)} = (\mathbf{t}) \cdot \boldsymbol{\omega}_i \cdot U_{y,im}^{(1)} \quad (12)$$

$$\dot{U}_{z,im}^{(1)} = (\mathbf{t}) \cdot \boldsymbol{\omega}_i \cdot U_{z,im}^{(1)} \quad (13)$$

### C.3.2 Second-Order

$$\dot{U}_{x,ijmn}^{(2\pm)} = (\mathbf{t}) \cdot \boldsymbol{\omega}_{ij}^{\pm} \cdot U_{x,ijmn}^{(2\pm)} \quad (14)$$

$$\dot{U}_{y,ijmn}^{(2\pm)} = (\mathbf{t}) \cdot \boldsymbol{\omega}_{ij}^{\pm} \cdot U_{y,ijmn}^{(2\pm)} \quad (15)$$

$$\dot{U}_{z,ijmn}^{(2\pm)} = (\mathbf{t}) \cdot \boldsymbol{\omega}_{ij}^{\pm} \cdot U_{z,ijmn}^{(2\pm)} \quad (16)$$

## C.4 Dynamic Pressure

### C.4.1 First-Order

$$P_{im}^{(1)} = (\rho_w g) \cdot a_{im} \cdot \exp(-\mathbf{t}\varepsilon_{im}) \omega_i \frac{\cosh[|\vec{k}_i|(h+z)]}{\cosh(|\vec{k}_i|h)} \cdot \exp(-\mathbf{t}(\vec{k}_{im} \cdot \vec{x})) \quad (17)$$

### C.4.2 Second-Order (only second-order potential term)

$$P_{ijmn}^{(2\pm)} = (\rho_w) \cdot a_{im} a_{jn} \cdot \exp(-\text{sgn}(\omega_{ij}^{\pm})\mathbf{t}\varepsilon_{ijmn}) \cdot B_{ijmn}^{\pm} \cdot \omega_{ij}^{\pm} \cdot \exp(-\text{sgn}(\omega_{ij}^{\pm})\mathbf{t}(\vec{k}_{im} \cdot \vec{x} \pm \vec{k}_{jn} \cdot \vec{x})) \quad (18)$$

## Appendix D

# FAST input files for the parked NREL 5-MW baseline turbine

## D.1 Primary Input File(\*.fst)

```
----- FAST INPUT FILE -----
NREL 5.0 MW Baseline Wind Turbine for Use in Offshore Analysis.
Properties from Dutch Offshore Wind Energy Converter (DOWEC) 6MW Pre-Design (10046_00
----- SIMULATION CONTROL -----
False      Echo      - Echo input data to "echo.out" (flag)
1          ADAMSprep - ADAMS preprocessor mode {1: Run FAST, 2: use FAST as a preproc
1          AnalMode - Analysis mode {1: Run a time-marching simulation, 2: create a
3          NumBl     - Number of blades (-)
4000.0     TMax      - Total run time (s)
0.01000    DT       - Integration time step (s)
----- TURBINE CONTROL -----
0          YCMode    - Yaw control mode {0: none, 1: user-defined from routine UserYa
9999.9     TYCon     - Time to enable active yaw control (s) [unused when YCMode=0
0          PCMode    - Pitch control mode {0: none, 1: user-defined from routine Pitc
0.0        TPCon     - Time to enable active pitch control (s) [unused when PCMode=0]
0          VSContrl  - Variable-speed control mode {0: none, 1: simple VS, 2: user-de
9999.9     VS_RtGnSp  - Rated generator speed for simple variable-speed generator c
9999.9     VS_RtTq   - Rated generator torque/constant generator torque in Region
9999.9     VS_Rgn2K  - Generator torque constant in Region 2 for simple variable-s
9999.9     VS_SlPc   - Rated generator slip percentage in Region 2 1/2 for simple
2          GenModel  - Generator model {1: simple, 2: Thevenin, 3: user-defined fr
True       GenTiStr  - Method to start the generator {T: timed using TimGenOn, F:
True       GenTiStp  - Method to stop the generator {T: timed using TimGenOf, F: w
9999.9     SpdGenOn  - Generator speed to turn on the generator for a startup (HSS
9999.9     TimGenOn  - Time to turn on the generator for a startup (s) [used only
9999.9     TimGenOf  - Time to turn off the generator (s) [used only when GenTiStp
1          HSSBrMode - HSS brake model {1: simple, 2: user-defined from routine UserH
0          THSSBrDp  - Time to initiate deployment of the HSS brake (s)
9999.9     TiDynBrk  - Time to initiate deployment of the dynamic generator brake
9999.9     TTPBrDp(1) - Time to initiate deployment of tip brake 1 (s)
9999.9     TTPBrDp(2) - Time to initiate deployment of tip brake 2 (s)
9999.9     TTPBrDp(3) - Time to initiate deployment of tip brake 3 (s) [unused for
9999.9     TBDepISp(1) - Deployment-initiation speed for the tip brake on blade 1 (r
9999.9     TBDepISp(2) - Deployment-initiation speed for the tip brake on blade 2 (r
9999.9     TBDepISp(3) - Deployment-initiation speed for the tip brake on blade 3 (r
9999.9     TYawManS  - Time to start override yaw maneuver and end standard yaw co
9999.9     TYawManE  - Time at which override yaw maneuver reaches final yaw angle
0.0        NacYawF   - Final yaw angle for yaw maneuvers (degrees)
9999.9     TPitManS(1) - Time to start override pitch maneuver for blade 1 and end s
9999.9     TPitManS(2) - Time to start override pitch maneuver for blade 2 and end s
9999.9     TPitManS(3) - Time to start override pitch maneuver for blade 3 and end s
9999.9     TPitManE(1) - Time at which override pitch maneuver for blade 1 reaches f
9999.9     TPitManE(2) - Time at which override pitch maneuver for blade 2 reaches f
9999.9     TPitManE(3) - Time at which override pitch maneuver for blade 3 reaches f
90.0      BLPitch(1) - Blade 1 initial pitch (degrees)
90.0      BLPitch(2) - Blade 2 initial pitch (degrees)
90.0      BLPitch(3) - Blade 3 initial pitch (degrees) [unused for 2 blade
90.0      BLPitchF(1) - Blade 1 final pitch for pitch maneuvers (degrees)
90.0      BLPitchF(2) - Blade 2 final pitch for pitch maneuvers (degrees)
90.0      BLPitchF(3) - Blade 3 final pitch for pitch maneuvers (degrees) [
----- ENVIRONMENTAL CONDITIONS -----
9.80665    Gravity   - Gravitational acceleration (m/s^2)
----- FEATURE FLAGS -----
True       FlapDOF1  - First flapwise blade mode DOF (flag)
True       FlapDOF2  - Second flapwise blade mode DOF (flag)
True       EdgeDOF   - First edgewise blade mode DOF (flag)
False     TeetDOF   - Rotor-teeter DOF (flag) [unused for 3 blades]
True       DrTrDOF   - Drivetrain rotational-flexibility DOF (flag)
True       GenDOF    - Generator DOF (flag)
False     YawDOF     - Yaw DOF (flag)
True       TwFADOF1  - First fore-aft tower bending-mode DOF (flag)
True       TwFADOF2  - Second fore-aft tower bending-mode DOF (flag)
True       TwSSDOF1  - First side-to-side tower bending-mode DOF (flag)
True       TwSSDOF2  - Second side-to-side tower bending-mode DOF (flag)
True       CompAero  - Compute aerodynamic forces (flag)
False     CompNoise  - Compute aerodynamic noise (flag)
----- INITIAL CONDITIONS -----
```

```

0.0      OoPDefl    - Initial out-of-plane blade-tip displacement (meters)
0.0      IPDefl    - Initial in-plane blade-tip deflection (meters)
0.0      TeetDefl  - Initial or fixed teeter angle (degrees) [unused for 3 blades]
0.0      Azimuth   - Initial azimuth angle for blade 1 (degrees)
0.0      RotSpeed  - Initial or fixed rotor speed (rpm)
0.0      NacYaw    - Initial or fixed nacelle-yaw angle (degrees)
0.0      TTDspFA   - Initial fore-aft tower-top displacement (meters)
0.0      TTDspSS   - Initial side-to-side tower-top displacement (meters)
-----
63.0     TipRad    - The distance from the rotor apex to the blade tip (meters)
1.5      HubRad    - The distance from the rotor apex to the blade root (meters)
1        PSpnElN   - Number of the innermost blade element which is still part of t
0.0      UndSling  - Undersling length [distance from teeter pin to the rotor apex]
0.0      HubCM     - Distance from rotor apex to hub mass [positive downwind] (mete
-5.01910 OverHang  - Distance from yaw axis to rotor apex [3 blades] or teeter pin
1.9      NacCMxn   - Downwind distance from the tower-top to the nacelle CM (meters)
0.0      NacCMyn   - Lateral distance from the tower-top to the nacelle CM (meters)
1.75     NacCMzn   - Vertical distance from the tower-top to the nacelle CM (meters)
87.6     TowerHt   - Height of tower above ground level [onshore] or MSL [offshore]
1.96256  Twr2Shft  - Vertical distance from the tower-top to the rotor shaft (meter
0.0      TwrRBHt   - Tower rigid base height (meters)
-5.0     ShftTilt  - Rotor shaft tilt angle (degrees)
0.0      Delta3    - Delta-3 angle for teetering rotors (degrees) [unused for 3 bla
-2.5     PreCone(1) - Blade 1 cone angle (degrees)
-2.5     PreCone(2) - Blade 2 cone angle (degrees)
-2.5     PreCone(3) - Blade 3 cone angle (degrees) [unused for 2 blades]
0.0      AzimBlUp  - Azimuth value to use for I/O when blade 1 points up (degrees)
-----
0.0      YawBrMass - Yaw bearing mass (kg)
240.00E3 NacMass   - Nacelle mass (kg)
56.78E3  HubMass   - Hub mass (kg)
0.0      TipMass(1) - Tip-brake mass, blade 1 (kg)
0.0      TipMass(2) - Tip-brake mass, blade 2 (kg)
0.0      TipMass(3) - Tip-brake mass, blade 3 (kg) [unused for 2 blades]
2607.89E3 NacYIner  - Nacelle inertia about yaw axis (kg m^2)
534.116  GenIner   - Generator inertia about HSS (kg m^2)
115.926E3 HubIner  - Hub inertia about rotor axis [3 blades] or teeter axis [2 bl
-----
90.0     GBoxEff   - Gearbox efficiency (%)
94.4     GenEff    - Generator efficiency [ignored by the Thevenin and user-define
97.0     GBRatio   - Gearbox ratio (-)
False    GBRevers  - Gearbox reversal {T: if rotor and generator rotate in oppos
0.5162E3 HSSBrTqF  - Fully deployed HSS-brake torque (N-m)
0        HSSBrDT   - Time for HSS-brake to reach full deployment once initiated (sec)
DynBrkFi - File containing a mech-gen-torque vs HSS-speed curve for a dynamic brak
867.637E6 DTTorSpr - Drivetrain torsional spring (N-m/rad)
6.215E6  DTTorDmp  - Drivetrain torsional damper (N-m/(rad/s))
-----
9999.9   SIG_SlPc   - Rated generator slip percentage (%) [used only when VSContrl=0 a
9999.9   SIG_SySp   - Synchronous (zero-torque) generator speed (rpm) [used only
9999.9   SIG_RtTq   - Rated torque (N-m) [used only when VSContrl=0 and GenModel=
9999.9   SIG_PORT   - Pull-out ratio (Tpullout/Trated) (-) [used only when VSCont
-----
9999.9   TEC_Freq   - Line frequency [50 or 60] (Hz) [used only when VSContrl=0 a
9998     TEC_NPol   - Number of poles [even integer > 0] (-) [used only when VSCon
9999.9   TEC_SRes   - Stator resistance (ohms) [used only when VSContrl=0 and Gen
9999.9   TEC_RRes   - Rotor resistance (ohms) [used only when VSContrl=0 and GenM
9999.9   TEC_VLL    - Line-to-line RMS voltage (volts) [used only when VSContrl=0
9999.9   TEC_SLR    - Stator leakage reactance (ohms) [used only when VSContrl=0
9999.9   TEC_RLR    - Rotor leakage reactance (ohms) [used only when VSContrl=0 a
9999.9   TEC_MR     - Magnetizing reactance (ohms) [used only when VSContrl=0 and
-----
0        PtfmModel - Platform model {0: none, 1: onshore, 2: fixed bottom o
"NRELOffshBrBslne5MW_Platform_Monopile_RF.dat" PtfmFile - Name of file contain
-----
99       TwrNodes  - Number of tower nodes used for analysis (-)
"NRELOffshBrBslne5MW_Tower_Onshore.dat"       TwrFile   - Name of file containin
-----
9028.32E6 YawSpr    - Nacelle-yaw spring constant (N-m/rad)
19.16E6   YawDamp   - Nacelle-yaw damping constant (N-m/(rad/s))
0.0       YawNeut   - Neutral yaw position--yaw spring force is zero at this yaw (de
-----
False     Furling   - Read in additional model properties for furling turbine (fl
FurlFile  - Name of file containing furling properties (quoted string) [unused when
-----
0        TeetMod   - Rotor-teeter spring/damper model {0: none, 1: standard, 2: use

```

```

0.0 TeetDmpP - Rotor-teeter damper position (degrees) [used only for 2 blades
0.0 TeetDmp - Rotor-teeter damping constant (N-m/(rad/s)) [used only for 2 b
0.0 TeetCDmp - Rotor-teeter rate-independent Coulomb-damping moment (N-m) [us
0.0 TeetSStP - Rotor-teeter soft-stop position (degrees) [used only for 2 bla
0.0 TeetHStP - Rotor-teeter hard-stop position (degrees) [used only for 2 bla
0.0 TeetSSSp - Rotor-teeter soft-stop linear-spring constant (N-m/rad) [used
0.0 TeetHSSp - Rotor-teeter hard-stop linear-spring constant (N-m/rad) [used
-----
0.0 TBDrConN - Tip-brake drag constant during normal operation, Cd*Area (m^2)
0.0 TBDrConD - Tip-brake drag constant during fully-deployed operation, Cd*Ar
0.0 TpBrDT - Time for tip-brake to reach full deployment once released (sec
-----
BLADE -----
"NRELOffshshrBsline5MW_Blade.dat" BldFile(1) - Name of file containin
"NRELOffshshrBsline5MW_Blade.dat" BldFile(2) - Name of file containin
"NRELOffshshrBsline5MW_Blade.dat" BldFile(3) - Name of file containin
-----
AERODYN -----
"NRELOffshshrBsline5MW_AeroDyn.ipt" ADFile - Name of file containin
-----
NOISE -----
NoiseFile - Name of file containing aerodynamic noise input parameters (quoted stri
-----
ADAMS -----
"NRELOffshshrBsline5MW_ADAMSSpecific.dat" ADAMSFile - Name of file containin
-----
LINEARIZATION CONTROL -----
"NRELOffshshrBsline5MW_Linear.dat" LinFile - Name of file containin
-----
OUTPUT -----
True SumPrint - Print summary data to "<RootName>.fsm" (flag)
1 OutFileFmt - Format for tabular (time-marching) output file(s) (1: text
True TabDelim - Generate a tab-delimited tabular output file. (flag)
"ES10.3E2" OutFmt - Format used for tabular output except time. Resulting fiel
0 TStart - Time to begin tabular output (s)
10 DecFact - Decimation factor for tabular output {1: output every
10.0 SttsTime - Amount of time between screen status messages (sec)
-3.09528 NcIMUxn - Downwind distance from the tower-top to the nacelle IMU (mete
0.0 NcIMUyn - Lateral distance from the tower-top to the nacelle IMU (meter
2.23336 NcIMUzn - Vertical distance from the tower-top to the nacelle IMU (meter
1.912 ShftGagL - Distance from rotor apex [3 blades] or teeter pin [2 blades] t
3 NTwGages - Number of tower nodes that have strain gages for output [0 to
10,11,12 TwrGagNd - List of tower nodes that have strain gages [1 to TwrNodes]
3 NBLGages - Number of blade nodes that have strain gages for output [0 to
5,9,13 BldGagNd - List of blade nodes that have strain gages [1 to BldNodes] (
OutList - The next line(s) contains a list of output parameters. See OutList.txt
"WindVxi , WindVyi , WindVzi" - Longitudinal, lateral,
"GenPwr , GenTq" - Electrical generator p
"OoPDefl1 , IPDefl1 , TwstDefl1" - Blade 1 out-of-plane a
"BldPitch1" - Blade 1 pitch angle
"Azimuth" - Blade 1 azimuth angle
"RotSpeed , GenSpeed" - Low-speed shaft and hi
"TTDspFA , TTDspSS , TTDspTwst" - Tower fore-aft and sid
"Spn2MLxbl , Spn2MLybl" - Blade 1 local edgewise
"RootFxc1 , RootFycl , RootFzcl" - Out-of-plane shear, in
"RootMxc1 , RootMycl , RootMzcl" - In-plane bending, out-
"RotTorq , LSSGagMya , LSSGagMza" - Rotor torque and low-s
"YawBrFxp , YawBrFyp , YawBrFzp" - Fore-aft shear, side-t
"YawBrMxp , YawBrMyp , YawBrMzp" - Side-to-side bending,
"TwrBsFxt , TwrBsFyt , TwrBsFzt" - Fore-aft shear, side-t
"TwrBsMxt , TwrBsMyt , TwrBsMzt" - Side-to-side bending,
"NacYaw , YawPos"
"RootMxbl , RootMybl , RootMzbl" - Blade 1 edgewise, flap
"NacYawErr , HorWndDir"
"WaveElev"
END of FAST input file (the word "END" must appear in the first 3 columns of this las
-----

```

## D.2 AeroDyn Input Files(\*.ipt)

```

NREL 5.0 MW offshore baseline aerodynamic input properties; Compatible with AeroDyn v1
SI SysUnits - System of units used for input and output [must be SI for FA
STEADY StallMod - Dynamic stall included [BEDDOES or STEADY] (unquoted string)
NO_CM UseCm - Use aerodynamic pitching moment model? [USE_CM or NO_CM] (unq
EQUIL InfModel - Inflow model [DYNIN or EQUIL] (unquoted string)
NONE IndModel - Induction-factor model [NONE or WAKE or SWIRL] (unquoted stri
0.005 AToler - Induction-factor tolerance (convergence criteria) (-)
PRANDt1 TLModel - Tip-loss model (EQUIL only) [PRANDt1, GTECH, or NONE] (unquo
PRANDt1 HLModel - Hub-loss model (EQUIL only) [PRANDt1 or NONE] (unquoted stri
"userwind" WindFile - Name of file containing wind data (quoted stri

```

```

90.0      HH          - Wind reference (hub) height [TowerHt+Twr2Shft+OverHang*SIN(Shf
0.0      TwrShad     - Tower-shadow velocity deficit (-)
9999.9    ShadHWid   - Tower-shadow half width (m)
9999.9    T_Shad_Refpt- Tower-shadow reference point (m)
1.225    AirDens     - Air density (kg/m^3)
1.464E-5 KinVisc    - Kinematic air viscosity [CURRENTLY IGNORED] (m^2/sec)
0.0125   DTAero     - Time interval for aerodynamic calculations (sec)
8        NumFoil    - Number of airfoil files (-)
"AeroData\Cylinder1.dat"      FoilNm      - Names of the airfoil fi
"AeroData\Cylinder2.dat"
"AeroData\DU40_A17.dat"
"AeroData\DU35_A17.dat"
"AeroData\DU30_A17.dat"
"AeroData\DU25_A17.dat"
"AeroData\DU21_A17.dat"
"AeroData\NACA64_A17.dat"
17      BldNodes    - Number of blade nodes used for analysis (-)
RNodes  AeroTwst  DRNodes  Chord  NFoil  PrnElm
2.8667  13.308    2.7333   3.542  1      PRINT
5.6000  13.308    2.7333   3.854  1      PRINT
8.3333  13.308    2.7333   4.167  2      PRINT
11.7500 13.308    4.1000   4.557  3      PRINT
15.8500 11.480    4.1000   4.652  4      PRINT
19.9500 10.162    4.1000   4.458  4      PRINT
24.0500  9.011     4.1000   4.249  5      PRINT
28.1500  7.795     4.1000   4.007  6      PRINT
32.2500  6.544     4.1000   3.748  6      PRINT
36.3500  5.361     4.1000   3.502  7      PRINT
40.4500  4.188     4.1000   3.256  7      PRINT
44.5500  3.125     4.1000   3.010  8      PRINT
48.6500  2.319     4.1000   2.764  8      PRINT
52.7500  1.526     4.1000   2.518  8      PRINT
56.1667  0.863     2.7333   2.313  8      PRINT
58.9000  0.370     2.7333   2.086  8      PRINT
61.6333  0.106     2.7333   1.419  8      PRINT

```



# Appendix E

## Abaqus files for modeling the jacket support structure

### E.1 Python script to read field output from .odb(\*.py)

```
from odbAccess import *
from textRepr import *
from abaqusConstants import *
import odbAccess
odb=openOdb(path='myjob.odb')

mySteps = odb.steps

numSteps = len(mySteps)

for i in range(numSteps):
    stepKey = mySteps.keys()[i]
    step = mySteps[stepKey]
    numFrames = len(step.frames)

regS1 = odb.rootAssembly.instances['PART-1-1'].nodeSets['BC_NODE']
regU1 = odb.rootAssembly.instances['PART-1-1'].nodeSets['ZERO_POINT']
regL1 = odb.rootAssembly.instances['PART-1-1'].elementSets['LEG1_MEMB1']
regL2 = odb.rootAssembly.instances['PART-1-1'].elementSets['LEG2_MEMB1']
regL3 = odb.rootAssembly.instances['PART-1-1'].elementSets['LEG3_MEMB1']
regL4 = odb.rootAssembly.instances['PART-1-1'].elementSets['LEG4_MEMB1']
regB1M1 = odb.rootAssembly.instances['PART-1-1'].elementSets['BRA1_MEMB1']
regB2M1 = odb.rootAssembly.instances['PART-1-1'].elementSets['BRA2_MEMB1']
regB3M1 = odb.rootAssembly.instances['PART-1-1'].elementSets['BRA3_MEMB1']
regB4M1 = odb.rootAssembly.instances['PART-1-1'].elementSets['BRA4_MEMB1']
regB1M2 = odb.rootAssembly.instances['PART-1-1'].elementSets['BRA1_MEMB2']
regB2M2 = odb.rootAssembly.instances['PART-1-1'].elementSets['BRA2_MEMB2']
regB3M2 = odb.rootAssembly.instances['PART-1-1'].elementSets['BRA3_MEMB2']
regB4M2 = odb.rootAssembly.instances['PART-1-1'].elementSets['BRA4_MEMB2']

frameRepository = step.frames

moment_out = open('abaqus_moment1.txt', 'w')
force_out = open('abaqus_forcel.txt', 'w')
disp_out_zero = open('abaqus_disp_zero.txt', 'w')
L1_out = open('abaqus_L1.txt', 'w')
L2_out = open('abaqus_L2.txt', 'w')
L3_out = open('abaqus_L3.txt', 'w')
L4_out = open('abaqus_L4.txt', 'w')
B1M1_out = open('abaqus_B1M1.txt', 'w')
B2M1_out = open('abaqus_B2M1.txt', 'w')
B3M1_out = open('abaqus_B3M1.txt', 'w')
B4M1_out = open('abaqus_B4M1.txt', 'w')
B1M2_out = open('abaqus_B1M2.txt', 'w')
B2M2_out = open('abaqus_B2M2.txt', 'w')
B3M2_out = open('abaqus_B3M2.txt', 'w')
B4M2_out = open('abaqus_B4M2.txt', 'w')

for frame in frameRepository:
    RForce = frame.fieldOutputs['RF']
    RMoment = frame.fieldOutputs['RM']
    UDisp = frame.fieldOutputs['U']
    URDisp = frame.fieldOutputs['UR']
    SForce = frame.fieldOutputs['SF']
    SMoment = frame.fieldOutputs['SM']
    Time = frame.frameValue
    FX = RForce.getSubset(region=regS1).values[0].data[0]
    FY = RForce.getSubset(region=regS1).values[0].data[1]
    FZ = RForce.getSubset(region=regS1).values[0].data[2]
    MX = RMoment.getSubset(region=regS1).values[0].data[0]
    MY = RMoment.getSubset(region=regS1).values[0].data[1]
    MZ = RMoment.getSubset(region=regS1).values[0].data[2]
    U_zero1 = UDisp.getSubset(region=regU1).values[0].data[0]
    U_zero2 = UDisp.getSubset(region=regU1).values[0].data[1]
    U_zero3 = UDisp.getSubset(region=regU1).values[0].data[2]
    UR_zero1 = URDisp.getSubset(region=regU1).values[0].data[0]
    UR_zero2 = URDisp.getSubset(region=regU1).values[0].data[1]
    UR_zero3 = URDisp.getSubset(region=regU1).values[0].data[2]
```

```

L1_F1 = SForce.getSubset(region=regL1).values[0].data[0]
L1_F2 = SForce.getSubset(region=regL1).values[0].data[1]
L1_F3 = SForce.getSubset(region=regL1).values[0].data[2]
L1_M1 = SMoment.getSubset(region=regL1).values[0].data[0]
L1_M2 = SMoment.getSubset(region=regL1).values[0].data[1]
L1_M3 = SMoment.getSubset(region=regL1).values[0].data[2]
L2_F1 = SForce.getSubset(region=regL2).values[0].data[0]
L2_F2 = SForce.getSubset(region=regL2).values[0].data[1]
L2_F3 = SForce.getSubset(region=regL2).values[0].data[2]
L2_M1 = SMoment.getSubset(region=regL2).values[0].data[0]
L2_M2 = SMoment.getSubset(region=regL2).values[0].data[1]
L2_M3 = SMoment.getSubset(region=regL2).values[0].data[2]
L3_F1 = SForce.getSubset(region=regL3).values[0].data[0]
L3_F2 = SForce.getSubset(region=regL3).values[0].data[1]
L3_F3 = SForce.getSubset(region=regL3).values[0].data[2]
L3_M1 = SMoment.getSubset(region=regL3).values[0].data[0]
L3_M2 = SMoment.getSubset(region=regL3).values[0].data[1]
L3_M3 = SMoment.getSubset(region=regL3).values[0].data[2]
L4_F1 = SForce.getSubset(region=regL4).values[0].data[0]
L4_F2 = SForce.getSubset(region=regL4).values[0].data[1]
L4_F3 = SForce.getSubset(region=regL4).values[0].data[2]
L4_M1 = SMoment.getSubset(region=regL4).values[0].data[0]
L4_M2 = SMoment.getSubset(region=regL4).values[0].data[1]
L4_M3 = SMoment.getSubset(region=regL4).values[0].data[2]
B1M1_F1 = SForce.getSubset(region=regB1M1).values[0].data[0]
B1M1_F2 = SForce.getSubset(region=regB1M1).values[0].data[1]
B1M1_F3 = SForce.getSubset(region=regB1M1).values[0].data[2]
B1M1_M1 = SMoment.getSubset(region=regB1M1).values[0].data[0]
B1M1_M2 = SMoment.getSubset(region=regB1M1).values[0].data[1]
B1M1_M3 = SMoment.getSubset(region=regB1M1).values[0].data[2]
B2M1_F1 = SForce.getSubset(region=regB2M1).values[0].data[0]
B2M1_F2 = SForce.getSubset(region=regB2M1).values[0].data[1]
B2M1_F3 = SForce.getSubset(region=regB2M1).values[0].data[2]
B2M1_M1 = SMoment.getSubset(region=regB2M1).values[0].data[0]
B2M1_M2 = SMoment.getSubset(region=regB2M1).values[0].data[1]
B2M1_M3 = SMoment.getSubset(region=regB2M1).values[0].data[2]
B3M1_F1 = SForce.getSubset(region=regB3M1).values[0].data[0]
B3M1_F2 = SForce.getSubset(region=regB3M1).values[0].data[1]
B3M1_F3 = SForce.getSubset(region=regB3M1).values[0].data[2]
B3M1_M1 = SMoment.getSubset(region=regB3M1).values[0].data[0]
B3M1_M2 = SMoment.getSubset(region=regB3M1).values[0].data[1]
B3M1_M3 = SMoment.getSubset(region=regB3M1).values[0].data[2]
B4M1_F1 = SForce.getSubset(region=regB4M1).values[0].data[0]
B4M1_F2 = SForce.getSubset(region=regB4M1).values[0].data[1]
B4M1_F3 = SForce.getSubset(region=regB4M1).values[0].data[2]
B4M1_M1 = SMoment.getSubset(region=regB4M1).values[0].data[0]
B4M1_M2 = SMoment.getSubset(region=regB4M1).values[0].data[1]
B4M1_M3 = SMoment.getSubset(region=regB4M1).values[0].data[2]
B1M2_F1 = SForce.getSubset(region=regB1M2).values[0].data[0]
B1M2_F2 = SForce.getSubset(region=regB1M2).values[0].data[1]
B1M2_F3 = SForce.getSubset(region=regB1M2).values[0].data[2]
B1M2_M1 = SMoment.getSubset(region=regB1M2).values[0].data[0]
B1M2_M2 = SMoment.getSubset(region=regB1M2).values[0].data[1]
B1M2_M3 = SMoment.getSubset(region=regB1M2).values[0].data[2]
B2M2_F1 = SForce.getSubset(region=regB2M2).values[0].data[0]
B2M2_F2 = SForce.getSubset(region=regB2M2).values[0].data[1]
B2M2_F3 = SForce.getSubset(region=regB2M2).values[0].data[2]
B2M2_M1 = SMoment.getSubset(region=regB2M2).values[0].data[0]
B2M2_M2 = SMoment.getSubset(region=regB2M2).values[0].data[1]
B2M2_M3 = SMoment.getSubset(region=regB2M2).values[0].data[2]
B3M2_F1 = SForce.getSubset(region=regB3M2).values[0].data[0]
B3M2_F2 = SForce.getSubset(region=regB3M2).values[0].data[1]
B3M2_F3 = SForce.getSubset(region=regB3M2).values[0].data[2]
B3M2_M1 = SMoment.getSubset(region=regB3M2).values[0].data[0]
B3M2_M2 = SMoment.getSubset(region=regB3M2).values[0].data[1]
B3M2_M3 = SMoment.getSubset(region=regB3M2).values[0].data[2]
B4M2_F1 = SForce.getSubset(region=regB4M2).values[0].data[0]
B4M2_F2 = SForce.getSubset(region=regB4M2).values[0].data[1]
B4M2_F3 = SForce.getSubset(region=regB4M2).values[0].data[2]
B4M2_M1 = SMoment.getSubset(region=regB4M2).values[0].data[0]
B4M2_M2 = SMoment.getSubset(region=regB4M2).values[0].data[1]
B4M2_M3 = SMoment.getSubset(region=regB4M2).values[0].data[2]
force_out.write(str(Time)+" "+str(FX)+" "+str(FY)+" "+str(FZ)+"\n")
moment_out.write(str(Time)+" "+str(MX)+" "+str(MY)+" "+str(MZ)+"\n")
disp_out_zero.write(str(Time)+" "+str(U_zero1)+" "+str(U_zero2)+" "+str(U_zero3)
+" "+str(UR_zero1)+" "+str(UR_zero2)+" "+str(UR_zero3)+"\n")

```

```

L1_out.write(str(Time)+" "+str(L1_F1)+" "+str(L1_F2)+" "+str(L1_F3)+" "+str(L1_M1)
+" "+str(L1_M2)+" "+str(L1_M3)+"\n")
L2_out.write(str(Time)+" "+str(L2_F1)+" "+str(L2_F2)+" "+str(L2_F3)+" "+str(L2_M1)
+" "+str(L2_M2)+" "+str(L2_M3)+"\n")
L3_out.write(str(Time)+" "+str(L3_F1)+" "+str(L3_F2)+" "+str(L3_F3)+" "+str(L3_M1)
+" "+str(L3_M2)+" "+str(L3_M3)+"\n")
L4_out.write(str(Time)+" "+str(L4_F1)+" "+str(L4_F2)+" "+str(L4_F3)+" "+str(L4_M1)
+" "+str(L4_M2)+" "+str(L4_M3)+"\n")
B1M1_out.write(str(Time)+" "+str(B1M1_F1)+" "+str(B1M1_F2)+" "+str(B1M1_F3)+" "
+str(B1M1_M1)+" "+str(B1M1_M2)+" "+str(B1M1_M3)+"\n")
B2M1_out.write(str(Time)+" "+str(B2M1_F1)+" "+str(B2M1_F2)+" "+str(B2M1_F3)+" "
+str(B2M1_M1)+" "+str(B2M1_M2)+" "+str(B2M1_M3)+"\n")
B3M1_out.write(str(Time)+" "+str(B3M1_F1)+" "+str(B3M1_F2)+" "+str(B3M1_F3)+" "
+str(B3M1_M1)+" "+str(B3M1_M2)+" "+str(B3M1_M3)+"\n")
B4M1_out.write(str(Time)+" "+str(B4M1_F1)+" "+str(B4M1_F2)+" "+str(B4M1_F3)+" "
+str(B4M1_M1)+" "+str(B4M1_M2)+" "+str(B4M1_M3)+"\n")
B1M2_out.write(str(Time)+" "+str(B1M2_F1)+" "+str(B1M2_F2)+" "+str(B1M2_F3)+" "
+str(B1M2_M1)+" "+str(B1M2_M2)+" "+str(B1M2_M3)+"\n")
B2M2_out.write(str(Time)+" "+str(B2M2_F1)+" "+str(B2M2_F2)+" "+str(B2M2_F3)+" "
+str(B2M2_M1)+" "+str(B2M2_M2)+" "+str(B2M2_M3)+"\n")
B3M2_out.write(str(Time)+" "+str(B3M2_F1)+" "+str(B3M2_F2)+" "+str(B3M2_F3)+" "
+str(B3M2_M1)+" "+str(B3M2_M2)+" "+str(B3M2_M3)+"\n")
B4M2_out.write(str(Time)+" "+str(B4M2_F1)+" "+str(B4M2_F2)+" "+str(B4M2_F3)+" "
+str(B4M2_M1)+" "+str(B4M2_M2)+" "+str(B4M2_M3)+"\n")

moment_out=open('abaqus_moment2.txt','w')
force_out=open('abaqus_force2.txt','w')

for frame in frameRepository:
    RForce =frame.fieldOutputs['RF']
    RMoment=frame.fieldOutputs['RM']
    Time = frame.frameValue
    FX = RForce.getSubset(region=regS1).values[1].data[0]
    FY = RForce.getSubset(region=regS1).values[1].data[1]
    FZ = RForce.getSubset(region=regS1).values[1].data[2]
    MX = RMoment.getSubset(region=regS1).values[1].data[0]
    MY = RMoment.getSubset(region=regS1).values[1].data[1]
    MZ = RMoment.getSubset(region=regS1).values[1].data[2]
    force_out.write(str(Time)+" "+str(FX)+" "+str(FY)+" "+str(FZ)+"\n")
    moment_out.write(str(Time)+" "+str(MX)+" "+str(MY)+" "+str(MZ)+"\n")

moment_out=open('abaqus_moment3.txt','w')
force_out=open('abaqus_force3.txt','w')

for frame in frameRepository:
    RForce =frame.fieldOutputs['RF']
    RMoment=frame.fieldOutputs['RM']
    Time = frame.frameValue
    FX = RForce.getSubset(region=regS1).values[2].data[0]
    FY = RForce.getSubset(region=regS1).values[2].data[1]
    FZ = RForce.getSubset(region=regS1).values[2].data[2]
    MX = RMoment.getSubset(region=regS1).values[2].data[0]
    MY = RMoment.getSubset(region=regS1).values[2].data[1]
    MZ = RMoment.getSubset(region=regS1).values[2].data[2]
    force_out.write(str(Time)+" "+str(FX)+" "+str(FY)+" "+str(FZ)+"\n")
    moment_out.write(str(Time)+" "+str(MX)+" "+str(MY)+" "+str(MZ)+"\n")

moment_out=open('abaqus_moment4.txt','w')
force_out=open('abaqus_force4.txt','w')

for frame in frameRepository:
    RForce =frame.fieldOutputs['RF']
    RMoment=frame.fieldOutputs['RM']
    Time = frame.frameValue
    FX = RForce.getSubset(region=regS1).values[3].data[0]
    FY = RForce.getSubset(region=regS1).values[3].data[1]
    FZ = RForce.getSubset(region=regS1).values[3].data[2]
    MX = RMoment.getSubset(region=regS1).values[3].data[0]
    MY = RMoment.getSubset(region=regS1).values[3].data[1]
    MZ = RMoment.getSubset(region=regS1).values[3].data[2]
    force_out.write(str(Time)+" "+str(FX)+" "+str(FY)+" "+str(FZ)+"\n")
    moment_out.write(str(Time)+" "+str(MX)+" "+str(MY)+" "+str(MZ)+"\n")

odb.close()

```

## E.2 Abaqus Input File(\*.inp)

```
*Heading
*Preprint, echo=NO, model=NO, history=NO, contact=NO
**
** PARTS
**
*Part, name=PART-1
*Node
1,      6000.,      6000.,      -50000.
2,      6000.,      6000.,      -45000.
3,      5967.,      5967.,      -44001.
4,      5939.,      5939.,      -43127.
5,      5333.,      5333.,      -24614.
6,     -6000.,      6000.,      -50000.
7,     -6000.,      6000.,      -45000.
8,     -5967.,      5967.,      -44001.
9,     -5939.,      5939.,      -43127.
10,    -5333.,      5333.,      -24614.
11,    -6000.,     -6000.,      -50000.
12,    -6000.,     -6000.,      -45000.
13,    -5967.,     -5967.,      -44001.
14,    -5939.,     -5939.,      -43127.
15,    -5333.,     -5333.,      -24614.
16,     6000.,     -6000.,      -50000.
17,     6000.,     -6000.,      -45000.
18,     5967.,     -5967.,      -44001.
19,     5939.,     -5939.,      -43127.
20,     5333.,     -5333.,      -24614.
21,     4820.,      4820.,      -8922.
22,     4385.,      4385.,       4378.
23,     4016.,      4016.,      15651.
24,     4000.,      4000.,      16150.
25,    -4820.,      4820.,      -8922.
26,    -4385.,      4385.,       4378.
27,    -4016.,      4016.,      15651.
28,    -4000.,      4000.,      16150.
29,    -4820.,     -4820.,      -8922.
30,    -4385.,     -4385.,       4378.
31,    -4016.,     -4016.,      15651.
32,    -4000.,     -4000.,      16150.
33,     4820.,     -4820.,      -8922.
34,     4385.,     -4385.,       4378.
35,     4016.,     -4016.,      15651.
36,     4000.,     -4000.,      16150.
41,     5620.,        0.,     -33373.
42,    -5620.,        0.,     -33373.
43,        0.,      5620.,     -33373.
44,        0.,     -5620.,     -33373.
45,     5064.,        0.,     -16371.
46,    -5064.,        0.,     -16371.
47,        0.,      5064.,     -16371.
48,        0.,     -5064.,     -16371.
49,     4592.,        0.,     -1958.
50,    -4592.,        0.,     -1958.
51,        0.,      4592.,     -1958.
52,        0.,     -4592.,     -1958.
53,     4193.,        0.,      10262.
54,    -4193.,        0.,      10262.
55,        0.,      4193.,      10262.
56,        0.,     -4193.,      10262.
57,     4000.,      4000.,      20150.
58,    -4000.,      4000.,      20150.
59,     4000.,     -4000.,      20150.
60,    -4000.,     -4000.,      20150.
61,        0.,        0.,      16150.
62,        0.,        0.,      18150.
63,        0.,        0.,      20150.
1001,        0.,        0.,      21150.
1011,        0.,        0.,      32150.
1021,        0.,        0.,      42150.
1031,        0.,        0.,      54150.
1041,        0.,        0.,      64150.
1051,        0.,        0.,      74150.
1061,        0.,        0.,      83150.
1071,        0.,        0.,      88150.
```

10041,	5863,	5863,	-40813
10042,	5787,	5787,	-38499
10043,	5711,	5711,	-36185
10044,	5636,	5636,	-33871
10045,	5560,	5560,	-31557
10046,	5484,	5484,	-29243
10047,	5408,	5408,	-26929
10081,	-5864.,	5863.,	-40813.
10082,	-5788.,	5787.,	-38499.
10083,	-5712.,	5711.,	-36185.
10084,	-5636.,	5636.,	-33871.
10085,	-5561.,	5560.,	-31557.
10086,	-5485.,	5484.,	-29243.
10087,	-5409.,	5408.,	-26929.
10121,	-5864.,	-5864.,	-40813.
10122,	-5788.,	-5788.,	-38499.
10123,	-5712.,	-5712.,	-36185.
10124,	-5636.,	-5636.,	-33871.
10125,	-5561.,	-5561.,	-31557.
10126,	-5485.,	-5485.,	-29243.
10127,	-5409.,	-5409.,	-26929.
10161,	5863.,	-5864.,	-40813.
10162,	5787.,	-5788.,	-38499.
10163,	5711.,	-5712.,	-36185.
10164,	5636.,	-5636.,	-33871.
10165,	5560.,	-5561.,	-31557.
10166,	5484.,	-5485.,	-29243.
10167,	5408.,	-5409.,	-26929.
10171,	5268.,	5268.,	-22653.
10172,	5204.,	5204.,	-20691.
10173,	5140.,	5140.,	-18730.
10174,	5076.,	5076.,	-16768.
10175,	5012.,	5012.,	-14807.
10176,	4948.,	4948.,	-12845.
10177,	4884.,	4884.,	-10884.
10181,	4765.,	4765.,	-7260.
10182,	4711.,	4711.,	-5597.
10183,	4656.,	4656.,	-3935.
10184,	4602.,	4602.,	-2272.
10185,	4548.,	4548.,	-610.
10186,	4493.,	4493.,	1053.
10187,	4439.,	4439.,	2715.
10191,	4338.,	4338.,	5787.
10192,	4292.,	4292.,	7196.
10193,	4246.,	4246.,	8605.
10194,	4200.,	4200.,	10014.
10195,	4154.,	4154.,	11423.
10196,	4108.,	4108.,	12832.
10197,	4062.,	4062.,	14241.
10211,	-5269.,	5268.,	-22653.
10212,	-5205.,	5204.,	-20691.
10213,	-5141.,	5140.,	-18730.
10214,	-5077.,	5076.,	-16768.
10215,	-5013.,	5012.,	-14807.
10216,	-4949.,	4948.,	-12845.
10217,	-4885.,	4884.,	-10884.
10221,	-4766.,	4765.,	-7260.
10222,	-4712.,	4711.,	-5597.
10223,	-4657.,	4656.,	-3935.
10224,	-4603.,	4602.,	-2272.
10225,	-4549.,	4548.,	-610.
10226,	-4494.,	4493.,	1053.
10227,	-4440.,	4439.,	2715.
10231,	-4339.,	4338.,	5787.
10232,	-4293.,	4292.,	7196.
10233,	-4247.,	4246.,	8605.
10234,	-4201.,	4200.,	10014.
10235,	-4155.,	4154.,	11423.
10236,	-4109.,	4108.,	12832.
10237,	-4063.,	4062.,	14241.
10251,	-5269.,	-5269.,	-22653.
10252,	-5205.,	-5205.,	-20691.
10253,	-5141.,	-5141.,	-18730.
10254,	-5077.,	-5077.,	-16768.
10255,	-5013.,	-5013.,	-14807.
10256,	-4949.,	-4949.,	-12845.

10257,	-4885.,	-4885.,	-10884.
10261,	-4766.,	-4766.,	-7260.
10262,	-4712.,	-4712.,	-5597.
10263,	-4657.,	-4657.,	-3935.
10264,	-4603.,	-4603.,	-2272.
10265,	-4549.,	-4549.,	-610.
10266,	-4494.,	-4494.,	1053.
10267,	-4440.,	-4440.,	2715.
10271,	-4339.,	-4339.,	5787.
10272,	-4293.,	-4293.,	7196.
10273,	-4247.,	-4247.,	8605.
10274,	-4201.,	-4201.,	10014.
10275,	-4155.,	-4155.,	11423.
10276,	-4109.,	-4109.,	12832.
10277,	-4063.,	-4063.,	14241.
10291,	5268.,	-5269.,	-22653.
10292,	5204.,	-5205.,	-20691.
10293,	5140.,	-5141.,	-18730.
10294,	5076.,	-5077.,	-16768.
10295,	5012.,	-5013.,	-14807.
10296,	4948.,	-4949.,	-12845.
10297,	4884.,	-4885.,	-10884.
10301,	4765.,	-4766.,	-7260.
10302,	4711.,	-4712.,	-5597.
10303,	4656.,	-4657.,	-3935.
10304,	4602.,	-4603.,	-2272.
10305,	4548.,	-4549.,	-610.
10306,	4493.,	-4494.,	1053.
10307,	4439.,	-4440.,	2715.
10311,	4338.,	-4339.,	5787.
10312,	4292.,	-4293.,	7196.
10313,	4246.,	-4247.,	8605.
10314,	4200.,	-4201.,	10014.
10315,	4154.,	-4155.,	11423.
10316,	4108.,	-4109.,	12832.
10317,	4062.,	-4063.,	14241.
10371,	4475.,	5967.,	-44001.
10372,	2983.,	5967.,	-44001.
10373,	1491.,	5967.,	-44001.
10374,	0.,	5967.,	-44001.
10375,	-1492.,	5967.,	-44001.
10376,	-2984.,	5967.,	-44001.
10377,	-4476.,	5967.,	-44001.
10381,	-5967.,	4475.,	-44001.
10382,	-5967.,	2983.,	-44001.
10383,	-5967.,	1491.,	-44001.
10384,	-5967.,	0.,	-44001.
10385,	-5967.,	-1492.,	-44001.
10386,	-5967.,	-2984.,	-44001.
10387,	-5967.,	-4476.,	-44001.
10391,	-4476.,	-5967.,	-44001.
10392,	-2984.,	-5967.,	-44001.
10393,	-1492.,	-5967.,	-44001.
10394,	0.,	-5967.,	-44001.
10395,	1491.,	-5967.,	-44001.
10396,	2983.,	-5967.,	-44001.
10397,	4475.,	-5967.,	-44001.
10401,	5967.,	-4476.,	-44001.
10402,	5967.,	-2984.,	-44001.
10403,	5967.,	-1492.,	-44001.
10404,	5967.,	0.,	-44001.
10405,	5967.,	1491.,	-44001.
10406,	5967.,	2983.,	-44001.
10407,	5967.,	4475.,	-44001.
10411,	5859.,	4454.,	-40689.
10412,	5779.,	2969.,	-38250.
10413,	5699.,	1484.,	-35812.
10421,	5548.,	-1334.,	-31184.
10422,	5476.,	-2667.,	-28994.
10423,	5404.,	-4000.,	-26804.
10431,	5859.,	-4455.,	-40689.
10432,	5779.,	-2970.,	-38250.
10433,	5699.,	-1485.,	-35812.
10441,	5548.,	1333.,	-31184.
10442,	5476.,	2666.,	-28994.
10443,	5404.,	3999.,	-26804.

10451,	-5860.,	4454.,	-40689.
10452,	-5780.,	2969.,	-38250.
10453,	-5700.,	1484.,	-35812.
10461,	-5549.,	-1334.,	-31184.
10462,	-5477.,	-2667.,	-28994.
10463,	-5405.,	-4000.,	-26804.
10471,	-5860.,	-4455.,	-40689.
10472,	-5780.,	-2970.,	-38250.
10473,	-5700.,	-1485.,	-35812.
10481,	-5549.,	1333.,	-31184.
10482,	-5477.,	2666.,	-28994.
10483,	-5405.,	3999.,	-26804.
10491,	4454.,	5859.,	-40689.
10492,	2969.,	5779.,	-38250.
10493,	1484.,	5699.,	-35812.
10501,	-1334.,	5548.,	-31184.
10502,	-2667.,	5476.,	-28994.
10503,	-4000.,	5404.,	-26804.
10511,	-4455.,	5859.,	-40689.
10512,	-2970.,	5779.,	-38250.
10513,	-1485.,	5699.,	-35812.
10521,	1333.,	5548.,	-31184.
10522,	2666.,	5476.,	-28994.
10523,	3999.,	5404.,	-26804.
10531,	4454.,	-5860.,	-40689.
10532,	2969.,	-5780.,	-38250.
10533,	1484.,	-5700.,	-35812.
10541,	-1334.,	-5549.,	-31184.
10542,	-2667.,	-5477.,	-28994.
10543,	-4000.,	-5405.,	-26804.
10551,	-4455.,	-5860.,	-40689.
10552,	-2970.,	-5780.,	-38250.
10553,	-1485.,	-5700.,	-35812.
10561,	1333.,	-5549.,	-31184.
10562,	2666.,	-5477.,	-28994.
10563,	3999.,	-5405.,	-26804.
10571,	5265.,	3999.,	-22554.
10572,	5198.,	2666.,	-20493.
10573,	5131.,	1333.,	-18432.
10581,	5003.,	-1205.,	-14509.
10582,	4942.,	-2410.,	-12647.
10583,	4881.,	-3615.,	-10785.
10591,	5265.,	-4000.,	-22554.
10592,	5198.,	-2667.,	-20493.
10593,	5131.,	-1334.,	-18432.
10601,	5003.,	1205.,	-14509.
10602,	4942.,	2410.,	-12647.
10603,	4881.,	3615.,	-10785.
10611,	-5266.,	3999.,	-22554.
10612,	-5199.,	2666.,	-20493.
10613,	-5132.,	1333.,	-18432.
10621,	-5003.,	-1205.,	-14509.
10622,	-4942.,	-2410.,	-12647.
10623,	-4881.,	-3615.,	-10785.
10631,	-5266.,	-4000.,	-22554.
10632,	-5199.,	-2667.,	-20493.
10633,	-5132.,	-1334.,	-18432.
10641,	-5003.,	1205.,	-14509.
10642,	-4942.,	2410.,	-12647.
10643,	-4881.,	3615.,	-10785.
10651,	3999.,	5265.,	-22554.
10652,	2666.,	5198.,	-20493.
10653,	1333.,	5131.,	-18432.
10661,	-1205.,	5003.,	-14509.
10662,	-2410.,	4942.,	-12647.
10663,	-3615.,	4881.,	-10785.
10671,	-4000.,	5265.,	-22554.
10672,	-2667.,	5198.,	-20493.
10673,	-1334.,	5131.,	-18432.
10681,	1205.,	5003.,	-14509.
10682,	2410.,	4942.,	-12647.
10683,	3615.,	4881.,	-10785.
10691,	3999.,	-5266.,	-22554.
10692,	2666.,	-5199.,	-20493.
10693,	1333.,	-5132.,	-18432.
10701,	-1205.,	-5003.,	-14509.

10702,	-2410.,	-4942.,	-12647.
10703,	-3615.,	-4881.,	-10785.
10711,	-4000.,	-5266.,	-22554.
10712,	-2667.,	-5199.,	-20493.
10713,	-1334.,	-5132.,	-18432.
10721,	1205.,	-5003.,	-14509.
10722,	2410.,	-4942.,	-12647.
10723,	3615.,	-4881.,	-10785.
10731,	4763.,	3615.,	-7181.
10732,	4706.,	2410.,	-5440.
10733,	4649.,	1205.,	-3699.
10741,	4540.,	-1097.,	-374.
10742,	4488.,	-2193.,	1210.
10743,	4436.,	-3289.,	2794.
10751,	4763.,	-3615.,	-7181.
10752,	4706.,	-2410.,	-5440.
10753,	4649.,	-1205.,	-3699.
10761,	4540.,	1096.,	-374.
10762,	4488.,	2192.,	1210.
10763,	4436.,	3288.,	2794.
10771,	-4763.,	3615.,	-7181.
10772,	-4706.,	2410.,	-5440.
10773,	-4649.,	1205.,	-3699.
10781,	-4541.,	-1097.,	-374.
10782,	-4489.,	-2193.,	1210.
10783,	-4437.,	-3289.,	2794.
10791,	-4763.,	-3615.,	-7181.
10792,	-4706.,	-2410.,	-5440.
10793,	-4649.,	-1205.,	-3699.
10801,	-4541.,	1096.,	-374.
10802,	-4489.,	2192.,	1210.
10803,	-4437.,	3288.,	2794.
10811,	3615.,	4763.,	-7181.
10812,	2410.,	4706.,	-5440.
10813,	1205.,	4649.,	-3699.
10821,	-1097.,	4540.,	-374.
10822,	-2193.,	4488.,	1210.
10823,	-3289.,	4436.,	2794.
10831,	-3615.,	4763.,	-7181.
10832,	-2410.,	4706.,	-5440.
10833,	-1205.,	4649.,	-3699.
10841,	1096.,	4540.,	-374.
10842,	2192.,	4488.,	1210.
10843,	3288.,	4436.,	2794.
10851,	3615.,	-4763.,	-7181.
10852,	2410.,	-4706.,	-5440.
10853,	1205.,	-4649.,	-3699.
10861,	-1097.,	-4541.,	-374.
10862,	-2193.,	-4489.,	1210.
10863,	-3289.,	-4437.,	2794.
10871,	-3615.,	-4763.,	-7181.
10872,	-2410.,	-4706.,	-5440.
10873,	-1205.,	-4649.,	-3699.
10881,	1096.,	-4541.,	-374.
10882,	2192.,	-4489.,	1210.
10883,	3288.,	-4437.,	2794.
10891,	4337.,	3288.,	5849.
10892,	4289.,	2192.,	7320.
10893,	4241.,	1096.,	8791.
10901,	4148.,	-1004.,	11609.
10902,	4104.,	-2008.,	12956.
10903,	4060.,	-3012.,	14303.
10911,	4337.,	-3289.,	5849.
10912,	4289.,	-2193.,	7320.
10913,	4241.,	-1097.,	8791.
10921,	4148.,	1004.,	11609.
10922,	4104.,	2008.,	12956.
10923,	4060.,	3012.,	14303.
10931,	-4337.,	3288.,	5849.
10932,	-4289.,	2192.,	7320.
10933,	-4241.,	1096.,	8791.
10941,	-4149.,	-1004.,	11609.
10942,	-4105.,	-2008.,	12956.
10943,	-4061.,	-3012.,	14303.
10951,	-4337.,	-3289.,	5849.
10952,	-4289.,	-2193.,	7320.



10953,	-4241.,	-1097.,	8791.
10961,	-4149.,	1004.,	11609.
10962,	-4105.,	2008.,	12956.
10963,	-4061.,	3012.,	14303.
10971,	3288.,	4337.,	5849.
10972,	2192.,	4289.,	7320.
10973,	1096.,	4241.,	8791.
10981,	-1004.,	4148.,	11609.
10982,	-2008.,	4104.,	12956.
10983,	-3012.,	4060.,	14303.
10991,	-3289.,	4337.,	5849.
10992,	-2193.,	4289.,	7320.
10993,	-1097.,	4241.,	8791.
11001,	1004.,	4148.,	11609.
11002,	2008.,	4104.,	12956.
11003,	3012.,	4060.,	14303.
11011,	3288.,	-4337.,	5849.
11012,	2192.,	-4289.,	7320.
11013,	1096.,	-4241.,	8791.
11021,	-1004.,	-4149.,	11609.
11022,	-2008.,	-4105.,	12956.
11023,	-3012.,	-4061.,	14303.
11031,	-3289.,	-4337.,	5849.
11032,	-2193.,	-4289.,	7320.
11033,	-1097.,	-4241.,	8791.
11041,	1004.,	-4149.,	11609.
11042,	2008.,	-4105.,	12956.
11043,	3012.,	-4061.,	14303.
21001 ,	6000 ,	6000 ,	-51000
21002 ,	6000 ,	6000 ,	-52000
21003 ,	6000 ,	6000 ,	-53000
21004 ,	6000 ,	6000 ,	-54000
21005 ,	6000 ,	6000 ,	-55000
21006 ,	6000 ,	6000 ,	-56000
21007 ,	6000 ,	6000 ,	-57000
21008 ,	6000 ,	6000 ,	-58000
21009 ,	6000 ,	6000 ,	-59000
21010 ,	6000 ,	6000 ,	-60000
21011 ,	6000 ,	6000 ,	-61000
21012 ,	6000 ,	6000 ,	-62000
21013 ,	6000 ,	6000 ,	-63000
21014 ,	6000 ,	6000 ,	-64000
21015 ,	6000 ,	6000 ,	-65000
21016 ,	6000 ,	6000 ,	-66000
21017 ,	6000 ,	6000 ,	-67000
21018 ,	6000 ,	6000 ,	-68000
21019 ,	6000 ,	6000 ,	-69000
21020 ,	6000 ,	6000 ,	-70000
21021 ,	6000 ,	6000 ,	-71000
21022 ,	6000 ,	6000 ,	-72000
21023 ,	6000 ,	6000 ,	-73000
21024 ,	6000 ,	6000 ,	-74000
21025 ,	6000 ,	6000 ,	-75000
21026 ,	6000 ,	6000 ,	-76000
21027 ,	6000 ,	6000 ,	-77000
21028 ,	6000 ,	6000 ,	-78000
21029 ,	6000 ,	6000 ,	-79000
21030 ,	6000 ,	6000 ,	-80000
21031 ,	6000 ,	6000 ,	-81000
21032 ,	6000 ,	6000 ,	-82000
21033 ,	6000 ,	6000 ,	-83000
21034 ,	6000 ,	6000 ,	-84000
21035 ,	6000 ,	6000 ,	-85000
21036 ,	6000 ,	6000 ,	-86000
21037 ,	6000 ,	6000 ,	-87000
21038 ,	6000 ,	6000 ,	-88000
21039 ,	6000 ,	6000 ,	-89000
21040 ,	6000 ,	6000 ,	-90000
21041 ,	6000 ,	6000 ,	-91000
21042 ,	6000 ,	6000 ,	-92000
21043 ,	6000 ,	6000 ,	-93000
21044 ,	6000 ,	6000 ,	-94000
21045 ,	6000 ,	6000 ,	-95000
21046 ,	6000 ,	6000 ,	-96000
21047 ,	6000 ,	6000 ,	-97000
21048 ,	6000 ,	6000 ,	-98000

21049	,	6000	,	6000	,	-99000
21050	,	6000	,	6000	,	-100000
22001	,	-6000	,	6000	,	-51000
22002	,	-6000	,	6000	,	-52000
22003	,	-6000	,	6000	,	-53000
22004	,	-6000	,	6000	,	-54000
22005	,	-6000	,	6000	,	-55000
22006	,	-6000	,	6000	,	-56000
22007	,	-6000	,	6000	,	-57000
22008	,	-6000	,	6000	,	-58000
22009	,	-6000	,	6000	,	-59000
22010	,	-6000	,	6000	,	-60000
22011	,	-6000	,	6000	,	-61000
22012	,	-6000	,	6000	,	-62000
22013	,	-6000	,	6000	,	-63000
22014	,	-6000	,	6000	,	-64000
22015	,	-6000	,	6000	,	-65000
22016	,	-6000	,	6000	,	-66000
22017	,	-6000	,	6000	,	-67000
22018	,	-6000	,	6000	,	-68000
22019	,	-6000	,	6000	,	-69000
22020	,	-6000	,	6000	,	-70000
22021	,	-6000	,	6000	,	-71000
22022	,	-6000	,	6000	,	-72000
22023	,	-6000	,	6000	,	-73000
22024	,	-6000	,	6000	,	-74000
22025	,	-6000	,	6000	,	-75000
22026	,	-6000	,	6000	,	-76000
22027	,	-6000	,	6000	,	-77000
22028	,	-6000	,	6000	,	-78000
22029	,	-6000	,	6000	,	-79000
22030	,	-6000	,	6000	,	-80000
22031	,	-6000	,	6000	,	-81000
22032	,	-6000	,	6000	,	-82000
22033	,	-6000	,	6000	,	-83000
22034	,	-6000	,	6000	,	-84000
22035	,	-6000	,	6000	,	-85000
22036	,	-6000	,	6000	,	-86000
22037	,	-6000	,	6000	,	-87000
22038	,	-6000	,	6000	,	-88000
22039	,	-6000	,	6000	,	-89000
22040	,	-6000	,	6000	,	-90000
22041	,	-6000	,	6000	,	-91000
22042	,	-6000	,	6000	,	-92000
22043	,	-6000	,	6000	,	-93000
22044	,	-6000	,	6000	,	-94000
22045	,	-6000	,	6000	,	-95000
22046	,	-6000	,	6000	,	-96000
22047	,	-6000	,	6000	,	-97000
22048	,	-6000	,	6000	,	-98000
22049	,	-6000	,	6000	,	-99000
22050	,	-6000	,	6000	,	-100000
23001	,	6000	,	-6000	,	-51000
23002	,	6000	,	-6000	,	-52000
23003	,	6000	,	-6000	,	-53000
23004	,	6000	,	-6000	,	-54000
23005	,	6000	,	-6000	,	-55000
23006	,	6000	,	-6000	,	-56000
23007	,	6000	,	-6000	,	-57000
23008	,	6000	,	-6000	,	-58000
23009	,	6000	,	-6000	,	-59000
23010	,	6000	,	-6000	,	-60000
23011	,	6000	,	-6000	,	-61000
23012	,	6000	,	-6000	,	-62000
23013	,	6000	,	-6000	,	-63000
23014	,	6000	,	-6000	,	-64000
23015	,	6000	,	-6000	,	-65000
23016	,	6000	,	-6000	,	-66000
23017	,	6000	,	-6000	,	-67000
23018	,	6000	,	-6000	,	-68000
23019	,	6000	,	-6000	,	-69000
23020	,	6000	,	-6000	,	-70000
23021	,	6000	,	-6000	,	-71000
23022	,	6000	,	-6000	,	-72000
23023	,	6000	,	-6000	,	-73000
23024	,	6000	,	-6000	,	-74000

23025	,	6000	,	-6000	,	-75000
23026	,	6000	,	-6000	,	-76000
23027	,	6000	,	-6000	,	-77000
23028	,	6000	,	-6000	,	-78000
23029	,	6000	,	-6000	,	-79000
23030	,	6000	,	-6000	,	-80000
23031	,	6000	,	-6000	,	-81000
23032	,	6000	,	-6000	,	-82000
23033	,	6000	,	-6000	,	-83000
23034	,	6000	,	-6000	,	-84000
23035	,	6000	,	-6000	,	-85000
23036	,	6000	,	-6000	,	-86000
23037	,	6000	,	-6000	,	-87000
23038	,	6000	,	-6000	,	-88000
23039	,	6000	,	-6000	,	-89000
23040	,	6000	,	-6000	,	-90000
23041	,	6000	,	-6000	,	-91000
23042	,	6000	,	-6000	,	-92000
23043	,	6000	,	-6000	,	-93000
23044	,	6000	,	-6000	,	-94000
23045	,	6000	,	-6000	,	-95000
23046	,	6000	,	-6000	,	-96000
23047	,	6000	,	-6000	,	-97000
23048	,	6000	,	-6000	,	-98000
23049	,	6000	,	-6000	,	-99000
23050	,	6000	,	-6000	,	-100000
24001	,	-6000	,	-6000	,	-51000
24002	,	-6000	,	-6000	,	-52000
24003	,	-6000	,	-6000	,	-53000
24004	,	-6000	,	-6000	,	-54000
24005	,	-6000	,	-6000	,	-55000
24006	,	-6000	,	-6000	,	-56000
24007	,	-6000	,	-6000	,	-57000
24008	,	-6000	,	-6000	,	-58000
24009	,	-6000	,	-6000	,	-59000
24010	,	-6000	,	-6000	,	-60000
24011	,	-6000	,	-6000	,	-61000
24012	,	-6000	,	-6000	,	-62000
24013	,	-6000	,	-6000	,	-63000
24014	,	-6000	,	-6000	,	-64000
24015	,	-6000	,	-6000	,	-65000
24016	,	-6000	,	-6000	,	-66000
24017	,	-6000	,	-6000	,	-67000
24018	,	-6000	,	-6000	,	-68000
24019	,	-6000	,	-6000	,	-69000
24020	,	-6000	,	-6000	,	-70000
24021	,	-6000	,	-6000	,	-71000
24022	,	-6000	,	-6000	,	-72000
24023	,	-6000	,	-6000	,	-73000
24024	,	-6000	,	-6000	,	-74000
24025	,	-6000	,	-6000	,	-75000
24026	,	-6000	,	-6000	,	-76000
24027	,	-6000	,	-6000	,	-77000
24028	,	-6000	,	-6000	,	-78000
24029	,	-6000	,	-6000	,	-79000
24030	,	-6000	,	-6000	,	-80000
24031	,	-6000	,	-6000	,	-81000
24032	,	-6000	,	-6000	,	-82000
24033	,	-6000	,	-6000	,	-83000
24034	,	-6000	,	-6000	,	-84000
24035	,	-6000	,	-6000	,	-85000
24036	,	-6000	,	-6000	,	-86000
24037	,	-6000	,	-6000	,	-87000
24038	,	-6000	,	-6000	,	-88000
24039	,	-6000	,	-6000	,	-89000
24040	,	-6000	,	-6000	,	-90000
24041	,	-6000	,	-6000	,	-91000
24042	,	-6000	,	-6000	,	-92000
24043	,	-6000	,	-6000	,	-93000
24044	,	-6000	,	-6000	,	-94000
24045	,	-6000	,	-6000	,	-95000
24046	,	-6000	,	-6000	,	-96000
24047	,	-6000	,	-6000	,	-97000
24048	,	-6000	,	-6000	,	-98000
24049	,	-6000	,	-6000	,	-99000
24050	,	-6000	,	-6000	,	-100000

```

*Element, type=B31
1001, 63, 1001
1011, 1001, 1011
1021, 1011, 1021
1031, 1021, 1031
1041, 1031, 1041
1051, 1041, 1051
1061, 1051, 1061
1071, 1061, 1071
10010, 1, 2
10020, 2, 3
10030, 3, 4
10050, 6, 7
10060, 7, 8
10070, 8, 9
10041, 4, 10041
10042, 10041, 10042
10043, 10042, 10043
10044, 10043, 10044
10045, 10044, 10045
10046, 10045, 10046
10047, 10046, 10047
10048, 10047, 5
10081, 9, 10081
10082, 10081, 10082
10083, 10082, 10083
10084, 10083, 10084
10085, 10084, 10085
10086, 10085, 10086
10087, 10086, 10087
10088, 10087, 10
10090, 11, 12
10100, 12, 13
10110, 13, 14
10121, 14, 10121
10122, 10121, 10122
10123, 10122, 10123
10124, 10123, 10124
10125, 10124, 10125
10126, 10125, 10126
10127, 10126, 10127
10128, 10127, 15
10130, 16, 17
10140, 17, 18
10150, 18, 19
10161, 19, 10161
10162, 10161, 10162
10163, 10162, 10163
10164, 10163, 10164
10165, 10164, 10165
10166, 10165, 10166
10167, 10166, 10167
10168, 10167, 20
10171, 5, 10171
10172, 10171, 10172
10173, 10172, 10173
10174, 10173, 10174
10175, 10174, 10175
10176, 10175, 10176
10177, 10176, 10177
10178, 10177, 21
10181, 21, 10181
10182, 10181, 10182
10183, 10182, 10183
10184, 10183, 10184
10185, 10184, 10185
10186, 10185, 10186
10187, 10186, 10187
10188, 10187, 22
10191, 22, 10191
10192, 10191, 10192
10193, 10192, 10193
10194, 10193, 10194
10195, 10194, 10195
10196, 10195, 10196
10197, 10196, 10197

```

10198, 10197, 23  
10200, 23, 24  
10211, 10, 10211  
10212, 10211, 10212  
10213, 10212, 10213  
10214, 10213, 10214  
10215, 10214, 10215  
10216, 10215, 10216  
10217, 10216, 10217  
10218, 10217, 25  
10221, 25, 10221  
10222, 10221, 10222  
10223, 10222, 10223  
10224, 10223, 10224  
10225, 10224, 10225  
10226, 10225, 10226  
10227, 10226, 10227  
10228, 10227, 26  
10231, 26, 10231  
10232, 10231, 10232  
10233, 10232, 10233  
10234, 10233, 10234  
10235, 10234, 10235  
10236, 10235, 10236  
10237, 10236, 10237  
10238, 10237, 27  
10240, 27, 28  
10251, 15, 10251  
10252, 10251, 10252  
10253, 10252, 10253  
10254, 10253, 10254  
10255, 10254, 10255  
10256, 10255, 10256  
10257, 10256, 10257  
10258, 10257, 29  
10261, 29, 10261  
10262, 10261, 10262  
10263, 10262, 10263  
10264, 10263, 10264  
10265, 10264, 10265  
10266, 10265, 10266  
10267, 10266, 10267  
10268, 10267, 30  
10271, 30, 10271  
10272, 10271, 10272  
10273, 10272, 10273  
10274, 10273, 10274  
10275, 10274, 10275  
10276, 10275, 10276  
10277, 10276, 10277  
10278, 10277, 31  
10280, 31, 32  
10291, 20, 10291  
10292, 10291, 10292  
10293, 10292, 10293  
10294, 10293, 10294  
10295, 10294, 10295  
10296, 10295, 10296  
10297, 10296, 10297  
10298, 10297, 33  
10301, 33, 10301  
10302, 10301, 10302  
10303, 10302, 10303  
10304, 10303, 10304  
10305, 10304, 10305  
10306, 10305, 10306  
10307, 10306, 10307  
10308, 10307, 34  
10311, 34, 10311  
10312, 10311, 10312  
10313, 10312, 10313  
10314, 10313, 10314  
10315, 10314, 10315  
10316, 10315, 10316  
10317, 10316, 10317  
10318, 10317, 35

10320, 35, 36  
10371, 3, 10371  
10372, 10371, 10372  
10373, 10372, 10373  
10374, 10373, 10374  
10375, 10374, 10375  
10376, 10375, 10376  
10377, 10376, 10377  
10378, 10377, 8  
10381, 8, 10381  
10382, 10381, 10382  
10383, 10382, 10383  
10384, 10383, 10384  
10385, 10384, 10385  
10386, 10385, 10386  
10387, 10386, 10387  
10388, 10387, 13  
10391, 13, 10391  
10392, 10391, 10392  
10393, 10392, 10393  
10394, 10393, 10394  
10395, 10394, 10395  
10396, 10395, 10396  
10397, 10396, 10397  
10398, 10397, 18  
10401, 18, 10401  
10402, 10401, 10402  
10403, 10402, 10403  
10404, 10403, 10404  
10405, 10404, 10405  
10406, 10405, 10406  
10407, 10406, 10407  
10408, 10407, 3  
10411, 4, 10411  
10412, 10411, 10412  
10413, 10412, 10413  
10414, 10413, 41  
10421, 41, 10421  
10422, 10421, 10422  
10423, 10422, 10423  
10424, 10423, 20  
10431, 19, 10431  
10432, 10431, 10432  
10433, 10432, 10433  
10434, 10433, 41  
10441, 41, 10441  
10442, 10441, 10442  
10443, 10442, 10443  
10444, 10443, 5  
10451, 9, 10451  
10452, 10451, 10452  
10453, 10452, 10453  
10454, 10453, 42  
10461, 42, 10461  
10462, 10461, 10462  
10463, 10462, 10463  
10464, 10463, 15  
10471, 14, 10471  
10472, 10471, 10472  
10473, 10472, 10473  
10474, 10473, 42  
10481, 42, 10481  
10482, 10481, 10482  
10483, 10482, 10483  
10484, 10483, 10  
10491, 4, 10491  
10492, 10491, 10492  
10493, 10492, 10493  
10494, 10493, 43  
10501, 43, 10501  
10502, 10501, 10502  
10503, 10502, 10503  
10504, 10503, 10  
10511, 9, 10511  
10512, 10511, 10512  
10513, 10512, 10513

10514, 10513, 43  
10521, 43, 10521  
10522, 10521, 10522  
10523, 10522, 10523  
10524, 10523, 5  
10531, 19, 10531  
10532, 10531, 10532  
10533, 10532, 10533  
10534, 10533, 44  
10541, 44, 10541  
10542, 10541, 10542  
10543, 10542, 10543  
10544, 10543, 15  
10551, 14, 10551  
10552, 10551, 10552  
10553, 10552, 10553  
10554, 10553, 44  
10561, 44, 10561  
10562, 10561, 10562  
10563, 10562, 10563  
10564, 10563, 20  
10571, 5, 10571  
10572, 10571, 10572  
10573, 10572, 10573  
10574, 10573, 45  
10581, 45, 10581  
10582, 10581, 10582  
10583, 10582, 10583  
10584, 10583, 33  
10591, 20, 10591  
10592, 10591, 10592  
10593, 10592, 10593  
10594, 10593, 45  
10601, 45, 10601  
10602, 10601, 10602  
10603, 10602, 10603  
10604, 10603, 21  
10611, 10, 10611  
10612, 10611, 10612  
10613, 10612, 10613  
10614, 10613, 46  
10621, 46, 10621  
10622, 10621, 10622  
10623, 10622, 10623  
10624, 10623, 29  
10631, 15, 10631  
10632, 10631, 10632  
10633, 10632, 10633  
10634, 10633, 46  
10641, 46, 10641  
10642, 10641, 10642  
10643, 10642, 10643  
10644, 10643, 25  
10651, 5, 10651  
10652, 10651, 10652  
10653, 10652, 10653  
10654, 10653, 47  
10661, 47, 10661  
10662, 10661, 10662  
10663, 10662, 10663  
10664, 10663, 25  
10671, 10, 10671  
10672, 10671, 10672  
10673, 10672, 10673  
10674, 10673, 47  
10681, 47, 10681  
10682, 10681, 10682  
10683, 10682, 10683  
10684, 10683, 21  
10691, 20, 10691  
10692, 10691, 10692  
10693, 10692, 10693  
10694, 10693, 48  
10701, 48, 10701  
10702, 10701, 10702  
10703, 10702, 10703

10704, 10703, 29  
10711, 15, 10711  
10712, 10711, 10712  
10713, 10712, 10713  
10714, 10713, 48  
10721, 48, 10721  
10722, 10721, 10722  
10723, 10722, 10723  
10724, 10723, 33  
10731, 21, 10731  
10732, 10731, 10732  
10733, 10732, 10733  
10734, 10733, 49  
10741, 49, 10741  
10742, 10741, 10742  
10743, 10742, 10743  
10744, 10743, 34  
10751, 33, 10751  
10752, 10751, 10752  
10753, 10752, 10753  
10754, 10753, 49  
10761, 49, 10761  
10762, 10761, 10762  
10763, 10762, 10763  
10764, 10763, 22  
10771, 25, 10771  
10772, 10771, 10772  
10773, 10772, 10773  
10774, 10773, 50  
10781, 50, 10781  
10782, 10781, 10782  
10783, 10782, 10783  
10784, 10783, 30  
10791, 29, 10791  
10792, 10791, 10792  
10793, 10792, 10793  
10794, 10793, 50  
10801, 50, 10801  
10802, 10801, 10802  
10803, 10802, 10803  
10804, 10803, 26  
10811, 21, 10811  
10812, 10811, 10812  
10813, 10812, 10813  
10814, 10813, 51  
10821, 51, 10821  
10822, 10821, 10822  
10823, 10822, 10823  
10824, 10823, 26  
10831, 25, 10831  
10832, 10831, 10832  
10833, 10832, 10833  
10834, 10833, 51  
10841, 51, 10841  
10842, 10841, 10842  
10843, 10842, 10843  
10844, 10843, 22  
10851, 33, 10851  
10852, 10851, 10852  
10853, 10852, 10853  
10854, 10853, 52  
10861, 52, 10861  
10862, 10861, 10862  
10863, 10862, 10863  
10864, 10863, 30  
10871, 29, 10871  
10872, 10871, 10872  
10873, 10872, 10873  
10874, 10873, 52  
10881, 52, 10881  
10882, 10881, 10882  
10883, 10882, 10883  
10884, 10883, 34  
10891, 22, 10891  
10892, 10891, 10892  
10893, 10892, 10893



10894, 10893, 53  
10901, 53, 10901  
10902, 10901, 10902  
10903, 10902, 10903  
10904, 10903, 35  
10911, 34, 10911  
10912, 10911, 10912  
10913, 10912, 10913  
10914, 10913, 53  
10921, 53, 10921  
10922, 10921, 10922  
10923, 10922, 10923  
10924, 10923, 23  
10931, 26, 10931  
10932, 10931, 10932  
10933, 10932, 10933  
10934, 10933, 54  
10941, 54, 10941  
10942, 10941, 10942  
10943, 10942, 10943  
10944, 10943, 31  
10951, 30, 10951  
10952, 10951, 10952  
10953, 10952, 10953  
10954, 10953, 54  
10961, 54, 10961  
10962, 10961, 10962  
10963, 10962, 10963  
10964, 10963, 27  
10971, 22, 10971  
10972, 10971, 10972  
10973, 10972, 10973  
10974, 10973, 55  
10981, 55, 10981  
10982, 10981, 10982  
10983, 10982, 10983  
10984, 10983, 27  
10991, 26, 10991  
10992, 10991, 10992  
10993, 10992, 10993  
10994, 10993, 55  
11001, 55, 11001  
11002, 11001, 11002  
11003, 11002, 11003  
11004, 11003, 23  
11011, 34, 11011  
11012, 11011, 11012  
11013, 11012, 11013  
11014, 11013, 56  
11021, 56, 11021  
11022, 11021, 11022  
11023, 11022, 11023  
11024, 11023, 31  
11031, 30, 11031  
11032, 11031, 11032  
11033, 11032, 11033  
11034, 11033, 56  
11041, 56, 11041  
11042, 11041, 11042  
11043, 11042, 11043  
11044, 11043, 35  
11050, 24, 57  
11060, 28, 58  
11070, 32, 60  
11080, 36, 59  
20001, 61, 62  
20002, 62, 63,  
21001, 1, 21001  
21002, 21001, 21002  
21003, 21002, 21003  
21004, 21003, 21004  
21005, 21004, 21005  
21006, 21005, 21006  
21007, 21006, 21007  
21008, 21007, 21008  
21009, 21008, 21009

21010, 21009, 21010  
21011, 21010, 21011  
21012, 21011, 21012  
21013, 21012, 21013  
21014, 21013, 21014  
21015, 21014, 21015  
21016, 21015, 21016  
21017, 21016, 21017  
21018, 21017, 21018  
21019, 21018, 21019  
21020, 21019, 21020  
21021, 21020, 21021  
21022, 21021, 21022  
21023, 21022, 21023  
21024, 21023, 21024  
21025, 21024, 21025  
21026, 21025, 21026  
21027, 21026, 21027  
21028, 21027, 21028  
21029, 21028, 21029  
21030, 21029, 21030  
21031, 21030, 21031  
21032, 21031, 21032  
21033, 21032, 21033  
21034, 21033, 21034  
21035, 21034, 21035  
21036, 21035, 21036  
21037, 21036, 21037  
21038, 21037, 21038  
21039, 21038, 21039  
21040, 21039, 21040  
21041, 21040, 21041  
21042, 21041, 21042  
21043, 21042, 21043  
21044, 21043, 21044  
21045, 21044, 21045  
21046, 21045, 21046  
21047, 21046, 21047  
21048, 21047, 21048  
21049, 21048, 21049  
21050, 21049, 21050  
22001, 6, 22001  
22002, 22001, 22002  
22003, 22002, 22003  
22004, 22003, 22004  
22005, 22004, 22005  
22006, 22005, 22006  
22007, 22006, 22007  
22008, 22007, 22008  
22009, 22008, 22009  
22010, 22009, 22010  
22011, 22010, 22011  
22012, 22011, 22012  
22013, 22012, 22013  
22014, 22013, 22014  
22015, 22014, 22015  
22016, 22015, 22016  
22017, 22016, 22017  
22018, 22017, 22018  
22019, 22018, 22019  
22020, 22019, 22020  
22021, 22020, 22021  
22022, 22021, 22022  
22023, 22022, 22023  
22024, 22023, 22024  
22025, 22024, 22025  
22026, 22025, 22026  
22027, 22026, 22027  
22028, 22027, 22028  
22029, 22028, 22029  
22030, 22029, 22030  
22031, 22030, 22031  
22032, 22031, 22032  
22033, 22032, 22033  
22034, 22033, 22034  
22035, 22034, 22035

22036, 22035, 22036  
22037, 22036, 22037  
22038, 22037, 22038  
22039, 22038, 22039  
22040, 22039, 22040  
22041, 22040, 22041  
22042, 22041, 22042  
22043, 22042, 22043  
22044, 22043, 22044  
22045, 22044, 22045  
22046, 22045, 22046  
22047, 22046, 22047  
22048, 22047, 22048  
22049, 22048, 22049  
22050, 22049, 22050  
23001, 16, 23001  
23002, 23001, 23002  
23003, 23002, 23003  
23004, 23003, 23004  
23005, 23004, 23005  
23006, 23005, 23006  
23007, 23006, 23007  
23008, 23007, 23008  
23009, 23008, 23009  
23010, 23009, 23010  
23011, 23010, 23011  
23012, 23011, 23012  
23013, 23012, 23013  
23014, 23013, 23014  
23015, 23014, 23015  
23016, 23015, 23016  
23017, 23016, 23017  
23018, 23017, 23018  
23019, 23018, 23019  
23020, 23019, 23020  
23021, 23020, 23021  
23022, 23021, 23022  
23023, 23022, 23023  
23024, 23023, 23024  
23025, 23024, 23025  
23026, 23025, 23026  
23027, 23026, 23027  
23028, 23027, 23028  
23029, 23028, 23029  
23030, 23029, 23030  
23031, 23030, 23031  
23032, 23031, 23032  
23033, 23032, 23033  
23034, 23033, 23034  
23035, 23034, 23035  
23036, 23035, 23036  
23037, 23036, 23037  
23038, 23037, 23038  
23039, 23038, 23039  
23040, 23039, 23040  
23041, 23040, 23041  
23042, 23041, 23042  
23043, 23042, 23043  
23044, 23043, 23044  
23045, 23044, 23045  
23046, 23045, 23046  
23047, 23046, 23047  
23048, 23047, 23048  
23049, 23048, 23049  
23050, 23049, 23050  
24001, 11, 24001  
24002, 24001, 24002  
24003, 24002, 24003  
24004, 24003, 24004  
24005, 24004, 24005  
24006, 24005, 24006  
24007, 24006, 24007  
24008, 24007, 24008  
24009, 24008, 24009  
24010, 24009, 24010  
24011, 24010, 24011

```

24012, 24011, 24012
24013, 24012, 24013
24014, 24013, 24014
24015, 24014, 24015
24016, 24015, 24016
24017, 24016, 24017
24018, 24017, 24018
24019, 24018, 24019
24020, 24019, 24020
24021, 24020, 24021
24022, 24021, 24022
24023, 24022, 24023
24024, 24023, 24024
24025, 24024, 24025
24026, 24025, 24026
24027, 24026, 24027
24028, 24027, 24028
24029, 24028, 24029
24030, 24029, 24030
24031, 24030, 24031
24032, 24031, 24032
24033, 24032, 24033
24034, 24033, 24034
24035, 24034, 24035
24036, 24035, 24036
24037, 24036, 24037
24038, 24037, 24038
24039, 24038, 24039
24040, 24039, 24040
24041, 24040, 24041
24042, 24041, 24042
24043, 24042, 24043
24044, 24043, 24044
24045, 24044, 24045
24046, 24045, 24046
24047, 24046, 24047
24048, 24047, 24048
24049, 24048, 24049
24050, 24049, 24050
*Element, TYPE=SPRING1, ELSET=SPR_xdir1
31001, 21001
32001, 22001
33001, 23001
34001, 24001
*Element, TYPE=SPRING1, ELSET=SPR_xdir2
31002, 21002
32002, 22002
33002, 23002
34002, 24002
*Element, TYPE=SPRING1, ELSET=SPR_xdir3
31003, 21003
32003, 22003
33003, 23003
34003, 24003
*Element, TYPE=SPRING1, ELSET=SPR_xdir4
31004, 21004
32004, 22004
33004, 23004
34004, 24004
*Element, TYPE=SPRING1, ELSET=SPR_xdir5
31005, 21005
32005, 22005
33005, 23005
34005, 24005
*Element, TYPE=SPRING1, ELSET=SPR_xdir6
31006, 21006
32006, 22006
33006, 23006
34006, 24006
*Element, TYPE=SPRING1, ELSET=SPR_xdir7
31007, 21007
32007, 22007
33007, 23007
34007, 24007
*Element, TYPE=SPRING1, ELSET=SPR_xdir8
31008, 21008

```

```

32008, 22008
33008, 23008
34008, 24008
*Element, TYPE=SPRING1, ELSET=SPR_xdir9
31009, 21009
32009, 22009
33009, 23009
34009, 24009
*Element, TYPE=SPRING1, ELSET=SPR_xdir10
31010, 21010
32010, 22010
33010, 23010
34010, 24010
*Element, TYPE=SPRING1, ELSET=SPR_xdir11
31011, 21011
32011, 22011
33011, 23011
34011, 24011
*Element, TYPE=SPRING1, ELSET=SPR_xdir12
31012, 21012
32012, 22012
33012, 23012
34012, 24012
*Element, TYPE=SPRING1, ELSET=SPR_xdir13
31013, 21013
32013, 22013
33013, 23013
34013, 24013
*Element, TYPE=SPRING1, ELSET=SPR_xdir14
31014, 21014
32014, 22014
33014, 23014
34014, 24014
*Element, TYPE=SPRING1, ELSET=SPR_xdir15
31015, 21015
32015, 22015
33015, 23015
34015, 24015
*Element, TYPE=SPRING1, ELSET=SPR_xdir16
31016, 21016
32016, 22016
33016, 23016
34016, 24016
*Element, TYPE=SPRING1, ELSET=SPR_xdir17
31017, 21017
32017, 22017
33017, 23017
34017, 24017
*Element, TYPE=SPRING1, ELSET=SPR_xdir18
31018, 21018
32018, 22018
33018, 23018
34018, 24018
*Element, TYPE=SPRING1, ELSET=SPR_xdir19
31019, 21019
32019, 22019
33019, 23019
34019, 24019
*Element, TYPE=SPRING1, ELSET=SPR_xdir20
31020, 21020
32020, 22020
33020, 23020
34020, 24020
*Element, TYPE=SPRING1, ELSET=SPR_xdir21
31021, 21021
32021, 22021
33021, 23021
34021, 24021
*Element, TYPE=SPRING1, ELSET=SPR_xdir22
31022, 21022
32022, 22022
33022, 23022
34022, 24022
*Element, TYPE=SPRING1, ELSET=SPR_xdir23
31023, 21023
32023, 22023

```

33023, 23023  
34023, 24023  
\*Element, TYPE=SPRING1, ELSET=SPR\_xdir24  
31024, 21024  
32024, 22024  
33024, 23024  
34024, 24024  
\*Element, TYPE=SPRING1, ELSET=SPR\_xdir25  
31025, 21025  
32025, 22025  
33025, 23025  
34025, 24025  
\*Element, TYPE=SPRING1, ELSET=SPR\_xdir26  
31026, 21026  
32026, 22026  
33026, 23026  
34026, 24026  
\*Element, TYPE=SPRING1, ELSET=SPR\_xdir27  
31027, 21027  
32027, 22027  
33027, 23027  
34027, 24027  
\*Element, TYPE=SPRING1, ELSET=SPR\_xdir28  
31028, 21028  
32028, 22028  
33028, 23028  
34028, 24028  
\*Element, TYPE=SPRING1, ELSET=SPR\_xdir29  
31029, 21029  
32029, 22029  
33029, 23029  
34029, 24029  
\*Element, TYPE=SPRING1, ELSET=SPR\_xdir30  
31030, 21030  
32030, 22030  
33030, 23030  
34030, 24030  
\*Element, TYPE=SPRING1, ELSET=SPR\_xdir31  
31031, 21031  
32031, 22031  
33031, 23031  
34031, 24031  
\*Element, TYPE=SPRING1, ELSET=SPR\_xdir32  
31032, 21032  
32032, 22032  
33032, 23032  
34032, 24032  
\*Element, TYPE=SPRING1, ELSET=SPR\_xdir33  
31033, 21033  
32033, 22033  
33033, 23033  
34033, 24033  
\*Element, TYPE=SPRING1, ELSET=SPR\_xdir34  
31034, 21034  
32034, 22034  
33034, 23034  
34034, 24034  
\*Element, TYPE=SPRING1, ELSET=SPR\_xdir35  
31035, 21035  
32035, 22035  
33035, 23035  
34035, 24035  
\*Element, TYPE=SPRING1, ELSET=SPR\_xdir36  
31036, 21036  
32036, 22036  
33036, 23036  
34036, 24036  
\*Element, TYPE=SPRING1, ELSET=SPR\_xdir37  
31037, 21037  
32037, 22037  
33037, 23037  
34037, 24037  
\*Element, TYPE=SPRING1, ELSET=SPR\_xdir38  
31038, 21038  
32038, 22038  
33038, 23038

```

34038, 24038
*Element, TYPE=SPRING1, ELSET=SPR_xdir39
31039, 21039
32039, 22039
33039, 23039
34039, 24039
*Element, TYPE=SPRING1, ELSET=SPR_xdir40
31040, 21040
32040, 22040
33040, 23040
34040, 24040
*Element, TYPE=SPRING1, ELSET=SPR_xdir41
31041, 21041
32041, 22041
33041, 23041
34041, 24041
*Element, TYPE=SPRING1, ELSET=SPR_xdir42
31042, 21042
32042, 22042
33042, 23042
34042, 24042
*Element, TYPE=SPRING1, ELSET=SPR_xdir43
31043, 21043
32043, 22043
33043, 23043
34043, 24043
*Element, TYPE=SPRING1, ELSET=SPR_xdir44
31044, 21044
32044, 22044
33044, 23044
34044, 24044
*Element, TYPE=SPRING1, ELSET=SPR_xdir45
31045, 21045
32045, 22045
33045, 23045
34045, 24045
*Element, TYPE=SPRING1, ELSET=SPR_xdir46
31046, 21046
32046, 22046
33046, 23046
34046, 24046
*Element, TYPE=SPRING1, ELSET=SPR_xdir47
31047, 21047
32047, 22047
33047, 23047
34047, 24047
*Element, TYPE=SPRING1, ELSET=SPR_xdir48
31048, 21048
32048, 22048
33048, 23048
34048, 24048
*Element, TYPE=SPRING1, ELSET=SPR_xdir49
31049, 21049
32049, 22049
33049, 23049
34049, 24049
*Element, TYPE=SPRING1, ELSET=SPR_xdir50
31050, 21050
32050, 22050
33050, 23050
34050, 24050
*Element, TYPE=SPRING1, ELSET=SPR_ydir1
41001, 21001
42001, 22001
43001, 23001
44001, 24001
*Element, TYPE=SPRING1, ELSET=SPR_ydir2
41002, 21002
42002, 22002
43002, 23002
44002, 24002
*Element, TYPE=SPRING1, ELSET=SPR_ydir3
41003, 21003
42003, 22003
43003, 23003
44003, 24003

```

```

*Element, TYPE=SPRING1, ELSET=SPR_ydir4
41004, 21004
42004, 22004
43004, 23004
44004, 24004
*Element, TYPE=SPRING1, ELSET=SPR_ydir5
41005, 21005
42005, 22005
43005, 23005
44005, 24005
*Element, TYPE=SPRING1, ELSET=SPR_ydir6
41006, 21006
42006, 22006
43006, 23006
44006, 24006
*Element, TYPE=SPRING1, ELSET=SPR_ydir7
41007, 21007
42007, 22007
43007, 23007
44007, 24007
*Element, TYPE=SPRING1, ELSET=SPR_ydir8
41008, 21008
42008, 22008
43008, 23008
44008, 24008
*Element, TYPE=SPRING1, ELSET=SPR_ydir9
41009, 21009
42009, 22009
43009, 23009
44009, 24009
*Element, TYPE=SPRING1, ELSET=SPR_ydir10
41010, 21010
42010, 22010
43010, 23010
44010, 24010
*Element, TYPE=SPRING1, ELSET=SPR_ydir11
41011, 21011
42011, 22011
43011, 23011
44011, 24011
*Element, TYPE=SPRING1, ELSET=SPR_ydir12
41012, 21012
42012, 22012
43012, 23012
44012, 24012
*Element, TYPE=SPRING1, ELSET=SPR_ydir13
41013, 21013
42013, 22013
43013, 23013
44013, 24013
*Element, TYPE=SPRING1, ELSET=SPR_ydir14
41014, 21014
42014, 22014
43014, 23014
44014, 24014
*Element, TYPE=SPRING1, ELSET=SPR_ydir15
41015, 21015
42015, 22015
43015, 23015
44015, 24015
*Element, TYPE=SPRING1, ELSET=SPR_ydir16
41016, 21016
42016, 22016
43016, 23016
44016, 24016
*Element, TYPE=SPRING1, ELSET=SPR_ydir17
41017, 21017
42017, 22017
43017, 23017
44017, 24017
*Element, TYPE=SPRING1, ELSET=SPR_ydir18
41018, 21018
42018, 22018
43018, 23018
44018, 24018
*Element, TYPE=SPRING1, ELSET=SPR_ydir19

```



41019, 21019  
42019, 22019  
43019, 23019  
44019, 24019  
\*Element, TYPE=SPRING1, ELSET=SPR\_ydir20  
41020, 21020  
42020, 22020  
43020, 23020  
44020, 24020  
\*Element, TYPE=SPRING1, ELSET=SPR\_ydir21  
41021, 21021  
42021, 22021  
43021, 23021  
44021, 24021  
\*Element, TYPE=SPRING1, ELSET=SPR\_ydir22  
41022, 21022  
42022, 22022  
43022, 23022  
44022, 24022  
\*Element, TYPE=SPRING1, ELSET=SPR\_ydir23  
41023, 21023  
42023, 22023  
43023, 23023  
44023, 24023  
\*Element, TYPE=SPRING1, ELSET=SPR\_ydir24  
41024, 21024  
42024, 22024  
43024, 23024  
44024, 24024  
\*Element, TYPE=SPRING1, ELSET=SPR\_ydir25  
41025, 21025  
42025, 22025  
43025, 23025  
44025, 24025  
\*Element, TYPE=SPRING1, ELSET=SPR\_ydir26  
41026, 21026  
42026, 22026  
43026, 23026  
44026, 24026  
\*Element, TYPE=SPRING1, ELSET=SPR\_ydir27  
41027, 21027  
42027, 22027  
43027, 23027  
44027, 24027  
\*Element, TYPE=SPRING1, ELSET=SPR\_ydir28  
41028, 21028  
42028, 22028  
43028, 23028  
44028, 24028  
\*Element, TYPE=SPRING1, ELSET=SPR\_ydir29  
41029, 21029  
42029, 22029  
43029, 23029  
44029, 24029  
\*Element, TYPE=SPRING1, ELSET=SPR\_ydir30  
41030, 21030  
42030, 22030  
43030, 23030  
44030, 24030  
\*Element, TYPE=SPRING1, ELSET=SPR\_ydir31  
41031, 21031  
42031, 22031  
43031, 23031  
44031, 24031  
\*Element, TYPE=SPRING1, ELSET=SPR\_ydir32  
41032, 21032  
42032, 22032  
43032, 23032  
44032, 24032  
\*Element, TYPE=SPRING1, ELSET=SPR\_ydir33  
41033, 21033  
42033, 22033  
43033, 23033  
44033, 24033  
\*Element, TYPE=SPRING1, ELSET=SPR\_ydir34  
41034, 21034

42034, 22034  
43034, 23034  
44034, 24034  
\*Element, TYPE=SPRING1, ELSET=SPR\_ydir35  
41035, 21035  
42035, 22035  
43035, 23035  
44035, 24035  
\*Element, TYPE=SPRING1, ELSET=SPR\_ydir36  
41036, 21036  
42036, 22036  
43036, 23036  
44036, 24036  
\*Element, TYPE=SPRING1, ELSET=SPR\_ydir37  
41037, 21037  
42037, 22037  
43037, 23037  
44037, 24037  
\*Element, TYPE=SPRING1, ELSET=SPR\_ydir38  
41038, 21038  
42038, 22038  
43038, 23038  
44038, 24038  
\*Element, TYPE=SPRING1, ELSET=SPR\_ydir39  
41039, 21039  
42039, 22039  
43039, 23039  
44039, 24039  
\*Element, TYPE=SPRING1, ELSET=SPR\_ydir40  
41040, 21040  
42040, 22040  
43040, 23040  
44040, 24040  
\*Element, TYPE=SPRING1, ELSET=SPR\_ydir41  
41041, 21041  
42041, 22041  
43041, 23041  
44041, 24041  
\*Element, TYPE=SPRING1, ELSET=SPR\_ydir42  
41042, 21042  
42042, 22042  
43042, 23042  
44042, 24042  
\*Element, TYPE=SPRING1, ELSET=SPR\_ydir43  
41043, 21043  
42043, 22043  
43043, 23043  
44043, 24043  
\*Element, TYPE=SPRING1, ELSET=SPR\_ydir44  
41044, 21044  
42044, 22044  
43044, 23044  
44044, 24044  
\*Element, TYPE=SPRING1, ELSET=SPR\_ydir45  
41045, 21045  
42045, 22045  
43045, 23045  
44045, 24045  
\*Element, TYPE=SPRING1, ELSET=SPR\_ydir46  
41046, 21046  
42046, 22046  
43046, 23046  
44046, 24046  
\*Element, TYPE=SPRING1, ELSET=SPR\_ydir47  
41047, 21047  
42047, 22047  
43047, 23047  
44047, 24047  
\*Element, TYPE=SPRING1, ELSET=SPR\_ydir48  
41048, 21048  
42048, 22048  
43048, 23048  
44048, 24048  
\*Element, TYPE=SPRING1, ELSET=SPR\_ydir49  
41049, 21049  
42049, 22049

```

43049, 23049
44049, 24049
*Element, TYPE=SPRING1, ELSET=SPR_ydir50
41050, 21050
42050, 22050
43050, 23050
44050, 24050
*Elset, elset=TP_BEAM
20001, 20002
*Elset, elset=BEAM1
10371, 10372, 10373, 10374, 10375, 10376, 10377, 10378
10381, 10382, 10383, 10384, 10385, 10386, 10387, 10388
10391, 10392, 10393, 10394, 10395, 10396, 10397, 10398
10401, 10402, 10403, 10404, 10405, 10406, 10407, 10408
10411, 10412, 10413, 10414, 10421, 10422, 10423, 10424
10431, 10432, 10433, 10434, 10441, 10442, 10443, 10444
10451, 10452, 10453, 10454, 10461, 10462, 10463, 10464
10471, 10472, 10473, 10474, 10481, 10482, 10483, 10484
10491, 10492, 10493, 10494, 10501, 10502, 10503, 10504
10511, 10512, 10513, 10514, 10521, 10522, 10523, 10524
10531, 10532, 10533, 10534, 10541, 10542, 10543, 10544
10551, 10552, 10553, 10554, 10561, 10562, 10563, 10564
10571, 10572, 10573, 10574, 10581, 10582, 10583, 10584
10591, 10592, 10593, 10594, 10601, 10602, 10603, 10604
10611, 10612, 10613, 10614, 10621, 10622, 10623, 10624
10631, 10632, 10633, 10634, 10641, 10642, 10643, 10644
10651, 10652, 10653, 10654, 10661, 10662, 10663, 10664
10671, 10672, 10673, 10674, 10681, 10682, 10683, 10684
10691, 10692, 10693, 10694, 10701, 10702, 10703, 10704
10711, 10712, 10713, 10714, 10721, 10722, 10723, 10724
10731, 10732, 10733, 10734, 10741, 10742, 10743, 10744
10751, 10752, 10753, 10754, 10761, 10762, 10763, 10764
10771, 10772, 10773, 10774, 10781, 10782, 10783, 10784
10791, 10792, 10793, 10794, 10801, 10802, 10803, 10804
10811, 10812, 10813, 10814, 10821, 10822, 10823, 10824
10831, 10832, 10833, 10834, 10841, 10842, 10843, 10844
10851, 10852, 10853, 10854, 10861, 10862, 10863, 10864
10871, 10872, 10873, 10874, 10881, 10882, 10883, 10884
10891, 10892, 10893, 10894, 10901, 10902, 10903, 10904
10911, 10912, 10913, 10914, 10921, 10922, 10923, 10924
10931, 10932, 10933, 10934, 10941, 10942, 10943, 10944
10951, 10952, 10953, 10954, 10961, 10962, 10963, 10964
10971, 10972, 10973, 10974, 10981, 10982, 10983, 10984
10991, 10992, 10993, 10994, 11001, 11002, 11003, 11004
11011, 11012, 11013, 11014, 11021, 11022, 11023, 11024
11031, 11032, 11033, 11034, 11041, 11042, 11043, 11044
*Elset, elset=BEAM2
10020, 10030, 10060, 10070, 10081, 10082, 10083, 10084
10085, 10086, 10087, 10088, 10100, 10110, 10121
10122, 10123, 10124, 10125, 10126, 10127, 10128, 10140
10150, 10161, 10162, 10163, 10164, 10165, 10166, 10167
10168, 10041, 10042, 10043, 10044, 10045, 10046, 10047
10048
*Elset, elset=BEAM3
10171, 10172, 10173, 10174, 10175, 10176, 10177, 10178
10181, 10182, 10183, 10184, 10185, 10186, 10187, 10188
10191, 10192, 10193, 10194, 10195, 10196, 10197, 10198
10200, 10211, 10212, 10213, 10214, 10215, 10216, 10217
10218, 10221, 10222, 10223, 10224, 10225, 10226, 10227
10228, 10231, 10232, 10233, 10234, 10235, 10236, 10237
10238, 10240, 10251, 10252, 10253, 10254, 10255, 10256
10257, 10258, 10261, 10262, 10263, 10264, 10265, 10266
10267, 10268, 10271, 10272, 10273, 10274, 10275, 10276
10277, 10278, 10280, 10291, 10292, 10293, 10294, 10295
10296, 10297, 10298, 10301, 10302, 10303, 10304, 10305
10306, 10307, 10308, 10311, 10312, 10313, 10314, 10315
10316, 10317, 10318, 10320
*Elset, elset=BEAM4, generate
11050, 11080, 10
*Elset, elset=PILE, generate
10010, 10130, 40
21001, 21050, 1
22001, 22050, 1
23001, 23050, 1
24001, 24050, 1
*Elset, elset=TW1

```

```

1001,
*Elset, elset=TW2
1011,
*Elset, elset=TW3
1021,
*Elset, elset=TW4
1031,
*Elset, elset=TW5
1041,
*Elset, elset=TW6
1051,
*Elset, elset=TW7
1061,
*Elset, elset=TW8
1071,
*Nset, nset=TW_top_node
1071,
*Nset, nset=TP_slave_node
24, 28, 32, 36, 57, 58, 59, 60, 61, 63
*Nset, nset=X2S2
49, 50, 51, 52
*Nset, nset=TP_master_node
62,
*Nset, nset=BC_node, generate
21050, 24050, 1000
*SPRING, ELSET=SPR_xdir1, nonlinear
1
-92700, -200
-88460, -7
-78678, -5
-51463, -2
0, 0
51463, 2
78678, 5
88460, 7
92700, 200
*SPRING, ELSET=SPR_xdir2, nonlinear
1
-241200, -200
-229684, -9
-203713, -6
-132675, -3
0, 0
132675, 3
203713, 6
229684, 9
241200, 200
*SPRING, ELSET=SPR_xdir3, nonlinear
1
-445500, -200
-423651, -11
-375082, -7
-243627, -4
0, 0
243627, 4
375082, 7
423651, 11
445500, 200
*SPRING, ELSET=SPR_xdir4, nonlinear
1
-547200, -200
-525026, -17
-470522, -11
-311498, -6
0, 0
311498, 6
470522, 11
525026, 17
547200, 200
*SPRING, ELSET=SPR_xdir5, nonlinear
1
-787500, -200
-751842, -19
-669132, -13
-438120, -6
0, 0

```

```

438120,      6
669132,     13
751842,     19
787500,     200
*SPRING, ELSET=SPR_xdir6, nonlinear
1
-198000,    -525
-336600,    -315
-475200,    -105
-330000,    -35
  0,         0
 330000,     35
 475200,    105
 336600,    315
 198000,    525
*SPRING, ELSET=SPR_xdir7, nonlinear
1
-248500,    -525
-379850,    -315
-511200,    -105
-355000,    -35
  0,         0
 355000,     35
 511200,    105
 379850,    315
 248500,    525
*SPRING, ELSET=SPR_xdir8, nonlinear
1
-2505600,   -200
-2380588,   -20
-2105253,   -13
-1365055,   -7
  0,         0
 1365055,    7
 2105253,   13
 2380588,   20
 2505600,   200
*SPRING, ELSET=SPR_xdir9, nonlinear
1
-3094200,   -200
-2940972,   -22
-2602129,   -15
-1688508,   -7
  0,         0
 1688508,    7
 2602129,   15
 2940972,   22
 3094200,   200
*SPRING, ELSET=SPR_xdir10, nonlinear
1
-3744000,   -200
-3559751,   -24
-3150933,   -16
-2045917,   -8
  0,         0
 2045917,    8
 3150933,   16
 3559751,   24
 3744000,   200
*SPRING, ELSET=SPR_xdir11, nonlinear
1
-3722400,   -200
-3537689,   -29
-3129671,   -19
-2030412,   -10
  0,         0
 2030412,   10
 3129671,   19
 3537689,   29
 3722400,   200
*SPRING, ELSET=SPR_xdir12, nonlinear
1
-4363200,   -200
-4166643,   -32
-3709493,   -21
-2430070,   -11

```

```

0, 0
2430070, 11
3709493, 21
4166643, 32
4363200, 200
*SPRING, ELSET=SPR_xdir13, nonlinear
1
-5054400, -200
-4821302, -34
-4285850, -23
-2801053, -11
0, 0
2801053, 11
4285850, 23
4821302, 34
5054400, 200
*SPRING, ELSET=SPR_xdir14, nonlinear
1
-5796000, -200
-5523141, -36
-4903174, -24
-3197898, -12
0, 0
3197898, 12
4903174, 24
5523141, 36
5796000, 200
*SPRING, ELSET=SPR_xdir15, nonlinear
1
-6588000, -200
-6272154, -38
-5561459, -25
-3620601, -13
0, 0
3620601, 13
5561459, 25
6272154, 38
6588000, 200
*SPRING, ELSET=SPR_xdir16, nonlinear
1
-9417600, -200
-8991304, -36
-8002343, -24
-5239773, -12
0, 0
5239773, 12
8002343, 24
8991304, 36
9417600, 200
*SPRING, ELSET=SPR_xdir17, nonlinear
1
-10557000, -200
-10031500, -37
-8872656, -25
-5754420, -12
0, 0
5754420, 12
8872656, 25
10031500, 37
10557000, 200
*SPRING, ELSET=SPR_xdir18, nonlinear
1
-11761200, -200
-11179488, -39
-9892261, -26
-6419832, -13
0, 0
6419832, 13
9892261, 26
11179488, 39
11761200, 200
*SPRING, ELSET=SPR_xdir19, nonlinear
1
-13030200, -200
-12389443, -41
-10967137, -27

```

```

-7121558,      -14
   0,          0
  7121558,      14
10967137,      27
12389443,      41
13030200,      200
*SPRING, ELSET=SPR_xdir20, nonlinear
1
-14363999,     -200
-13661364,     -43
-12097285,     -29
-7859598,      -14
   0,          0
  7859598,      14
12097285,      29
13661364,      43
14363999,      200
*SPRING, ELSET=SPR_xdir21, nonlinear
1
-15762598,     -200
-14995252,     -45
-13282704,     -30
-8633951,      -15
   0,          0
  8633951,      15
13282704,      30
14995252,      45
15762598,      200
*SPRING, ELSET=SPR_xdir22, nonlinear
1
-17225995,     -200
-16391106,     -47
-14523394,     -31
-9444618,      -16
   0,          0
  9444618,      16
14523394,      31
16391106,      47
17225995,      200
*SPRING, ELSET=SPR_xdir23, nonlinear
1
-18754190,     -200
-17848926,     -49
-15819354,     -33
-10291597,     -16
   0,          0
 10291597,      16
15819354,      33
17848926,      49
18754190,      200
*SPRING, ELSET=SPR_xdir24, nonlinear
1
-20347180,     -200
-19368712,     -51
-17170585,     -34
-11174891,     -17
   0,          0
 11174891,      17
17170585,      34
19368712,      51
20347180,      200
*SPRING, ELSET=SPR_xdir25, nonlinear
1
-22004963,     -200
-20950463,     -53
-18577087,     -35
-12094497,     -18
   0,          0
12094497,      18
18577087,      35
20950463,      53
22004963,      200
*SPRING, ELSET=SPR_xdir26, nonlinear
1
-23727534,     -200
-22594181,     -55

```

```

-20038858,      -37
-13050416,      -18
  0,            0
 13050416,      18
 20038858,      37
 22594181,      55
 23727534,      200
*SPRING, ELSET=SPR_xdir27, nonlinear
1
-25514888,      -200
-24299864,      -57
-21555900,      -38
-14042649,      -19
  0,            0
 14042649,      19
 21555900,      38
 24299864,      57
 25514888,      200
*SPRING, ELSET=SPR_xdir28, nonlinear
1
-27367015,      -200
-26067513,      -59
-23128212,      -39
-15071194,      -20
  0,            0
 15071194,      20
 23128212,      39
 26067513,      59
 27367015,      200
*SPRING, ELSET=SPR_xdir29, nonlinear
1
-29283903,      -200
-27897127,      -61
-24755794,      -41
-16136052,      -20
  0,            0
 16136052,      20
 24755794,      41
 27897127,      61
 29283903,      200
*SPRING, ELSET=SPR_xdir30, nonlinear
1
-31265537,      -200
-29788707,      -63
-26438646,      -42
-17237224,      -21
  0,            0
 17237224,      21
 26438646,      42
 29788707,      63
 31265537,      200
*SPRING, ELSET=SPR_xdir31, nonlinear
1
-33311896,      -200
-31651966,      -64
-27992780,      -43
-18152233,      -21
  0,            0
 18152233,      21
 27992780,      43
 31651966,      64
 33311896,      200
*SPRING, ELSET=SPR_xdir32, nonlinear
1
-35422954,      -200
-33664837,      -66
-29780565,      -44
-19318982,      -22
  0,            0
 19318982,      22
 29780565,      44
 33664837,      66
 35422954,      200
*SPRING, ELSET=SPR_xdir33, nonlinear
1
-37598676,      -200

```



```

-35739673,      -68
-31623620,      -45
-20522045,      -23
  0,             0
 20522045,       23
 31623620,       45
 35739673,       68
 37598676,       200
*SPRING, ELSET=SPR_xdir34, nonlinear
1
-39839023,      -200
-37876476,      -70
-33521946,      -47
-21761421,      -23
  0,             0
 21761421,       23
 33521946,       47
 37876476,       70
 39839023,       200
*SPRING, ELSET=SPR_xdir35, nonlinear
1
-42143944,      -200
-40075244,      -72
-35475543,      -48
-23037111,      -24
  0,             0
 23037111,       24
 35475543,       48
 40075244,       72
 42143944,       200
*SPRING, ELSET=SPR_xdir36, nonlinear
1
-44513381,      -200
-42335978,      -74
-37484409,      -49
-24349113,      -25
  0,             0
 24349113,       25
 37484409,       49
 42335978,       74
 44513381,       200
*SPRING, ELSET=SPR_xdir37, nonlinear
1
-46947262,      -200
-44658677,      -76
-39548546,      -51
-25697429,      -25
  0,             0
 25697429,       25
 39548546,       51
 44658677,       76
 46947262,       200
*SPRING, ELSET=SPR_xdir38, nonlinear
1
-49069898,      -200
-46639826,      -77
-41258491,      -51
-26764840,      -26
  0,             0
 26764840,       26
 41258491,       51
 46639826,       77
 49069898,       200
*SPRING, ELSET=SPR_xdir39, nonlinear
1
-50361212,      -200
-47867190,      -77
-42344241,      -51
-27469178,      -26
  0,             0
 27469178,       26
 42344241,       51
 47867190,       77
 50361212,       200
*SPRING, ELSET=SPR_xdir40, nonlinear
1

```

```

-51652525,      -200
-49094553,      -77
-43429991,      -51
-28173516,      -26
   0,           0
 28173516,       26
 43429991,       51
 49094553,       77
 51652525,      200
*SPRING, ELSET=SPR_xdir41, nonlinear
1
-52943838,      -200
-50321917,      -77
-44515740,      -51
-28877853,      -26
   0,           0
 28877853,       26
 44515740,       51
 50321917,       77
 52943838,      200
*SPRING, ELSET=SPR_xdir42, nonlinear
1
-54235151,      -200
-51549281,      -77
-45601490,      -51
-29582191,      -26
   0,           0
 29582191,       26
 45601490,       51
 51549281,       77
 54235151,      200
*SPRING, ELSET=SPR_xdir43, nonlinear
1
-55526464,      -200
-52776645,      -77
-46687240,      -51
-30286529,      -26
   0,           0
 30286529,       26
 46687240,       51
 52776645,       77
 55526464,      200
*SPRING, ELSET=SPR_xdir44, nonlinear
1
-56817777,      -200
-54004009,      -77
-47772990,      -51
-30990867,      -26
   0,           0
 30990867,       26
 47772990,       51
 54004009,       77
 56817777,      200
*SPRING, ELSET=SPR_xdir45, nonlinear
1
-58109090,      -200
-55231373,      -77
-48858739,      -51
-31695205,      -26
   0,           0
 31695205,       26
 48858739,       51
 55231373,       77
 58109090,      200
*SPRING, ELSET=SPR_xdir46, nonlinear
1
-59400403,      -200
-56458736,      -77
-49944489,      -51
-32399543,      -26
   0,           0
 32399543,       26
 49944489,       51
 56458736,       77
 59400403,      200
*SPRING, ELSET=SPR_xdir47, nonlinear

```

```

1
-60691717,      -200
-57686100,      -77
-51030239,      -51
-33103881,      -26
   0,           0
 33103881,      26
 51030239,      51
 57686100,      77
 60691717,      200
*SPRING, ELSET=SPR_xdir48, nonlinear
1
-61983030,      -200
-58913464,      -77
-52115989,      -51
-33808219,      -26
   0,           0
 33808219,      26
 52115989,      51
 58913464,      77
 61983030,      200
*SPRING, ELSET=SPR_xdir49, nonlinear
1
-63274343,      -200
-60140828,      -77
-53201739,      -51
-34512556,      -26
   0,           0
 34512556,      26
 53201739,      51
 60140828,      77
 63274343,      200
*SPRING, ELSET=SPR_xdir50, nonlinear
1
-64565656,      -200
-61368192,      -77
-54287488,      -51
-35216894,      -26
   0,           0
 35216894,      26
 54287488,      51
 61368192,      77
 64565656,      200
*SPRING, ELSET=SPR_ydir1, nonlinear
2
  -92700,       -200
  -88460,        -7
  -78678,        -5
  -51463,        -2
    0,           0
   51463,         2
   78678,         5
   88460,         7
   92700,        200
*SPRING, ELSET=SPR_ydir2, nonlinear
2
  -241200,       -200
  -229684,        -9
  -203713,        -6
  -132675,        -3
    0,           0
   132675,         3
   203713,         6
   229684,         9
   241200,        200
*SPRING, ELSET=SPR_ydir3, nonlinear
2
  -445500,       -200
  -423651,       -11
  -375082,        -7
  -243627,        -4
    0,           0
   243627,         4
   375082,         7
   423651,        11
   445500,        200

```

```

*SPRING, ELSET=SPR_ydir4, nonlinear
2
-547200, -200
-525026, -17
-470522, -11
-311498, -6
0, 0
311498, 6
470522, 11
525026, 17
547200, 200
*SPRING, ELSET=SPR_ydir5, nonlinear
2
-787500, -200
-751842, -19
-669132, -13
-438120, -6
0, 0
438120, 6
669132, 13
751842, 19
787500, 200
*SPRING, ELSET=SPR_ydir6, nonlinear
2
-198000, -525
-336600, -315
-475200, -105
-330000, -35
0, 0
330000, 35
475200, 105
336600, 315
198000, 525
*SPRING, ELSET=SPR_ydir7, nonlinear
2
-248500, -525
-379850, -315
-511200, -105
-355000, -35
0, 0
355000, 35
511200, 105
379850, 315
248500, 525
*SPRING, ELSET=SPR_ydir8, nonlinear
2
-2505600, -200
-2380588, -20
-2105253, -13
-1365055, -7
0, 0
1365055, 7
2105253, 13
2380588, 20
2505600, 200
*SPRING, ELSET=SPR_ydir9, nonlinear
2
-3094200, -200
-2940972, -22
-2602129, -15
-1688508, -7
0, 0
1688508, 7
2602129, 15
2940972, 22
3094200, 200
*SPRING, ELSET=SPR_ydir10, nonlinear
2
-3744000, -200
-3559751, -24
-3150933, -16
-2045917, -8
0, 0
2045917, 8
3150933, 16
3559751, 24

```

```

    3744000,      200
*SPRING, ELSET=SPR_ydir11, nonlinear
2
-3722400,      -200
-3537689,      -29
-3129671,      -19
-2030412,      -10
    0,          0
    2030412,      10
    3129671,      19
    3537689,      29
    3722400,      200
*SPRING, ELSET=SPR_ydir12, nonlinear
2
-4363200,      -200
-4166643,      -32
-3709493,      -21
-2430070,      -11
    0,          0
    2430070,      11
    3709493,      21
    4166643,      32
    4363200,      200
*SPRING, ELSET=SPR_ydir13, nonlinear
2
-5054400,      -200
-4821302,      -34
-4285850,      -23
-2801053,      -11
    0,          0
    2801053,      11
    4285850,      23
    4821302,      34
    5054400,      200
*SPRING, ELSET=SPR_ydir14, nonlinear
2
-5796000,      -200
-5523141,      -36
-4903174,      -24
-3197898,      -12
    0,          0
    3197898,      12
    4903174,      24
    5523141,      36
    5796000,      200
*SPRING, ELSET=SPR_ydir15, nonlinear
2
-6588000,      -200
-6272154,      -38
-5561459,      -25
-3620601,      -13
    0,          0
    3620601,      13
    5561459,      25
    6272154,      38
    6588000,      200
*SPRING, ELSET=SPR_ydir16, nonlinear
2
-9417600,      -200
-8991304,      -36
-8002343,      -24
-5239773,      -12
    0,          0
    5239773,      12
    8002343,      24
    8991304,      36
    9417600,      200
*SPRING, ELSET=SPR_ydir17, nonlinear
2
-10557000,     -200
-10031500,     -37
-8872656,      -25
-5754420,      -12
    0,          0
    5754420,      12
    8872656,      25

```

```

10031500,      37
10557000,      200
*SPRING, ELSET=SPR_ydir18, nonlinear
2
-11761200,     -200
-11179488,     -39
-9892261,      -26
-6419832,      -13
   0,           0
  6419832,      13
  9892261,      26
 11179488,      39
 11761200,      200
*SPRING, ELSET=SPR_ydir19, nonlinear
2
-13030200,     -200
-12389443,     -41
-10967137,     -27
-7121558,      -14
   0,           0
  7121558,      14
 10967137,      27
 12389443,      41
 13030200,      200
*SPRING, ELSET=SPR_ydir20, nonlinear
2
-14363999,     -200
-13661364,     -43
-12097285,     -29
-7859598,      -14
   0,           0
  7859598,      14
 12097285,      29
 13661364,      43
 14363999,      200
*SPRING, ELSET=SPR_ydir21, nonlinear
2
-15762598,     -200
-14995252,     -45
-13282704,     -30
-8633951,      -15
   0,           0
  8633951,      15
 13282704,      30
 14995252,      45
 15762598,      200
*SPRING, ELSET=SPR_ydir22, nonlinear
2
-17225995,     -200
-16391106,     -47
-14523394,     -31
-9444618,      -16
   0,           0
  9444618,      16
 14523394,      31
 16391106,      47
 17225995,      200
*SPRING, ELSET=SPR_ydir23, nonlinear
2
-18754190,     -200
-17848926,     -49
-15819354,     -33
-10291597,     -16
   0,           0
 10291597,      16
 15819354,      33
 17848926,      49
 18754190,      200
*SPRING, ELSET=SPR_ydir24, nonlinear
2
-20347180,     -200
-19368712,     -51
-17170585,     -34
-11174891,     -17
   0,           0
 11174891,      17

```

```

17170585,      34
19368712,      51
20347180,      200
*SPRING, ELSET=SPR_ydir25, nonlinear
2
-22004963,     -200
-20950463,     -53
-18577087,     -35
-12094497,     -18
   0,           0
12094497,      18
18577087,      35
20950463,      53
22004963,      200
*SPRING, ELSET=SPR_ydir26, nonlinear
2
-23727534,     -200
-22594181,     -55
-20038858,     -37
-13050416,     -18
   0,           0
13050416,      18
20038858,      37
22594181,      55
23727534,      200
*SPRING, ELSET=SPR_ydir27, nonlinear
2
-25514888,     -200
-24299864,     -57
-21555900,     -38
-14042649,     -19
   0,           0
14042649,      19
21555900,      38
24299864,      57
25514888,      200
*SPRING, ELSET=SPR_ydir28, nonlinear
2
-27367015,     -200
-26067513,     -59
-23128212,     -39
-15071194,     -20
   0,           0
15071194,      20
23128212,      39
26067513,      59
27367015,      200
*SPRING, ELSET=SPR_ydir29, nonlinear
2
-29283903,     -200
-27897127,     -61
-24755794,     -41
-16136052,     -20
   0,           0
16136052,      20
24755794,      41
27897127,      61
29283903,      200
*SPRING, ELSET=SPR_ydir30, nonlinear
2
-31265537,     -200
-29788707,     -63
-26438646,     -42
-17237224,     -21
   0,           0
17237224,      21
26438646,      42
29788707,      63
31265537,      200
*SPRING, ELSET=SPR_ydir31, nonlinear
2
-33311896,     -200
-31651966,     -64
-27992780,     -43
-18152233,     -21
   0,           0

```

```

18152233,      21
27992780,      43
31651966,      64
33311896,      200
*SPRING, ELSET=SPR_ydir32, nonlinear
2
-35422954,     -200
-33664837,     -66
-29780565,     -44
-19318982,     -22
   0,           0
 19318982,      22
 29780565,      44
 33664837,      66
 35422954,      200
*SPRING, ELSET=SPR_ydir33, nonlinear
2
-37598676,     -200
-35739673,     -68
-31623620,     -45
-20522045,     -23
   0,           0
 20522045,      23
 31623620,      45
 35739673,      68
 37598676,      200
*SPRING, ELSET=SPR_ydir34, nonlinear
2
-39839023,     -200
-37876476,     -70
-33521946,     -47
-21761421,     -23
   0,           0
 21761421,      23
 33521946,      47
 37876476,      70
 39839023,      200
*SPRING, ELSET=SPR_ydir35, nonlinear
2
-42143944,     -200
-40075244,     -72
-35475543,     -48
-23037111,     -24
   0,           0
 23037111,      24
 35475543,      48
 40075244,      72
 42143944,      200
*SPRING, ELSET=SPR_ydir36, nonlinear
2
-44513381,     -200
-42335978,     -74
-37484409,     -49
-24349113,     -25
   0,           0
 24349113,      25
 37484409,      49
 42335978,      74
 44513381,      200
*SPRING, ELSET=SPR_ydir37, nonlinear
2
-46947262,     -200
-44658677,     -76
-39548546,     -51
-25697429,     -25
   0,           0
 25697429,      25
 39548546,      51
 44658677,      76
 46947262,      200
*SPRING, ELSET=SPR_ydir38, nonlinear
2
-49069898,     -200
-46639826,     -77
-41258491,     -51
-26764840,     -26

```



```

0, 0
26764840, 26
41258491, 51
46639826, 77
49069898, 200
*SPRING, ELSET=SPR_ydir39, nonlinear
2
-50361212, -200
-47867190, -77
-42344241, -51
-27469178, -26
0, 0
27469178, 26
42344241, 51
47867190, 77
50361212, 200
*SPRING, ELSET=SPR_ydir40, nonlinear
2
-51652525, -200
-49094553, -77
-43429991, -51
-28173516, -26
0, 0
28173516, 26
43429991, 51
49094553, 77
51652525, 200
*SPRING, ELSET=SPR_ydir41, nonlinear
2
-52943838, -200
-50321917, -77
-44515740, -51
-28877853, -26
0, 0
28877853, 26
44515740, 51
50321917, 77
52943838, 200
*SPRING, ELSET=SPR_ydir42, nonlinear
2
-54235151, -200
-51549281, -77
-45601490, -51
-29582191, -26
0, 0
29582191, 26
45601490, 51
51549281, 77
54235151, 200
*SPRING, ELSET=SPR_ydir43, nonlinear
2
-55526464, -200
-52776645, -77
-46687240, -51
-30286529, -26
0, 0
30286529, 26
46687240, 51
52776645, 77
55526464, 200
*SPRING, ELSET=SPR_ydir44, nonlinear
2
-56817777, -200
-54004009, -77
-47772990, -51
-30990867, -26
0, 0
30990867, 26
47772990, 51
54004009, 77
56817777, 200
*SPRING, ELSET=SPR_ydir45, nonlinear
2
-58109090, -200
-55231373, -77
-48858739, -51

```

```

-31695205,      -26
   0,           0
 31695205,      26
48858739,       51
55231373,       77
58109090,      200
*SPRING, ELSET=SPR_ydir46, nonlinear
2
-59400403,     -200
-56458736,     -77
-49944489,     -51
-32399543,     -26
   0,           0
 32399543,      26
49944489,       51
56458736,       77
59400403,      200
*SPRING, ELSET=SPR_ydir47, nonlinear
2
-60691717,     -200
-57686100,     -77
-51030239,     -51
-33103881,     -26
   0,           0
 33103881,      26
51030239,       51
57686100,       77
60691717,      200
*SPRING, ELSET=SPR_ydir48, nonlinear
2
-61983030,     -200
-58913464,     -77
-52115989,     -51
-33808219,     -26
   0,           0
 33808219,      26
52115989,       51
58913464,       77
61983030,      200
*SPRING, ELSET=SPR_ydir49, nonlinear
2
-63274343,     -200
-60140828,     -77
-53201739,     -51
-34512556,     -26
   0,           0
 34512556,      26
53201739,       51
60140828,       77
63274343,      200
*SPRING, ELSET=SPR_ydir50, nonlinear
2
-64565656,     -200
-61368192,     -77
-54287488,     -51
-35216894,     -26
   0,           0
 35216894,      26
54287488,       51
61368192,       77
64565656,      200
*****
** new sets for outputs at legs and braces
*****
*Nset, nset=ZERO_POINT, generate
10741, 10881, 20
*Elset, elset=LEG1_MEMB1
10271,
*Elset, elset=LEG2_MEMB1
10261,
*Elset, elset=LEG3_MEMB1
10251,
*Elset, elset=LEG4_MEMB1
10121,
*Elset, elset=BRA1_MEMB1
11031,

```

```

*Elset, elset=BRA2_MEMB1
10871,
*Elset, elset=BRA3_MEMB1
10711,
*Elset, elset=BRA4_MEMB1
10551,
*Elset, elset=BRA1_MEMB2
10951,
*Elset, elset=BRA2_MEMB2
10791,
*Elset, elset=BRA3_MEMB2
10631,
*Elset, elset=BRA4_MEMB2
10471,
*Elset, elset=PILE_END
10050,
** Section: Section-6-TW1 Profile: Profile-6
*Beam Section, elset=TW1, material=STEEL, temperature=GRADIENTS, section=PIPE
2800., 32.
0.,-1.,0.
** Section: Section-7-TW2 Profile: Profile-7
*Beam Section, elset=TW2, material=STEEL, temperature=GRADIENTS, section=PIPE
2788., 32.
0.,-1.,0.
** Section: Section-8-TW3 Profile: Profile-8
*Beam Section, elset=TW3, material=STEEL, temperature=GRADIENTS, section=PIPE
2659., 30.
0.,-1.,0.
** Section: Section-9-TW4 Profile: Profile-9
*Beam Section, elset=TW4, material=STEEL, temperature=GRADIENTS, section=PIPE
2541., 28.
0.,-1.,0.
** Section: Section-10-TW5 Profile: Profile-10
*Beam Section, elset=TW5, material=STEEL, temperature=GRADIENTS, section=PIPE
2400., 24.
0.,-1.,0.
** Section: Section-11-TW6 Profile: Profile-11
*Beam Section, elset=TW6, material=STEEL, temperature=GRADIENTS, section=PIPE
2282., 22.
0.,-1.,0.
** Section: Section-12-TW7 Profile: Profile-12
*Beam Section, elset=TW7, material=STEEL, temperature=GRADIENTS, section=PIPE
2164., 30.
0.,-1.,0.
** Section: Section-13-TW8 Profile: Profile-13
*Beam Section, elset=TW8, material=STEEL, temperature=GRADIENTS, section=PIPE
2059., 30.
0.,-1.,0.
** Section: Section-1-PILE Profile: Profile-1
*Beam Section, elset=PILE, material=STEEL, temperature=GRADIENTS, section=PIPE
1041., 60.
0.,-1.,0.
** Section: Section-3-BEAM2 Profile: Profile-3
*Beam Section, elset=BEAM2, material=STEEL, temperature=GRADIENTS, section=PIPE
600., 50.
0.,-1.,0.
** Section: Section-4-BEAM3 Profile: Profile-4
*Beam Section, elset=BEAM3, material=STEEL, temperature=GRADIENTS, section=PIPE
600., 35.
0.,0.,-1.
** Section: Section-2-BEAM1 Profile: Profile-2
*Beam Section, elset=BEAM1, material=STEEL, temperature=GRADIENTS, section=PIPE
400., 20.
0.,0.,-1.
** Section: Section-5-BEAM4 Profile: Profile-5
*Beam Section, elset=BEAM4, material=STEEL, temperature=GRADIENTS, section=PIPE
600., 40.
0.,-1.,0.
** Section: Section-6-TP_BEAM Profile: Profile-6
*Beam Section, elset=TP_BEAM, material=CONCRETE, temperature=GRADIENTS, section=RECT
9600, 9600
0.,-1.,0.
*Element, type=MASS, elset=NAC_mass
50002, 1071
*Mass, elset=NAC_mass
350000.,

```

```

*End Part
** -----
** ASSEMBLY
** -----
*Assembly, name=Assembly
**
*Instance, name=PART-1-1, part=PART-1
*End Instance
*Nset, nset=TW_TOP, instance=PART-1-1
1071,
*Nset, nset=TP_BOTTOM, instance=PART-1-1
61,
*Nset, nset=JACKET_TOP, instance=PART-1-1
24, 28, 32, 36
*Surface, type=NODE, name=TRANSITION_PIECE_BOTTOM
JACKET_TOP, 1.
** Constraint: TP_JACKET
**Coupling, constraint name=TP_JACKET, ref node = TP_BOTTOM, surface=TRANSITION_PIECE_BOTTOM
**Kinematic
** Constraint: Constraint-2
**MPC
**TIE, PART-1-1.TP_slave_node, PART-1-1.TP_master_node
*End Assembly
** -----
** MATERIALS
** -----
*Material, name=STEEL
*Damping, beta=0.01
*Density
7.85e-06,
*Elastic
2.1e+08, 0.3
*Material, name=RIGID_MASS
*Damping, beta=0.01
*Density
7.85e-06,
*Elastic
2.9e+27, 0.0
*Material, name=CONCRETE
*Damping, alpha=3.18005, beta=0.216071
*Density
1.806e-06,
*Elastic
2.1e+08, 0.3
** -----
** Amplitude
** -----
*Amplitude, name=Fx_amp, INPUT=YawBrFxp.out
*Amplitude, name=Fy_amp, INPUT=YawBrFyp.out
*Amplitude, name=Fz_amp, INPUT=YawBrFzp.out
*Amplitude, name=Mx_amp, INPUT=YawBrMxp.out
*Amplitude, name=My_amp, INPUT=YawBrMyp.out
*Amplitude, name=Mz_amp, INPUT=YawBrMzp.out
** -----
** BOUNDARY CONDITIONS
** -----
** Name: BC-1 Type: Symmetry/Antisymmetry/Encastre
*Boundary
**PART-1-1.BC_node, ENCASTRE
PART-1-1.BC_node, 3, 3
**PART-1-1.BC_node, 2, 2
PART-1-1.BC_node, 6, 6
** -----
** Define Hydrodynamic load
** -----
*AQUA
-50000, 0.0, 9800, 1026.05e-09
*WAVE,TYPE=GRIDDED, DATA FILE=gridwave_3d_P1.binary
0.,0.,0.,1.,0.
**-----
** STEP: dynamic analysis step
**-----
*Step, name=Step-2, nlgeom=YES, inc=400000
*Dynamic, application=TRANSIENT FIDELITY
**Dynamic
1,600,1e-08,0.10

```

```

**-----
** Wind LOADS
**-----
** Name: CFORCE-1   Type: Moment
*Clod, follower, amplitude=MZ_AMP
TW_TOP, 6, 0.0001
** Name: CFORCE-2   Type: Moment
*Clod, follower, amplitude=MY_AMP
TW_TOP, 5, 0.0001
** Name: CFORCE-3   Type: Moment
*Clod, follower, amplitude=MX_AMP
TW_TOP, 4, 0.0001
** Name: CFORCE-4   Type: Concentrated force
*Clod, follower, amplitude=FZ_AMP
TW_TOP, 3, 0.0001
** Name: CFORCE-5   Type: Concentrated force
*Clod, follower, amplitude=FY_AMP
TW_TOP, 2, 0.0001
** Name: CFORCE-6   Type: Concentrated force
*Clod, follower, amplitude=FX_AMP
TW_TOP, 1, 0.0001
**-----
** WAVE LOADS
**-----
*DLOAD
, GRAV, 9800, 0., 0., -1.
*DLOAD
PART-1-1.BEAM1, FI, , 1000., 2., 0.
PART-1-1.BEAM2, FI, , 1400., 2., 0.
PART-1-1.BEAM3, FI, , 1400., 2., 0.
PART-1-1.BEAM4, FI, , 1400., 2., 0.
*DLOAD
PART-1-1.BEAM1, FDD, , 1000., 1.
PART-1-1.BEAM2, FDD, , 1400., 1.
PART-1-1.BEAM3, FDD, , 1400., 1.
PART-1-1.BEAM4, FDD, , 1400., 1.
**DLOAD
**PART-1-1.BEAM1, PB, , 1000.
**PART-1-1.BEAM2, PB, , 1400.
**PART-1-1.BEAM3, PB, , 1400.
**PART-1-1.BEAM4, PB, , 1400.
**
** OUTPUT REQUESTS
**
**Restart, write, frequency=0
**
** FIELD OUTPUT: F-Output-2
**
*OUTPUT,FIELD, Frequency=1
*NODE OUTPUT, NSET=PART-1-1.BC_node
RF
*NODE OUTPUT, NSET=PART-1-1.X2S2
U
*ELEMENT OUTPUT, ELSET=PART-1-1.TW1
SF
*NODE OUTPUT, NSET=PART-1-1.ZERO_POINT
U
*NODE OUTPUT, NSET=PART-1-1.TW_top_node
U
*ELEMENT OUTPUT, ELSET=PART-1-1.LEG1_MEMB1
SF
*ELEMENT OUTPUT, ELSET=PART-1-1.LEG2_MEMB1
SF
*ELEMENT OUTPUT, ELSET=PART-1-1.LEG3_MEMB1
SF
*ELEMENT OUTPUT, ELSET=PART-1-1.LEG4_MEMB1
SF
*ELEMENT OUTPUT, ELSET=PART-1-1.BRA1_MEMB1
SF
*ELEMENT OUTPUT, ELSET=PART-1-1.BRA2_MEMB1
SF
*ELEMENT OUTPUT, ELSET=PART-1-1.BRA3_MEMB1
SF
*ELEMENT OUTPUT, ELSET=PART-1-1.BRA4_MEMB1
SF
*ELEMENT OUTPUT, ELSET=PART-1-1.BRA1_MEMB2

```

```
SF
*ELEMENT OUTPUT, ELSET=PART-1-1.BRA2_MEMB2
SF
*ELEMENT OUTPUT, ELSET=PART-1-1.BRA3_MEMB2
SF
*ELEMENT OUTPUT, ELSET=PART-1-1.BRA4_MEMB2
SF
*ELEMENT OUTPUT, ELSET=PART-1-1.PILE_END
SF
*End Step
```

## Bibliography

- [1] N. Sharma and R. Dean. Second-order directional seas and associated wave forces. *Society of Petroleum Engineers Journal*, 4:129–140, 1981.
- [2] M.S. Longuet-Higgins, D.E. Cartwright, and N.D. Smith. Observations of the directional spectrum of sea waves using the motions of a floating buoy. In *Ocean Wave Spectra, Proceedings of the Royal Society of London. Series A, Mathematical and Physical Sciences*, 1962.
- [3] O.M. Faltinsen. *Sea Loads On Ships and Offshore Structures*. Cambridge University Press, 1990.
- [4] G. G. Stokes. On the theory of oscillatory waves. *Trans.Camb. Phil. Soc.*, 8:441–455, 1847.
- [5] P.D. Scavounos. *Ocean Wave Interaction with Ships and Offshore Energy Systems [Lecture Note]*. Massachusetts Institute of Technology, 2002.
- [6] C.-H. Lee. WAMIT theory manual. Technical Report MIT Report 95-2, Department of Ocean Engineering, Massachusetts Institute of Technology, Cambridge, MA, 1995.
- [7] R. G. Dean and R.A. Dalrymple. *Water Wave Mechanics for Engineers and Scientists*. Prentice-Hall, Inc., 1991.
- [8] R. Miche. Le pouvoir reflechissant des ouvrages maritime exposés à l’action de la houle. In *Annale Ponts et Chaussées.*, 1951.
- [9] S-L.J. Hu and D. Zhao. Non-Gaussian properties of second-order random waves. *Journal of Engineering Mechanics*, 119:44–364, 1993.
- [10] C. T. Stansberg. Non-Gaussian extremes in numerically generated second-order random waves on deep water. In *8th International Offshore and Polar Engineering Conference*, Montreal, Canada, 1998.
- [11] Det Norske Veritas. *Recommended practice - DNV-RP-C205 - Environmental conditions and environmental loads*. DNV, 2010.
- [12] T. Marthinsen and S.R. Winterstein. On the skewness of random surface waves. In *2nd International Offshore and Polar Engineering Conference*, San Francisco, CA, 1992.
- [13] O. Nwogu. Nonlinear evolution of directional wave spectra in shallow water. In *Proceeding of Costal Engineering*, 1994.
- [14] P. Agarwal and L. Manuel. Incorporating irregular nonlinear waves in coupled simulation and reliability studies of offshore wind turbines. *Applied Ocean Research*, 33(3):215 – 227, 2011.
- [15] B.A. Harper, J. D. Kepert, and J. D. Ginger. Guidelines for converting between various wind averaging periods in tropical cyclone conditions. Technical Report WMO/TD-No.1555, World Meteorological Organization, 2010.
- [16] G. H. Bryan and R. Rotunno. Evaluation of an analytical model for the maximum intensity of tropical cyclones. *Journal of the Atmospheric Sciences*, 66:3042–3060, 2009.
- [17] H. A. Panofsky and J. A Dutton. *Atmospheric turbulence: models and methods for engineering applications*. John Wiley and Sons, Inc., 1984.
- [18] M. D. Powell, P.J. Vickery, and T.A. Reinhold. Reduced drag coefficient for high wind speeds in tropical cyclones. *Nature*, 442:279–283, 2003.

- [19] S. A. Hsu, B. W. Blanchard, and Z. Yan. A simplified equation for Paulson's  $\psi_m(z/l)$  formulation for overwater applications. *Journal of Applied Meteorology*, 38:623–625, 1999.
- [20] H. Ishizaki. Wind profiles, turbulence intensities and gust factors for design in typhoon-prone region. *Journal of Wind Engineering and Industrial Aerodynamics*, 13:55–66, 1983.
- [21] M.K. Ochi. *Hurricane-generated seas*. Elsevier Ocean Engineering Book Series, Elsevier, 2003.
- [22] International Electrotechnical Commission. *IEC 61400-1 Wind Turbines - Part 1: Design, Edition 3*, 2007.
- [23] P. Agarwal and L. Manuel. Simulation of offshore wind turbine response for ultimate limit states. *Engineering Structures*, 31:2236–2246, 2009.
- [24] P. Agarwal and L. Manuel. On the modeling of nonlinear waves for prediction of long-term offshore wind turbine loads. *Journal of Offshore Mechanics and Arctic Engineering*, 131(4):041601, 2009.
- [25] I. R. Young. Directional spectra of hurricane wind waves. *Journal of Geophysical Research*, 111, 2006.
- [26] L. H. Holthuijsen. *Waves in Oceanic and Coastal Waters*. Cambridge University Press, 2007.
- [27] J. Portilla, F.J. Ocampo-Torres, and J. Monbaliu. Spectral partitioning and identification of wind sea and swell. *Journal of Atmospheric and Oceanic Technology*, 26:107–122, 2009.
- [28] G.J. Komen, S. Hasselmann, and K. Hasselmann. On the existence of a fully developed wind-sea spectrum. *Journal of Physical Oceanography*, 14:1271–1285, 1984.
- [29] R. Sharma, J. Hensel, C. Baxter, and S-H J. Hu. Development of a technology type factor for jacket structures for offshore wind turbines in rhode island, technical report for the Rhode Island ocean special area management plan. Technical report, University of Rhode Island, Kingston, RI, 2010.
- [30] W. Wang, C. Bruyere, M. Duda, J. Dudhia, D. Gill, H. C. Lin, and J. Man-del. Advanced research WRF Version 3 modeling system user's guide), 2015. [[http://www2.mmm.ucar.edu/wrf/users/docs/user\\_guide\\_V3/ARWUsersGuideV3.pdf](http://www2.mmm.ucar.edu/wrf/users/docs/user_guide_V3/ARWUsersGuideV3.pdf); accessed 15-March-2015].
- [31] J.G. Kaimal, J.G. Wyngaard, Y. Izumi, and O.R. Cotr. Spectral characteristics of surface layer turbulence. *Quarterly Journal of the Royal Meteorological Society*, 98:563–589, 1972.
- [32] J. M. Jonkman and M. L. Buhl, Jr. FAST User's Guide. Technical Report NREL/EL-500-38230, National Renewable Energy Laboratory, Golden, CO, 2005.
- [33] P. S. Veers. Three-dimensional Wind Simulation. Technical Report SAND88-0152, Sandia National Laboratory, Albuquerque, NM, 1988.
- [34] E. Simiu and R. H. Scanlan. *Wind Effects on Structures: Fundamentals and Applications to Design*. John Wiley and Sons, 3rd edition, 1996.
- [35] G. Solari and G. Piccardo. Probabilistic 3-D turbulence modeling for gust buffeting of structures. *Probabilistic Engineering Mechanics*, 16:73–86, 2001.
- [36] Abaqus. Abaqus Analysis Users Manual. Technical Report Vol. 6.13., Dassault Systemes, 2013.
- [37] J. M. Jonkman, S. Butterfield, W. Musial, and G. Scott. Definition of a 5-MW Reference Wind Turbine for Off-shore System Development. Technical Report NREL/TP-500-38060, National Renewable Energy Laboratory, Golden, CO, 2009.



- [38] F. Vorpahl, W. Popko, and D. Kaufer. Description of a basic model of the upwind reference jacket for code comparison in the OC4 Project under IEA Wind Annex 30. Technical report, Institute for Wind Energy and Energy System Technology IWES, Bremerhaven, 2011.
- [39] Vemula N.K., DeVries W., Fischer T., Cordle A., and Schmidt B. Design solution for the UpWind reference offshore support structure. Technical Report UpWind WP4 D4.2.5, Fraunhofer Institute for Wind Energy and Energy System Technology (IWES), Germany, 2010.
- [40] Det Norske Veritas. *DNV-OS-J101: Design of offshore wind turbine structures*, 2004.
- [41] T. Fischer and M. Kuehn. Site sensitive support structure and machine design for offshore wind farms. In *EWEC*, 2009.
- [42] W. Popko, F. Vorpahl, A. Zuga, M. Kohlmeier, J. Jonkman, and A et al. Robertson. Offshore Code Comparison Collaboration Continuation (OC4), Phase I - results of coupled simulations of an offshore wind turbine with jacket support structure. In *The 22nd International Offshore and Polar Engineering conference (ISOPE)*, Rhodes, Greece, 2012.
- [43] H. Song, R. Damiani, A. Robertson, and J. Jonkman. A new structural-dynamics module for offshore multi-member substructures within the wind turbine computer-aided engineering tool fast. In *The 23rd International Offshore and Polar Engineering conference (ISOPE)*, Anchorage, Alaska, 2013.
- [44] American Petroleum Institute (API). *API RP 2A-WSD: Recommended Practice for Planning Designing and Constructing Fixed Offshore structures - Working Stress Design.*, 2007.
- [45] J.F. Manwell, J.G. McGowan, and A.L. Rogers. *Wind Energy Explained: Theory, Design and Application, 2nd Edition*. Wiley and Sons: West Sussex, 2002.
- [46] H. Matlock. Correlations for design of laterally loaded piles in soft clay. In *Proceedings of the Offshore Technology Conference*, Houston, Texas, 1970.
- [47] R. E. Melchers. *Structural Reliability Analysis and Prediction*. Wiley and Sons, New York, 1999.
- [48] P. Agarwal. *Structural reliability of offshore wind turbines*. Ph.D. Dissertation, The University of Texas at Austin, 2008.

# Appendix F. The University of Miami Coupled Model for Combined Simulation of Hurricane Wind and Wave Fields

## Summary of University of Miami Work

This project aimed to develop a meteorologically-based simulation and design tool that addresses uncertain risks to U.S. offshore wind farms from destructive wind and wave conditions in the hurricane-prone Gulf of Mexico and U.S. Eastern Seaboard wind energy development sites. This process involves adapting a leading, coupled, atmosphere-wave-ocean model developed by the research group at the University of Miami (UM) for hurricane research and prediction to provide correlated wind and wave fields as input to the NREL-developed FAST turbine design tools. The University of Miami Coupled Model (UMCM) has been configured to provide high-resolution coupled model simulations of hurricanes for use in the analysis of wind and wave loads conducted by the University of Texas (UT). We have completed the UMCM simulations of two major hurricanes: Hurricane Ike (2008) over the Gulf of Mexico and Superstorm Sandy (2012) over the U.S. Eastern Seaboard. The UMCM model output was provided to both NREL and UT groups during the course of this project for studies of downscaling wind and wave effects to turbine scale. Documentation of the UMCM software and model output is included here. This appendix focuses on scientific results and model evaluation with observations of Hurricane Ike and Superstorm Sandy.

## Objectives

The main objectives of this work are to 1) configure and test the UMCM over the Gulf of Mexico and the U.S. East Coast/Atlantic Seaboard for use in predicting wind turbine loads, 2) conduct coupled atmosphere-wave-ocean model experiments using UMCM to better understand the wind, surface waves, and ocean currents in hurricanes near landfall and their impacts on offshore wind turbines, and 3) provide UMCM simulations of hurricanes over the Gulf of Mexico and for downscaling studies at turbine and structural scales. Figure F1 shows a schematic of the coupled system and conceptual model for this project.

The UMCM was developed for research and prediction of marine and coastal weather systems including tropical cyclones and winter storms. It is a fully coupled atmosphere-wave-ocean model that consists of three model components: the Weather Research and Forecasting (WRF) model, the University of Miami Wave Model (UMWM), and the Hybrid Coordinate Ocean Model (HYCOM). We have developed a unified air-sea interface module that couples multiple atmosphere, wave, and ocean models using the Earth System Modeling Framework (ESMF). It provides a physically based and computationally efficient coupling at the air-sea interface that is flexible for use in a multi-model system and portable for transition to the next-generation coupled atmosphere-wave/ocean-land models. The UMCM has been tested and evaluated using the coupled air-sea observations collected in recent field campaigns in the Northern seas and Gulf of Mexico and for tropical cyclones in the Atlantic and Pacific basins. The UMCM is used to provide fully coupled model predictions of wind, ocean wave, and current fields as input to turbine design calculations.

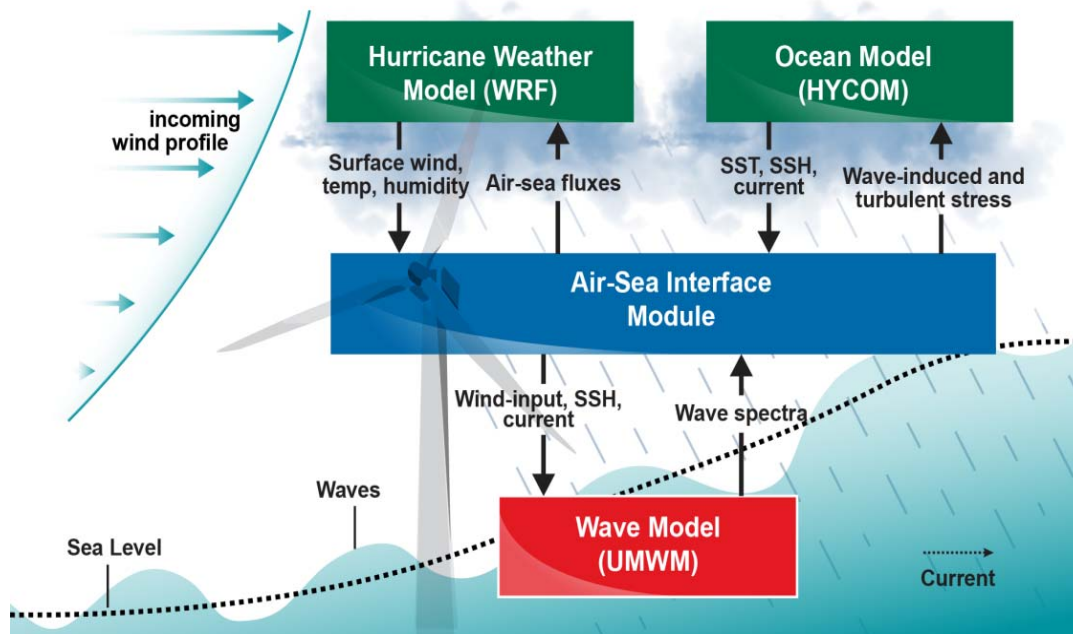


**Figure F1. Schematic of the fully coupled atmosphere-wave-ocean modeling system University of Miami Coupled Model that consists of WRF (atmospheric model), University of Miami Wave Model (wave model), and the Hybrid Coordinate Ocean Model (HYCOM) (ocean circulation model), as well as the meteorological and oceanic variables in the coupled system**

The development of the UMCM is based on basic coupled atmosphere-wave-ocean coupling physics described in Chen et al. (2007, 2013). The latest version includes a standardized, unified, air-sea coupling module, which provides routines that are compatible with different atmosphere, wave and ocean component models. The development of the Earth System Modeling Framework (ESMF (Hill et al. 2004), a software library for geophysical model coupling, made the design and development of the unified air-sea coupled model feasible. ESMF provides the facilities for grid and field data manipulation, as well as conventions for coupled model software design and parallel processing. The UMCM can be constructed using different atmosphere, wave, and ocean circulation models, connected together through an ESMF coupling interface.

## UMCM Component Model Descriptions

### *Atmosphere Model*

The atmospheric model in UMCM is the Weather Research and Forecasting (WRF) model V3.5 with Advanced Research WRF (ARW) dynamical core (Skamarock et al. 2008). WRF is a state-of-the-art non-hydrostatic atmospheric model with a large number of model physics options and a storm-following, moving nest capability for hurricane forecasting. It is defined on a 12 km horizontal resolution domain with 36 vertical levels and spans the area from 103.0 W to 55.0 W in longitude, and from 7.0 N to 45.0 N in latitude. There are two square-shaped, vortex-following, inner nests of 4 km and 1.3 km horizontal resolution that are 2,000 km and 440 km wide, respectively. The surface layer is based on Monin-Obukhov theory and the boundary layer parameterization is based on the Yonsei University scheme (YSU, Hong et al. 2006). The cloud microphysics is based on the single-moment 5-species scheme WSM5 (Hong et al. 2004), which is used on 1.3 and 4 km nested domains. The Kain-Fritsch cumulus parameterization is based on the 12 km domain (Kain and Fritsch 1993) in addition to WSM5. WRF passes the vertical wind

profile and air density to the wave model and radiative and heat fluxes and precipitation rate to the ocean circulation model.

### ***Ocean Surface Wave Model***

The ocean wave model in UMCM is the University of Miami Wave Model (UMWM) V1.1.0 (Donelan et al. 2012), a spectral ocean wave model that predicts wave energy spectra and atmosphere and ocean momentum fluxes based on input winds and ocean currents. UMWM is initialized from a calm state, and the full wave development for the initial atmospheric conditions happens within 6 hours. The model covers the same domain as the WRF parent domain, except that it is defined on a 4 km horizontal resolution. The wave energy spectrum is defined on 36 directional bins and 37 frequency bins ranging from 0.0313 Hz to 2 Hz. UMWM passes vectorial atmosphere stress to the atmosphere model, and vectorial ocean stress to the ocean circulation model.

### ***Ocean Circulation Model***

The ocean circulation model in UMCM is the HYbrid Coordinate Ocean Model (HYCOM) V2.2.34 (Wallcraft et al. 2009). It is a 3-dimensional hydrostatic ocean model with a hybrid vertical coordinate, z-level in shallow water, terrain-following  $\sigma$ -coordinate in intermediate water, and isopycnal (constant density) in deep water. In this study, we use the nonlocal K-profile vertical-mixing scheme by Large et al. (1994). Its domain is defined on a 0.04 degree (deg) horizontal resolution grid that spans almost as large a domain as that of WRF and UMWM, and with 32 vertical levels. In this region, the grid spacing of 0.04 deg corresponds to the spacing between 3,250 m in the north, and 4,400 m in the south of the domain. Thus, the grid spacing closely matches that of the UMWM grid and the WRF inner 4 km nest. HYCOM passes sea-surface temperature to the atmosphere model and surface current field and water density to the wave model. The air-sea interface module is defined on an exchange grid that covers the WRF and UMWM domains, at the horizontal resolution of 4 km. All fields are interpolated to the exchange grid, on which the calculation of air-sea exchange is defined, and are co-located in discrete time. In the current model configuration, fields from WRF and UMWM are exchanged every 60 seconds (s), whereas HYCOM fields are exchanged every 120 s.

### ***Initial and Lateral Boundary Conditions***

The WRF model initial and lateral boundary conditions are from the National Center for Environmental Prediction (NCEP) Global Forecasting System (GFS) 6-hourly fields at 0.5 deg horizontal resolution. The initial and boundary conditions for the ocean model are provided by the global, data-assimilated, 0.08 deg horizontal resolution daily HYCOM fields. Figure F2 shows an example of the UMCM domains and model forecast of Hurricane Sandy initialized by the global GFS and HYCOM fields at 0000 UTC on 28 October 2012.

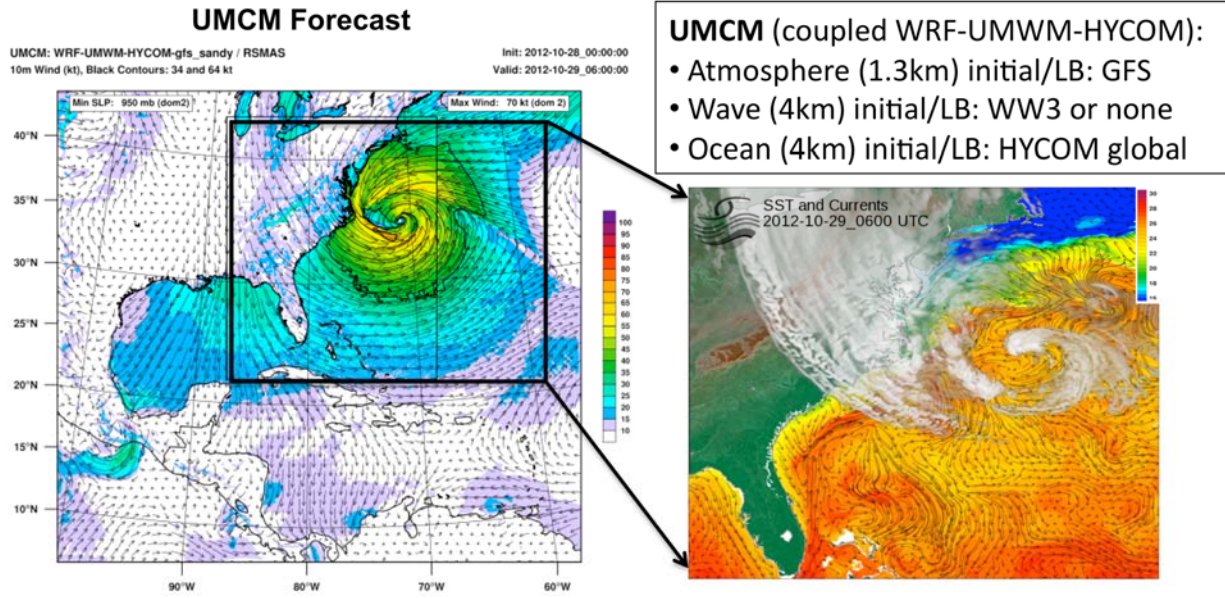


**Figure F2. UCMC model forecast of surface wind (left) and sea surface temperature and precipitating cloud fields (right) for Hurricane Sandy at 0600 UTC on October 29, 2012**

### Combined Models

Each of the three component models in UCMC have separate origins and were originally designed to simulate their respective physical systems separately. The unified air-sea interface serves not only as a coupler but also includes coupling computations related to air-sea heat, moisture, and momentum fluxes that are done consistently at each coupling time step. The common grid is configured at the highest horizontal grid spacing of the three component models. In the current coupling configuration, it is set to 1.3 km, which is consistent with WRF. The UMWM and HYCOM grid resolution is at 4 km. The coupling time step for between the atmosphere-wave models is 1 minute and for the ocean model is 2 minutes.

The WRF model incorporates two-way interacting moving nests at an increasing resolution over a storm and which follows it as it moves. In the specific configuration used for simulations of Hurricane Ike, the outermost domain has a 12 km horizontal resolution. This resolution provides forcing for the lateral boundaries of a 4 km middle resolution domain, which in turn provides forcing for the lateral boundaries of a moving 1.33 km fine-resolution domain centered over the hurricane using a vortex-tracking algorithm developed at the UM. The outermost domain of WRF is initialized and forced using output from a global weather forecast model, typically the National Weather Service's GFS or the European Center's Integrated Forecast System (IFS) models. The influence of observational data (from satellites, aircraft, etc.) has been incorporated in the global forecast data. UCMC can also assimilate additional, more localized observational data as it runs.

### Completed Work at the University of Miami

- UM group has completed the coupled atmosphere-wave-ocean model simulation of Hurricane Ike (2008) and forecast of Superstorm Sandy (2012) using the University of Miami Coupled Model (UMCM). UMCM has 1.3 km grid resolution for the atmosphere and 4 km for the wave and ocean model components. The UCMC full model fields



(including all vertical levels and nested horizontal model grids) were made available at an hourly output.

- A site-specific, high-frequency model output at 1-minute intervals for 10 sites along the eastern seaboard selected by the UT group. This special model output was provided for the UT group in support of their downscale modeling effort. The 1-min coupled model output includes winds, ocean surface wave height, and 2-D wave spectra and other surface variables. In addition to the wind and wave data, UM also provided the ocean current profiles at each site for UT, which may be of value for estimating loads both above and below the ocean surface.
- At NREL and UT request, we have also produced full model fields at 10-minute interval, which is higher frequency than the normal 1-hour interval output. The full fields include 3D winds, temperature, humidity, significant wave height and wave periods, 3D ocean currents, temperature, and so on. UM provided the full UMCM output to NREL for 1) future research applications, 2) advanced visualization of high-resolution atmosphere-wave-ocean fields in hurricanes at NREL, and 3) open distribution online for users outside NREL (see Appendix G).

## Results

### *Superstorm Sandy (2012)*

Superstorm Sandy formed as a tropical storm in the Caribbean Sea on 23 October 2012, and later intensified into a Category 1 hurricane of the western Atlantic Ocean. It interacted with a strong mid-latitude system and became a “superstorm” that made landfall over the U.S. northeastern coastal region. UM conducted a UMCM forecast starting at 0000 UTC on 27 October 2012, using the NOAA GFS model forecast fields as the initial and lateral boundary conditions for WRF and the global HYCOM forecast fields for the regional HYCOM in UMCM. Figure A3 shows the UMCM forecast storm track and intensity (red lines) compared with the National Hurricane Center (NHC) best track data (black lines). Both the storm track and intensity were well-forecasted by UMCM.

## Verification of UMCM Forecasts with NHC and NDBC Data

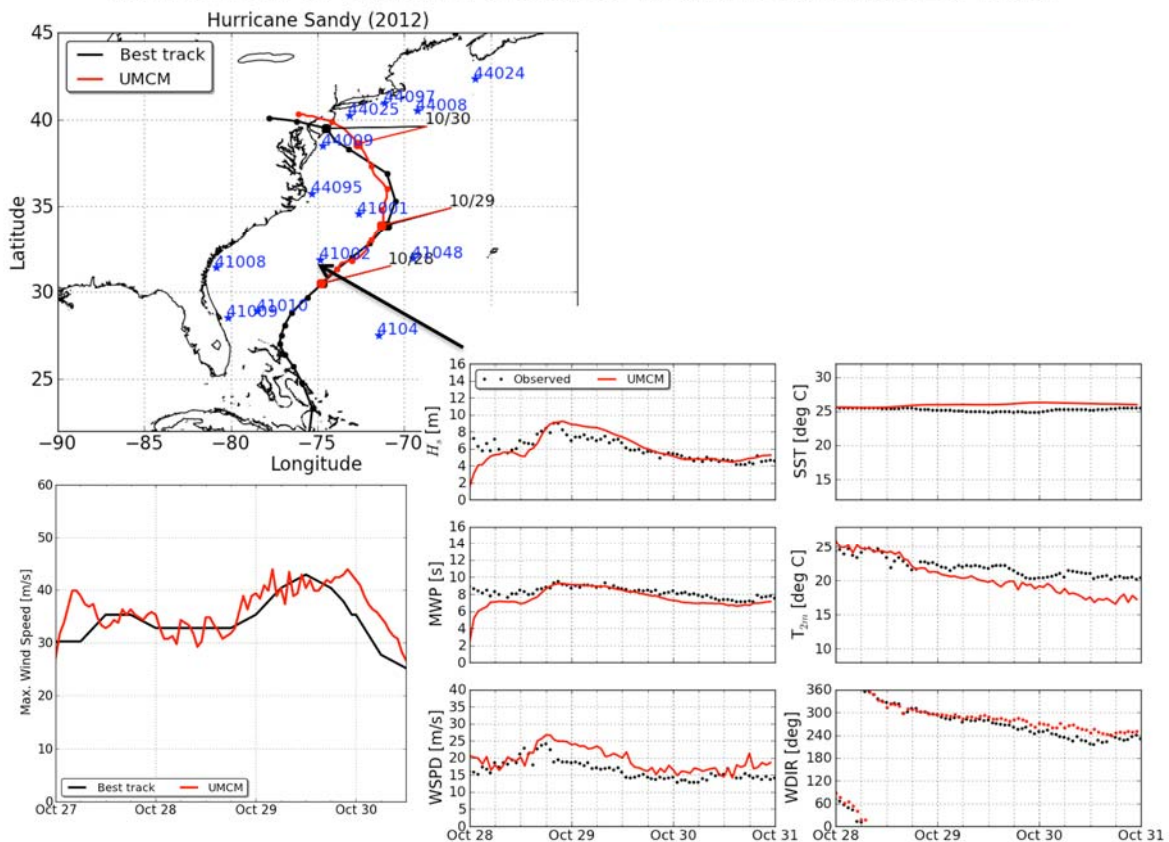


**Figure F3.** The UMCM forecast (red) and National Hurricane Center best track data (black) of Superstorm Sandy track (top left) and intensity (bottom left). Model forecast (red) and the National Data Buoy Center (NDBC) buoy observation (black) of significant wave height ( $H_s$ ), mean wave period (MWP), wind speed (WSPD), sea-surface temperature (SST), and 2-m air temperature ( $T_{air}$ ).

The UMCM is evaluated and verified with in-situ observations from the National Data Buoy Center (NDBC) buoys. An example of the model verification against the buoy observation is shown in Figure F3. NDBC 41002 was near the center of Superstorm Sandy when the storm passed the buoy location on 28 October 2012.

Hurricanes have major impacts on the coastal ocean and land when making landfall. The characteristics of winds, surface waves, and ocean currents are shown in Figure A4. The storm impacts are asymmetric around the storm. On the right side of the center, the wind is mostly southeasterly and easterly onshore flow. The surface waves and sea surface height are the highest when Sandy was making landfall on 30 October. On the left side, the wind changed direction before and after landfall. The wave height peaked before the landfall and then decreased when the wind became offshore at and after the landfall. The 2-D wave spectra shows that the sea swells (long waves) dominated on the right side, whereas the wind-sea (short waves) and swell are both present on the left.

## Winds and Waves at Virtual Turbine Sites in Superstorm Sandy

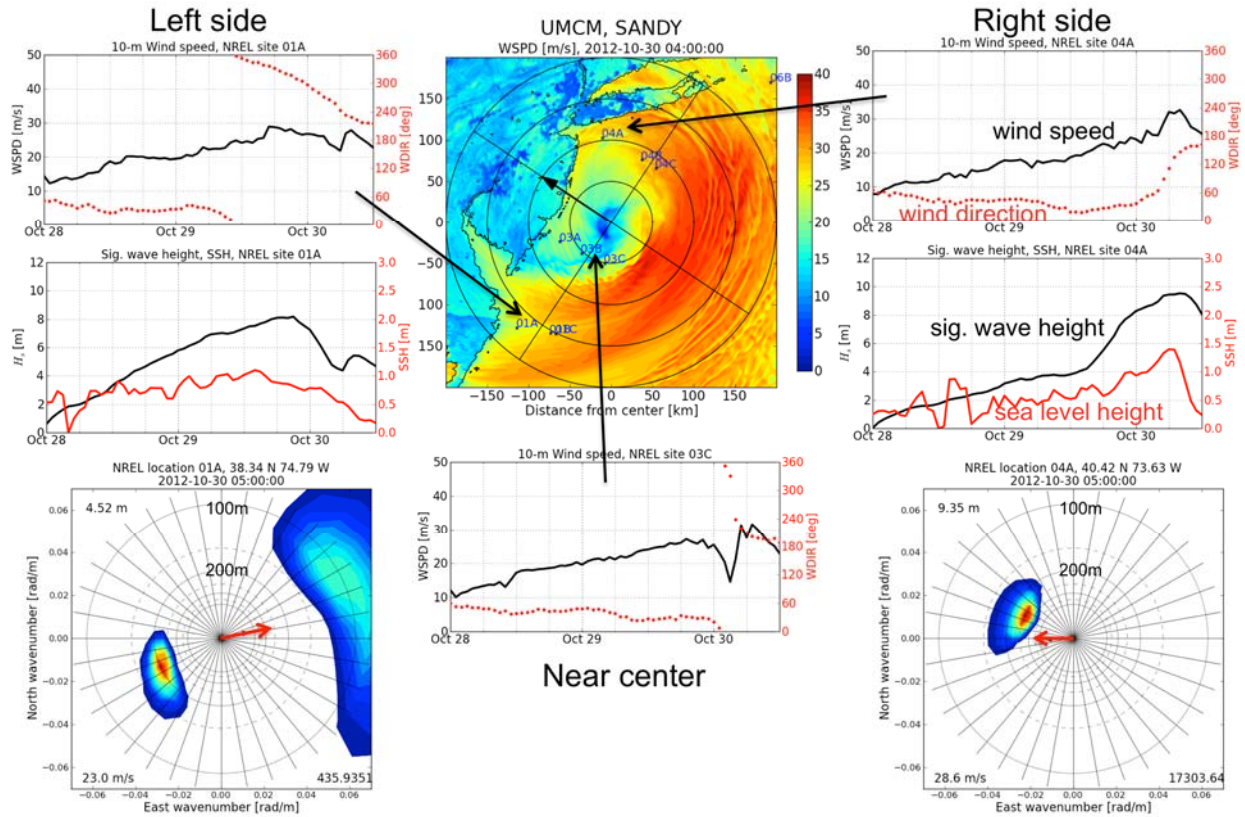


**Figure F4. UMC forecasts of wind speed (red) and direction (black), significant wave height (red), sea level height (black), and 2-D wave spectra (color coded for power of wave spectrum and red arrow represents wind vector) at three selected virtual turbine sites on the left, right, and near the center of Superstorm Sandy right before the landfall on 30 October 2012.**

There is a significant vertical wind shear from the surface to the 200 m level in Superstorm Sandy as shown in Figure F5. The wind speed varies from 25 to  $> 40 \text{ m s}^{-1}$ .



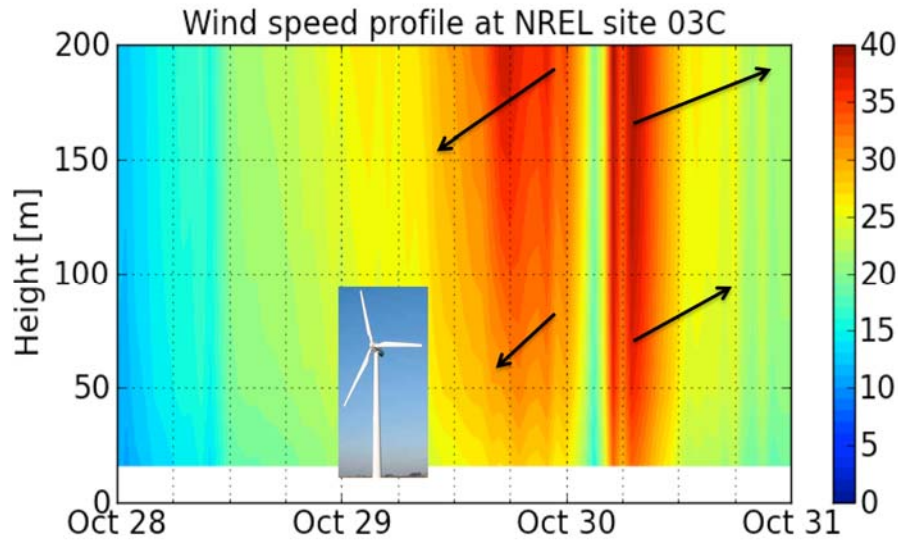


**Figure F5. The UMCM forecast of wind speed (color) near the center of the storm at location 03C (marked on the surface wind speed map in Figure F3). The black vectors indicate wind directions.**

### ***Hurricane Ike (2008)***

The UMCM forecast fields in Hurricane Ike (2008) have been verified against the in situ observations from the NDBC sites in the Gulf of Mexico during the hurricane passage in September 2008. The fields of verification include 10-m surface wind speed (WSPD), sea level pressure (SLP), surface air temperature ( $T_a$ ), sea-surface temperature (SST), significant wave height (SWH), and mean wave period (MWP). The site-specific comparisons are subject to storm track forecast error. In order to evaluate hurricane-induced features, a storm-relative approach with correction for track error is usually used for verification at sites within the storm when it passed the site. Here we include examples from two nearshore sites that are outside of the storm with an Earth-relative reference, and two within the storm along the Hurricane Ike path with a storm-relative comparison (Figures F6 through F10).

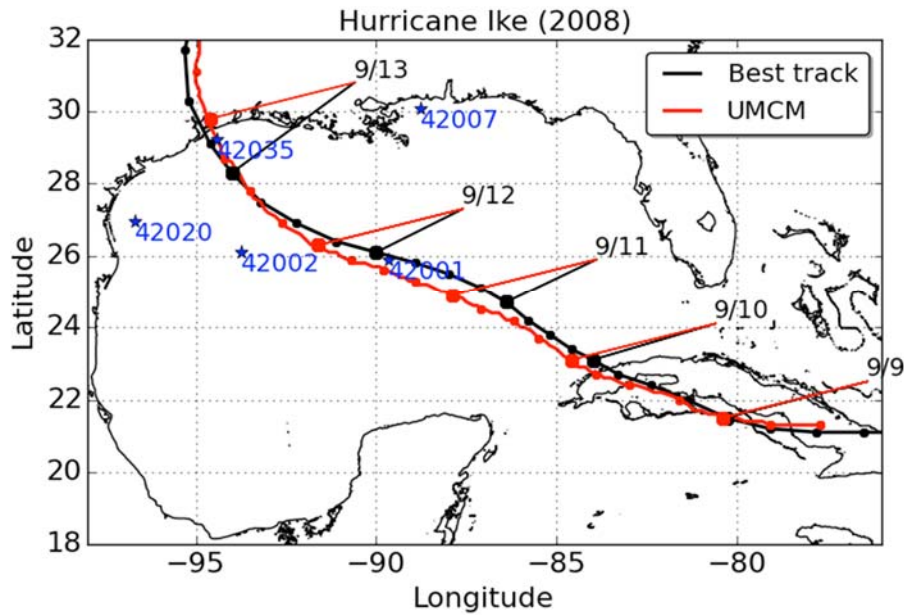


Figure F6. Map of model storm track forecast compared with the National Hurricane Center (NHC) Best Track estimate and locations of the NDBC sites

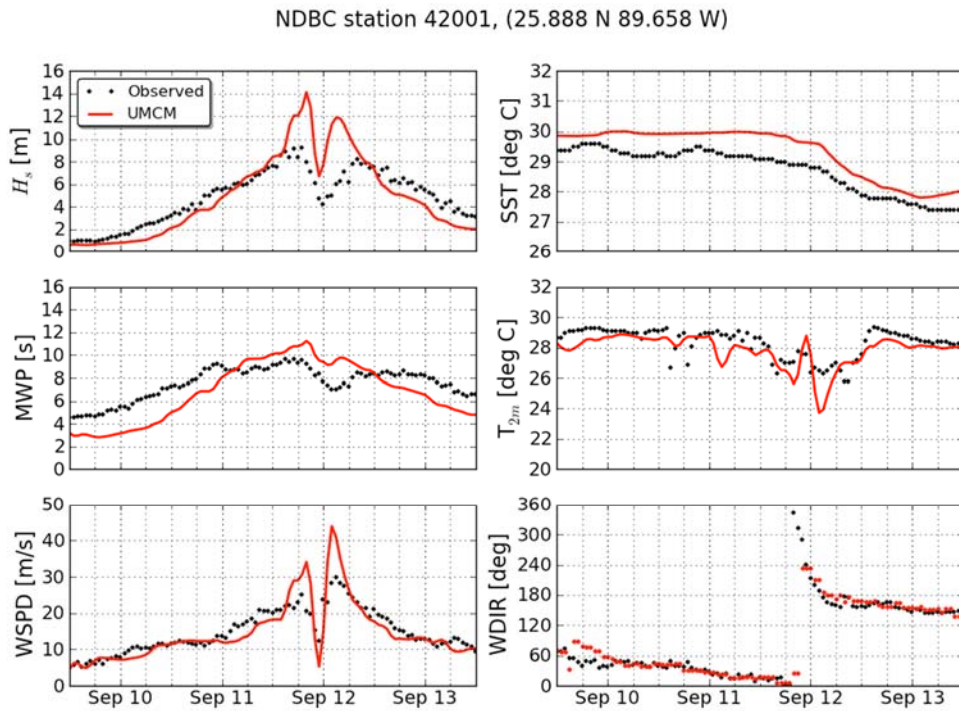


Figure F7. Comparison of UCM forecasts and NDBC Buoy 42001 data

NDBC station 42002, (25.790 N 93.666 W)

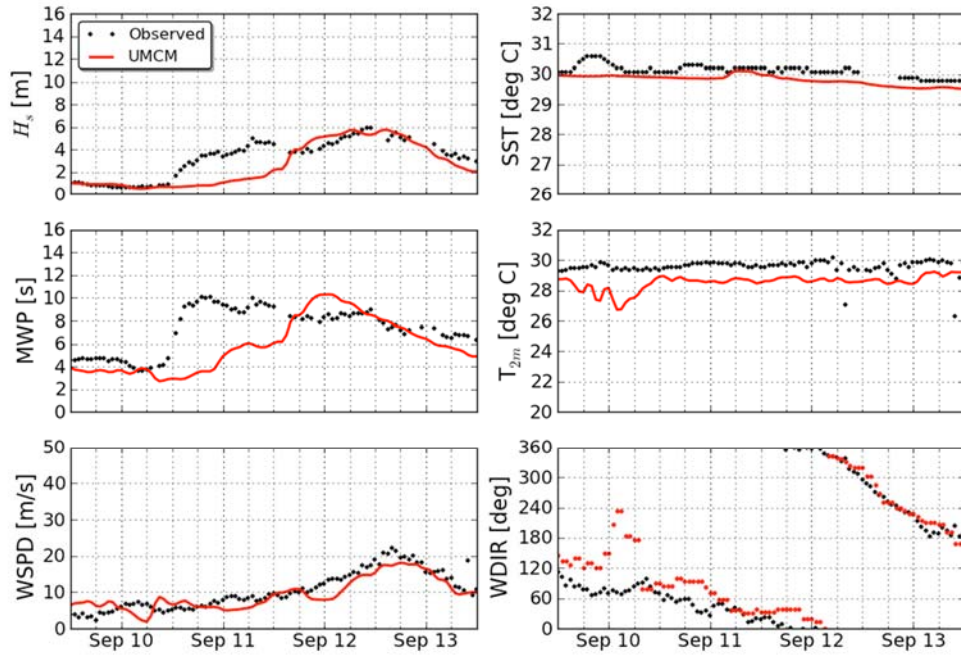


Figure F8. Comparison of UCMC forecasts and NDBC Buoy 42002 data

NDBC station 42007, (30.090 N 88.769 W)

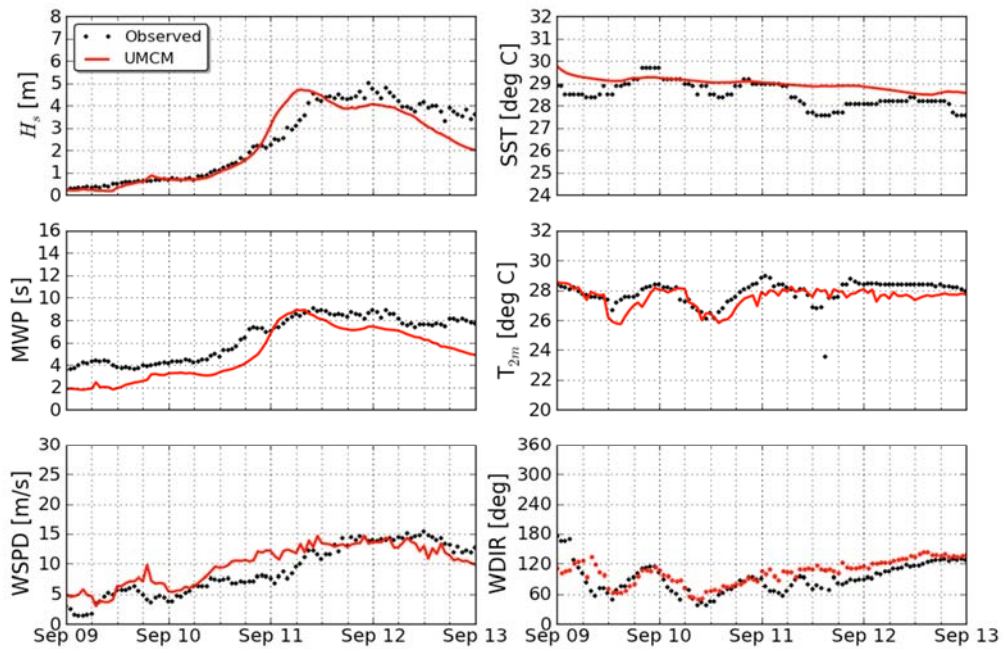


Figure F9. Comparison of UCMC forecasts and NDBC Buoy 42007 data

NDBC station 42020, (26.968 N 96.694 W)

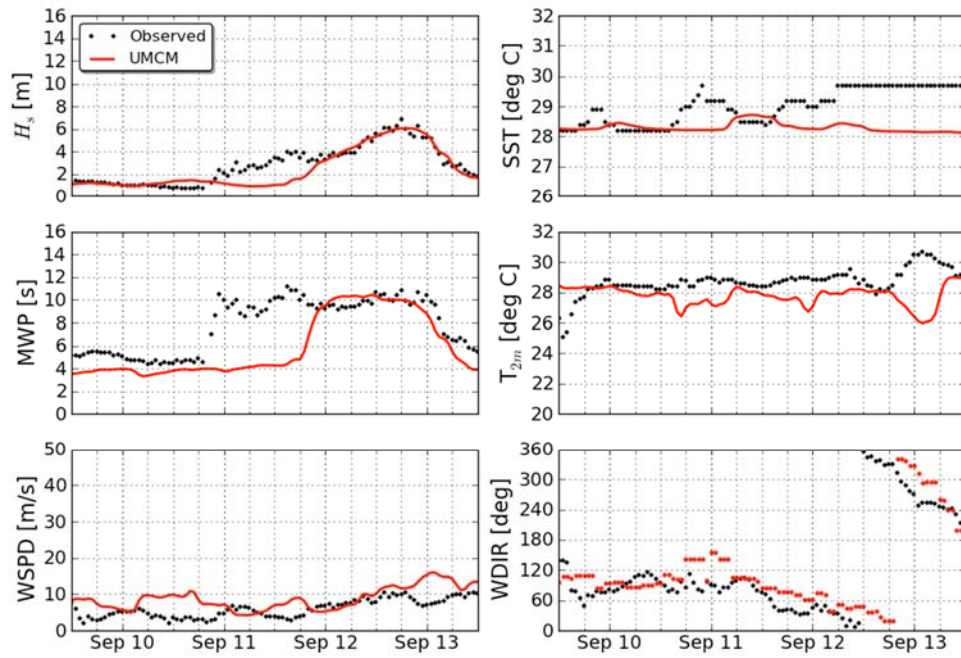


Figure F10. Comparison of UCMCM forecasts and NDBC Buoy 42020 data

## References

- Chen, S. S., J. F. Price, W. Zhao, M. A. Donelan, and E. J. Walsh (2007), The CBLAST Hurricane program and the next-generation fully coupled atmosphere-wave-ocean models for hurricane research and prediction, *Bull. American Meteor. Soc.*, **88**, 311–317.
- Chen, S. S., W. Zhao, M. A. Donelan, and H. L. Tolman (2013), Directional wind-wave coupling in fully coupled atmosphere-wave-ocean models: Results from CBLAST-hurricane, *J. Atmos. Sci.*, **70**, 3198–3215.
- Donelan, M. A., M. Curcic, S. S. Chen, and A. K. Magnusson (2012), Modeling waves and wind stress, *J. Geophys. Res.*, **117**, C00J23.
- Hill, C., C. DeLuca, V. Balaji, M. Suarez, and A. da Silva (2004), Architecture of the Earth System Modeling Framework, *Computing in Science and Engineering*, **6**, 18–28.
- Hong, S.-Y., J. Dudhia, and S.-H. Chen (2004), A revised approach to ice microphysical processes for the bulk parameterization of clouds and precipitation, *Mon. Wea. Rev.*, **132**, 103–120.
- Hong, S.-Y., Y. Noh, and J. Dudhia (2006), A new vertical diffusion package with an explicit treatment of entrainment processes, *Mon. Wea. Rev.*, **121**, 2318–2341.
- Kain, J. S., and J. M. Fritsch (1993), Convective parameterization for mesoscale models: The Kain-Fritsch scheme, in *The representation of cumulus convection in numerical models*, edited by K. A. Emanuel and A. M. S. D. J. Raymond, Eds., p. 246pp.
- Large, W. G., J. C. McWilliams, and S. C. Doney (1994), Oceanic vertical mixing: A review and a model with a nonlocal boundary layer parameterization, *Reviews of Geophysics*, **32**, 363–403.
- McWilliams, J. C., and P. P. Sullivan (2000), Vertical mixing by Langmuir circulations, *Spill Science and Technology Bulletin*, **6**, 225–237.
- Wallcraft, A. J., E. J. Metzger, and S. N. Carroll (2009), Software design description for the Hybrid Coordinate Ocean Model (HYCOM) version 2.2, Tech. rep., nRL/MR/732009-9166.



## Appendix G. Large Data Access System

The University of Miami Combined Model (UMCM) pairs atmospheric Weather Research and Forecasting (WRF) data with University of Miami Wave Model (UMWM) and Hybrid Coordinate Ocean Model data. The data set hosted at the National Renewable Energy Laboratory (NREL) contains detailed data for hurricanes Ike (2010) and Sandy (2012), stored in a series of NetCDF-format files, totaling 1.3 Terabytes. The UMCM data store can be accessed at <http://opendap.nrel.gov> (also listed on <http://data.gov> at <http://catalog.data.gov/dataset/combined-wind-wave-hurricane-model>). Users internal to NREL can access the data slicing application at <http://jett.hpc.nrel.gov>.

Each data set contains a number of files, one per time stamp, and each file contains a grid of measurements using a custom map projection. The details of the data and their resolution are as follows:

- Ike
  - Time resolution:
    - 1 sample/hour from 9/8 12:00 to 9/12 6:00
    - 1 sample/10 minute (min) from 9/12 6:00 to 9/13 9:00
    - 252 samples in time
- Sandy
  - Time resolution:
    - 1 sample/10 min from 10/28 00:10 to 10/31 00:00
    - 432 samples in time.

At 58 additional sites, the data set contains higher resolution “spectral” data from the UMWM for Hurricane Sandy. Figure G1 shows the location of these points relative to the tracks of Ike and Sandy. Of those sites, 26 were selected as potential areas of interest for offshore wind development, and 32 were selected as validation locations for comparison with National Data Buoy Center (NDBC) data. At these locations, 4,319 samples are available, providing a 1 min/sample resolution.

## Data Access Systems

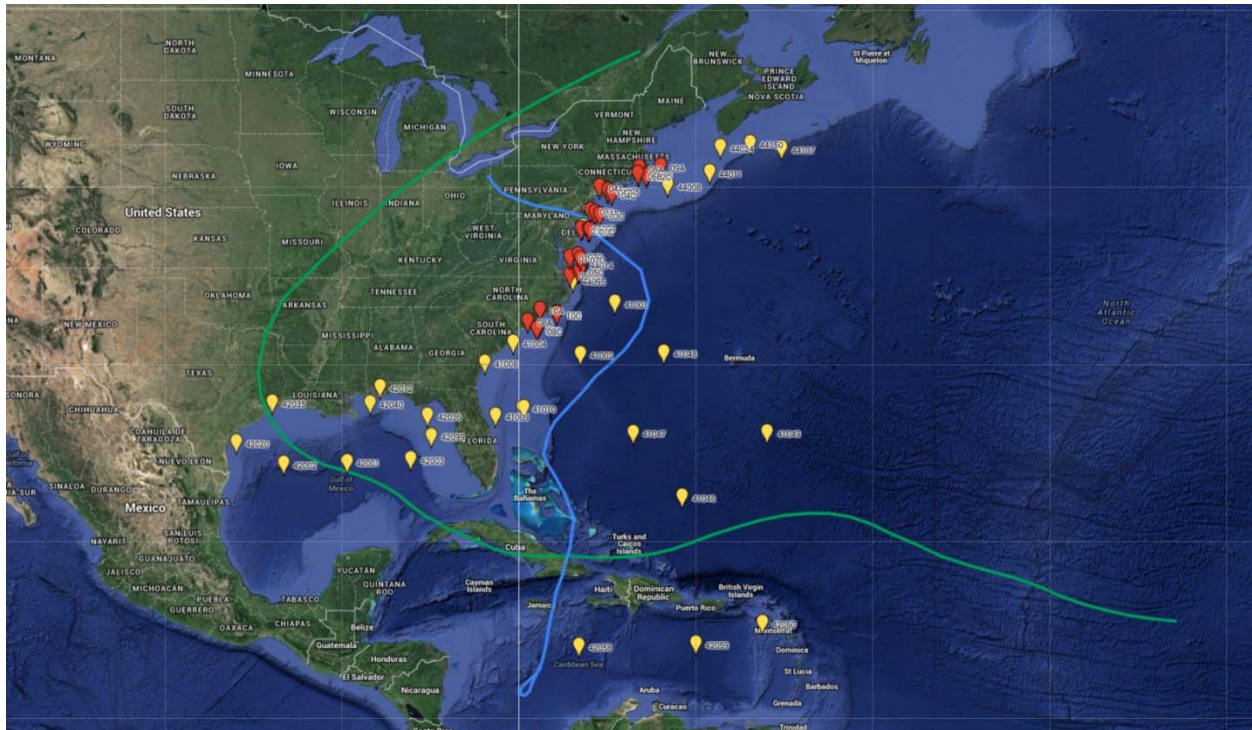


**Figure G1. Locations of 1 minute/sample resolution "spectral" data placed amidst storm tracks are indicated by the red balloons**

Source: Orthoimagery courtesy of Google Inc.

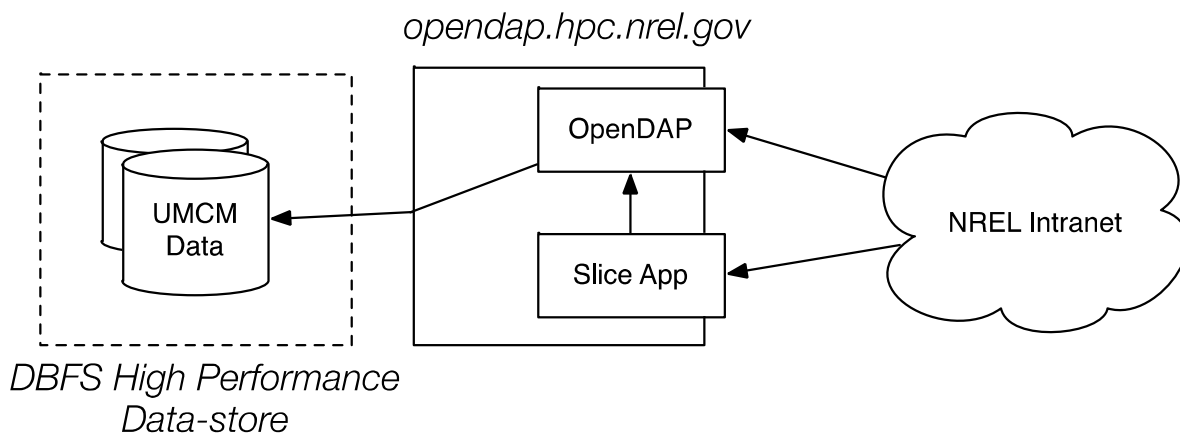


**Figure G2. Configuration of OpenDAP Hyrax server and slicing application for the database file system (DBFS)**

The data is stored in the NREL data center in the native NetCDF format on the DBFS high-performance data store. Remote Web access to the data is provided by a Hyrax data server, which accepts queries using the OpenDAP protocol as well as a basic Web access. OpenDAP queries allow for arbitrary subsetting of the data using any number of client frameworks (e.g., Python, Matlab, etc.). In this way, only the necessary subset of data is retrieved from the server on the fly as computations are performed. Visualization can be accomplished similarly, by requesting a subset of relevant data.

Additionally, staff at the NREL Computational Sciences Center have developed a custom Web framework for performing automatic time-series data extraction at an arbitrary location with any subset of model variables. In this way, National Wind Technology Center researchers can extract just those variables of greatest interest at exactly the sites they wish. These data “slices” are requested through a Web interface. Data extraction is fielded by a queue-based system and researchers are notified when their data is ready to download as spreadsheet by email. Figure G2 shows the configured elements of this data access system. At the time of writing, this framework can only be accessed internally, but is designed for public access should that be deemed valuable at a later time.

## **Analysis Example**

To provide an example of analysis opportunities using these resources, we identified three locations corresponding to points of interest for offshore wind turbine researchers. These locations are 03A (39.2691,-74.2267), 03B (39.1576, -73.9192), and 07A (36.934,-75.5453). Locations 03A and 03B are off the coast of Atlantic City along the direct path of Hurricane Sandy, amounting to a worst-case scenario for this storm. Location 07A is off the coast of Virginia outside the main path of the storm. Both locations are in a state of active wind turbine planning and development. Figure G3 and Figure G4 show the locations in detail with the path of Hurricane Sandy in blue.



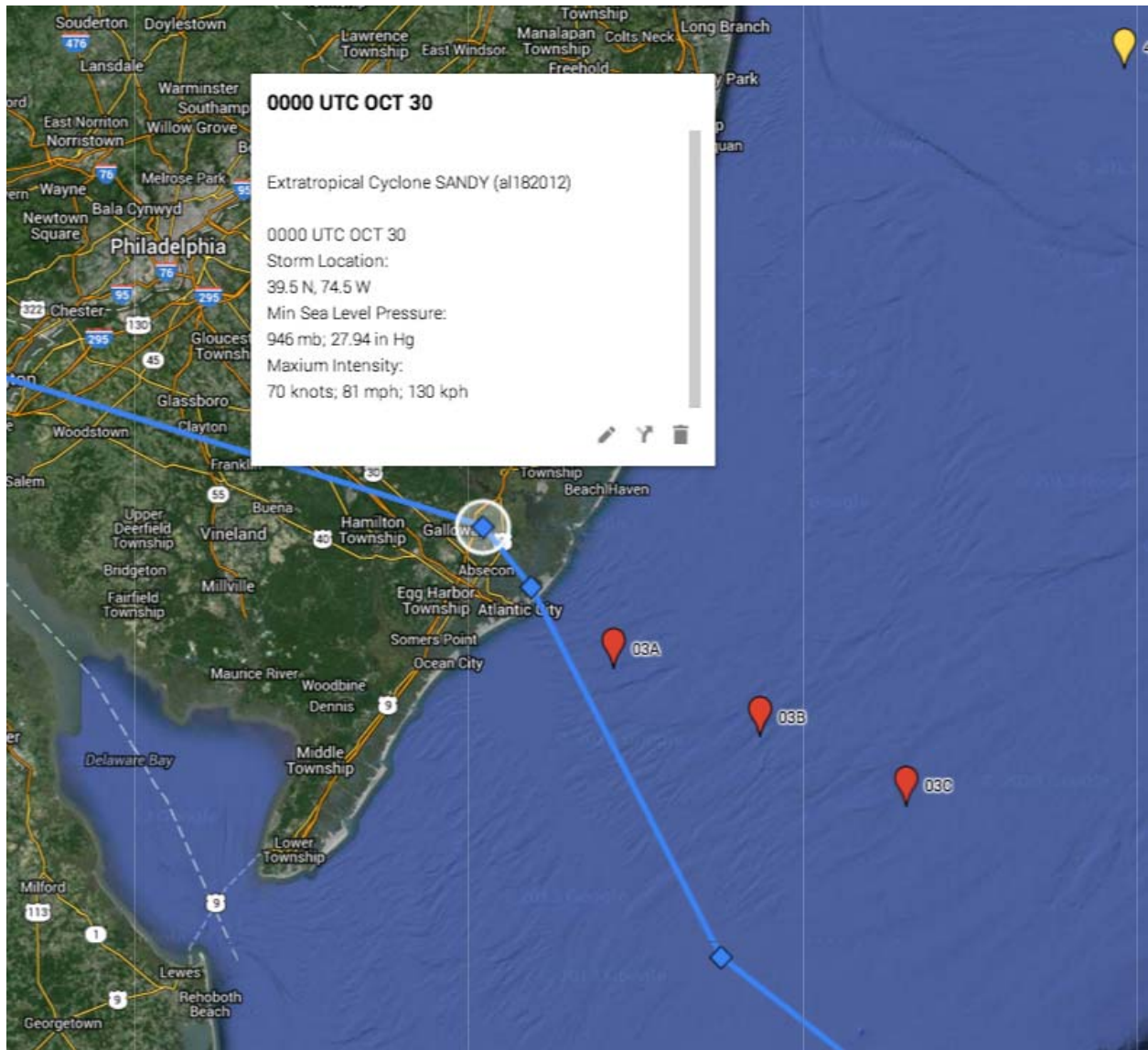


**Figure G3. Close-up of locations 03A and 03B**  
 Source: Orthoimagery courtesy of Google Inc.

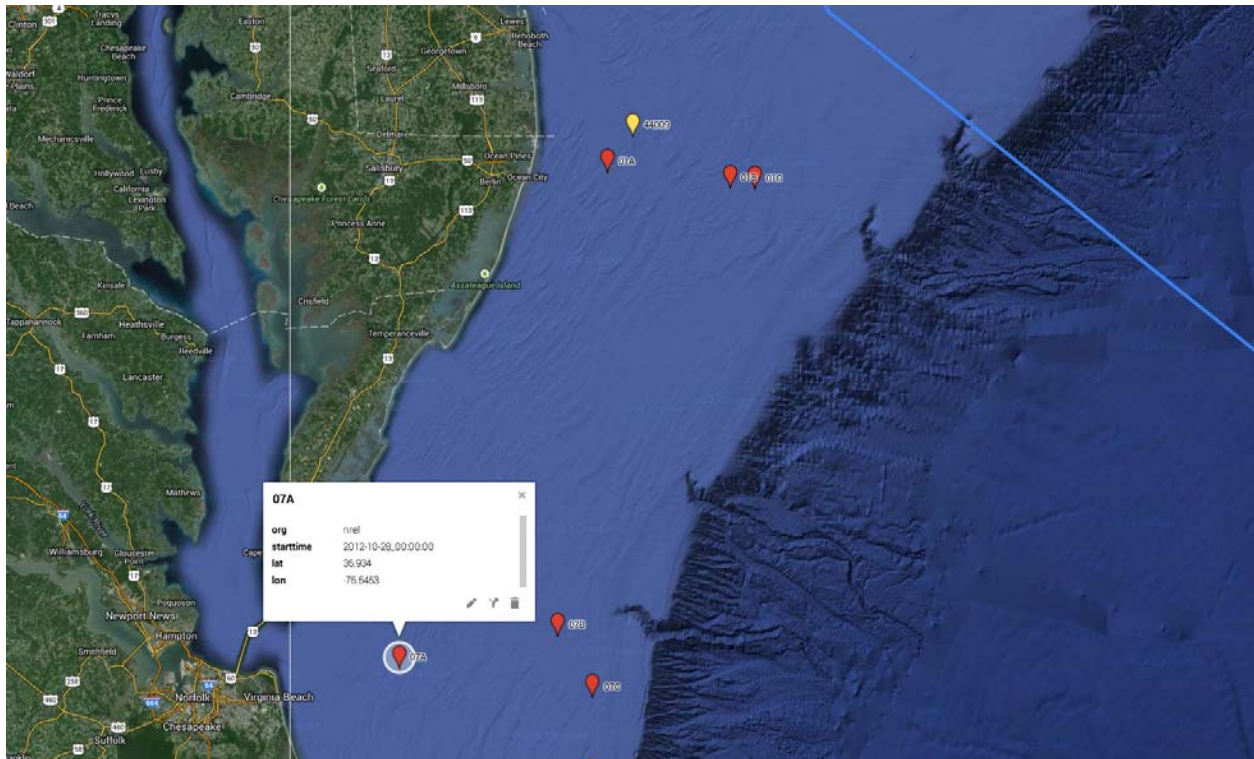


**Figure G4. Close-up of location 07A**

Source: Orthoimagery courtesy of Google Inc.

Example time series for location 03B are given in Figures G5 through G8. Figure G5 and Figure G7 show the entire duration of the storm for 1 and 10 min resolutions, respectively. Figure G6 and Figure G8 show a close-up view of data from this time series around the time the storm crosses over the location (i.e., at landfall). It is clear to see that the 10-min sample/snapshot in Figure G8 is beginning to reach the limits of usefulness in terms of the resolution; however, the main trends are still clear. The higher resolution in Figure G6 gives a crisp view of the behavior of the storm at landfall.

The peak wind event for location 03B occurs at approximately 03:00 on 30 October 2012, reaching a maximum average wind speed of 32 m/s (71 mph). The maximum wave event is approximately 6 hours earlier, reaching 11 meter wave heights with a period of 11 seconds. Wind direction changes radically between these two events (max wave and max wind), from approximately 200 degrees (SSW) to 80 degrees (ENE). The change in wind direction creates a maximum wind-wave misalignment in this period of 30–35 degrees. Sites 03A and 03B show similar patterns (see Figure G9 and Figure G10). Site 07A exhibits the greatest misalignment in wind and wave directions: nearly 70 degrees phase mismatch during a period of greater than 30 m/s wind speeds and more than 10 m waves. Site 03A, which is more inland, appears quite similar to 03B, although less severe.

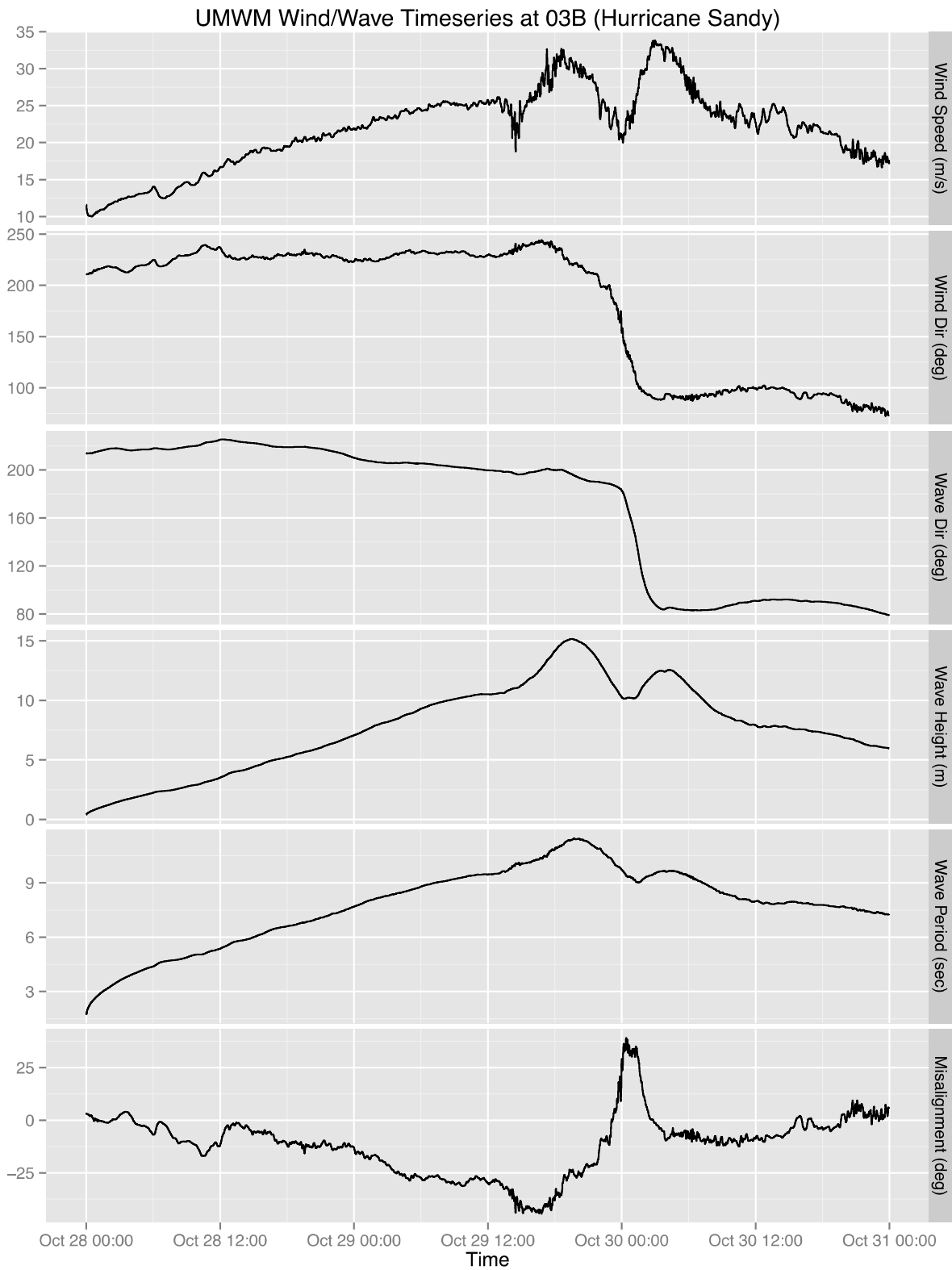


**Figure G5. Time series at location 03B, 1 min/sample resolution**

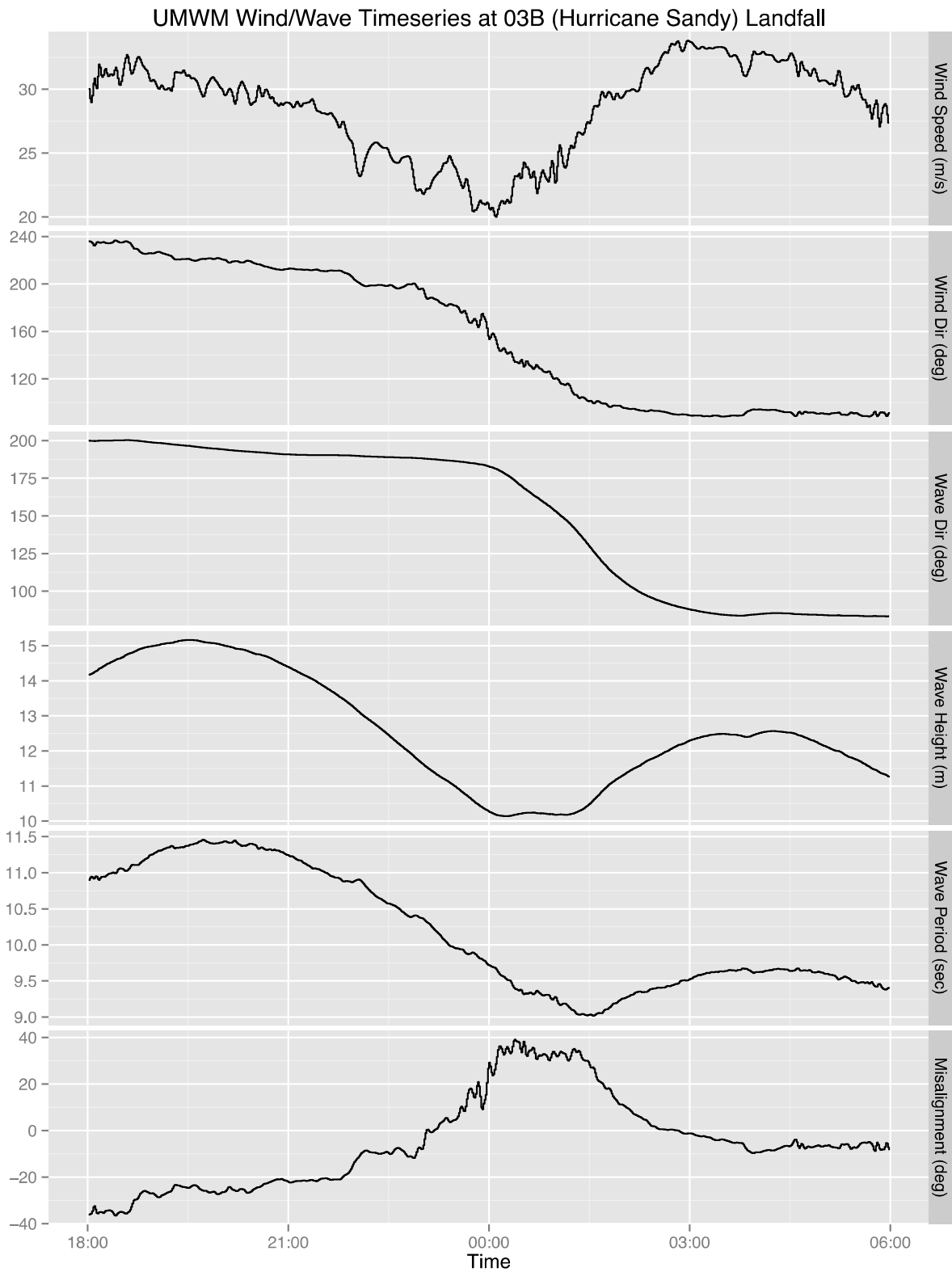


**Figure G6. Time series at location 03B, 1 min/sample resolution, close-up at landfall**

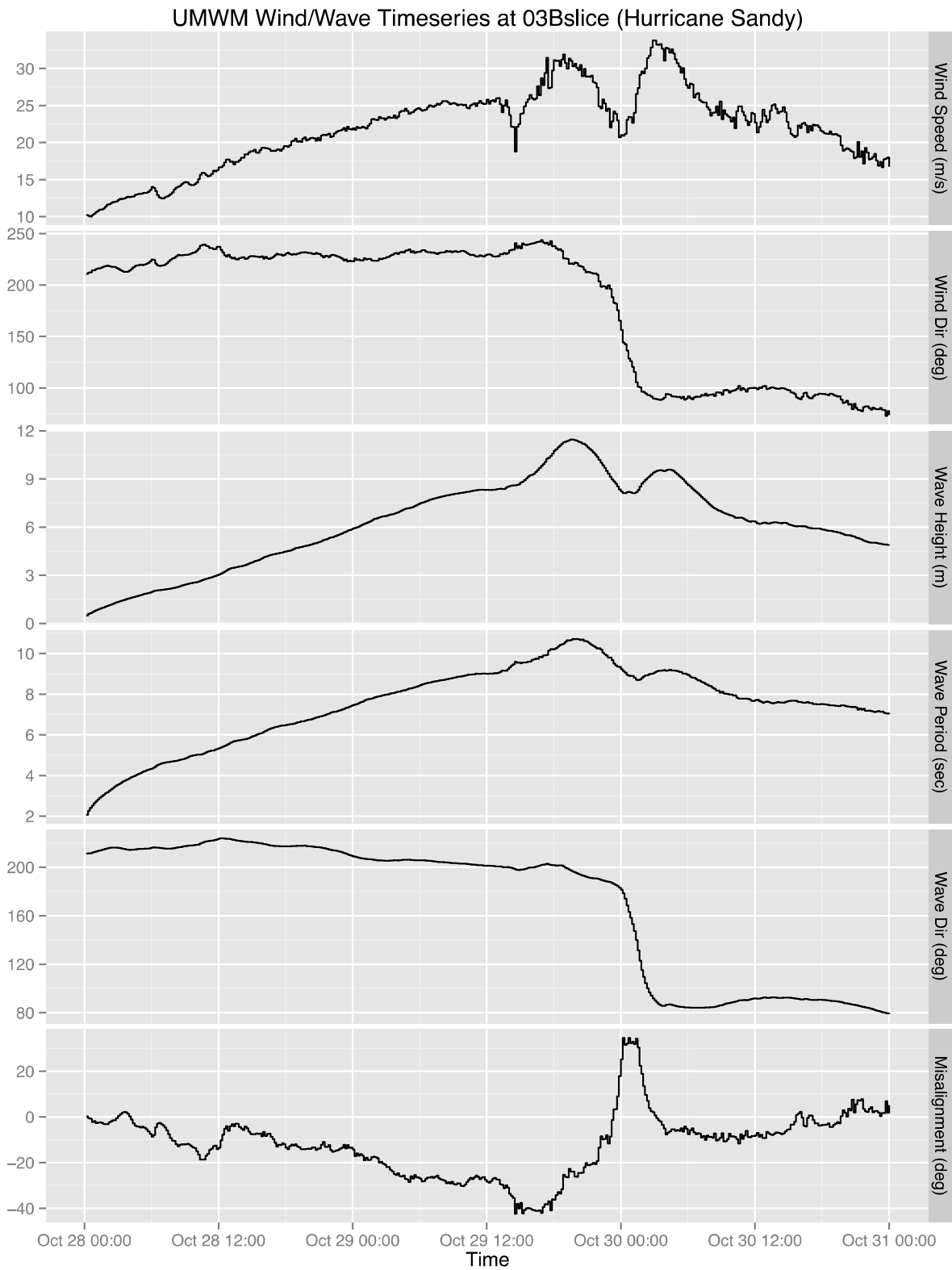


**Figure G7. Time series at location 03B, 10 min/sample resolution, extracted with NREL data slice tool**

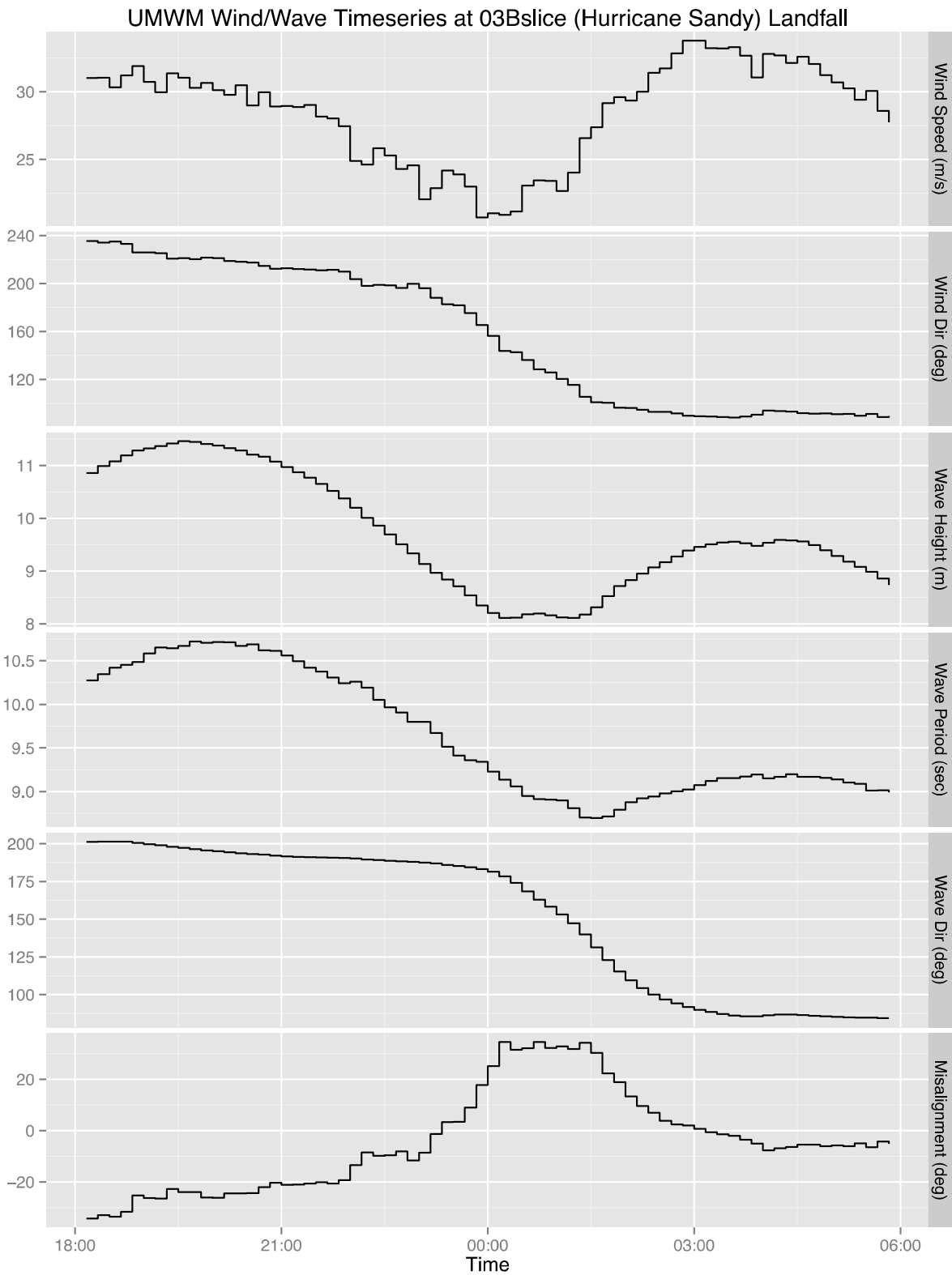


**Figure G8. Time series at location 03B, 10 min/sample resolution, close up at landfall**

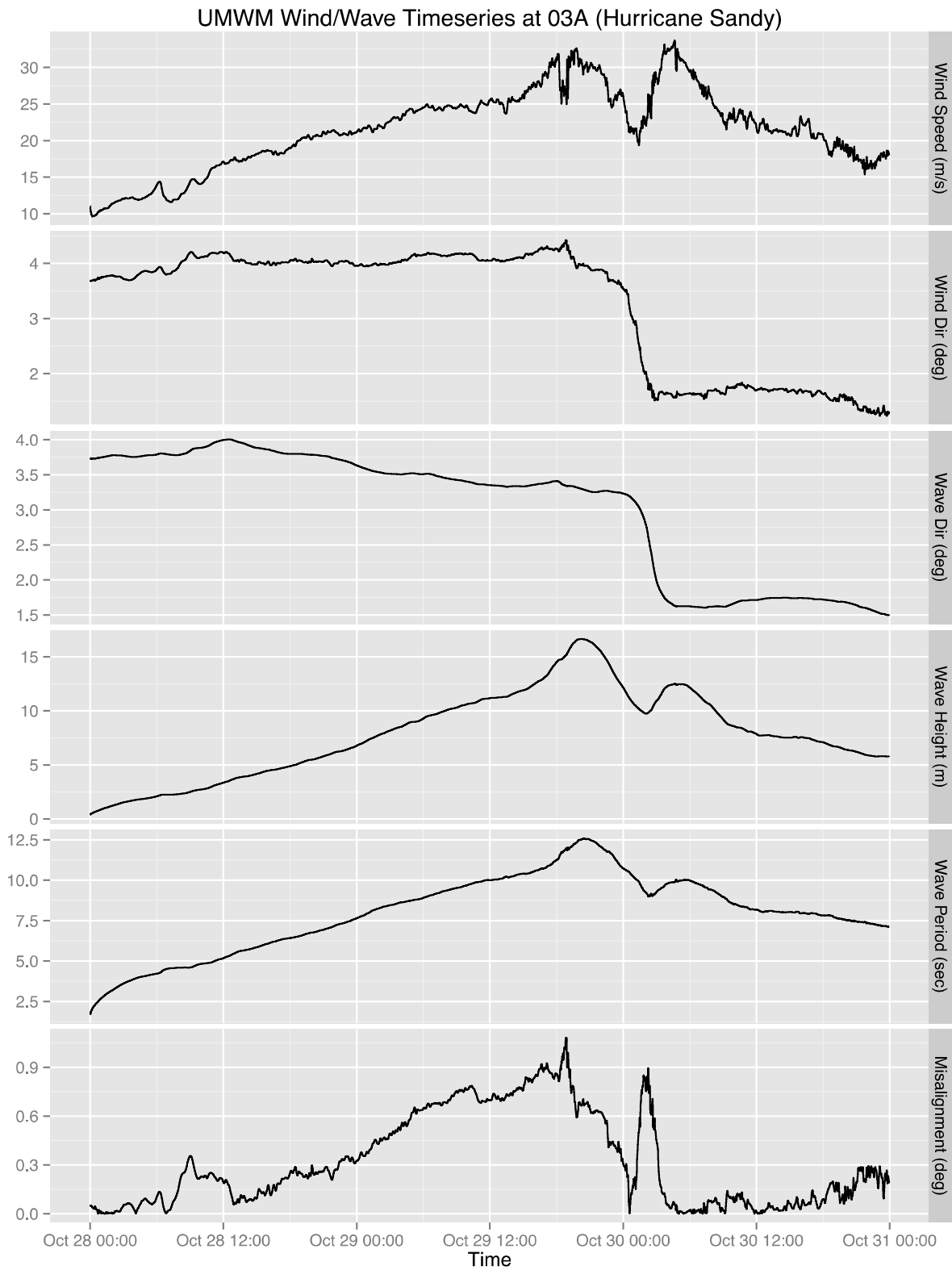


**Figure G9. Time series at location 03A, 1 min/sample resolution**

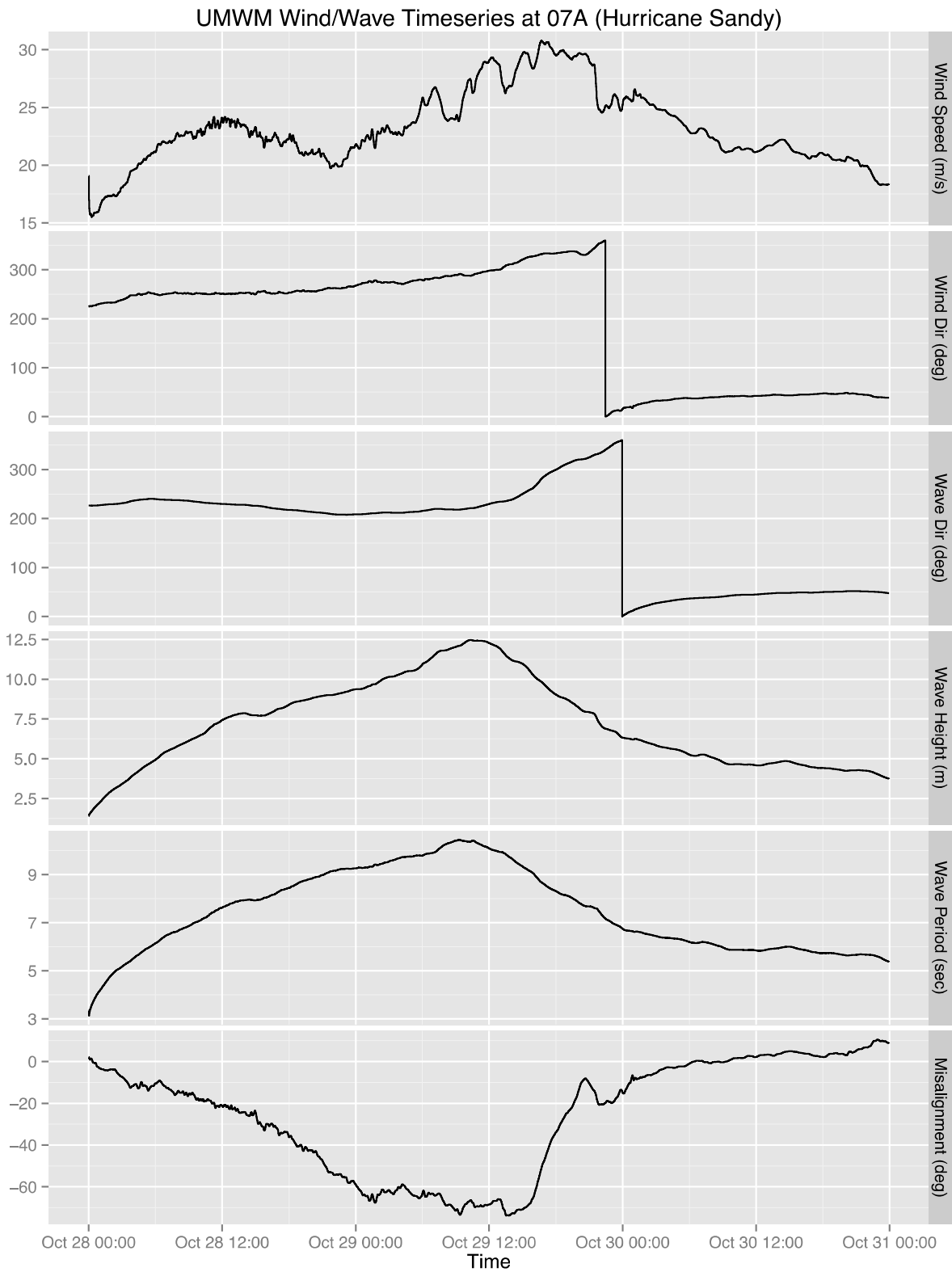


**Figure G10. Time series for location 07A, 1 min/sample resolution**